



NTNU – Trondheim
Norwegian University of
Science and Technology

Application of AC Superconducting Windings in Large PM Synchronous Generators for Wind Power

Raghbendra Tiwari

Master of Science in Electric Power Engineering

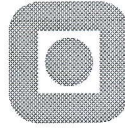
Submission date: June 2012

Supervisor: Arne Nysveen, ELKRAFT

Co-supervisor: Stev E. Skaar, SmartMotor AS

Norwegian University of Science and Technology
Department of Electric Power Engineering

Department of Electric Power Engineering



MASTER'S THESIS

Student's name: Raghbendra Tiwari

Area: Electric Power Engineering

Title: **PM windpower generators with superconducting AC windings**

Description:

To reduce the size and weight of electrical machines, the use of superconductors are of special interest. Today most of the machines made are using superconductors exposed to dc-magnetic fields only. Thus the research has focused on synchronous machines with superconductors in the field winding. New superconductors based on MgB_2 that can tolerate ac current and ac external fields opens up for the possibility of using superconductors in the armature windings. A project work conducted by the student fall 2011 showed that a PM machine with concentrated windings is a good candidate for this technology.

In this work the student shall work on using the technology on large direct-driven PM windpower generators.

More specifically the work shall focus on:

- Give a technological background and motivation for using ac superconductors in synchronous machines.
- Describe the design methodology for PM windpower generators and how the superconducting windings can be applied
- Perform a design comparison with PM generators with traditional copper windings. Important parameters are volume and weight, losses and electrical parameters.

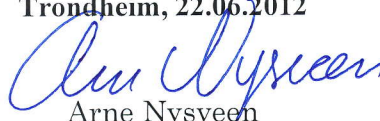
Details in the analysis and selection of machines to be analysed can be clarified with the supervisors.

Start date: 06.02.2012

Deadline: 02.07.2012

Co-supervisor: Stev Skaar, SmartMotor

Trondheim, 22.06.2012


Arne Nysveen
Professor

Abstract

Superconductors are known for carrying very high current density without any loss of energy. This characteristic helps to achieve very high power capacity with compact size of machine. In application of superconductors, the main obstacle has been the cooling of the conductors since it operates at very low temperatures below ambient. After the discovery of high temperature superconductor (HTS) in 1986, several prototype machines have been built using in DC field winding. The application of superconductor in AC armature winding has not been feasible due to excessive AC losses. These losses are caused due to penetration of time varying magnetic field.

This thesis concerns the possibility of the application of superconductor in armature windings of permanent magnet synchronous generator. A 10 MW wind power generator with copper winding has been taken as reference machine and the machine has been redesigned with several pole-slot combinations using superconductor. Permanent magnet has been used as the source of field. Three alternatives have been designed with superconductor in armature winding and the machine with 176 poles, 192 slots has been selected as the best among them based upon the active weight of the generator, outer volume, utilization factor, power factor, full load losses, and total harmonic distortion and cogging torque. The selected machine has been found to be 62 ton in weight where as that of reference machine is 90 ton. Moreover, the outer volume of the superconducting machine is about 2.5 times lesser than that of the copper winding reference machine. The reduction in volume of generator will consequently reduce the volume of nacelle and the reduction in weight will reduce the transportation cost. The major reference of comparison has been the utilization factor of the machines which is $110 \text{ kN}\cdot\text{m}/\text{m}^3$ for the proposed superconducting machine whereas that for reference machine has been $44.6 \text{ kN}\cdot\text{m}/\text{m}^3$.

The total loss in superconducting machine has not been calculated due to unavailability of actual AC losses in superconductors. Therefore, a tolerable limit of AC losses has been calculated using the losses incurred by the reference machine which is $0.82 \text{ mW}/\text{A}\cdot\text{m}$ at 20 K when a perpendicular AC field of 0.39 T is applied. Normalized AC losses lower than this value will make the superconducting machine to possess lower loss in comparison to reference machine.

Some measures to improve the power factor of superconducting machine by increasing the thickness of magnet have also been studied. It has been found that an increase by 20 mm of additional layer of magnet makes the proposed superconducting machine to have better power factor than the reference machine. Hence, the SC machine consumes less reactive power from the grid and needs a smaller power electronic converter in the system.

In this work, it has been put forth that permanent magnet synchronous generators with AC superconductors will make a system compact in size and weight provided AC superconductors with lower losses than aforementioned value are manufactured.

Preface

This Master's thesis work has been carried out at Norwegian University of Science and Technology (NTNU) in co-operation with SmartMotor AS, Trondheim. The work is basically focused on the possibility of application of superconductors in armature windings of permanent magnet machines. A MATLAB based SmartTool developed by SmartMotor AS has been used for optimization of geometrical parameters of the machines. The design has later on been checked for its magnetic characteristics in COMSOL.

In this report, Chapter 1 presents the general idea about the superconductors and its characteristics, applications and some information about the prototype equipment developed so far.

Chapter 2 describes about the permanent magnet synchronous generators and its application in wind power. This chapter also includes the description on superconductors in permanent magnet synchronous machines, AC losses associated with it and the cooling system employed in general for cryostat cooling.

Chapter 3 explains the design considerations of permanent magnet machines in brief. The importance of utilization factor of the machine and the impact of some important parameters like pole slot combination, current density and thickness of magnet has been explained in brief.

Chapter 4 covers the methodology employed and the selection of machine parameters for this thesis work. Some important results of the superconducting machines have been listed in this chapter.

Chapter 5 contains the discussion of this work and the comparison of several characteristics of the designed superconducting machine to the copper winding machine based on the results presented in Chapter 4.

Chapter 6 presents the conclusion of this work with a list of future work envisaged in this field.

Acknowledgement

I would like to express my sincere thanks to my supervisor, Prof. Arne Nysveen for providing an opportunity to study on a renowned topic of superconductor and for his ingenious ideas during the work.

I am grateful to my co-supervisor Stev E. Skaar for his continuous guidance throughout this work.

I would also thank to Alexy Matveev, SmartMotor AS, Trondheim for providing logistics required during this Master's thesis.

I am thankful to Niklas Magnusson, SINTEF Energy AS for sharing his experiences about research on superconductor and providing relevant ideas for my work in regular meetings.

I would like to extend my thanks to Dr. Roy Nilsen, Wärtsilä Norway AS for his help in coordinating with SmartMotor and SINTEF to carry out this project.

My thanks also go to Ravindra Ummaneni for his support in SmartTool and COMSOL works.

My regards extend to my friends whose company and discussions always helped me feel homely. Finally, I would recall my parents whose blessings were always encouraging me to move ahead towards my destiny.

Acronyms

AC	Alternating Current
BCS	Bardeen (B), Cooper (C), Schrieffer (S)
BSCCO-2212	$\text{Bi}_2\text{Sr}_2\text{CaCu}_2\text{O}_8$, Bismuth strontium calcium copper oxide
BSCCO-2223	$(\text{Bi, Pb})_2\text{Sr}_2\text{Ca}_2\text{Cu}_3\text{O}_{10}$
DC	Direct Current
FCL	Fault Current Limiters
FEA	Finite Element Analysis
HTS	High Temperature Superconductor
IGC	Intermagetics General Corporation
LHe	Liquid Helium
LN_2	Liquid Nitrogen
LNe	Liquid Neon
LTS	Low Temperature Superconductor
MAGLEV	Magnetic Levitation
MgB_2	Magnesium di-boride
MRI	Magnetic Resonance Imaging
OPIT	Oxide-powder-in-tube
PMSM	Permanent Magnet Synchronous Machine
SC	Super-conductor
SMES	Superconducting Magnetic Energy Storage
YBCO-123	$\text{YBa}_2\text{Cu}_3\text{O}_7$, Yttrium barium copper oxide

Table of contents

Problem description	i
Abstract	ii
Preface	iii
Acknowledgement	iv
Acronyms	v
Table of contents	vi
1 Introduction	1
1.1 Background	1
1.2 Research motivation.....	1
1.3 Superconductors in general.....	2
1.4 Characteristics of superconductors	3
1.5 Type I and type II superconductors	4
1.6 Applications of superconductors.....	5
1.6.1 Cables	6
1.6.2 Transformer.....	7
1.6.3 Motor and generators.....	7
2 Permanent magnet synchronous machines	9
2.1 General	9
2.2 PMSM in wind power	9
2.3 Application of superconductor in wind power generators	10
2.4 AC losses in superconductors	11
2.5 Limit of AC losses in Superconductor	13
2.6 Cooling technology of superconductors.....	14
3 Design considerations	17
3.1 General	17
3.2 Utilization factor	18
3.3 Impact of current increment	20
3.4 Effect of geometrical parameters.....	21
3.5 Pole slot combination	22

3.6	Air gap length selection	23
3.7	Magnet thickness.....	24
4	Methodology.....	25
4.1	General	25
4.2	Design tools	25
4.2.1	SmartTool	25
4.2.2	COMSOL.....	26
4.3	Reference machine	26
4.4	Modification in reference machine	27
4.5	Analysis with superconductor	30
4.5.1	Geometrical dimension of slot with Superconductor	30
4.5.2	Losses evaluation	32
4.6	Selection of geometrical parameters	32
4.6.1	Air gap length selection.....	32
4.6.2	Magnet thickness	32
4.6.3	Cooling systems arrangement.....	32
4.7	Results.....	33
4.7.1	Machine – 1 (176 pole/192 slot machine)	33
4.7.2	Machine – 2 (154 pole/168 slot machine)	35
4.7.3	Machine – 3 (132 pole/144 slot machine)	37
5	Discussion	41
5.1	General	41
5.2	Comparison of machines w.r.t. utilization factor	41
5.3	Comparison of machines w.r.t. weight.....	42
5.4	Comparison of machines w.r.t. volume.....	44
5.5	Comparison of machines w.r.t. power factor and terminal equipment	45
5.6	Comparison of machines w.r.t. magnetic saturation	46
5.7	Comparison of losses in the machines	48
5.8	Harmonics and cogging torque.....	50
5.8.1	Harmonics.....	50

5.8.2	Cogging torque	52
5.9	Selection of machine	52
5.10	Limit of AC loss in superconductor	55
5.11	Effect of increased thickness of magnet	59
6	Conclusion and future work.....	61
6.1	Conclusion	61
6.2	Future work	62
	References.....	63
	Appendices.....	67
Appendix A	Possible pole slot combinations	73
Appendix B	Specification of MgB2 superconductor	74
Appendix C	Derivation of power loss in slot	75
Appendix D	FEA results of reference machine	76
Appendix E	FEA results of Machine – 1 (176 pole 192 slots).....	88
Appendix F	FEA results of Machine – 2 (154 pole 168 slots).....	101
Appendix G	FEA results of Machine – 3 (132 pole 144 slots).....	113
Appendix H	FEA results of Machine – 1 (176 pole 192 slots with 50 mm magnet).....	125
Appendix I	FEA results of reference machine with segmentation of magnet	137

List of figures

- Figure 1.1: Characteristic of superconductor [1]. 2
- Figure 1.2: The origin of superconductivity in conventional superconductors [2]..... 3
- Figure 1.3: Superconductivity in a 3D space defined by current density, temperature, and magnetic field [5]. 4
- Figure 1.4: Perfect diamagnetic property of superconductor (Meissner effect) [7]. 4
- Figure 1.5: Characteristics of Type I superconductors [2]. 5
- Figure 1.6: Characteristic of Type II superconductor [2]..... 5
- Figure 2.1: Topology of direct driven wind power generation system..... 9
- Figure 2.2: Cost comparison of conventional and SC machine [17]. 10
- Figure 2.3: Cost comparison of current and future SC machine [17]. 10
- Figure 2.4: Schematic diagram of direct cooling system. 15
- Figure 3.1: Effect of current density factor on phase angle..... 21
- Figure 3.2: Phasor diagram of PMSM..... 21
- Figure 3.3 Phasor diagram of PMSM with increased current. 22
- Figure 3.4: Effect of number of pole/slot on yoke thickness. 23
- Figure 3.5: Phasor diagram after increment in magnet thickness. 24
- Figure 4.1: SmartTool simulation of reference machine 02/11/2010. 27
- Figure 4.2 COMSOL Simulation of 10 MW machine (yellow area indicates a magnetic flux density around 2 T). 28
- Figure 4.3: COMSOL simulation of redesigned reference machine. 28
- Figure 4.4: Slot configuration. 31
- Figure 4.5: Cross-section of superconductor [43]..... 31
- Figure 4.6: Optimized parameters for Machine - 1..... 34
- Figure 4.7: Optimized parameters for Machine - 2..... 36
- Figure 4.8: Optimized parameters for Machine - 3..... 38
- Figure 5.1: Weight of the active materials of machines. 43
- Figure 5.2: Torque to weight ratio of all machines. 43
- Figure 5.3: Power to weight ratio of all machines. 43
- Figure 5.4: Power density vs. torque density (logarithmic scale) [44]..... 44
- Figure 5.5: Outer volume of all machines. 45

Figure 5.6: Active and reactive capacity of all machines. 46

Figure 5.7: Comparison of magnetic saturation ($B=0$ to 1.7 T for all machines). 47

Figure 5.8: Effect of segmentation on magnet losses [47]. 49

Figure 5.9: Axial and circumferential segmentation of magnet [48]. 49

Figure 5.10: Induced losses in magnets of reference machine with and without segmentation. 50

Figure 5.11: Waveform and harmonic content of phase voltage of Machine - 1..... 51

Figure 5.12: Waveform and harmonic content of line voltage of Machine - 1. 51

Figure 5.13: Comparison of diameter and weight of all machines. 53

Figure 5.14: Comparison of Copper winding machine and SC winding machine. 53

Figure 5.15: Variation of flux density at the center of a slot. 57

Figure 5.16: Cross-section of a mono-filamentary wire [56]. 58

Figure 5.18: Effect on weight of magnet..... 60

Figure 5.19: Effect on reactive power due to magnet thickness. 60

List of tables

Table 1.1: Main driving forces for HTS applications in electrical power [11].	6
Table 1.2 Status of HTS prototype development worldwide [11].	6
Table 2.1: Magnetic loss per cycle of sample geometries [22].	12
Table 2.2: Equivalent losses in superconductor at different operating temperatures.	13
Table 3.1 Permitted flux densities of the magnetic circuit for various standard electrical machines [28].	18
Table 4.1: Reference parameters of the machine for the design process.	25
Table 4.2: Changes in parameters of reference machine after modification.	29
Table 4.3: Major parameters of Machine - 1.	33
Table 4.4: Major parameters of Machine - 2.	35
Table 4.5: Major parameters of Machine - 3.	37
Table 4.6: Summary of all parameters for all machines.	39
Table 5.1: Geometrical and electromagnetic parameters of the machines.	41
Table 5.2: Utilization factor of the machines based on mechanical torque and apparent power.	42
Table 5.3: Power and Torque related parameters of reference machine and SC machines.	42
Table 5.4: Reactive power comparison of all machines.	45
Table 5.5: Summary of losses in all machines.	48
Table 5.6: Losses in reference machine with and without segmentation of magnet.	49
Table 5.7: THD in phase and line voltage of all machines.	51
Table 5.8: Cogging torque and torque ripple of all machines.	52
Table 5.9: Map of the characteristics of superconducting machines.	54
Table 5.10: List of parameters changed with increase in thickness of magnet.	59

Chapter 1

1 Introduction

1.1 Background

The phenomenon of superconductivity was discovered in 1911 by Heike Kamerlingh Onnes and since then many metal and compounds have been introduced as superconductors. Some low temperature superconductors (LTS) have been used for long in commercial applications like Magnetic Resonance Imaging (MRI) but the high temperature superconductors (HTS), discovered in 1986, are yet to be commercialized. Several prototypes of electrical equipment using superconductors have been developed worldwide so far and have been tested.

Superconductors have been tested in electrical machines as a source of DC field. They incur significant AC losses when applied in presence of time varying magnetic field. The purpose of this thesis work is to study the possibility of the application of superconductor in AC armature winding.

A 10 MW wind turbine generator with copper winding has been taken as a reference machine and has been analyzed with superconducting armature windings. The objective is to design the generator compact in size and hence in weight which will help to keep the power per tower to be the same but with higher power to weight ratio. The AC losses associated with it have to be referred from the experimental results of measurement of AC losses being carried out at SINTEF.

1.2 Research motivation

The efficiency, weight and dimensions are the major governing parameters in design of AC electrical machines. The efficiency depends on the losses in the machines which includes losses in magnet, losses in stator and rotor yoke and most pronouncing in armature windings in case of a copper winding machine. The dimension of the machine is increased to extract the heat generated in the machine due to such losses. The capacity of cooling of a machine limits the magnitude of current in the armature windings. Since copper conductors bears finite resistance, it leads to generation of high amount of heat as the capacity of the machine increases. Therefore, the armature current i.e. the current density in the armature winding is controlled to a significantly lower value of about 4 A/mm² in these machines.

Superconductors exhibit zero resistance at its operating temperature and this special characteristic provides room for increased current density. The higher current density in armature helps to achieve a compact machine compared to copper winding machine of same power. An expression which is explained later in Chapter 3 can be mentioned to describe this case as follows:

$$S_i = K \cdot \bar{A} \cdot \hat{B}_{\delta l} \quad (1.1)$$

Where, S_i = Apparent power capacity of the machine

K = constant depending upon physical parameters of the machine

$\hat{B}_{\delta l}$ = Air-gap flux density (T)

\bar{A} = Linear current density (A/m)

Comparing to copper winding machine, if the air-gap flux density ($\hat{B}_{\delta l}$) of a machine is kept constant and the linear current density (\bar{A}) is increased using superconductor, the capacity of the machine can be increased to a higher value. Conversely, if the power has to be kept constant, the power density or torque density of the machine can be increased by increasing the same parameter and a compact machine can be achieved. This decrement in dimension will provide opportunity to increase the power to weight ratio for same power per tower of the wind turbine and consequently increases the economic benefit as well due to reduced weight.

1.3 Superconductors in general

Superconductors are capable of conducting electricity without any loss of energy under specified operating conditions. When current flows in an ordinary conductor, for example copper wire, some energy is lost. As shown in Figure 1.1, unlike the ordinary conductors, when a superconductor is cooled below its critical temperature (T_c), its resistivity abruptly disappears and exhibits zero resistance in the circuit.

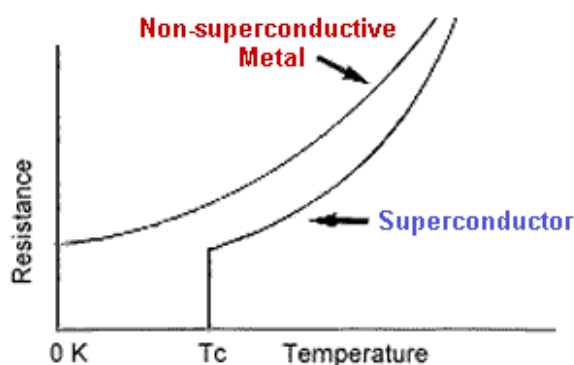


Figure 1.1: Characteristic of superconductor [1].

In metals such as copper and aluminum, electricity is conducted as outer energy level electrons share its electrons from one atom to another. These atoms form a vibrating lattice within the metal conductor due to some fixed ions; the warmer the metal the more it vibrates. As the electrons begin moving through the mess, they collide with tiny impurities or imperfections in the lattice. When the electrons collide into these obstacles they fly off in all directions and lose energy in the form of heat.

Inside a superconductor the behavior of electrons is completely different. The impurities and lattice are still there, but the movement of the superconducting electrons through the obstacle course is quite different. As the superconducting electrons travel through the conductor, they pass unobstructed through the complex lattice. Because they

do not collide into any obstacles like ion and impurities and create no friction, they can conduct electricity with no loss in the current and no loss of energy.

The understanding of superconductivity was first forwarded in 1957 by three American physicists – John Bardeen, Leon Cooper, and John Schrieffer, through their Theories of Superconductivity, known as the BCS theory. The BCS theory explains superconductivity at temperatures close to absolute zero i.e. for low temperature superconductors. According to Cooper, atomic lattice vibrations are directly responsible for unifying the entire current. They force the electrons to pair up into teams that pass all of the obstacles which cause resistance in the conductor. These teams of electrons are known as Cooper pairs. The electrons which normally repel one another, experience an overwhelming attraction in superconductors. According to the theory, as one negatively charged electron passes by positively charged ions in the lattice of the superconductor, the lattice distorts. This in turn causes phonons to be emitted which form a channel of positive charges around the electron [2]. Phonons are small deformations due to attraction between positively charged ion and electron. This distortion creates a highly positive area around electron and attracts another electron to come to same place to form a pair of electrons, known as Cooper pair [3].

Before the electron passes by and the lattice springs back to its normal position, a second electron is drawn into this channel as shown in Figure 1.2. It is through this process that two electrons, which should repel one another, link up. The forces exerted by the phonons overcome the electrons' natural repulsion. The electron pairs are coherent with one another as they pass through the conductor in unison. The electrons are screened by the phonons and are separated by some distance. It is this exchange that keeps the Cooper pairs together and continues it to be in superconducting state [4].

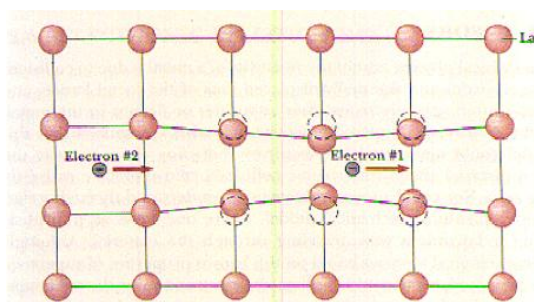


Figure 1.2: The origin of superconductivity in conventional superconductors [2].

1.4 Characteristics of superconductors

Superconductors hold its superconducting characteristics when operated under a regime bounded by three inter-related matters, current density, operating temperature, and magnetic field as shown in Figure 1.3. The highest temperature at which a material possesses no electrical resistivity is called its critical temperature (T_c). The upper limit of its current carrying capability is called the critical current density (J_c) and critical magnetic field (H_c) is that above which it ceases to be a superconductor. The superconductor reverts to its normal state if any of these limits exceed.

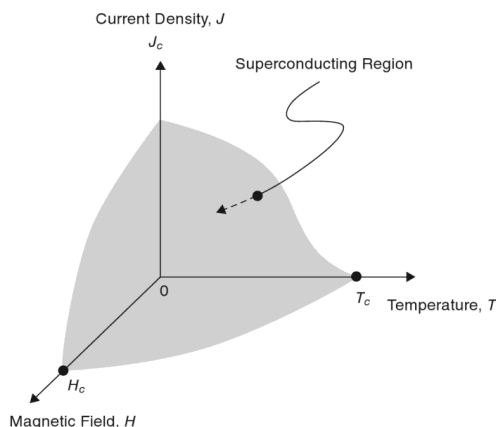


Figure 1.3: Superconductivity in a 3D space defined by current density, temperature, and magnetic field [5].

In addition, the superconducting characteristic also follows Meissner effect, discovered in 1933 by Walther Meissner and Robert Ochsenfeld. According to this, a superconductor exhibit perfect diamagnetic property (susceptibility is -1) i.e. there is no magnetic field inside the superconducting material. The property remains valid when the applied field is weak, that is below the critical magnetic field (H_c) and it is cooled below its critical temperature (T_c) [6]. It happens due to setting up of electric currents near its surface. The magnetic field set up by these surface currents cancels the applied magnetic field within the bulk of the superconductor.

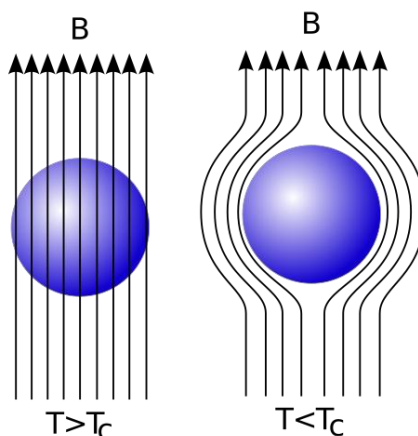


Figure 1.4: Perfect diamagnetic property of superconductor (Meissner effect) [7].

1.5 Type I and type II superconductors

After long time of the discovery of superconductors, few compounds were discovered to exhibit mixed characteristics beyond its critical magnetic field (H_c) and were named type II superconductors.

Type I superconductors completely follows the Meissner effect i.e. expels the magnetic field and remains superconductor below its critical magnetic field of H_c and critical operating temperature of T_c as shown in Figure 1.5 [2]. Type I superconductors are well described by the BCS theory. These types of superconductors have been of limited practical usefulness because the critical magnetic fields are very small and the superconducting state disappears suddenly at that temperature [8].

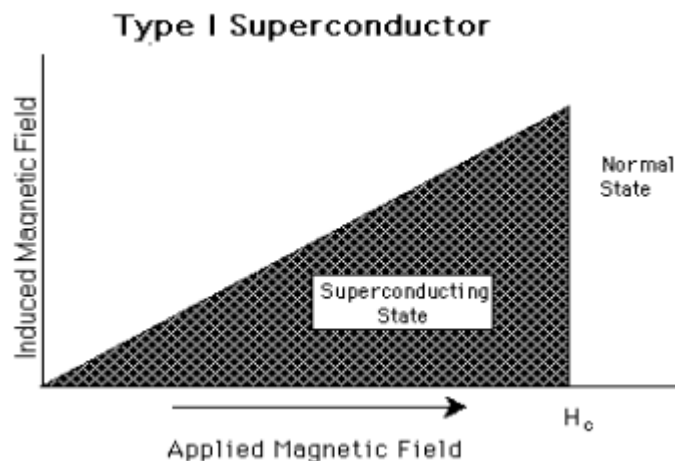


Figure 1.5: Characteristics of Type I superconductors [2].

Type II superconductors are characterized by two critical fields. As shown in Figure 1.6, below the lower critical field H_{c1} , applied magnetic field is completely excluded from the conductor by the surface currents on the thin layer of the superconductor [9]. At fields between H_{c1} and H_{c2} , the field begins to penetrate into the material. The occurrence of this state is said to be mixed state, with some of the material in normal state and part still superconducting [2]. These types of superconductors have been found to have much higher critical fields and therefore could carry much higher current densities while remaining in the superconducting state. All the high temperature superconductors (HTSs) fall under this category.

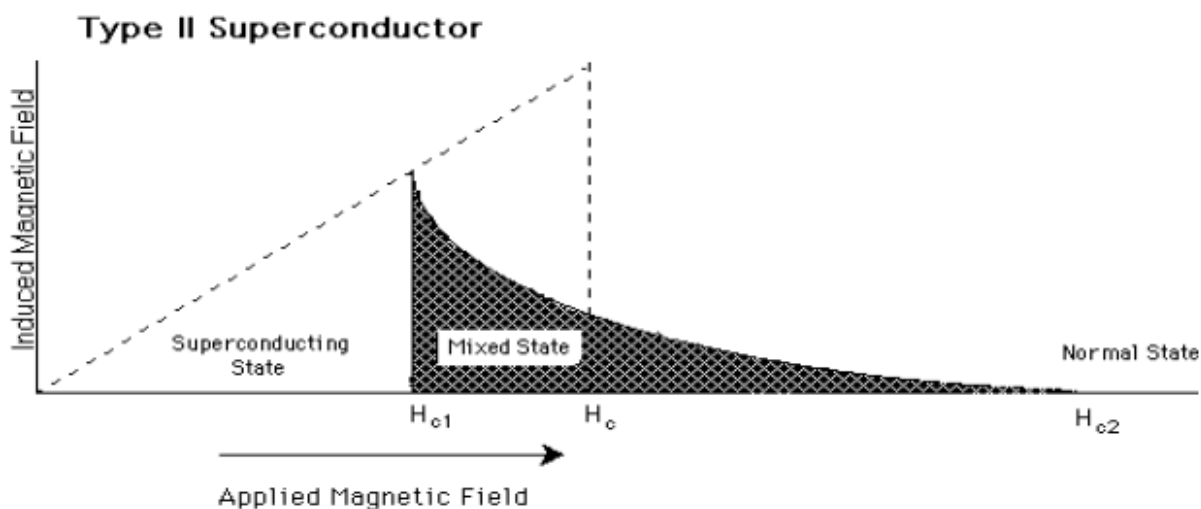


Figure 1.6: Characteristic of Type II superconductor [2].

1.6 Applications of superconductors

Among the two types of Superconductors, low temperature superconductors (LTS) are being used commercially for magnet market. That market consisted magnetic resonance imaging (MRI) and nuclear magnetic resonance (NMR), and magnets for high-energy physics accelerators and plasma fusion devices, together with smaller niches for research magnets for several years. LTS are still in use in MRIs [10].

High temperature superconductors (HTS) represents a new class of conductor with unique properties, which would not only allow electric power devices to be more compact but also enable new applications as shown in Table 1.1.

Table 1.1: Main driving forces for HTS applications in electrical power [11].

Benefits	Property	Applications	Conductor
Higher Efficiency	$R = 0$	Motors, Generators, Cables, Transformers	Wire
Higher power density	j_c	Motors, Generators, Cables, Transformers	Wire
Novel opportunities	$R = 0$	SMES	Wire
	$dm/dB < 0$	Magnetic bearings	Bulk
	Transition	Current limiters, Switches	Wire & sheet

1.6.1 Cables

HTS cables are expected to have high current carrying capability, which can be alternative for replacement of existing underground cables to increase transmission capacity in the same duct. HTS cables can be loaded with very high current with almost no loss and, thus, design with lower voltage levels can be possible. Various cable prototypes have been demonstrated, all exclusively based on Ag-sheathed Bi-2223. Among them, Southwire cable (Table 1.2) was energized during summer 2000. So far, cooling system represents a serious challenge [11].

Table 1.2 Status of HTS prototype development worldwide [11].

Application	HTS (Supplier)	Company	Prototype development
Current Limiter	Bi2212-bulk (ABB)	ABB	6.4 MVA, tested
	YBCO-film (Siemens)	Siemens	1.2 MVA, tested
Cable	Bi2223-PIT (ASC)	Pirelli	24 kV – 2.4 kA, 120 m
	Bi2223-PIT (SEI)	SEI/TEPCO	66 kV – 1 kA, 100 m, tested
	Bi2223-PIT (IGC)	Southwire	12.5 kV – 1.25 kA, 33m, tested
	Bi2223-PIT (ASC)	NKT	36 kV – 2 kA, 30 m, tested
Transformer	Bi2223-PIT (ASC)	ABB	0.63 MVA, tested
	Bi2223-PIT (VAC)	Siemens	1 MVA (traction), tested
Motor	Bi2223-PIT (ASC)	ASC	5000 PS, tested
Flywheel	YBCO Bulk	Mitsubishi	1.4 kWh, tested

1.6.2 Transformer

The application of HTS in transformers provides the potential of reduction (compared to conventional) in losses (<30%), volume (~ 50 %), and weight (~ 70 %). Furthermore, it offers over-load ability without accelerated aging and possible integration of a fault current limitation function.

In addition, benefits come from reducing the short-circuit current in the system and lower transformer impedance. The superconducting wire has current-limiting capability. This can reduce the interrupting ratings of circuit breakers. The lower transformer impedance will improve voltage regulation and stability and increase real and reactive power availability to the power system [12].

Presently, the main obstacle remains strong J_c reduction in magnetic fields and high AC-losses at coil ends. The feasibility of such HTS transformers has been demonstrated by ABB's 3-phase 630 kVA (20 kV/0.42 kV) prototype, which was operated in an electric grid for 1 year. In a pre-study on a 10 MVA prototype, it was concluded that fault current limitation integration is feasible, even with fast recovery to operation. Waukesha, together with IGC (Intermagnetics General Corp.) as wire supplier and Oak Ridge National Lab has tested a 1-phase 1 MVA (13.8/6.9 kV) device, with a next prototype (5-10 MVA) under development. Siemens has also completed a 1 MVA model for traction applications, which is cooled to 66 K to enhance the wire performance [11]. If the issues like cryogenic insulation, high voltage termination, and cryo-cooler refrigeration optimization can be addressed, there is good scope of commercializing a high MVA transformer [12].

1.6.3 Motor and generators

Superconducting motors and generators have several potential advantages. They can be power-dense, light weight, small volume, highly efficient, and reliable [12].

The potential benefits of a HTS motor are similar to that of HTS transformer. A viable synchronous machine can be with a superconducting rotor consisting of Bi – HTS based windings. An all-superconducting machine where the armature winding is also superconducting, is not viable with the current Bi-based tapes because of the high AC-losses (caused by AC-currents in the armature winding). The main challenges are the low J_c of Bi-wires in magnetic fields and high conductor costs. A 5000 hp synchronous machine (6.6 kV, 1800 rpm, volume 7.5 m³) has been reported with an efficiency of 97.2 %. Siemens has also tested a 400 kW prototype [11].

Several motor and generator system have been demonstrated using MgB₂ superconductor. One design is the superconducting homopolar motor being developed for the Navy; the present design uses NbTi superconductors operating at 4 K. MgB₂ offers the potential of higher power densities, high temperature margins, and lighter weight coils for these superconducting homopolar motors. Other superconducting motor systems have been demonstrated using liquid neon and helium gas operating in the 20 – 30 K range; MgB₂ superconducting coils have generated magnetic fields in the 0.5 – 2.0 T field range at these

temperatures. Presently, Hypertech is building MgB_2 superconducting rotor coils for a cryogenic 2 MW generator demonstration for NASA that will be cooled with liquid hydrogen at 20 K [12].

The other applications of superconductors cover fault current limiter (FCL), magnetic resonance imaging (MRI) and powerful magnets for several purposes. Magnetic-levitation is an application where superconductors perform extremely well. A landmark for the commercial use of MAGLEV technology exists in Japan which was built in cooperation with national fund project in 1990.

Power utilities have also begun to use superconductor-based transformers and fault limiters. The Swiss-Swedish company ABB has already demonstrated the first superconducting transformer to a utility power network in March of 1997. ABB has also recently announced the development of a 6.4 MVA fault current limiter. This new generation of HTS superconducting fault limiters is being called upon due to their ability to respond in just milliseconds to limit tens of kilo-amperes of current [13].

Chapter 2

2 Permanent magnet synchronous machines

2.1 General

Since the development of alternating current, AC machines have been widely found desirable for any kind of applications. Two most common types of rotating AC machines are induction (asynchronous) and synchronous machines. A synchronous machine has two windings: an AC armature winding located in the stator and a field (DC) winding located on the rotor. Rotating machines (motors and generators) employ copper windings on rotor and stator. In some kind of machines like PMSM, permanent magnet is used as a source of field.

2.2 PMSM in wind power

In hydro and turbo applications, generators run at constant speed and it is important to maintain the output voltage and the reactive power demand in the system by controlling the excitation current. Therefore, these systems employ wound rotor synchronous generator. In the past, when constant speed (with gear between turbine and generator) generators were being used for wind power application, the same type of generators were being preferred. But in recent days, direct driven generators (without gear) are predominant in use since such system has some favorable features like reduced losses in the drive system and less noise than the system with mechanical gear [14]. PM excited synchronous machines avoids the field current supply from secondary source as needed by the wound-rotor generators but on the other hand, lacks the reactive power compensation facilities. The terminal voltage of such system is controlled by the power electronic converter connected to the generator output terminals, therefore, the control of generator voltage is not critical and constant excitation i.e. permanent magnet machine has become highly preferable for this purpose.

The PMSM is compact in comparison to wound rotor machine since it avoids the bulkiness of external excitation system. In wind power application, direct driven PMSM needs to generate very high torque because of its very low speed compared to the same rated power of conventional constant speed machines. Because of this high requirement of torque at low speed, it is usually designed with large diameters and consequently it becomes heavier. To decrease the weight of the rotor and stator yokes and to keep the end-winding losses small, direct driven PMSM are usually designed with concentrated winding and with a small pole pitch [15].

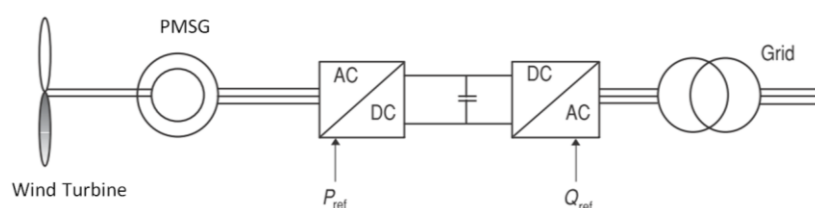


Figure 2.1: Topology of direct driven wind power generation system.

A general topology of the combination of all equipment of a wind power is shown in Figure 2.1. The generated power of the PMSM is fed to the two stage power converter and the controlled output is fed to the grid via power transformer.

2.3 Application of superconductor in wind power generators

In the AC machines, current in the windings create resistive losses, which leads to incur significant loss of energy. The heat generated due to this loss also enforces to make the machine larger in size to provide additional cooling. Thus, any efficiency improvement is likely to yield significant savings in energy and resources. Superconductors offer zero resistance to electrical current, thus the use of it eliminates any resistive loss in the machine as well as produces a reduced size and weight of the machine. In other terms, it can ease to achieve higher power from the same machine that uses copper windings. The discovery of HTSs in 1986 has provided the further flexibility to develop a variety of rotating machines employing superconducting windings. HTS motors are ideal for use in pumps, fans, compressors, blowers, and belt drives deployed in utility and industrial applications, particularly for those requiring continuous operation. Such motors are also suitable for large process industries such as steel milling, pulp and paper processing, chemical, oil and gas refining, mining and other heavy-duty applications [16].

In recent days, the requirement of high power wind turbine is being shouted as alternative of novel source of renewable energy. The study shows that application of high temperature superconductors (HTS) in wind power generators can be economical and can lead to lighter weight of the system for high power machines. As presented in Figure 2.2, the wind power generator above 8 MW seems to be cost effective with the application of superconductor in field windings. The superconducting technology is still to become a matured technology and the break-even point for application of superconductor in wind power application may come down to 3 – 4 MW as predicted in Figure 2.3.

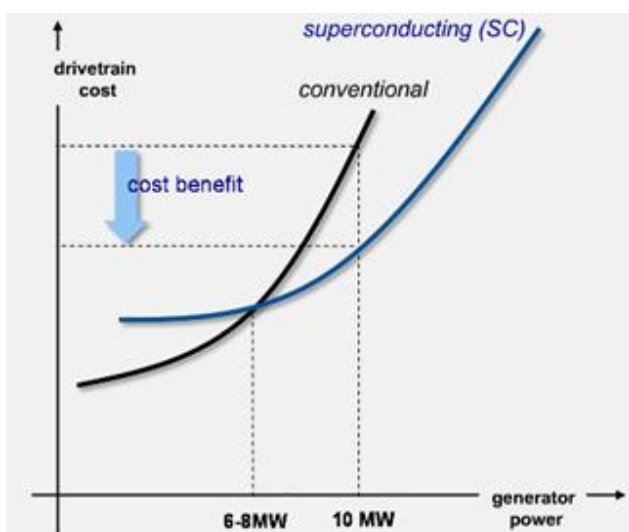


Figure 2.2: Cost comparison of conventional and SC machine [17].

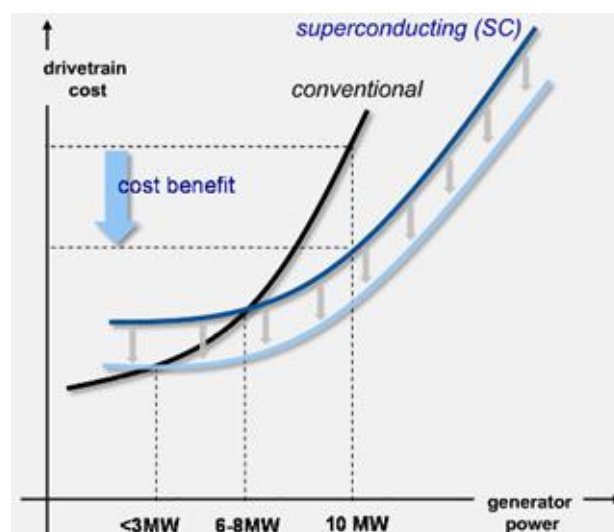


Figure 2.3: Cost comparison of current and future SC machine [17].

Although several characteristics of superconductor is superior to conventional machines with copper winding, the ac losses in superconductor due to time varying magnetic field is restricting its use only as a field winding. When it is used as field winding, the rotation of SC on the rotor experiences a constant and virtually static field due to the same rotational speed of the rotor and the magnetic field produced by the stator current and thereby it eludes from ac losses. But its application in armature winding in stator faces varying magnetic field and leads to undesirable ac losses [18].

2.4 AC losses in superconductors

A superconductor offers zero electrical resistance in its superconducting state and causes no losses. However, it remains valid when the superconductor is not exposed to magnetic fields above its lower critical field H_{c1} . If the applied magnetic field (H) exceeds H_{c1} , which is usually the case, the superconductor no longer remains lossless [19]. It is therefore, obvious for high temperature superconductors (HTS) to incur AC losses.

The magnetic field can be externally applied or generated by a transport current. The magnitude of the losses depends, for a given conductor, on the operating temperature (T), the magnetic field (B), the transport current (I) and the frequency (f) [20].

$$P_{ac} = P_{ac}(T, B, I, f) \quad (2.1)$$

The total AC loss in a superconductor consists of magnetization and transport-current losses. The magnetization loss in a time varying external magnetic field is due to hysteresis and coupling currents. Screening currents inside the superconducting filaments cause hysteresis loss. A decrease in the filament dimensions reduces the hysteresis loss [9].

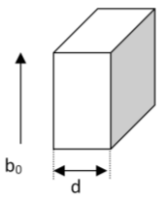
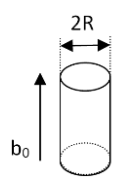
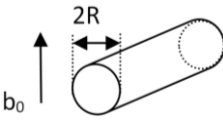
A transport current in a superconductor generates a magnetic field around the conductor, which is called the self-field. With an alternating transport current, the alternating self-field penetrates the superconductor during each current cycle. Even if there is no external magnetic field, the variation of the self-field inside the material causes a hysteresis loss, which is called self-field loss [21]. For a circular or elliptical wire, self-field losses (Q_t) per unit volume per cycle are given by:

$$Q_t = \frac{\mu_0 I_c^2}{\pi} \left[(1 - i) \cdot \ln(1 - i) + \frac{(2 - i)i}{2} \right] \quad (2.2)$$

Where, $i = I_0/I_c$ and I_0 = transport current and I_c = critical current of the superconductor. At the critical current, the loss per cycle per unit length for an elliptical wire with a critical current I_c is $0.16\mu_0 I_c^2$ [22].

The hysteresis loss is influenced by the geometry of the superconductor, the direction of the applied magnetic field (b_0) and the penetration depth (b_p)¹. Smaller the cross-section of superconductors, lesser is the hysteresis losses. The loss equation for tape shaped and cylindrical shaped conductors in parallel field as calculated by Bean [24] can be depicted as in Table 2.1.

Table 2.1: Magnetic loss per cycle of sample geometries [22].

Sample geometry	Magnetic loss per unit volume per cycle Q_h (J/m ³)		Penetration depth (b_p)
	$\frac{2b_0^2}{3\mu_0}\beta$	$\beta < 1$	$\frac{\mu_0 J_c d}{2}$
	$\frac{2b_0^2}{\mu_0} \left(1 - \frac{2}{3}\beta\right)$	$\beta > 1$	
	$\frac{2b_0^2}{3\mu_0}\beta(2 - \beta)$	$\beta < 1$	$\mu_0 J_c R$
	$\frac{2b_0^2}{3\mu_0} \frac{(2 - \beta^{-1})}{\beta}$	$\beta > 1$	
	$\frac{4b_0^2}{3\mu_0}\beta(2 - \beta)$	$\beta < 1$	$\frac{2\mu_0 J_c R}{\pi}$
	$\frac{4b_0^2}{3\mu_0} \frac{(2 - \beta^{-1})}{\beta}$	$\beta > 1$	

In the Table 2.1, $\beta = \frac{b_0}{b_p}$ denotes the level of penetration of field in the superconductor.

The AC losses in Superconductor mentioned in above equations are approximately proportional to the operating frequency. The total AC losses per unit length, P_{ac} in W/m is given by

$$P_{ac} = f \cdot C_f \cdot A \cdot Q \quad (2.3)$$

Where C_f is a dimensionless fitting parameter, A is the cross-section area of the shape and Q is the total loss per unit volume per cycle i.e. sum of all losses [20].

¹ **Penetration depth** is the distance to which a magnetic field penetrates into a superconductor and becomes equal to $1/e$ times that of the magnetic field at the surface of the superconductor [23] C. Kittel, "Introduction To Solid State Physics," ed: John Wiley & Sons, 2005, pp. 273-278.

2.5 Limit of AC losses in Superconductor

The alternating magnetic field in these devices causes energy dissipation (AC loss) despite the zero resistance of the superconductor in stationary circumstances. The dissipated heat must be removed from the low-temperature environment by a refrigerator, whose power consumption is 10s of times the AC loss. To remove these losses, a cooling device has to be used, the capacity of which depends on the value of cooling penalty factor. The cooling penalty factor (η_{cp}) is determined by the Carnot factor (η_{carnot}) and the efficiency of the cooling device ($\eta_{cooling}$).

$$\eta_{cp} = \eta_{carnot} \cdot \frac{1}{\eta_{cooling}} \quad (2.4)$$

where the Carnot factor is the number of Watts needed in an ideal cooling machine to remove one Watt at low temperature:

$$\eta_{carnot} = \frac{T_{amb} - T_{low}}{T_{low}} \quad (2.5)$$

T_{amb} is the ambient temperature and T_{low} is the operating temperature of the superconductor [20].

Comparing the losses of different HTSs or between HTSs and conventional conductors (copper or aluminium), the losses per unit carried current and unit length (P_{Am}) in W/A·m is a relevant figure of measurement. Also, when comparing the losses at different operating temperatures, the cooling penalty factor (the number of Watts needed in a cooling device to remove one Watt dissipated at the operating temperature of the HTS) has to be taken into account. A conventional, oil filled, transformer has typically a current density of 2-4 A/mm². This current density and the resistivity of copper $\rho_{cu} = 2 \times 10^{-8} \Omega\text{m}$ (at operating temperature, 80°C) yield $P_{ac} = J_{cu} \cdot \rho_{cu} = 40 - 80 \times 10^{-3} \text{ W/A}\cdot\text{m}$ in its copper windings. At 77 K, the cooling penalty factor is about 10, and hence an HTS operating at this temperature with losses of 4 – 8 mW/A·m has equally high losses as the copper conductor. To limit the losses to only 10% of the corresponding losses in copper, losses of the order of 0.4 – 0.8 mW/A·m can be tolerated. Therefore, for power-engineering applications around 77 K the maximum permissible AC loss is approximately 0.5 mW/A·m at operating conditions [9].

The equivalent losses at different temperatures using eq. (2.4) and (2.5) is presented as in Table 2.2.

Table 2.2: Equivalent losses in superconductor at different operating temperatures.

Type of conductor	Operating temperature	Penalty factor	Tolerable losses
Copper conductor	80 °C (353 K)	-	40 – 80 mW/A·m
Superconductor	77 K	10	4 – 8 mW/A·m
Superconductor	45 K	20	2 – 4 mW/A·m
Superconductor	4.2 K	240	0.17 – 0.33 mW/A·m

As shown in Table 2.2, at low temperatures, the cooling penalty factor is much higher (about 240 at 4.2 K), and although there exist good conductors operating in the liquid helium range, the high cooling penalty factor makes them uneconomical for the use in AC electric power applications [25].

In AC applications, AC losses in HTS are proportional to the square of the conductor dimension perpendicular to the surrounding magnetic field, i.e. the thickness for a planar conductor. Multifilament Bi-2223/Ag composites with close twist pitch have much reduced AC losses. Bi-2223 wire in magnetic field with round and square cross-section with reasonable AC-losses (0.53 mW/A·m) has already been demonstrated [11].

2.6 Cooling technology of superconductors

All known superconductors must operate at cryogenic temperatures between 4 and 80 K. The technology of creating such low temperatures is quite complex and it needs quite sophisticated cooling equipment called refrigerators or cryo-coolers. Cryo-coolers cool down the superconductors or superconducting magnets from ambient temperature (300K) to 30 K or even 4 K for LTS coils.

Mostly five cryogenic fluids Helium (He), Hydrogen (H₂), Neon (Ne), Nitrogen (N₂) and Oxygen (O₂) are considered for cryo-cooling. Of these fluids, H₂ and O₂ are not preferred due to the fire hazard associated with them. Since LTS superconductors niobium-titanium (Nb-Ti) and niobium-tin (Nb₃Sn) require operation at close to 4 K, liquid He (LHe) is the only viable choice for LTS. Almost all LTS superconductors employ LHe as coolant. However, HTS superconductors (BSCCO-2223 and YBCO-123) can operate at LN₂ temperature (77 K) for low-field applications and at LNe temperature (27 K) for high-field applications.

i. Direct cooling with cryogens

Low temperature superconductor (LTS) magnets employing NbTi and Nb₃Sn superconductors are generally cooled by submerging them in LHe. Since the NbTi conductor is bathed in LHe, any heat generated in the conductor is transferred to the liquid coolant. This heat load is absorbed by converting LHe into gaseous He (GHe) using the latent heat of vaporization. In these magnets, superconductors remain in the superconducting state as long as the heat flux (heat per unit area) available at the conductor surface is less than what the LHe can remove; this limit is called the critical heat flux. Once the critical heat flux is exceeded, the superconductor temperature begins to rise, and eventually the superconductor transitions to its normal state when its temperature exceeds its critical temperature (T_c) [5].

As displayed in Figure 2.4, high pressure tubes carrying liquid Helium or liquid Neon depending upon the operating temperature of the superconducting wire used are employed inside the slot surrounded by the armature conductors. The pressurized tubes consist several orifices and sprays the cold coolant to the conductors to keep it below the critical temperature [26].

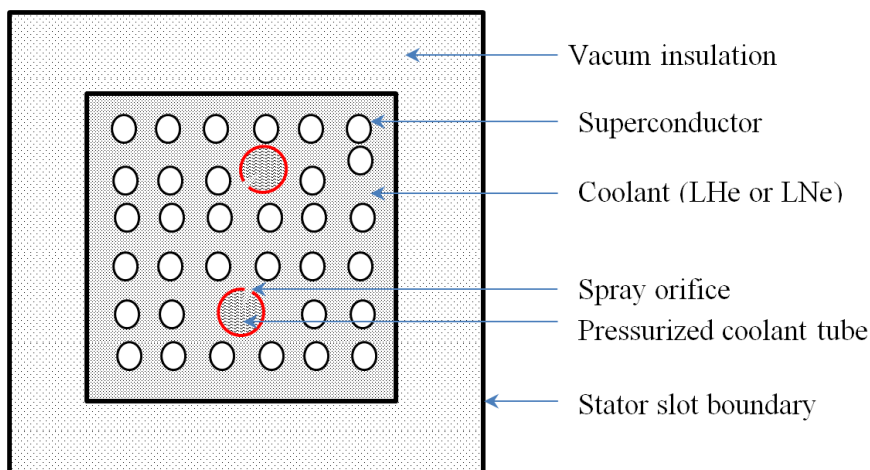


Figure 2.4: Schematic diagram of direct cooling system.

ii. Indirect or conduction cooling

High field application magnets and coils are operated using convenient conduction cooling with cryo-cooler refrigerators. Superconducting coils are epoxy impregnated to create monolithic structures that are mechanically strong and easy to handle. Such coils are cooled from their outside surface by conduction. Cooling schemes are generally carried out by implementing good thermal contact between HTS coils and (1) tubes carrying coolant and (2) directly by a cryo-cooler refrigerator cooler. The coolant in the cooling tubes could be a cold gas or a liquid cryogen. The coolant operates in a closed cycle, rejecting its heat load outside the magnet system in a refrigerator or other equivalent cooler. The coolant could also be a cryogen taken from a storage container. In addition a cryo-cooler refrigerator is thermally interfaced to an HTS coil being cooled [5].

Referring to the same Figure 2.4 of direct cooling system, pressurized coolant tubes can carry vapor He or Ne and the slot can be filled with liquid He or Ne. The heat generated in the armature can be extracted by LHe or LNe and the heat in the coolant can be transferred to vapor tube.

The AC superconducting coils in armature winding of wind generator may employ direct or indirect cooling scheme depending upon the number of turns in the slot and it will also rely on the cost of the cooling system for a particular application. The cryo-cooler can be accommodated in the nacelle of the wind turbine beside the generating unit. The additional weight of cryo-cooler in the nacelle is compensated by the reduction in the weight of the generator by the use of superconductors which provides an overall reduced weight on the tower than in case of copper winding machine.

This page is intentionally left blank.

Chapter 3

3 Design considerations

3.1 General

The design of a generator is a complex challenge where getting the highest performance for the least costs is desirable [27]. Machine design is an iterative process and can be commenced by defining certain basic characteristics. Some important basic parameters are pointed out as:

- Machine type (Synchronous, asynchronous, DC, reluctance machine, etc.)
- Type of construction (external pole, internal pole, axial flux, radial flux, etc.)
- Rated mechanical power
- Rated rotational speed
- Rated voltage
- Number of phases
- Number of pole pairs (p) of the machine (with frequency drives, this is also a subject of optimization)
- Economic boundary conditions

Besides these parameters, there are several other parameters which are optimized during the design process. During optimization, there used to be some free parameters which are kept almost constant during the design process to simplify the task. The following parameters can be selected as the free parameters:

- Outer diameter of the stator
- Length of the stator stack
- Width of the stator slot
- Depth of the stator slot
- Diameter of the air gap
- Air-gap length
- Peak value of air gap flux density
- Magnet thickness (in case of PM machine)
- Pole pair number and frequency

In electrical machine design, there are certain empirically defined ranges of flux densities which are applied in the preliminary phase of the design. Table 3.1 presents the values of electromagnetic loading for standard electrical machines [28].

Starting from these basics, the machine is optimized according to the specific requirements. In practical cases, the rotor and stator may be stressed to higher values than in the Table 3.1 to achieve higher torque density.

Table 3.1 Permitted flux densities of the magnetic circuit for various standard electrical machines [28].

Machine parts	Peak flux density (B) in Tesla	
	Salient pole Synchronous machines	Non-salient pole synchronous machines
Air gap	0.85 – 1.05	0.8 – 1.05
Stator yoke	1.0 – 1.5	1.5 – 2.0
Tooth	1.6 – 2.0	1.5 – 2.0
Rotor yoke	1.0 – 1.5	1.3 – 1.6

There are also some key indicators that guide the optimization process during the design of AC machines.

3.2 Utilization factor

An important rule within generator design is the relationship between mechanical power P_m , torque T , rotational speed in radians per second ω , air-gap rotor diameter D_i and axial rotor length L_i stated in terms of two equations [27].

$$P_m = \omega T \quad (3.1)$$

$$T = k \cdot D_i^2 \cdot L_i \quad (3.2)$$

where k is constant. The equations show that the torque is proportional to square of diameter and the power is proportional to the torque, hence a large diameter at which torque is generated will produce more power. A direct-drive generator for wind turbines is operated at low rotational speed and the rotor is directly mechanically connected to the rotor hub, which results in a large diameter to produce higher torque. The consequences are heavy mass and high costs. At a low rotational speed, an increased number of poles in the rotor are required to produce a reasonable frequency and a higher force. The frequency (f_e) is determined by number of poles (P) and the rotational speed (n_m) per minute [27].

$$f_e = \frac{n_m P}{120} \quad (3.3)$$

An increased number of poles are beneficial up to a certain point where core losses and magnetic leakage flux will influence the machine performance. As stated, the machine geometry and energy density can be optimized to find the best possible solution for a desired generator design. PM machines have a higher power to weight ratio compared to electrically excited machines. No additional power supply for field excitation gives higher reliability without slip rings and improved efficiency [29]. PM has been considered to be superior for direct drive generators in this work as a compact solution is desirable.

For the sizing of electrical machines, i.e. for determining their main dimensions and for comparing the stress limits of their electromagnetically active materials as well, the

utilization factor (C) has been proved to be suitable up to now [30]. It is defined as the torque corresponding to the apparent power (S_i) referred to the air-gap bore volume (V_{bore}):

$$C = \frac{S_i}{2\pi n_m V_{bore}} \quad (3.4)$$

where the air gap volume is defined as

$$V_{bore} = \frac{\pi D_i^2}{4} L_i \quad (3.5)$$

According to eq. (3.4), the quantity C consists electromagnetically of the thermally effective current coverage (a quantity referred to bore circumference πD_i), also known as linear current density or current loading (\bar{A}) given by

$$\bar{A} = \frac{2mN_s I_s}{\pi D_i} \quad (3.6)$$

where m is the number of phases, N_s is the number of turns in a coil and I_s is the rms phase current of the machine.

The air-gap emf can be expressed as

$$U_s = \frac{1}{\sqrt{2}} \omega N_s K_{ws1} \hat{\Phi}_l \quad (3.7)$$

where K_{ws1} is the winding factor and the air-gap flux density ($\hat{B}_{\delta l}$) (a quantity referred to pole unit area) is related to pole pitch (τ_p) and air-gap flux ($\hat{\Phi}_l$) as:

$$\hat{B}_{\delta l} = \frac{\pi \hat{\Phi}_l}{2\tau_p L_i} \quad (3.8)$$

The angular speed ω can be expressed in rpm as

$$\omega = 2\pi f_e \quad (3.9)$$

The apparent power of the machine in eq. (3.4) can be re-written in terms of I_s and U_s as

$$S_i = m U_s I_s \quad (3.10)$$

Substituting U_s and I_s from eq. (3.6), (3.7), (3.8) and (3.9),

$$S_i = \frac{\pi^2}{\sqrt{2}} \frac{n_m}{60} K_{ws1} \bar{A} \hat{B}_{\delta l} D_i^2 L_i \quad (3.11)$$

For fixed dimensions, the apparent power can be expressed as

$$S_i = K \cdot \bar{A} \cdot \hat{B}_{\delta l} \quad (3.12)$$

Where, K is a constant depending upon the rotational speed and geometry of the machine.

In electrical terms, for a fixed geometry of machine, the output power can be controlled varying the linear current density (\bar{A}) or the air gap flux density ($\hat{B}_{\delta l}$) or both [28].

Conventional machine design technology limits the torque density, described by the utilization factor $C = T/V$ with torque T and machine volume V , to a value of approximately 10 KN/m^3 for air-cooled permanent magnet synchronous motors. The magnitude results from a maximum Lorentz force product – air gap flux density ($\hat{B}_{\delta l}$) times linear stator current (\bar{A}). The achievable flux density deeply depends on the material and configuration of the magnets. However, another great influence is exerted by the magnetization curve of the soft magnetic material and the width of flux conducting section as teeth and yoke [31].

3.3 Impact of current increment

The main purpose of using superconductor in a machine is to increase the current density in the windings and to reduce the physical dimensions. The current density in a superconductor can be increased to its critical limit but it has implications to synchronous reactance and power factor. The analytical description of the impact of current to power factor can be derived as follows.

Let Machine – 1 has a terminal voltage of U_{N1} and is operating at a rated current of I_{s1} , then its rated apparent power will be,

$$S_{n1} = \sqrt{3}U_{n1}I_{s1} \quad (3.13)$$

And, the base impedance will be,

$$X_{1,base} = \frac{U_{n1}^2}{S_{n1}} \quad (3.14)$$

Similarly, for Machine – 2 of same design and geometrical dimensions, if the current rating of the machine is increased by a factor k ,

$$S_{n2} = \sqrt{3}U_{n1}I_{s2} = \sqrt{3}kU_{n1}I_{s1} = k \cdot S_{n1} \quad (3.15)$$

$$X_{2,base} = \frac{U_{n1}^2}{S_{n2}} = \frac{U_{n1}^2}{k \cdot S_{n1}} = \frac{X_{1,base}}{k}$$

The base impedance of the second machine is less than that of first machine. Since the phase inductance of a machine depends upon the geometrical parameters, decrement in base impedance increases the per unit value of synchronous reactance of the machine.

The same expression in terms of power factor can be written as:

$$\cos\phi_1 = \frac{P_1}{S_{n1}} \quad (3.16)$$

And,

$$\cos\phi_2 = \frac{P_2}{S_{n2}} \quad (3.17)$$

From, eq. (3.15), (3.16) and (3.17), if the active power P_1 and P_2 are same; the new power factor will be less by a factor of k .

$$\cos\phi_2 = \frac{\cos\phi_1}{k} \quad (3.18)$$

Graphically, the variation in phase angle has been as elucidated in Figure 3.1.

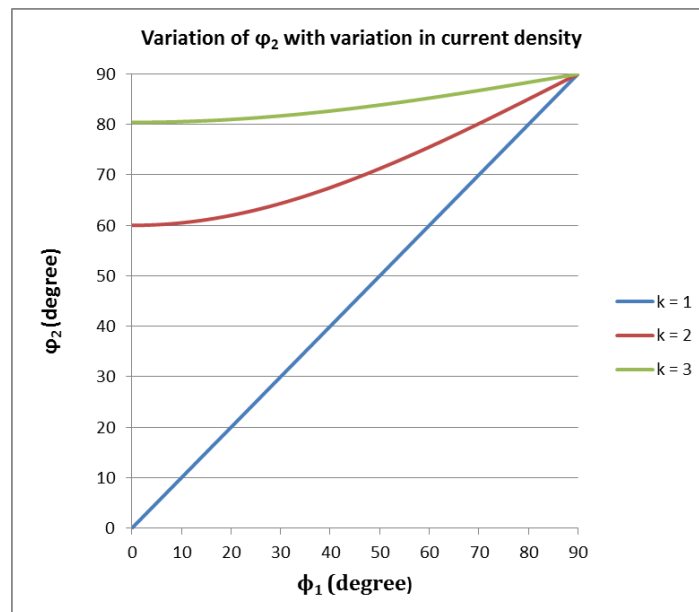


Figure 3.1: Effect of current density factor on phase angle.

This has also been justified with phasor diagram later in Section 3.4 and Figure 3.2.

3.4 Effect of geometrical parameters

The most important characteristics of a machine depend upon the geometry of the machine. As stated in Section 3.2, the output power, torque, synchronous reactance and no-load losses vary with the size of the machine.

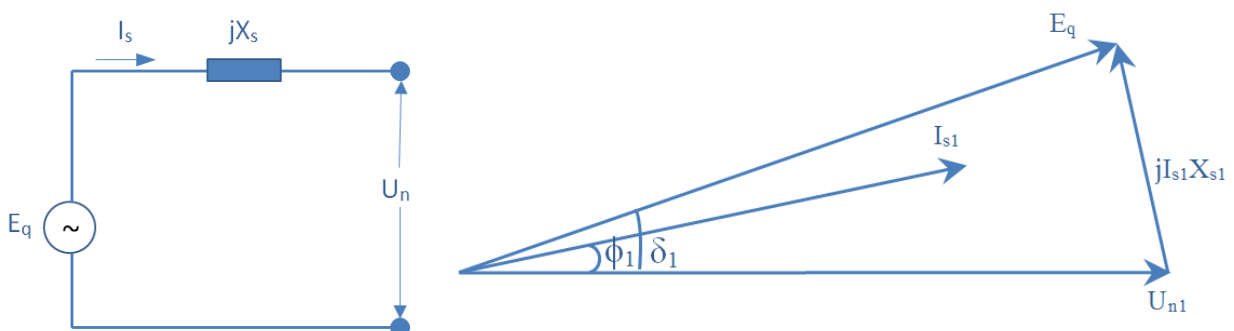


Figure 3.2: Phasor diagram of PMSM.

The phasor diagram of a permanent magnet synchronous machine (PMSM) can be drawn as shown in Figure 3.2. An expression for the power output with reference to the Figure 3.2 can be written as,

$$P = \frac{E_q U_n}{X_s} \sin \delta \quad (3.19)$$

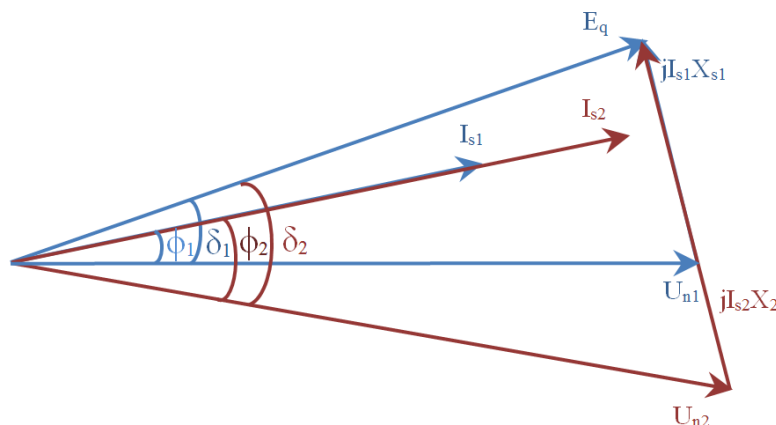


Figure 3.3 Phasor diagram of PMSM with increased current.

Keeping the geometrical parameters of a machine constant, the current density in the conductors can be a variable to increase the capacity of the machine. The induced voltage (E_q) will remain constant due to constant excitation from permanent magnets and the increase in current rating increases the drop in synchronous reactance (X_s) and consequently the power angle (δ) in the machine increases as depicted in Figure 3.1 and 3.2. From eq. (3.13), it can be observed that the increment of these parameters directly enhances the output power of the machine.

In other way, it can be conferred that if the output power required is kept constant, the increment of current density in the stator facilitates to build a compact machine i.e. the volume of the machine can be squeezed to enhance the torque density and hence the utilization factor.

3.5 Pole slot combination

The use of permanent magnet machines with a high pole number for low speed direct – drive applications has recently gained great interest [32]. By getting rid of the gearbox, a PM direct drive can provide better performance and be lighter than the machine with a gearbox. For these machines, concentrated windings around the teeth, with their simple structure and short end windings, are experienced to be very attractive [33]. Therefore, the direct-driven wind power machines rotating at very low angular speed needs very high number of pole slot combinations. In addition to this, the increased number of poles and slots reduces the thickness of rotor and stator yoke. As shown in Figure 3.4, for the same air gap flux density and same circumference of the machine, the increased number of poles requires thinner rotor yoke which consequently reduces the weight of the machine as well [34].

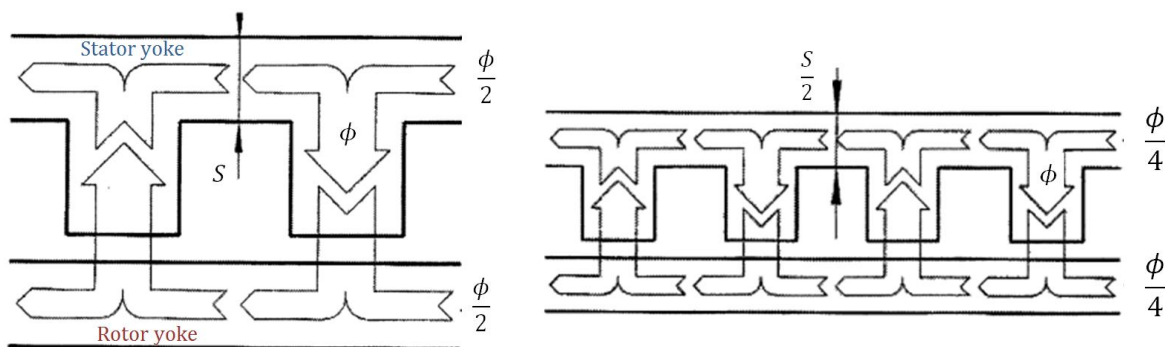


Figure 3.4: Effect of number of pole/slot on yoke thickness.

While selecting the combination of pole and slot, it becomes important to achieve the features like low vibrations under operation, and thus low noise, high starting torque, high efficiency, particularly when using laminated cores, high flexibility in design, particularly with regard to the main dimensions. These characteristics can be achieved if the number of slots (s) and the number of poles (p) defined by the relations,

$$|s - p| = 2 * m \quad (3.20)$$

and,
$$s = 12 * n * m \quad (3.21)$$

where n and m are natural numbers. The iron cores of these concentric winding machines are arranged such that iron cores having windings alternate with iron cores without windings, the cores being disposed in groups corresponding to three phase operation of the machine with $2 * m$ groups of winding per phase, with adjacent wound cores within a group being connected in series, and groups of cores being connected in series or in parallel [35].

According to eq. (3.20) and (3.21), there can be several combinations as mentioned in Appendix A. Other parameters to be considered while selecting the pole slot combination are cogging torque in the machine and harmonics. Very low cogging torque can be achieved if the slot and pole numbers are chosen so that the least common multiple (LCM) between these numbers is large [36].

3.6 Air gap length selection

The length of the air gap of a machine has a significant influence on the characteristics of an electrical machine. In principle, a small air gap gives a low magnetizing current, while the eddy current losses of the rotor and stator surface increase because of permeance harmonics created by the open or semi-closed slots. A small air gap also increases the surface losses in the rotor caused by the current linkage harmonics of the stator. Although the air gap is of great significance, no theoretical optimum has been solved for its length, but usually empirical equations are employed instead in the definition of the length of the air gap. In machines with an exceptionally large diameter, an air-gap ratio of

$$\frac{\delta}{D_i} \approx 0.001 \quad (3.22)$$

has to be selected because of the mechanical properties of the frame and the shaft of the machine [28].

Another empirical expression for selecting minimum air gap above the magnet surface is as,

$$\delta \approx 0.0002 + 0.003\sqrt{r_i L_i} \quad (3.23)$$

Where, r_i and L_i are the air-gap radius and stack length of the machine [37].

3.7 Magnet thickness

Taking the reference of eq. (3.12), the constant K depends upon the geometrical dimension of the machine. A superconducting machine is a high current density machine and is supposedly compact machine compared to copper winding machine of same power. For constant value of K , if the air gap flux is kept constant as well, the output power depends proportionally upon the current density in the machine. The high current density may lead to saturation in the yoke and demand for higher rotor and stator yoke thickness which can finally end up to a heavy machine. Therefore, optimization of appropriate magnet thickness to have a balance between air-gap flux density and current density is very important.

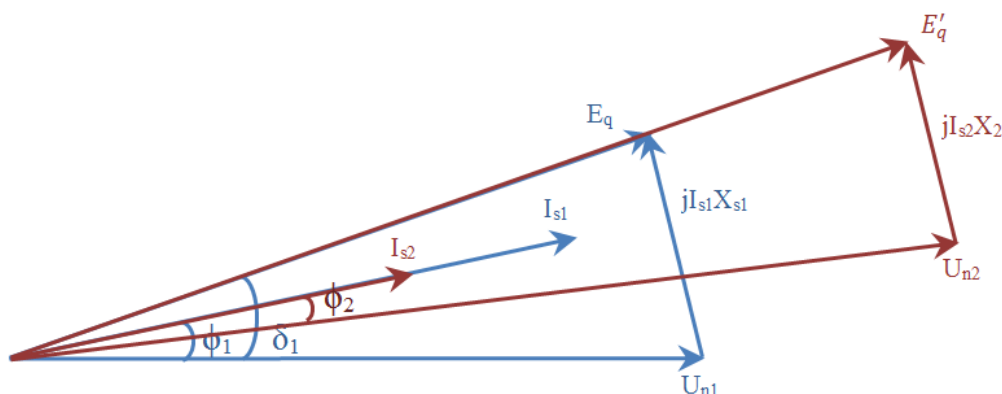


Figure 3.5: Phasor diagram after increment in magnet thickness.

As displayed in Figure 3.5, the increment in magnet thickness increases the induced voltage E_q to E'_q and the current in the winding decreases for the same power. The increased thickness also increases the equivalent air-gap length and the synchronous reactance decreases which gives additional reduction in drop in the reactance and makes the power angle (same as power factor angle in this case) small which finally gives increased terminal voltage.

The further consequence of the increment in magnet thickness yields to reduced current capacity of the converter and lesser power capacity requirement.

Chapter 4

4 Methodology

4.1 General

Machine design is an iterative process. In this work, a MATLAB based application SmartTool and COMSOL with MATLAB are the major tools in design of a superconducting synchronous generator for wind power application. A proposed design of 10 MW wind turbine generator has been taken as a reference machine. The geometrical parameters of the machine have been optimized with superconducting armature windings in place of copper windings using SmartTool. The overall weight of the machine, utilization factor, power factor and the magnetic saturation has been the parameters of major concern for optimization. The optimized design has later on been checked for magnetic characteristics using finite element analysis (FEA) in COMSOL with MATLAB. It has been an iterative process throughout the design. The relative permeability and magnetic flux density at full load condition have been regarded as the parameters for the approval of magnetic characteristics.

Three basic parameters of the machine as discussed in Section 3.1 have been kept constant in the design process are listed in Table 4.1.

Table 4.1: Reference parameters of the machine for the design process.

Parameters	Value
Rated mechanical power	10000 kW
Rated rotational speed	12.95 rpm
Desired rated voltage	3300 V

The free parameters that have been kept fixed for each set of design as mentioned in Section 3.1 are the number of poles and slots, air gap length, magnet thickness and slot dimensions. Different machines with superconductors have been designed onwards based on aforementioned parameters and the best one among them has been proposed as the alternative of reference machine with copper winding.

4.2 Design tools

4.2.1 SmartTool

A Norwegian company SmartMotor AS has developed a tool for design of radial flux PMSG with surface mounted magnets and concentrated coils. The tool can calculate and optimize different solution for a desirable machine design, and will give a quick outline of mass, stack length and active costs related to efficiency. The tool performs several iterations using well known design equations and approximations for radial flux topology. Either an outer or an inner rotor can be selected. The tool is based on MATLAB codes with analytical equations with a graphic user interface. An appurtenant machine model is generated by the tool based

on the results from the analytical calculations, including rotor back iron, stator back iron, permanent magnets, stator windings and air gap. The introductory generator design should be transferred to COMSOL to perform more accurate calculations. A list of fixed input parameters used in the simulation tool is shown in Table 4.1. One or more of the parameters can be chosen as variables to be optimized, where calculations on a selected number of machines will be performed. The output panel shows the calculated values for the input parameters of the desired design [38].

The reference machine has been proposed using SmartTool V3.2 and later on it was upgraded to version 3.3. This work has been carried out using the latest version of SmartTool.

4.2.2 COMSOL

The COMSOL Multiphysics engineering simulation software environment facilitates all steps in the modeling process – defining the geometry, meshing, specifying physics, solving, and then visualizing results.

While estimating the performance of a machine, analytical calculations may not be accurate enough. Design calculations for coil inductance, air gap flux and magnetic leakage, iron losses, back-emf, forces on conductors and cogging torque are difficult to evaluate accurately by analytical calculations. They should be complimented with finite element analysis (FEA) for better accuracy.

FEA is a numerical technique for solving partial differential equations (PDE) as well as integral equations. The solutions either solve a steady state problem by eliminating the differential equation completely, or reproducing the PDE as an approximating system of ordinary differential equations (ODE). The ODE's are evaluated by numerical techniques such as Euler's method, Simpson, Runge-Kutta, etc [39].

4.3 Reference machine

The reference machine for this analysis is a proposed 10 MW wind generator with copper winding in armature. The reference machine is with an outer diameter of 12 meter, stack length of 1.2 meter and an efficiency of 96.2 %. The weight of the generator active materials is 60 ton, but a total weight of 200 ton has been envisaged in the proposition. A high pole number of 198 poles and a low rotational speed of 12.95 rpm results in a frequency of 20 Hz. A 20 MVA converter is suggested in order to connect the generator to a 50/60 Hz grid [40].

A major challenge of reducing the weight and mechanical loading of the tower have been pointed out in the proposal. The proposed design of reference machine is focused on the design of a 10 MW direct driven radial flux PMSG with concentrated windings and variable speed. The rated machine power and maximum rated rotational speed of the machine are 10 MW and 12.95 rpm respectively. The optimized machine parameters in SmartTool are shown in Figure 4.1.

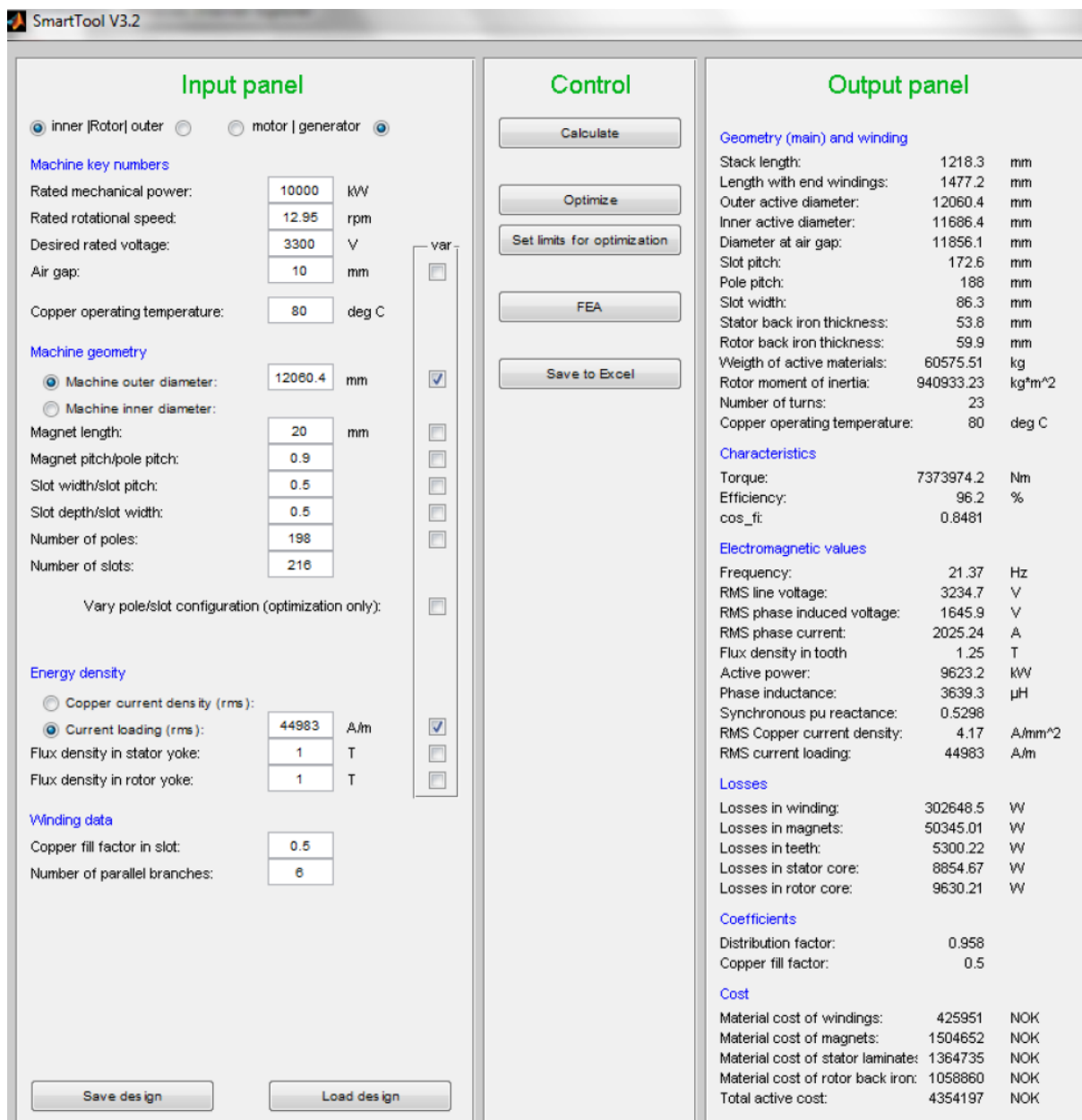


Figure 4.1: SmartTool simulation of reference machine 02/11/2010.

4.4 Modification in reference machine

The reference machine with copper winding has been observed to be excessively stressed to magnetic saturation since the flux density in most of the part of the yoke is 2 T (Figure 4.2). The saturation in yoke leads to noise and vibrations in the machine and higher core losses as well [41]. Therefore, the reference machine has been redesigned with thicker yoke to limit the magnetic flux density up to 1.7 T keeping the air gap diameter and the stack length of the machine fixed at the same value.

The redesigned machine has been regarded as the reference machine for further analysis. The optimized parameters of the machine are displayed in Figure 4.3 and the complete result is attached in Appendix D.

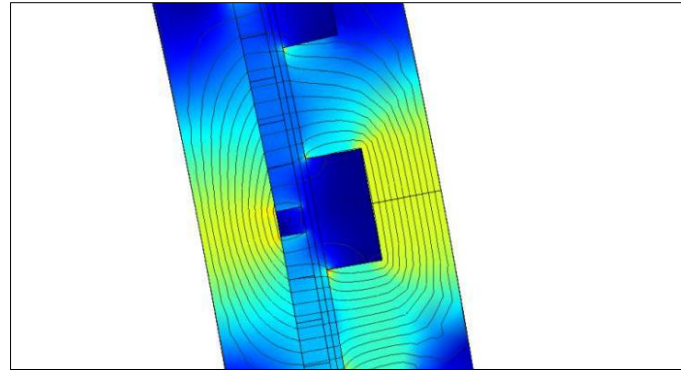


Figure 4.2 COMSOL Simulation of 10 MW machine (yellow area indicates a magnetic flux density around 2 T).

SmartTool V3.3

Input panel

inner | Rotor | outer
 motor | generator
 generator

Machine key numbers

Rated mechanical power: kW

Rated rotational speed: rpm

Desired rated voltage: V

Air gap length: mm

Copper operating temperature: deg C

Machine geometry

Machine outer diameter: mm
 Machine inner diameter: mm

Magnet length: mm

Magnet pitch/pole pitch:

Slot width/slot pitch:

Slot depth/slot width:

Number of poles:

Number of slots:

Vary pole/slot configuration (optimization only):

Energy density

Copper current density (rms): A/m
 Current loading (rms): A/m
 Stator loss per area: T

Flux density in stator yoke: T

Flux density in rotor yoke: T

Winding data

Copper fill factor under wedge:

Number of parallel branches:

Slot wedge

Thickness slot wedge: mm

Semimagnetic wedge?

Regular input:
 Geometry input:

Control

Output panel

Geometry (main) and winding

Stack length:	1218.4	mm
Length with end windings:	1479.3	mm
Outer active diameter:	12141.2	mm
Inner active diameter:	11600	mm
Diameter at air gap:	11857.1	mm
Slot pitch:	172.6	mm
Pole pitch:	188	mm
Slot depth:	43.1	mm
Slot width:	86.3	mm
Stator back iron thickness:	92.6	mm
Rotor back iron thickness:	103.6	mm
Weight of active materials:	90459.86	kg
Rotor moment of inertia:	1460904	kg*m ²
Number of turns:	25	
Copper operating temperature:	80	deg C

Characteristics

Torque:	7373974	Nm
Efficiency:	96.1	%
cos_phi:	0.8366	

Electromagnetic values

Frequency:	21.37	Hz
RMS line voltage:	3365.9	V
RMS phase induced voltage:	1692.9	V
RMS phase current:	1957.17	A
Flux density in tooth:	1.18	T
Average flux density in air gap:	0.59	T
Active power:	9545.6	kW
Phase inductance:	4051.7	µH
Synchronous pu reactance:	0.5478	
RMS Copper current density:	4.381	A/mm ²
RMS current loading:	47247.1	A/m

Losses

Losses in winding:	334380.	W
No Load Losses in magnets:	36149.45	W
No Load Losses in teeth:	12143.47	W
No Load Losses in stator yoke:	11527.05	W
No Load Losses in rotor yoke:	206.04	W
Stator loss per area:	7873	W/m ²

Coefficients

Distribution factor:	0.958	
AC/DC Loss factor:	1.2	
Magnetic air gap shear force:	43047	N/m ²

Cost

Material cost of windings:	6092	NOK
Material cost of magnets:	6020	NOK
Material cost of stator laminate:	41836	NOK
Material cost of rotor back iron:	36512	NOK
Total active cost:	90460	NOK

Figure 4.3: COMSOL simulation of redesigned reference machine.

The dimensions displayed in the SmartTool input output panel of the machines are with very fine accuracy which may not be practical during manufacturing but can be truncated to its nearest practical values to have very little effect on the electrical parameters.

The noticeable changes in the new machine are the weight of the machine, RMS copper current density, stator back iron thickness, rotor back iron thickness and losses as listed in Table 4.2.

Table 4.2: Changes in parameters of reference machine after modification.

Parameters	Reference machine	Re-designed machine
Weight of the machine	60575.5 Kg	90459.8 Kg
RMS copper current density	4.17 A/mm ²	4.38 A/mm ²
Stator back iron thickness	53.8 mm	92.6 mm
Rotor back iron thickness	59.9 mm	103.6 mm
Losses		
Losses in winding	302.65 kW	334.38 kW
No load losses in magnets	50.345 kW	36.15 kW
No load losses in teeth	5.3 kW	12.14 kW
No load losses in stator yoke	8.85 kW	11.53 kW
No load losses in rotor yoke	9.63 kW	0.21 kW

The increased current density causes increased heat generation inside the slot and it must be within the permissible limit of temperature rise. The effect of the increment in current density has been assessed below.

Temperature coefficient of copper at 20 °C (α_{20})= 0.0039/K [42].

Conductivity (σ) of copper at 80 °C,

$$\begin{aligned}\sigma_{80} &= \frac{\sigma_{20}}{1 + \alpha_{20}(T_{80} - T_{20})} \\ &= \frac{58 \times 10^6}{1 + 0.0039(80 - 20)} = 47 \times 10^6 \text{ S/m}\end{aligned}$$

Power loss in the slot per unit length,

$$\begin{aligned}P_{loss} &= \frac{J_{ac}^2}{\sigma_{80}} \cdot A_{slot,eff} \text{ (derived in Appendix C)} \\ &= \frac{(4.38 \times 10^6)^2}{47 \times 10^6} \cdot (43 \times 86 \times 10^{-6}) \cdot 0.5 \\ &= 754.7 \text{ W/m}\end{aligned}$$

Surface area for heat conduction = $(43+86) \times 10^{-3} \times 2 = 0.26 \text{ m}^2/\text{m}$

$$\text{Heat conduction along the slot per unit length} = \frac{754.7 \text{ W/m}}{0.26 \text{ m}^2/\text{m}} = 2.9 \text{ kW/m}^2$$

In the original reference machine, the current density is $J_{ac} = 4.17 \text{ A/mm}^2$, which give the heat loss along the slot per unit length equal to 2.63 kW/m^2 . The additional requirement in heat conduction along the slot per unit length is only 0.3 kW/m^2 . Also, the current loading (\bar{A}) in the redesigned machine after the increment in current density is 47.25 kA/m . The changes in both parameters in the re-designed machine are tolerable for a copper winding machine. For SC machine design, the magnetic characteristics of the redesigned machine have been taken as reference. All the optimized machines have been stressed equally i.e. with maximum magnetic flux density level of 1.7 to in stator and rotor yoke and teeth of the slots.

4.5 Analysis with superconductor

4.5.1 Geometrical dimension of slot with Superconductor

The dimension of slot required for superconducting armature winding has been calculated based on the parameters of the modified design of the wind power generator. The reference for cross-section area of the MgB_2 superconductor has been taken from the data of sample wire manufactured by Columbus Superconductor, Italy (detail specification in Appendix B). The sample is being tested at SINTEF Energy AS for measurement of AC losses.

The number of turns has been approximated from the several preliminary simulations of the machine with superconductor which has been assumed to be re-adjusted along with filling factor during iterative process.

Cross-section area of the SC (A_{sc}) = 1.476 mm^2

Number of turns in each slot (N) = 50 (assumed for initial iterations)

Total cross-section of SC in each slot ($A_{sc,tot}$) = $50 \times 1.476 \approx 74 \text{ mm}^2$

Assuming 50 % of the space will only be occupied by the conductors and the rest will be for circulation of cooling agent (gaseous Helium or liquid Neon),

Area required for SC placement = $74/0.5 = 148 \text{ mm}^2 \approx 150 \text{ mm}^2$

It is recommended that the minimum slot width that can be practically feasible for construction in large machines is 30 mm. In case of SC machine, 10 mm of space from each side of conductor will be allocated for thermal insulation. Therefore, the conductor area will be of 10 mm x 15 mm and the slot dimension will result to be of 30 mm x 35 mm above the slot wedge. A slot wedge thickness is assumed to be of 3 mm; hence the slot dimension will be 30 mm x 38 mm. The physical arrangement can be depicted as in Figure 4.4.

The sharp edge of the slots as shown in the figure may give rise to local saturation and can be chamfered during manufacturing to avoid such problem. The mechanical support required to hold the superconductor area can be designed during development of machine such that there will be no heat conduction between the stator and the conductor.

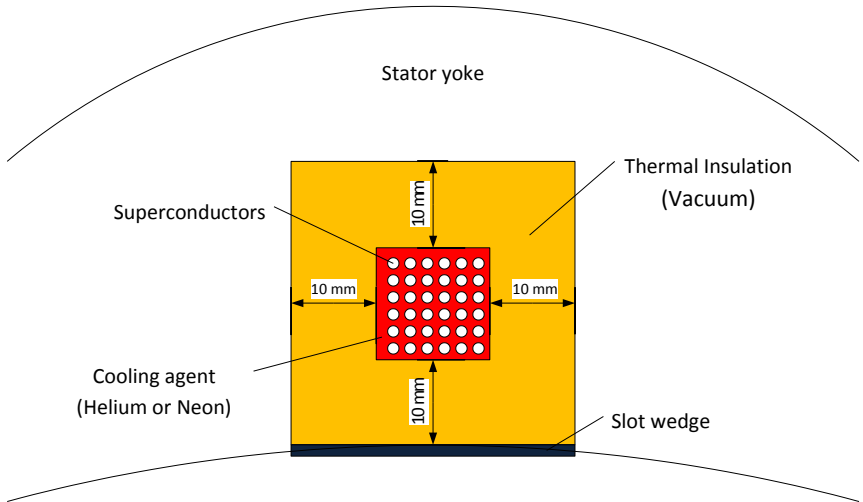


Figure 4.4: Slot configuration.

The cross-section of the superconductors placed inside the slots in the above figure will be circular as shown in Figure 4.5. It consists of several superconducting filaments embedded inside the conducting sheath (white in the picture) in matrix form. The matrix of filaments is twisted inside the sheath to reduce the coupling current losses caused due to AC magnetic field.



Figure 4.5: Cross-section of superconductor [43].

In the prototype synchronous machines built in past, all machines are equipped with superconducting field windings and the stator winding is wound with copper without iron. Ironless machines have been preferred to avoid the saturation due to very high magnetic field produced by the superconducting magnets. But in this case, the machine has been designed for superconducting armature windings and permanent magnet as the source of field. To avoid the excessive AC losses in the SC due to its direct exposure to time varying magnetic field, conventional iron machine has been wound with SC. The iron yoke gives path for the magnetic flux and AC losses have been minimized in expense of reduced capacity of machine unlike to the ironless machine. This also facilitates for less cooling requirements as the losses in SC will be lower compared to ironless armature winding machine.

4.5.2 Losses evaluation

The losses evaluation for the modified reference machine with copper winding at 21.4 Hz has been carried out using SmartTool and the same for the machine with superconductor has been carried out using the same tool by assuming the conductivity of the copper to be 58×10^{12} S/m instead of its original value of 58×10^6 S/m. The SmartTool in this case displays almost no copper loss (load loss) even though, SC exhibits considerable AC loss in practical case. The actual loss is supposed to be added from the experimental results from SINTEF. The FEA analysis of both the cases have been carried out until the machine has been loaded such that there is no room for further stressing the machine magnetically.

4.6 Selection of geometrical parameters

4.6.1 Air gap length selection

As mentioned earlier, machine design is an iterative process and after testing the several combinations of geometrical parameters, the air-gap diameter of the superconducting machine seems to be about 8 m.

According to eq. (3.22),

$$\text{Air gap length } (\delta) = 0.001 \cdot D_i = 0.001 * 8 \text{ m} = 8 \text{ mm}$$

And, according to eq. (3.23), for air-gap radius (r_i) = 4 m and Stack length (L_i) = 1 m,

$$\text{Air gap length } (\delta) \approx 0.0002 + 0.003 \sqrt{r_i \cdot L_i} = 6.3 \text{ mm}$$

In large machines with prefabricated windings and open slots, the air-gap length must be selected high enough (60–100% increase) to reduce pulsation losses [28].

Therefore, the air gap length has been selected to be 10 mm.

4.6.2 Magnet thickness

The magnet thickness of the reference machine is 20 mm. As presented in Section 3.7 and Figure 3.3, the increment in magnet increases the air gap flux density. This provides space to keep the current density in optimal range and hence the weight of the generator by making the stator and rotor yoke thinner. A thin layer of magnet in a machine demands for higher current density for the same power and leads to poor power factor of the machine.

Therefore, magnet thickness for the SC machines has been selected to be 30 mm.

4.6.3 Cooling systems arrangement

The cooling system requirement depends upon the operating temperature of the superconductor as described in Section 2.6. In this case, gaseous Helium can be the best alternative of cooling since the operating temperature for the MgB_2 conductor is most favorable at 20 K. Depending upon the possibility of higher temperature operating environment, liquid Neon can also be an alternative since the boiling point of LNe is 27 K. Direct cooling system inside the slot can be arranged for an effective cooling of the

superconducting windings. All the end turns can be cooled in gross or separately. Further research and design may give some better picture of cooling arrangement.

4.7 Results

After several iterative procedures using SmartTool and COMSOL, three alternative combinations have been optimized using superconductors. There should not have been any losses in the windings in superconducting machines but some winding losses appear in the SmartTool input/output panel which due to the assumption of finite value of conductivity for superconductors (58×10^{12} S/m). This loss has been neglected and has been further analyzed in following chapters with AC losses caused due to time varying magnetic field. The cost displayed in the same panel presents the weight of the individual elements of the machine since the cost has been set as 1 NOK/Kg for each element in the SmartTool cost data.

4.7.1 Machine - 1 (176 pole/192 slot machine)

Following the pole and slot combination principle as mentioned in Section 3.5, the first machine has been optimized with 192 slots and 176 poles. The optimized geometrical and electrical parameters are shown in Figure 4.6 and the complete result is annexed in Appendix E. Some of the important parameters of this combination are:

Table 4.3: Major parameters of Machine - 1.

Parameters	Values
Air-gap diameter	8302 mm
Stack length	1008 mm
Weight of active materials	62590 Kg
Power factor ($\cos\phi$)	0.805
Synchronous pu reactance	0.594
RMS current density	145 A/mm ²
RMS current loading	90.76 kA/m

Some relevant finite element analysis (FEA) results for this combination are as follows:

Parameters	Values
Phase inductance	5124 μ H
Phase voltage (rms)	1433 V
Total harmonic distortion (THD) in phase voltage	11.7 %
Line voltage	2482 V
Total harmonic distortion (THD) in line voltage	0.95 %
Cogging torque amplitude at no-load	302.9 N·m
Mean torque at full load	7647.1 kN·m
Torque ripple amplitude at full load (pu)	0.76 %

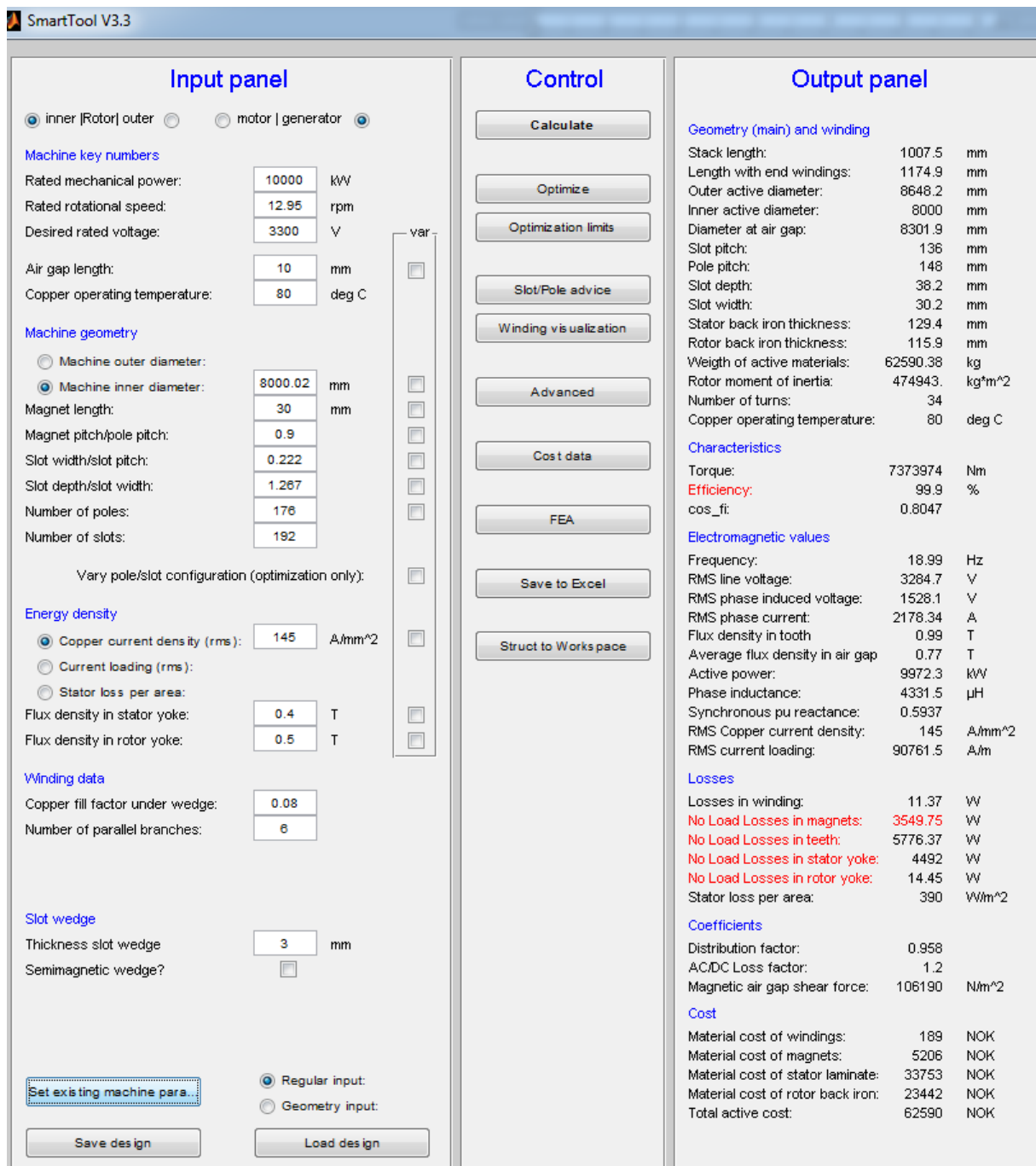


Figure 4.6: Optimized parameters for Machine - 1.

The no-load and full load losses in Machine -1 from FEA analysis has been obtained as:

Losses	No-load	Full load
Average PM loss (kW)	17.924	891.624
Max. stator core loss (kW)	14.641	36.722
Max. rotor core loss (kW)	0.223	27.327

4.7.2 Machine – 2 (154 pole/168 slot machine)

Following the similar procedure as for Machine – 1, the combination for Machine – 2 has been optimized with 154 pole and 168 slots. The optimized parameters are displayed in Figure 4.7 and the list of all results follow in Appendix F.

It can be noticed in the results that the lower number of pole slot combination causes the stator and rotor yoke thickness to increase as discussed in Section 3.5. The increased thickness of yokes consequently yields an increment in weight of the machine as well.

Some of the important parameters of this combination are listed in Table 4.4.

Table 4.4: Major parameters of Machine - 2.

Parameters	Values
Air-gap diameter	8367 mm
Stack length	1009 mm
Weight of active materials	74947 Kg
Power factor (Cos ϕ)	0.793
Synchronous pu reactance	0.610
RMS current density	160 A/mm ²
RMS current loading	87.18 kA/m

The finite element analysis (FEA) results for this machine are listed below:

Parameters	Values
Phase inductance	5797 μ H
Phase voltage (rms)	1404 V
Total harmonic distortion (THD) in phase voltage	13.2 %
Line voltage	2432 V
Total harmonic distortion (THD) in line voltage	1.15 %
Cogging torque amplitude at no-load	1587.0 N·m
Mean torque at full load	7671.7 kN·m
Torque ripple amplitude at full load (pu)	1.11 %

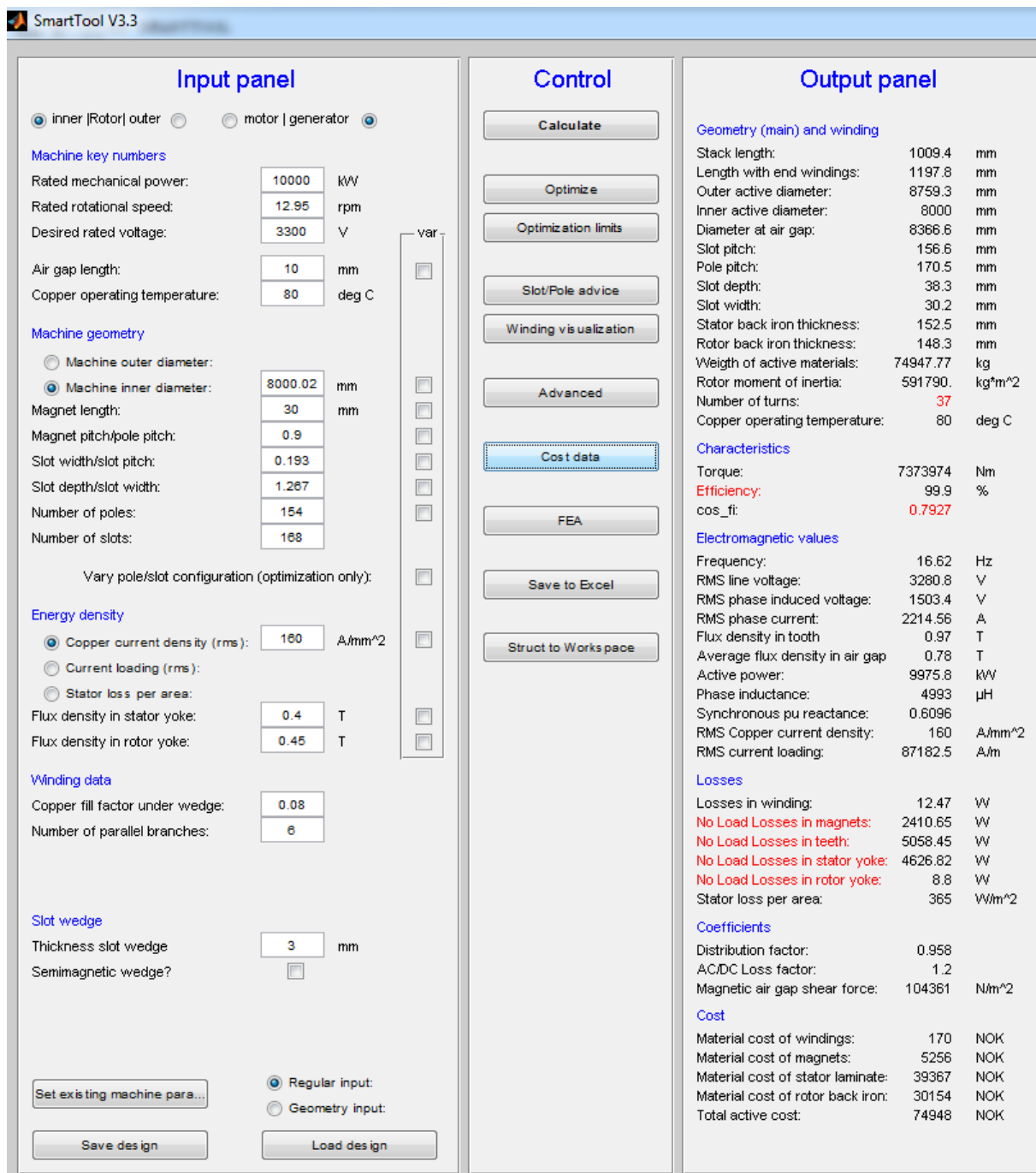


Figure 4.7: Optimized parameters for Machine - 2.

The no-load and full load losses in Machine -2 from FEA analysis has been obtained as:

Losses	No-load	Full load
Average PM loss (kW)	16.744	1126.868
Max. stator core loss (kW)	14.682	40.621
Max. rotor core loss (kW)	0.237	30.873

4.7.3 Machine – 3 (132 pole/144 slot machine)

The Machine – 3 has been optimized with 144 slots and 132 poles with the similar procedure as of previous machines. The optimized geometrical and electrical parameters are shown in Figure 4.8 and the complete list of results is presented in Appendix G.

Here, it can be observed that the reduction in number of pole and slot allows reducing the inner diameter of the machine which is 7.8 m in this case compared to 8 m for the previous machines. The further reduction in pole and slot has led to further increment in stator and yoke thickness and hence in the active weight of the generator.

Some of the important parameters of this Machine – 3 are listed in Table 4.5.

Table 4.5: Major parameters of Machine - 3.

Parameters	Values
Air-gap diameter	8254 mm
Stack length	1007 mm
Weight of active materials	93742 Kg
Power factor (Cos ϕ)	0.762
Synchronous pu reactance	0.647
RMS current density	190 A/mm ²
RMS current loading	88.07 kA/m

The finite element analysis (FEA) results for this combination are as follows:

Parameters	Values
Phase inductance	6963 μ H
Phase voltage (rms)	1370 V
Total harmonic distortion (THD) in phase voltage	15.0 %
Line voltage (rms)	2372 V
Total harmonic distortion (THD) in line voltage	1.52 %
Cogging torque amplitude at no-load	4744.7 N·m
Mean torque at full load	7756.7 kN·m
Torque ripple amplitude at full load (pu)	1.60 %

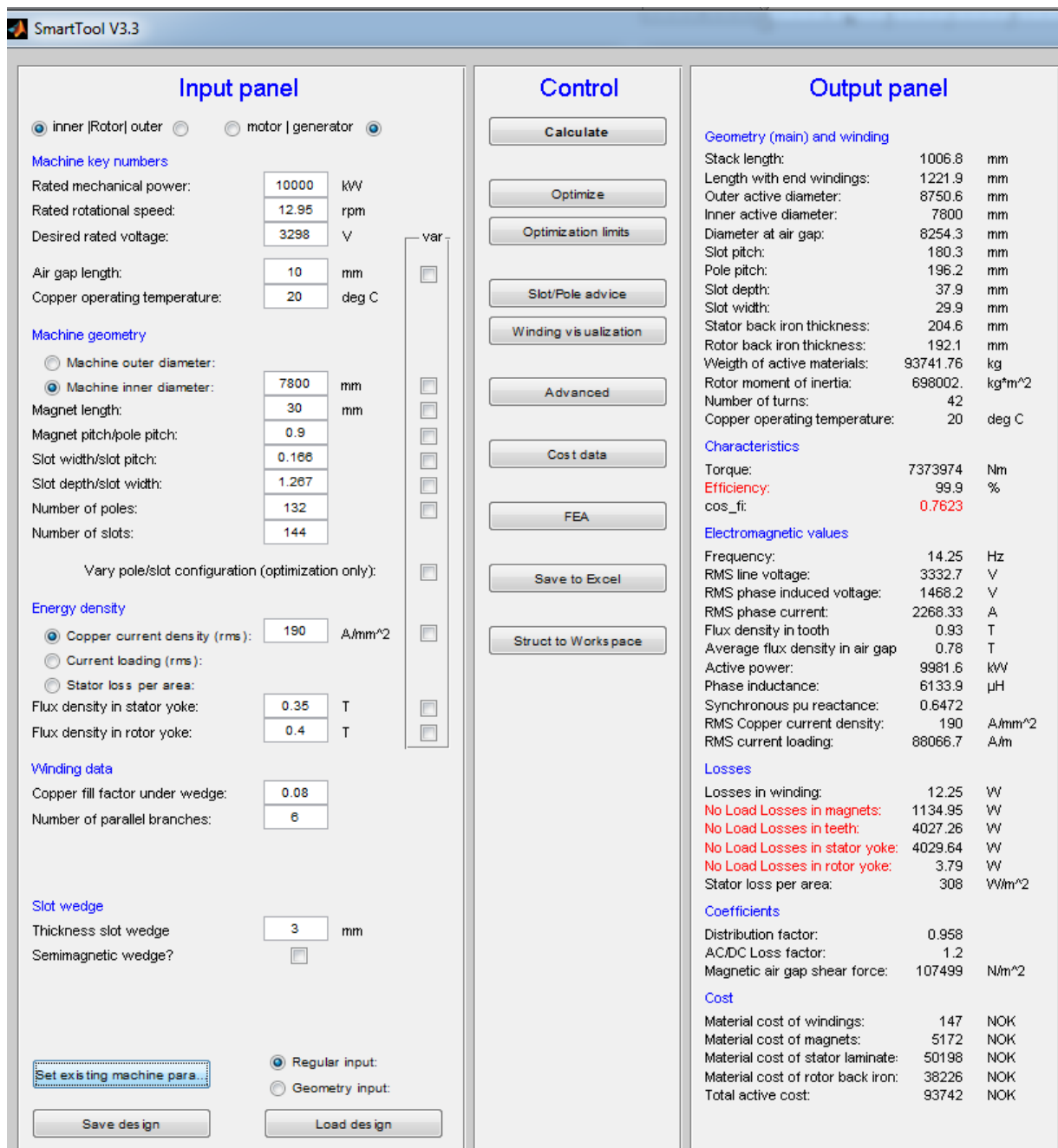


Figure 4.8: Optimized parameters for Machine - 3.

The no-load and full load losses in Machine -3 from FEA analysis has been obtained as:

Losses	No-load	Full load
Average PM loss (kW)	14.093	1497.059
Max. stator core loss (kW)	14.650	43.462
Max. rotor core loss (kW)	0.331	36.650

The parameters of the machines optimized using SmartTool can be summarized as in Table 4.6.

Table 4.6: Summary of all parameters for all machines.

Parameters	Reference machine	SC machine - 1	SC machine - 2	SC machine - 3
Rated mechanical power (MW)	10	10	10	10
Rated rotational speed (rpm)	12.95	12.95	12.95	12.95
Desired rated voltage (V)	3310	3300	3300	3300
Machine geometry				
Stack length (mm)	1218.4	1007.5	1009.4	1006.8
outer active diameter (mm)	12141	8648	8759	8751
Diameter at air gap (mm)	11857	8302	8367	8254
Characteristics				
Torque (Nm)	7373974	7373974	7373974	7373974
Efficiency (%)	96.1	99.9*	99.9*	99.9*
Power factor	0.837	0.805	0.793	0.762
Electromagnetic values				
Synchronous pu reactance	0.5478	0.5937	0.6096	0.6472
RMS copper current density (A/mm ²)	4.38	145	160	190
RMS current loading (A/m)	47247.1	90761.5	87182.5	88066.7
Losses				
Losses in winding (kW)	334.38	0	0	0
No load losses in magnets (kW)	36.15	3.55	2.41	1.14
No load losses in teeth (kW)	12.14	5.78	5.06	4.03
No load losses in stator yoke (kW)	11.53	4.49	4.63	4.03
No load losses in rotor yoke (kW)	0.21	0.015	0.009	0.004
Stator loss per area (kW/m ²)	7.87	0.39	0.37	0.31
Weight of parts				
Weight of active materials (Kg)	90460	62590.4	74948	93742
Magnets (Kg)	6020	5206	5226	5172

* Efficiency of the SC machines does not include the AC losses in superconductors.

This page is intentionally left blank.

Chapter 5

5 Discussion

5.1 General

The machine design is optimization of a combination of multiple parameters. During design, it is very difficult to optimize all the parameters favorably. In most of the cases, the tradeoff between particular parameters decides the final machine. In this chapter, the reference machine with copper winding and the 3 alternatives of proposed superconducting machines have been compared in several aspects and finally one alternative has been proposed.

The major geometrical and electromagnetic parameters of the machines are enlisted in Table 5.1.

Table 5.1: Geometrical and electromagnetic parameters of the machines.

Parameters	Reference machine	Machine 1	Machine 2	Machine 3
Air-gap diameter (mm)	11857	8302	8367	8254
Stack length (mm)	1218	1008	1009	1007
Weight of active materials (Kg)	90460	62590	74947	93742
Power factor (Cosφ)	0.837	0.805	0.793	0.762
Synchronous reactance (pu)	0.548	0.594	0.610	0.647
RMS current density (A/mm ²)	4.38	145	160	190
RMS current loading (kA/mm)	47.25	90.76	87.18	88.07

5.2 Comparison of machines w.r.t. utilization factor

The utilization factor based on mechanical torque from FEA results and apparent power of the machine can be calculated using the expressions discussed in Section 3.2.

$$k = \frac{T}{D_i^2 \cdot L_i}, \quad \text{unit } \frac{kN \cdot m}{m^3}$$

$$C = \frac{P_m}{\cos\phi \cdot D_i^2 \cdot L_i \cdot n_m}, \quad \text{unit } \frac{[kVA]}{m^3 \cdot rpm}$$

Table 5.2: Utilization factor of the machines based on mechanical torque and apparent power.

Parameters	Reference machine	Machine 1	Machine 2	Machine 3
Rated Power, kW	10000	10000	10000	10000
Mechanical torque (kN·m)	7640.2	7647.1	7671.7	7756.7
Air-gap diameter (mm)	11857	8302	8367	8254
Stack length (mm)	1218	1008	1009	1007
Power factor (Cosφ)	0.837	0.805	0.793	0.762
Utilization factor (<i>k</i>)	44.6	110.1	108.6	113.1
Utilization factor (<i>C</i>)	5.4	13.8	13.8	14.8

Table 5.2 presents that the Utilization factor of superconducting machines based on both the torque and apparent power are around 2.5 times higher than that of the reference machine. Among the SC machines, Machine -3 has the highest value of utilization factors by a very small margin. Therefore, it is difficult to choose any one of the SC machines based only upon utilization factors.

5.3 Comparison of machines w.r.t. weight

One of the major objectives of the design of superconducting machine is to reduce the weight of the machine in comparison to conventional copper winding machine. The key indicators based on weight are power density (power to weight ratio) and torque density (torque to weight). Mechanical torque has been taken from the finite element analysis for accurate indications.

Table 5.3: Power and Torque related parameters of reference machine and SC machines.

Parameters	Reference machine	Machine 1	Machine 2	Machine 3
Rated mechanical power (kW)	10000	10000	10000	10000
Stator back iron thickness (mm)	92.6	129.4	152.5	204.6
Rotor back iron thickness (mm)	103.6	115.9	148.3	192.1
Weight of active materials (Kg)	90460	62590	74947	93742
Power density (W/Kg)	110	160	133	106
Mean load torque at Full load (kN·m)	7640.2	7647.1	7671.7	7756.7
Torque density (N·m/Kg)	84.5	122.2	102.4	82.8

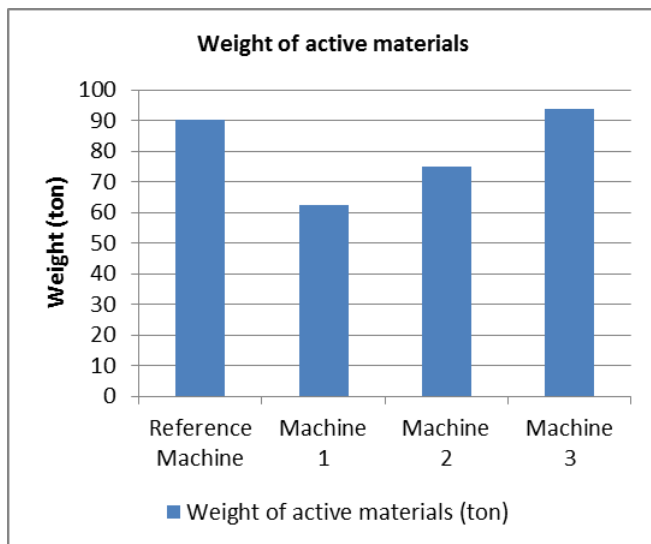


Figure 5.1: Weight of the active materials of machines.

As presented in Table 5.3 and Figure 5.1, the weight of the machine -1 is the lowest one and is lower by about 28 ton than the reference machine with copper winding. The weight of the SC machine -1, 2 and 3 are in increasing order. It is due to the flux density in the yoke. The highest number of poles and slot combination of machine – 1 causes least flux in the rotor and stator yoke and therefore, it has thinnest yokes and least weight among the 3 machines.

The reduction in weight by such amount consequently lessens the weight on the tower and the transportation weight as well. These indirect advantages of reduction of weight also save significant cost in case of offshore wind power.

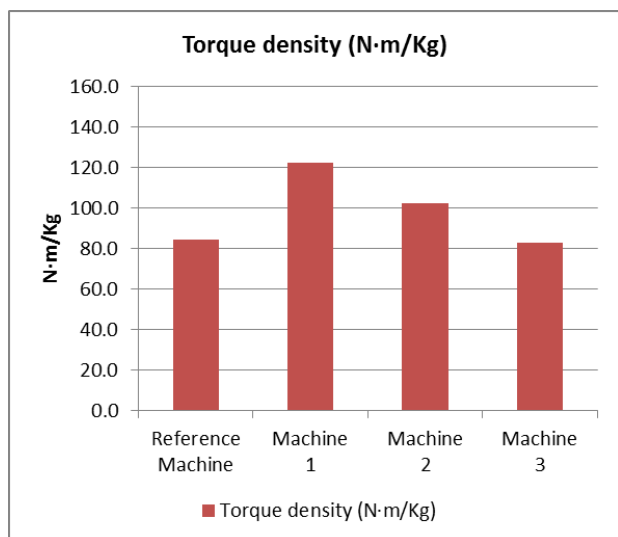


Figure 5.2: Torque to weight ratio of all machines.

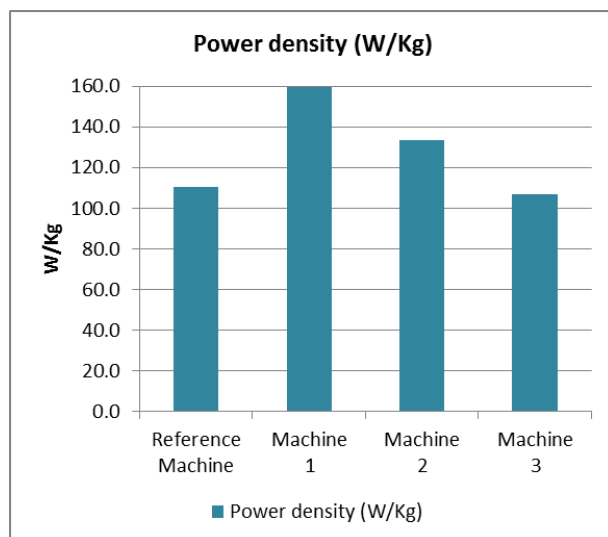


Figure 5.3: Power to weight ratio of all machines.

In addition, few key indicators of machines torque density (N·m/Kg) and power density (W/Kg) as shown in Figure 5.2 and Figure 5.3 also prove the machine – 1 with superconductor to be superior among the proposed 3 machines and the reference machine with copper winding.

For further comparison, a state-of-the-art design has been taken as the reference as shown in Figure 5.4. The figure demonstrates an area of state-of-the-art designs. The generators with power density and torque density data falling between this area are following the state-of-the-art technology whereas the generators with their corresponding data located to the right and up relative to the area are better than the conventional technology and the designs falling to the left and down relative to the area are worse than the state of the art technology [44].

After plotting the power density and torque density points of all the three proposed SC machines, it is clear that all three alternatives are above the state of the art technology area but the Machine -1 is well above and the best among the three.

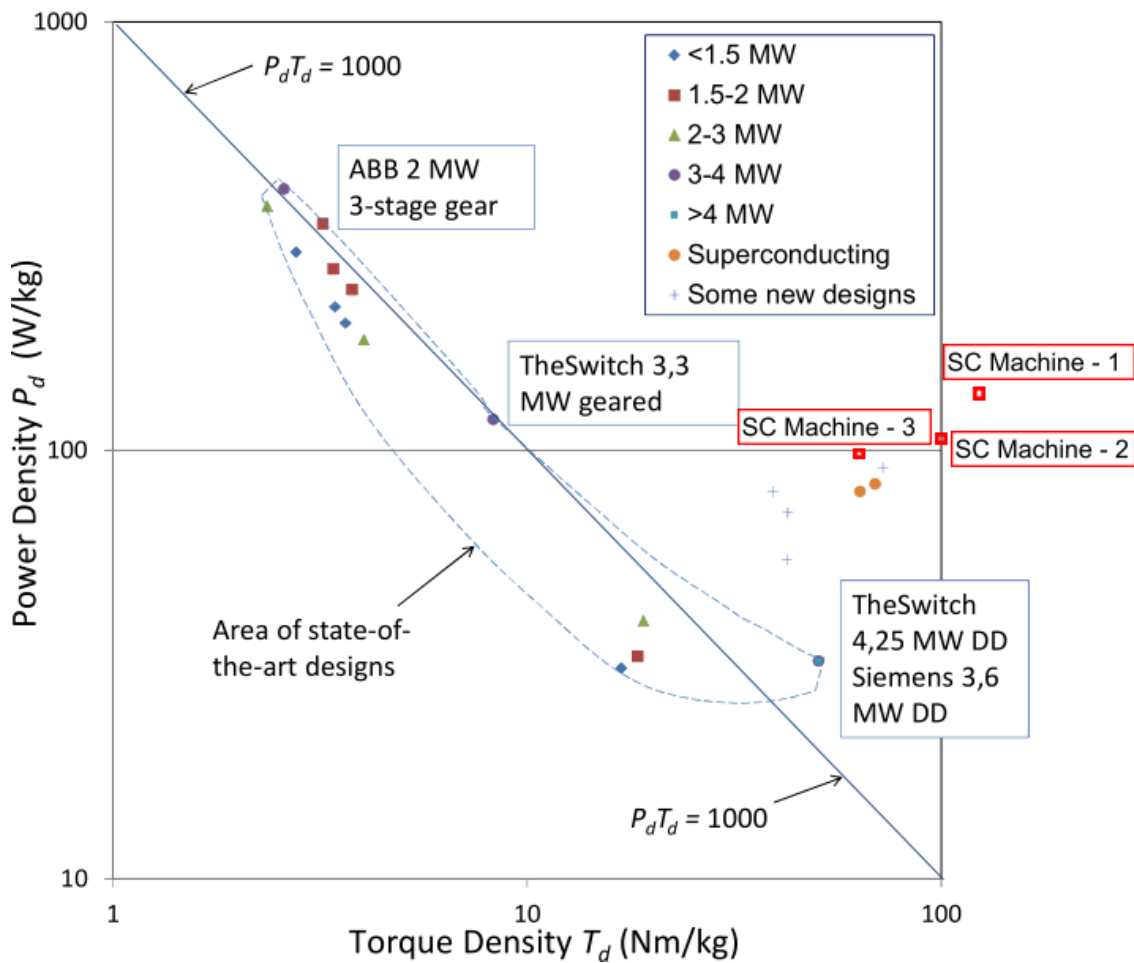


Figure 5.4: Power density vs. torque density (logarithmic scale) [44].

5.4 Comparison of machines w.r.t. volume

As described in Section 3.4, the increase in current density using superconductor makes the machine compact in volume and the Figure 5.5 delineates this impact. It is clear from the figure that all the SC machines are less than half in volume compared to the reference machine. The SC machine – 1 occupies the least volume among the all and has almost 2.4 times less volume than the reference machine.

The significant decrease in volume of the generator reduces the volume of nacelle and this will have some indirect impact in reduction in material cost and transportation cost as well.

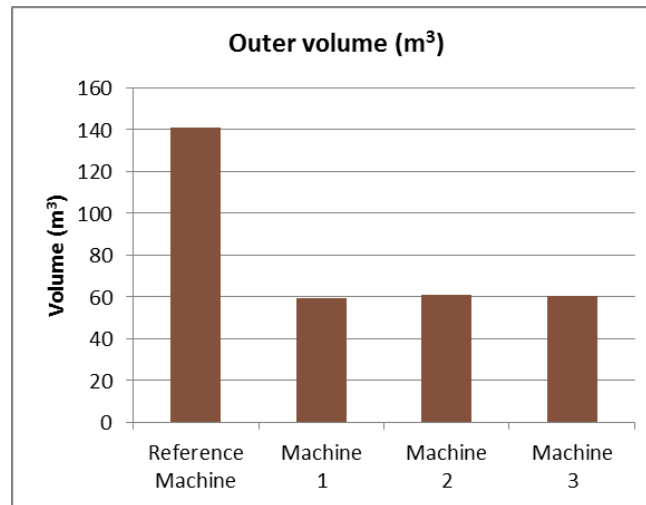


Figure 5.5: Outer volume of all machines.

5.5 Comparison of machines w.r.t. power factor and terminal equipment

The power factor of all the generators is positive (leading) means each machine will inject active power to the grid whereas consume reactive power. The power factor and synchronous reactance of the machines are listed in Table 5.4.

In all of the three proposed synchronous machines with superconducting armature winding, the reactive power is required to be supplied from the grid. The poor power factor of the machines will increase the size of the converter and consequently, the cost as well. The reactive power demand by each machine is listed in Table 5.4.

It is clear from the values listed in Table 5.4 that the power factor of Machine – 1 is the best among the proposed three SC machines. Here, the reference machine with copper winding is better in this context.

Table 5.4: Reactive power comparison of all machines.

Parameters	Reference machine	Machine 1	Machine 2	Machine 3
Rated power (P), kW	10000	10000	10000	10000
Power factor (cosφ)	0.8366	0.8047	0.7927	0.7623
Apparent power ² (S), kVA	11953	12427	12615	13118
Reactive Power ³ (Q), kVAr	6548	7378	7690	8490
Additional reactive power demand compared to reference machine, kVAr	-	830	1142	1942

$$^2 S = P / \cos\phi$$

$$^3 Q = S \cdot \sin\phi$$

The demand in reactive power can be graphically represented as in Figure 5.6.

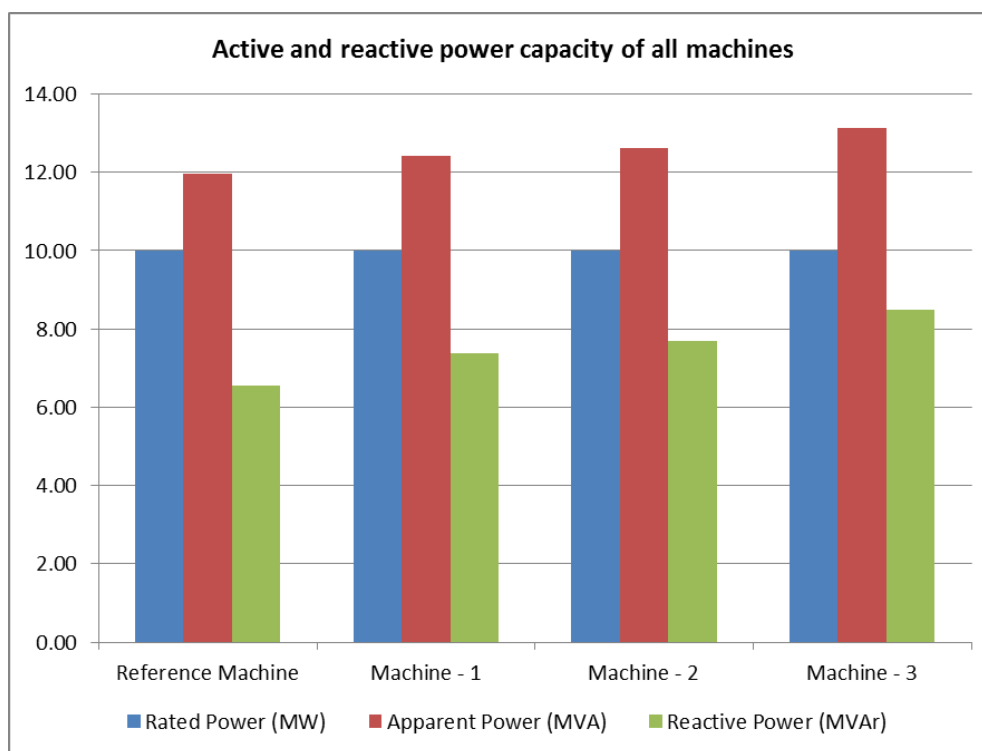


Figure 5.6: Active and reactive capacity of all machines.

From the Table 5.4 and Figure 5.6, it is evident that the reactive power demand by machine – 1 is 830 kVAR more than the reference machine. This increase will cause the converter to increase in size but on the other hand, it has already been described in Figure 5.1 that the weight of the generator decreases by almost 28 ton and consequently decreases the weight burden to the tower of the wind turbine and also decreases the size of the nacelle. In addition, the converter is located at the base of the tower and an increment in weight does not affect to the way the weight of the generator does.

5.6 Comparison of machines w.r.t. magnetic saturation

The dimension of the all the machines have been optimized such that the maximum flux density in the rotor and stator yoke will not exceed 1.7 T. The reference machine has also been optimized at same flux density. The higher flux density in core than this value will cause saturation of the core and will lead to higher core losses. Excessive noise and vibration are also the consequences of saturation of core. The flux density in the yoke of the machines displayed in Figure 5.7 varies from lower to higher value as the color changes from blue to red. The small white spots in the Figure 5.7 are beyond 1.7 T. The relative permeability of the machine will also vary accordingly and the corresponding figures are attached in Appendix. From the Figure 5.7, it can be observed that all the machines are magnetically equally stressed. Any further improvement in any one of the machines will demand almost similar change to other machines. Hence, on the basis of magnetically saturation, all the machines are fully optimized.

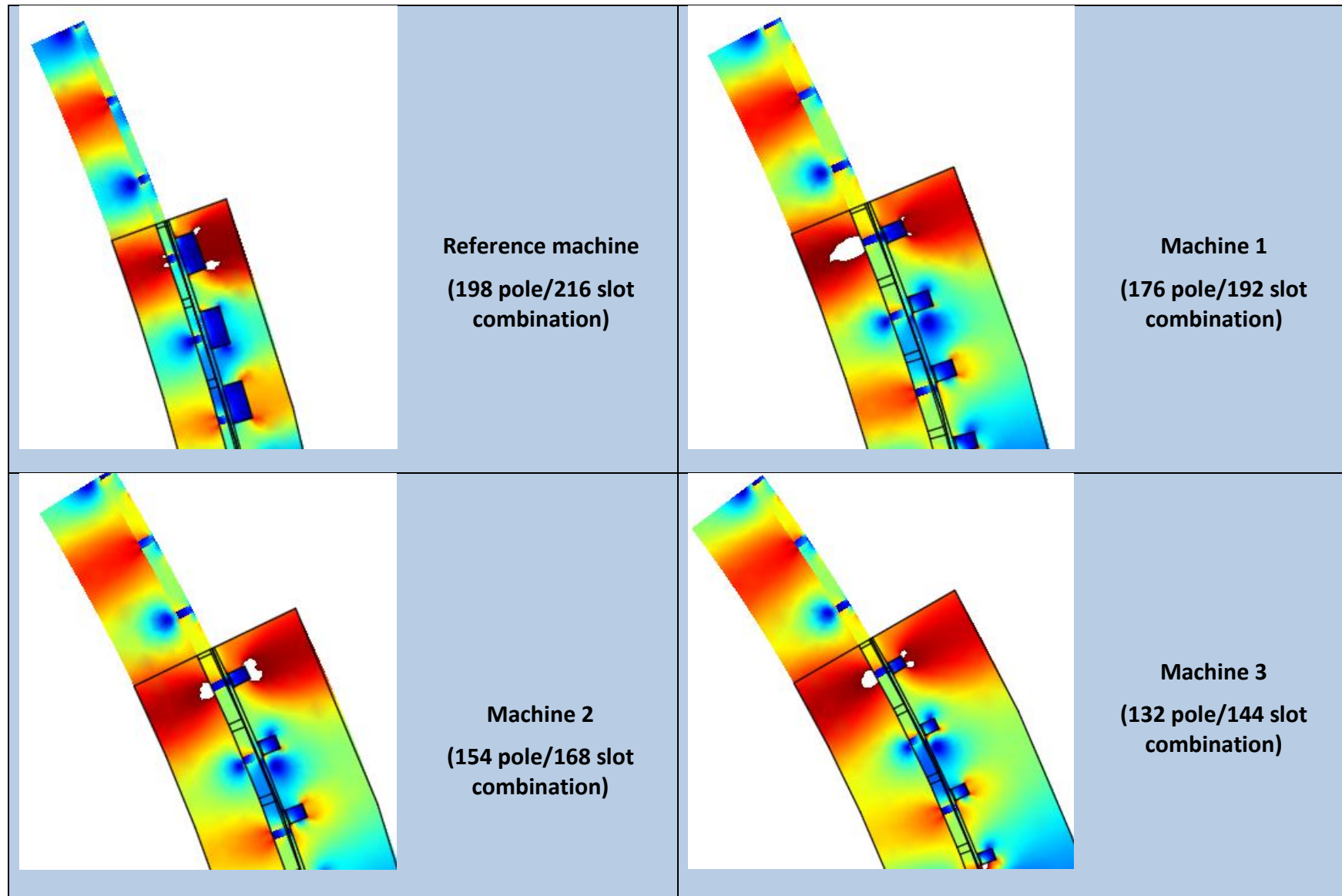


Figure 5.7: Comparison of magnetic saturation ($B=0$ to 1.7 T for all machines).

5.7 Comparison of losses in the machines

Further to the comparison between the machines, it is important to discuss the no-load losses and full load losses of the machines. Finite element analysis results have been taken as reference for more precise information. The losses in the machines have been extracted in Table 5.5 from the complete results presented in Appendix D, E, F and G.

Table 5.5: Summary of losses in all machines.

Parameters	Reference Machine	Machine 1	Machine 2	Machine 3
FEA results				
Iron loss in stator at no-load (kW)	23.593	14.641	14.682	14.650
Iron loss in rotor at no-load (kW)	1.5612	0.224	0.2374	0.331
Induced loss in magnets at no-load (kW)	677.416	17.924	16.744	14.093
Iron loss in stator at full load (kW)	60.757	36.722	40.621	43.462
iron loss in rotor at full load (kW)	36.787	27.327	30.873	36.650
Induced loss in magnets at full load (kW)	1526.113	891.624	1126.868	1497.059
Losses in winding (kW)	334.380	0*	0*	0*
Total losses at full - load(kW)	1958.037	955.653	1198.362	1577.171

*Note: AC losses in superconducting machines are not included.

From Table 5.5, it can be observed that the total loss at full load in a 10 MW of reference machine is about 2 MW which is excessively high and very abnormal for a practical machine. The major contributor of the loss is induced loss in magnets. In these machines, the magnetic poles have been simulated as a single piece of magnet which are effected by eddy current loss and time harmonics of the stator currents [45]. Therefore, these FEA results can be taken only as a reference for comparison purpose. Even the losses of all the machines are excessively high, for similar structure of magnet i.e. single piece of magnet per pole for all the machines, the machine - 1 with superconductor incurs the least loss and is about 50% of the reference machine.

The induced losses in magnets can be reduced greatly by segmentation of the magnets as shown in Figure 5.8. The segmenting can be in axial and circumferential and the number of segments can be decided depending upon the type of magnet and the possible length of manufacturability as shown in Figure 5.9. Both the axial and circumferential segmentation significantly reduces the losses and the combined effect will be even better in the direction of reduction of induced losses in magnets [46].

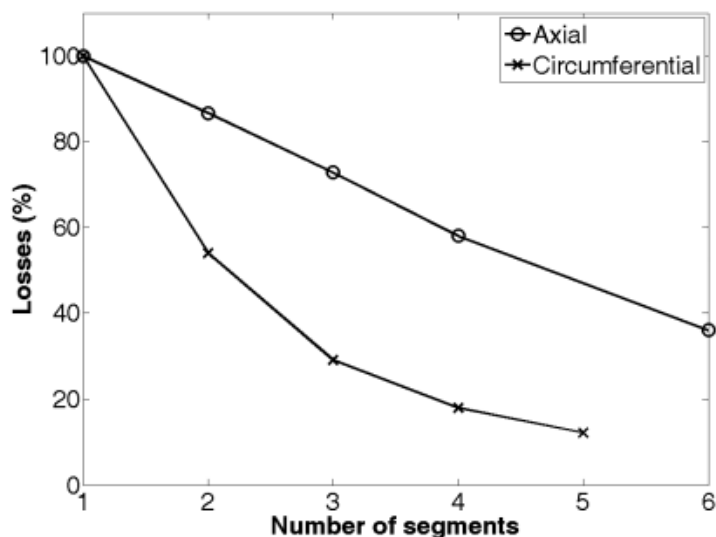


Figure 5.8: Effect of segmentation on magnet losses [47].

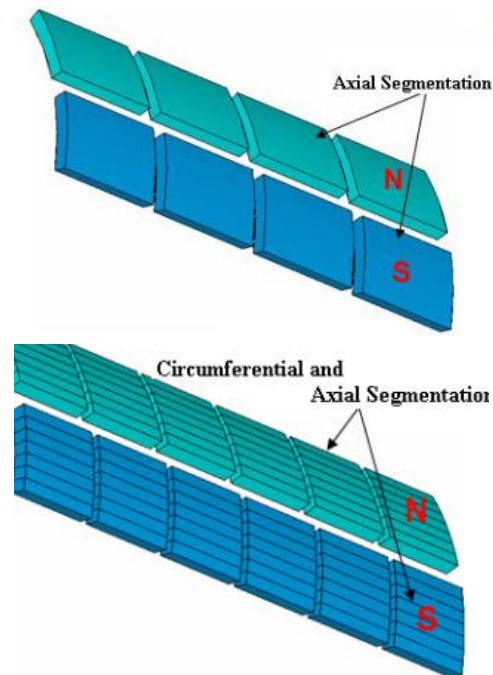


Figure 5.9: Axial and circumferential segmentation of magnet [48].

The improvement in full load losses for reference machine obtained from the FEA simulation with 17 segments (pole width is 17 cm and 1 cm of each segment) of the magnet along circumferential direction is presented in Table 5.6

Table 5.6: Losses in reference machine with and without segmentation of magnet.

Parameters	Reference Machine	Reference machine with 17 segments of magnet
FEA results		
Induced loss in magnets at no-load (kW)	677.42	13.01
Iron loss in stator at full load (kW)	60.76	60.99
iron loss in rotor at full load (kW)	36.79	37.31
Induced loss in magnets at full load (kW)	1526.11	18.41
Losses in winding (kW)	334.38	335.25
Total losses at full - load(kW)	1958.04	451.96

The results in Table 5.6 and the graphical representation in Figure 5.10 evidently assert that the induced loss in magnet at full load with segmentation is only 7 % of the same without segmentation. The stack length of the machine is 1.2 m and due to manufacturability limits, there will be some further segmentation in axial direction as depicted in Figure 5.9 and hence further reduction in induced losses can be achieved.

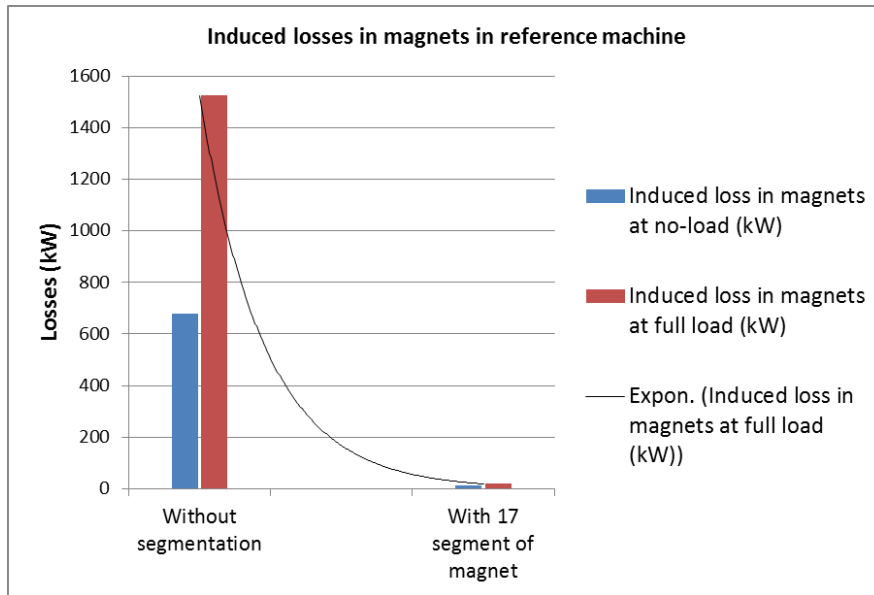


Figure 5.10: Induced losses in magnets of reference machine with and without segmentation.

Based on the results listed in Table 5.6 and Figure 5.8, it can be assumed that the similar segmentation for the SC machine will yield similar reduction in induced losses and will have very low total loss at full load. Since the major objective of this work was to study the effect of superconducting windings on dimensions of the machine, the segmented magnet has not been implemented and simulated. In the way to further development of superconducting machine, it is regarded as a future work to analyze the machine with segmentation of magnet or a conducting foil around the rotor to avoid the induced losses in magnets.

5.8 Harmonics and cogging torque

5.8.1 Harmonics

Harmonic content in voltage or current is used to measure the power quality of any system. Harmonics is the presence of component multiple of fundamental frequency component in voltage or current of a machine. Total harmonic distortion (THD) is one of the most important parameter to measure the harmonic content in output emf of any machine. THD is the summation of all the harmonic component of voltage compared to the fundamental component. It can be expressed mathematically as in eq. (5.1).

$$THD = \frac{\sqrt{V_2^2 + V_3^2 + V_4^2 + \dots + V_n^2}}{V_1} \times 100 \% \quad (5.1)$$

Where, $V_2, V_3, V_4 \dots V_n$ are harmonic component and V_1 is the fundamental component of the emf of a machine.

A regulation promulgated by Danish Energy Authority mentions that THD for large wind power generators should be smaller than 1.5 % [49].

The THD present in the phase voltage and line voltage of the reference machine and proposed SC machines are listed in Table 5.7.

Table 5.7: THD in phase and line voltage of all machines.

Parameters	Reference machine	Machine - 1	Machine - 2	Machine - 3
Phase voltage, 1 st harmonics (rms), V	1628	1433	1404	1370
Phase voltage maximum (rms), V	1610	1277	1234	1186
THD (%)	1.14 %	11.70 %	13.20 %	15.00 %
Line voltage, 1 st harmonics (rms), V	2820	2482	2432	2372
Line voltage maximum (rms), V	2847	2467	2409	2336
THD (%)	1.13%	0.95%	1.15%	1.52%

It can be observed from the Table 5.7 and Figure 5.11 that there is quite high content of harmonics in phase emf of superconducting machines compared to the reference machine. It is due to the presence of high amplitude harmonic emf, predominantly due to 3rd harmonics. But, in three phase power system, line voltage is the important parameter rather than the phase voltage and evidently as shown in Figure 5.12, the 3rd harmonic component is completely eliminated due to star connection of the generator terminals. Consequently, the total harmonic distortion of the SC machines reduces to 1.0 – 1.5 % which is in range of the tolerable limit recommended by Danish Energy Authority for wind power machines.

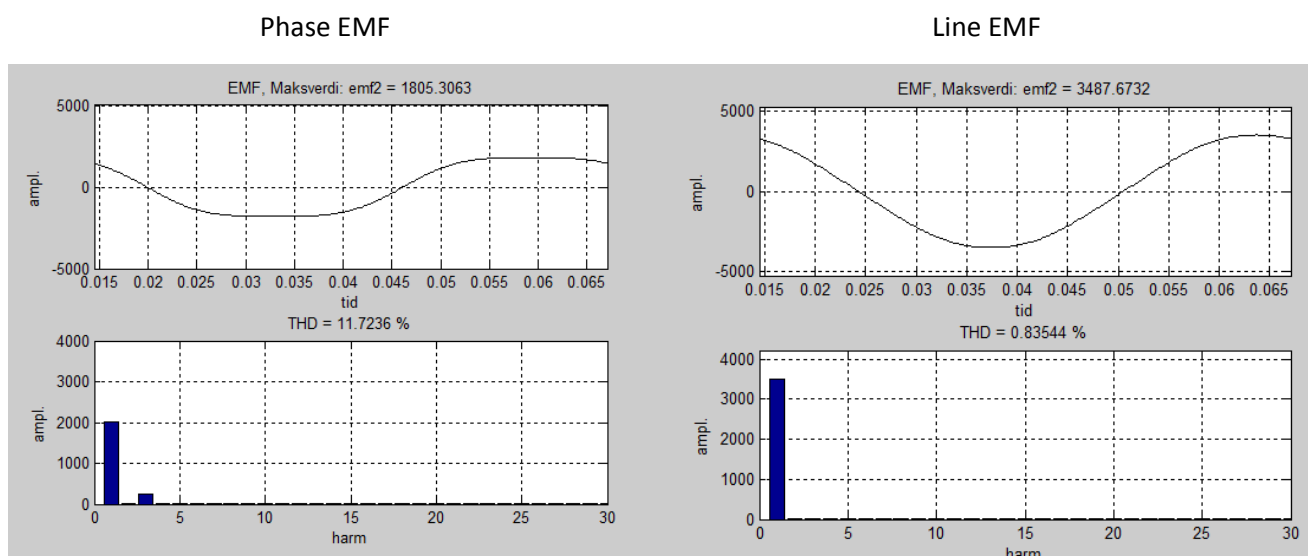


Figure 5.11: Waveform and harmonic content of phase voltage of Machine - 1.

Figure 5.12: Waveform and harmonic content of line voltage of Machine - 1.

From Table 5.7, the numerical values of THD for machine – 1 is even lower than that of reference machine and the other SC machines.

5.8.2 Cogging torque

Cogging torque is the torque due to the interaction between the permanent magnet poles on the rotor and the stator slots. Such torque causes ripple in mechanical torque produced by the machine which leads to mechanical vibration, acoustic noise and problems [50, 51]. Therefore, cogging torque should be minimized during the design process.

The cogging torque in the reference machine and the proposed machines with superconductors obtained from FEA results are shown in Table 5.8.

Table 5.8: Cogging torque and torque ripple of all machines.

Parameters	Reference machine	Machine - 1	Machine - 2	Machine - 3
Cogging torque amplitude at no-load (N.m)	393.2	302.8	1587	4744.7
Mean torque at full load (kN.m)	7640.16	7647.11	7671.71	7756.74
Torque ripple amplitude at full load (pu)	0.84 %	0.76 %	1.11 %	1.60 %

Here, it can be observed that the no-load cogging torque and torque ripple at full load produced in proposed SC machine -1 is lowest among all the SC machines and the reference machine.

5.9 Selection of machine

The analysis in Section 5.1 to 5.8 compares the several parameters of the reference machine (copper winding machine) and the three other machines optimized with superconducting armature winding.

Figure 5.13 summarizes the weight and volume characteristics of all machines. The vertical axis represents the weight of the machine. Here, the SC Machine – 1 is at lowest level representing the least weight and has smallest outer diameter among all the machines. It can also be noticed in the figure that moving from Machine – 1 in direction to Machine – 3, the yoke thickness is increasing. The decreasing number of pole and slot combination consequently increases the flux density in the core which causes the yoke to become thicker and the overall machine weight to be heavier. Hence, Machine – 1 has the best characteristics among the all machines discussed here.

As compared in previous sections, the superconducting machine -1 can be compared to the reference machine in Figure 5.14. The figure displays the advantage of SC machine with reduction in the volume of the nacelle corresponding to the reduction in volume of the generator. The volume and weight reduction in case of offshore wind power application have further indirect benefits like cost reduction in transport weight and in material cost of the nacelle.

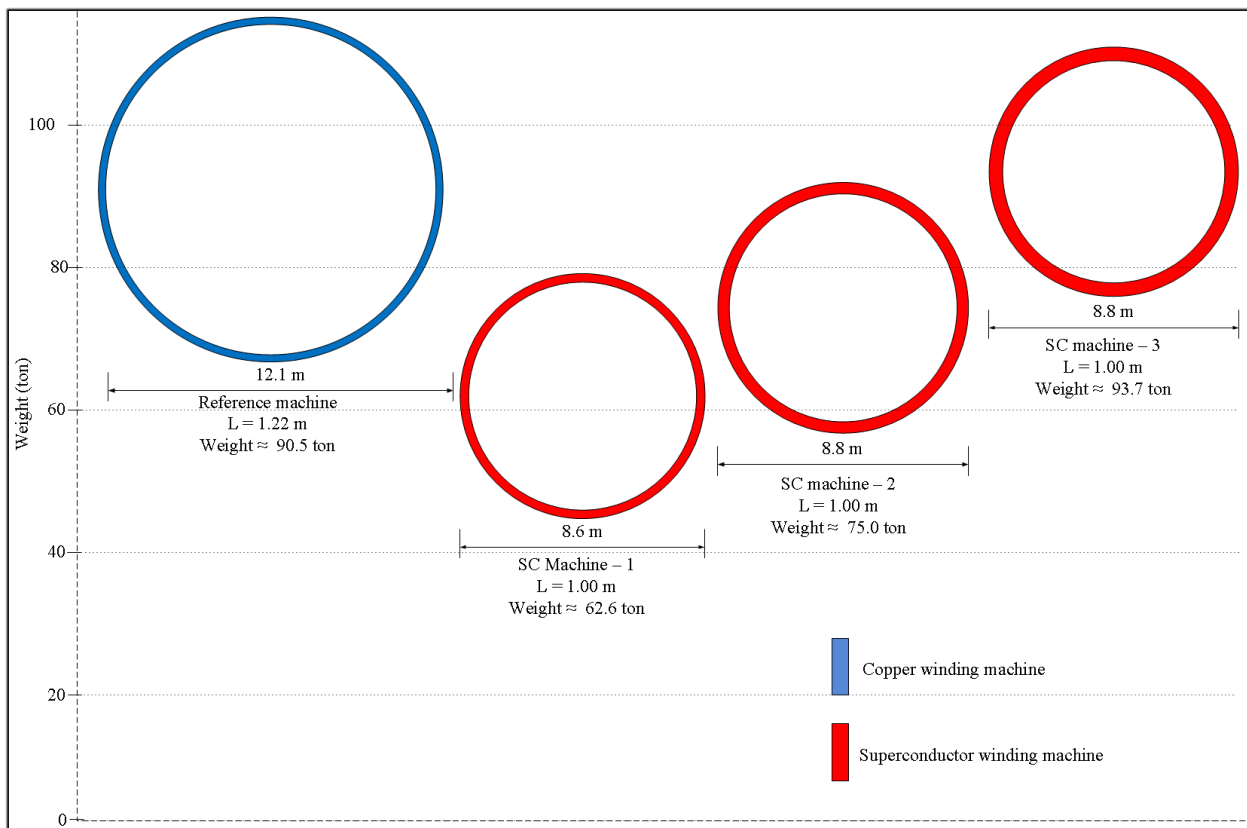


Figure 5.13: Comparison of diameter and weight of all machines.

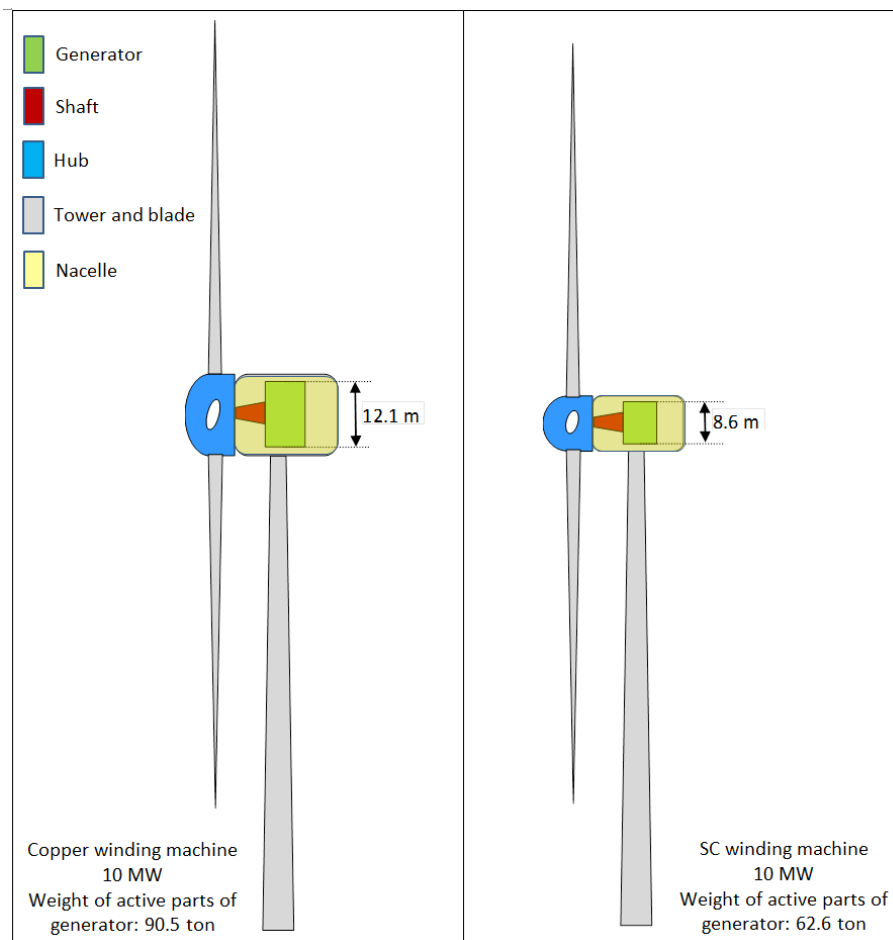


Figure 5.14: Comparison of Copper winding machine and SC winding machine.

The other characteristics can also be mapped as in Table 5.9. The mapping shows that Machine 1 (with 176 pole and 192 slots) has almost all characteristics better than the rest of the alternatives. The Torque resulted from FEA simulation is 7647.1 kN·m for Machine – 1 and 7756.7 kN·m for Machine – 3 which is about 1.4 % higher than the first one. Also, the weight of the magnet used in machine – 3 is 5172 Kg whereas that for machine – 1 is 5206 Kg. A merely 34 Kg extra weight of magnet cannot be an inferior quality since the machine -1 has very low weight compared to machine – 3 and all other features.

Table 5.9: Map of the characteristics of superconducting machines.

Parameters	Machine - 1	Machine - 2	Machine - 3	Remarks
Power (kW)	10000	10000	10000	
Torque (N.m)			x	Highest based on FEA results
Weight (Kg)	x			Lowest
Power to Weight ratio (W/Kg)	x			Highest
Torque to Weight ratio (N·m/Kg)	x			Highest
Outer volume	x			Lowest
Weight of the magnet used			x	Lowest
Power factor	x			Best
Synchronous reactance	x			Lowest
Utilization factor based on Torque (k)	x			Highest
Utilization factor based on apparent power (C)	x		x	Highest
Size of converter required	x			Smallest
Total harmonic distortion (THD)	x			Least
Torque ripple	x			Least

Based on all of the design characteristics of superconducting machines presented in this chapter, Machine – 1 can be selected as the best alternative with superconducting armature winding.

5.10 Limit of AC loss in superconductor

All the no-load loss components for SC machine are lower than that of reference machine. The SC machine draws smaller current at no-load than that of reference machine and therefore, has lower losses at no-load. In full load operation, the copper winding has a higher losses due to its finite resistivity and in this case, the reference machine has a copper loss of 334.38 kW where as there is no loss in SC machine (the 11.37 W of loss displayed in output panel of SmartTool is due to the finite conductivity of 58×10^{12} S/m set in SmartTool). There must be some AC losses due to varying magnetic field inside the slot i.e. inside the conductor area. The experimental results was supposed to take into account to determine the actual loss in the SC machine and to calculate the efficiency but it could not be received from SINTEF due to some delay in measurements. The measurements of AC losses for MgB₂ superconducting wire from Columbus Superconductor, Italy are yet to be carried out. Therefore, the permissible losses in the SC wire that can be tolerated for this design in comparison to reference machine have been determined.

According to [52], MgB₂ wires would be suitable for applications at 20 K in low magnetic fields (critical temperature, T_c of MgB₂ is 39 K [53]) which is easily obtainable using commercially available cryocoolers. Therefore, 20 K has been taken as operating temperature of MgB₂ superconducting wire.

$$\text{Carnot factor, } \eta_{carnot} = \frac{T_{amb} - T_{low}}{T_{low}} = \frac{300 - 20}{20} = 14$$

The actual efficiency of real refrigerators is often only 10% of the Carnot efficiency [54]. Therefore, taking into account the cooling efficiency of cryogenic refrigerator as 10%,

$$\text{Cooling penalty factor, } \eta_{cp} = \eta_{carnot} \frac{1}{\eta_{cooling}} = 14 \times \frac{1}{10\%} = 140$$

Since the superconductors in the AC armature winding will be thermally isolated from the rest of the machine parts, the losses in the windings will only be accountable for the cryogenic cooling system. The comparable loss for the SC machine w.r.t. copper winding machine is only the losses in winding. The relation between AC losses in SC (P_{ac}) and equivalent losses in copper winding (P_{cu}) can be established as:

$$P_{ac} \times \eta_{cp} < P_{cu}$$

$$\Rightarrow P_{ac} < \frac{P_{cu}}{\eta_{cp}} = \frac{334380 \text{ W}}{140} = 2388 \text{ W}$$

i.e. 2388 W of full load AC losses can be tolerated in SC machine at a varying field with peak flux density of 0.39 T.

One of the comparable parameter of AC losses in superconductor is per unit current and per unit length losses in mW/A·m.

Active length of the machine (L) = 1008 mm

Straight tooth width (W_{ts}) = 105 mm

Slot width (W_s) = 30 mm

The mean length of the end turn outside the slot can be assumed to be half circle with a diameter of ($W_{ts} + W_s$) = 135 mm diameter.

Length of end winding of one turn of SC machine (l_{end}) = ($L + \pi \times 135/2$) mm = 1220 mm

Total length conductor used in the machine (l_{tot}) = $l_{end} \times$ number of turns \times number of slots
 $= 1.22 \text{ m} \times 34 \times 192$
 $= 7965 \text{ m}$

Full load current (I_{fl}) = 2178 A

Number of parallel paths (z) = 6

Full load current through each conductor (I_{flc}) = $\frac{I_{fl}}{z} = \frac{2178 \text{ A}}{6} = 363 \text{ A}$

Per unit current per unit length losses in SC = $\frac{P_{cu}}{I_{flc} \times l_{tot}} = \frac{2388 \text{ W}}{363 \text{ A} \times 7965 \text{ m}}$
 $= 0.82 \frac{\text{mW}}{\text{A.m}}$

According to [55], the AC loss measurement on Ag/Bi (2223) at 77 K, frequency of 47 Hz and an applied field of $B = 63 \text{ mT}$, the normalized power loss (P_{ac}/I_c) per metre of conductor length without twisting is 0.68 mW/Am and 0.53 mW/Am with twist, respectively.

Calculations of AC losses using mathematical equations presented in Table 2.1

Taking reference of the Inspection Report of DC superconductor from Columbus superconductor attached in Appendix B,

Cross-section of superconductor wire (A) = 1.476 mm²

Then, the radius of the conductor,

$$R = \sqrt{\frac{A}{\pi}} = \sqrt{\frac{1.476}{\pi}} = 0.685 \text{ mm}$$

At an operating temperature of $T = 20 \text{ K}$, Critical current density $J_c = 281.2 \text{ A/mm}^2$ and critical transport current $I_c = 415 \text{ A}$.

Using the expression mentioned in Table 2.1,

$$\text{Penetration depth } (b_p) = \frac{2\mu_0 J_c R}{\pi} = \frac{(2 \times 4\pi \cdot 10^{-7} \times 281.2 \cdot 10^{-6} \times 0.685 \cdot 10^{-3})}{\pi}$$

$$= 0.154 \text{ T}$$

From the results shown in Figure 5.15, the peak magnetic field inside the slot is 0.39 T, i.e. $b_0 = 0.39$ T.

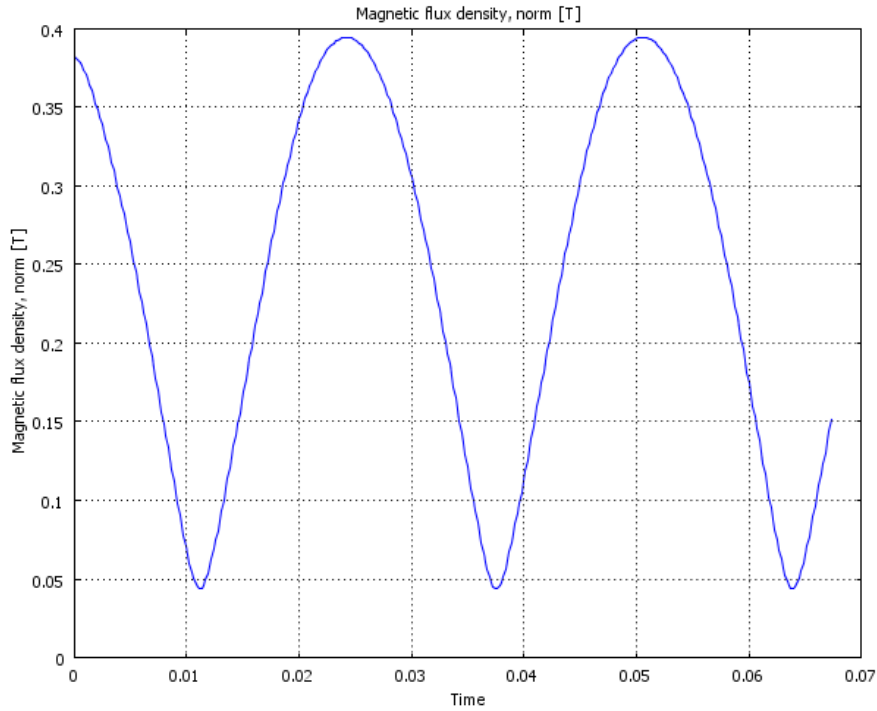


Figure 5.15: Variation of flux density at the center of a slot.

Now,

$$\beta = \frac{b_0}{b_p} = \frac{0.39 \text{ T}}{0.154 \text{ T}} = 2.53$$

The hysteresis loss per unit volume per cycle will be

$$Q_h = \frac{4b_0^2}{3\mu_0} \left(\frac{(2 - \beta^{-1})}{\beta} \right)$$

$$= 102.36 \cdot 10^3 \text{ J/m}^3/\text{cycle}$$

The total loss can be calculated using the eq. (2.3)

$$P_{ac} [W/m] = f \cdot C_f \cdot A \cdot Q_h = 2.87 \text{ W/m}$$

Here, the fitting parameter, C_f has been taken as 1 in this case since the sample superconductor from Columbus Superconductor is of DC type and the coupling effect is quite dominant in such type making all the filament matrix to behave has a single conductor.

Normalized AC loss per unit length per ampere,

$$P_{ac} \left[\frac{W}{A \cdot m} \right] = \frac{P_{ac} \left[\frac{W}{m} \right]}{I_{f1c}} = \frac{2.87 \frac{W}{m}}{363 \text{ A}} = 7.9 \frac{mW}{A \cdot m}$$

Similarly, the AC loss due to transport current (Q_t) can be calculated using eq. (2.2)

$$Q_t = \frac{\mu_0 I_c^2}{\pi} \left[(1 - i) \cdot \ln(1 - i) + \frac{(2 - i)i}{2} \right]$$

where,

$$i = \frac{I_0}{I_c} = \frac{363 \text{ A}}{415 \text{ A}} = 0.875$$

$$Q_t = \frac{4\pi \cdot 10^{-7} \times 415^2}{\pi} \left[(1 - 0.875) \cdot \ln(1 - 0.875) + \frac{(2 - 0.875) \cdot 0.875}{2} \right]$$

$$= 0.016 \text{ J/m}^3/\text{cycle}$$

Since this calculated loss due to transport current is very small compared to hysteresis loss, it can be neglected for this analysis.

The experimental measurements for a mono-filamentary MgB₂ wire as shown in Figure 5.16 shows a loss of $4 \times 10^4 \text{ J/m}^3/\text{cycle}$ at an AC magnetic field of 400 mT and an operating temperature of 30 K [56]. The normalized loss according to this measurement in this case using the eq. (2.3) results to be 1.12 W/m and for a current of 363 A, it will be as 3 mW/A·m.

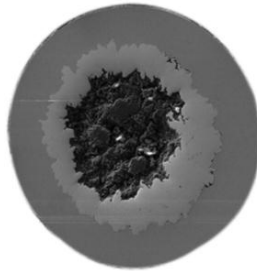


Figure 5.16: Cross-section of a mono-filamentary wire [56].

The above calculations can be summarized as follows:

Context	Normalized loss in mW/A·m
Tolerable loss in proposed superconducting machine at an operating temperature of 20 K, AC field of 0.39 T and with a round cross-section of conductor to be 1.476 mm ²	0.82 mW/A·m
Hysteresis loss in the proposed machine – 1 with DC superconductor wire where maximum coupling between filament has been considered (using eq. in Table 2.1)	7.90 mW/A·m
Hysteresis loss in proposed machine - 1 calculated using the experimental measurements in [56]	3.0 mW/A·m
AC loss on Ag/Bi (2223) at 77 K, frequency of 47 Hz and an applied field of B = 63 mT without twisting [55]	0.68 mW/A·m
AC loss on Ag/Bi (2223) at 77 K, frequency of 47 Hz and an applied field of B = 63 mT with twisting [55]	0.53 mW/A·m

From the calculations above, it can be conferred that to have same losses as in copper conductor machine, the AC superconductor wire should be manufactured such that it will possess at least 10 times lower loss than the dc superconductor attached in Appendix B. This requirement can be met by making thinner filament and applying twisting configurations or some other new technology to avoid coupling between the filaments.

The calculated value of 0.82 mW/A·m refers to 0.39 T of magnetic field which is 6 times higher than the losses measured in [55] and, therefore, the calculated loss requirement is challenging. But, the data corresponding to 20 K of operating temperature and the experimentally measured data from SINTEF would have been relevant for comparison. Since, further research is still going on in field of AC superconductors, the loss of 0.82 mW/A·m for an applied field of 0.39 T may be envisaged for a viable ac machines with superconducting armature windings.

Even the machine can achieve a utilization factor of about 2.5 times higher with the use of superconductor, the cost associated with it is relevant to discuss. The additional costs associated are mechanical arrangement of coils and cooling ducts, cooling of end turns and the cost of the cryo-cooler. In case of offshore wind power where the transportation cost and volume of the equipment also increase the cost significantly, the reduction in volume and weight of wind power generator with application of SC may lead to practical ease in the development.

5.11 Effect of increased thickness of magnet

As discussed earlier in Section 5.5, superconducting machines have lower power factor and consumes higher reactive power than the copper winding reference machine. This effect can be minimized to some extent by using some additional magnet on the rotor which is equivalent to increasing the excitation in a wound rotor machine.

The significant parameters affected by the change in magnet thickness can be summarized as in Table 5.10. The complete result is attached in Appendix H.

Table 5.10: List of parameters changed with increase in thickness of magnet.

Affected parameters	Reference machine	SC machine – 1 (with 30 mm magnet)	SC machine – 1 (with 50 mm magnet)
Power factor	0.84	0.80	0.91
Synchronous reactance	0.55	0.59	0.42
Weight of magnet used	6020 Kg	5206 Kg	8653 Kg
Total weight of active materials of the generator	90460 Kg	62590 Kg	53444 Kg
Reactive power requirement	5.48 MVar	5.94 MVar	4.17 MVar

From the Table 5.10, it can be observed that the weight of the proposed machine can further be decreased by about 9 ton using higher amount of magnet. Referring to eq. (3.12), the increase in magnet thickness increases the air-gap flux density ($\hat{B}_{\delta l}$) and a smaller current density (\bar{A}) is required to achieve the same power. The smaller current density adds up smaller field in the core and it helps to reduce the stator and rotor yoke thickness; and hence the total weight of the machine also comes down.

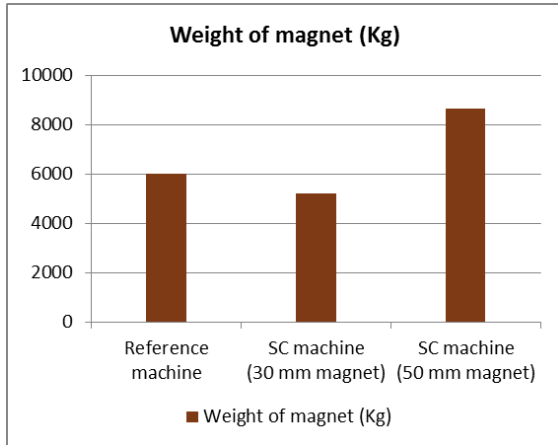


Figure 5.17: Effect on weight of magnet.

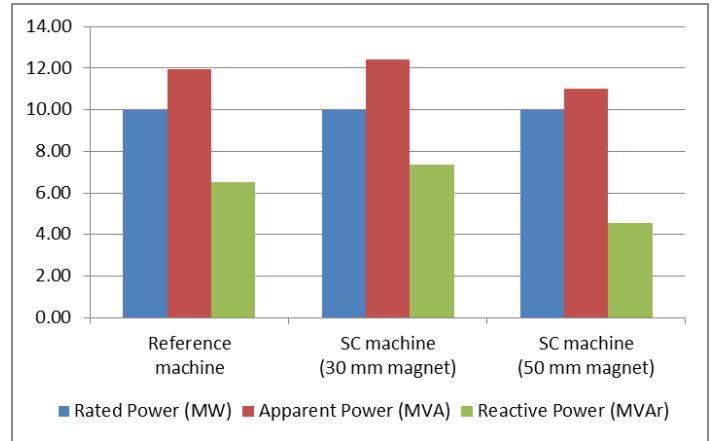


Figure 5.18: Effect on reactive power due to magnet thickness.

As presented in Figure 5.17, the weight of the magnet increases by weight by 3447 Kg (from 5206 Kg to 8653 Kg) and can be the additional burden in cost but it may be overcome by the reduction in total weight and size of the machine and consequently in reduction of the size of the nacelle and reduction in weight burden of the tower.

The increase in magnet thickness leads to increased induced voltage and hence better power factor than the proposed machine – 1 with 30 mm of magnet. The power factor of the machine improves from 0.80 to 0.90 which will help to decrease the size of the converter as well compared to the size required in combination with the copper winding reference machine. As displayed in Figure 5.18, the reactive power requirement decreases by almost 2 MVA than that in case of SC machine with 30 mm of magnet.

Based upon the above comparisons, a SC machine with 50 mm of magnet can also be an alternative which needs to be further analyzed for economic parameters, especially the cost comparison of magnet weight versus cost of converter capacity for reactive power demand.

Chapter 6

6 Conclusion and future work

6.1 Conclusion

As presented in this work, using superconductor, a 10 MW wind power generator with outer diameter of 12.1 m and a weight of 90 ton can be squeezed to a size with diameter of 8.8 m and a weight of 62 ton. Evidently, it seems promising in application of wind power machine where the weight burden on tower, transportation weight and volume of the appurtenances are of great importance. The reduction in volume of the superconducting machine increases the utilization factor by almost 2.5 times of the conventional copper winding machine based on both the mechanical torque and apparent power.

The AC losses associated with superconductors while employed in armature winding is a matter of serious concern. A penalty factor of 140 has been calculated for MgB_2 superconductor at an operating temperature of 20 K. It has been found that a superconductor with normalized AC loss of 0.82 mW/A·m can make a 10 MW superconducting machines to have equal loss as of copper winding machine. Therefore, any superconductor with a unit loss lower than 0.82 mW/A·m can be an alternative of copper winding machine in compact volume and reduced weight.

The mathematical calculation shows that a DC type MgB_2 superconductor will have a loss of 7.9 mW/A·m with a cross-section of 1.476 mm^2 at 20 K in presence of an AC magnetic field of 0.39 T. Hence, referring to the tolerable loss limit of 0.82 mW/A·m, it can be deduced that AC superconductors need some technology to reduce the losses in DC superconductors by at least 10 times to be feasible in comparison to copper winding machine.

Some negative aspects of the superconducting machines can also be observed are the poor power factor and the requirement of additional equipment for cooling of superconductors. These negative aspects of the machine can be compensated from a huge reduction of 28 ton weight in active parts of the generator and a 2.5 times reduction in its volume.

Another approach to have a further improvement in electrical characteristics of the superconducting machine is to increase the thickness of permanent magnet by 20 mm (from an earlier design with 30 mm to 50 mm) which yields a reduction of further 9 ton of weight than the SC machine with 30 mm of magnet and an improved power factor in the machine. Further to this, it demands about 2 MW of lesser reactive power than of copper winding machine but with an additional magnet of 2633 Kg. Therefore, the SC machine – 1, either with 30 mm or 50 mm of magnet can be selected depending upon the cost per unit of reactive power and magnet.

Finally, it can be concluded that wind power generators with superconducting armature windings can be an attractive alternative in future as the reduction in weight and volume of the machine saves significant material and cost.

6.2 Future work

- The conclusion lacks the comparison of electrical losses between the copper winding machine and that with superconductors due to unavailability of experimentally measured data of AC superconductors. The experiment is being carried out at SINTEF. The actual value of AC losses will give idea of cooling equipment and the feasibility of superconducting machines.
- The exact size and cost of cryo-cooler should be considered for final selection of the system. The analysis shows that the converter size may increase due to higher demand of reactive power and therefore, cost and efficiency of converter should also be taken into account for selection of an overall system.
- The increase in magnet thickness shows the system to be even more compact but the cost of magnet may be a burden. Detail cost analysis should be carried out of the machine.
- Superconducting machine seems to be attractive in context of weight and dimension but the mechanical assembly seems to be challenging. The arrangement of cooling in the slots, connecting the series coils, cooling of end turns need further research to execute in practice. Cooling seems even more challenging if the conductors are glued inside epoxy to avoid vibration due to electromagnetic forces acting on it.
- Since this work has been carried out with an imagination of superconductor inside the steel core slots with insulation around it. The FEA simulation with exact configuration i.e. insulation around the conductors inside the slots and with segmentation of magnets is also necessary to refine the presented results in this work.

References

- [1] J. Eck. (2010). *Type 1 Superconductors*. Available: <http://www.superconductors.org/Type1.htm>
- [2] R. W. Dull. (1994). *A Teachers Guide to Superconductivity for High School Students*.
- [3] T. Vieru. (2012, 2012.05.16). *Superconductivity Understood at a Microscopic Level*. Available: <http://news.softpedia.com/news/Superconductivity-Understood-at-a-Microscopic-Level-262433.shtml>
- [4] (1996, 2011/08/25). *Fundamentals of Superconductor*. Available: <http://www.ornl.gov/info/reports/m/ornlm3063r1/pt3.html>
- [5] S. S. Kalsi, "HTS Superconductors," in *Applications of High Temperature Superconductors to Electric Power Equipment*, ed: John Wiley & Sons, Inc., 2011, pp. 7-34.
- [6] M. Tinkham, *Introduction to Superconductivity*: Dover Publications, 2004.
- [7] *Meissner effect*. Wikipedia, The free encyclopedia, 2012, p.^pp. Pages.
- [8] R. Nave. *Superconductivity*. Available: <http://hyperphysics.phy-astr.gsu.edu/hbase/solids/scond.html>
- [9] M. P. Oomen, "AC loss in superconducting tapes and cables," Enschede, The Netherlands, 2000.
- [10] R. M. Scanlan, A. P. Malozemoff, and D. C. Larbalestier, "Superconducting materials for large scale applications," *Proceedings of the IEEE*, vol. 92, pp. 1639-1654, 2004.
- [11] M. Chen, L. Donzel, M. Lakner, and W. Paul, "High temperature superconductors for power applications," *Journal of the European Ceramic Society*, vol. 24, pp. 1815-1822, 2004.
- [12] M. Tomsic, M. Rindfleisch, J. Yue, K. McFadden, J. Phillips, M. D. Sumption, M. Bhatia, S. Bohnenstiehl, and E. W. Collings, "Overview of MgB₂ Superconductor Applications," *International Journal of Applied Ceramic Technology*, vol. 4, pp. 250-259, 2007.
- [13] J. Eck. (2010). *Uses for Superconductors*. Available: <http://www.superconductors.org/Uses.htm>
- [14] A. Grauers, "Design of Direct-driven Permanent-magnet Generators for Wind Turbines," Institutionen för elkraftteknik, Elmaskinteknik och kraftelektronik, Chalmers tekniska högskola, 1996.
- [15] O. Anaya-Lara, N. Jenkins, J. Ekanayake, and P. Cartwright, "Wind Energy Generation: Modelling and Control," ed: John Wiley & Sons, 2009, pp. 99-103.
- [16] S. S. Kalsi, "Rotating AC Machines," in *Applications of High Temperature Superconductors to Electric Power Equipment*, ed: John Wiley & Sons, Inc., 2011, pp. 59-128.
- [17] A. M. L.-. Energy. (2009). *Superconducting Generators, an "Industrial Revolution" in Energy*. Available: <http://www.amcleanenergy.com/why-offshore-first/page-4/>

- [18] W. Cao, "High-Temperature Superconducting Wind Turbine Generators," in *Wind Turbines*, D. I. Al-Bahadly, Ed., ed: InTech, 2011, pp. 623-638.
- [19] M. Daumling, S. K. Olsen, C. Træholt, D. W. A. Willen, and A. Kuhle, "AC loss in superconducting power cables," *Studies of High Temperature Superconductors (A. Narlikar, ed.)*, vol. 33, p. 39, 2000.
- [20] N. Magnusson, "AC Losses in High-temperature Superconducting Tapes: Calorimetric Measurement System and Semi-empirical Modelling," Ph.D. Dissertation, Electrical Power Engineering, Royal Institute of Technology, Stockholm, Sweden, 2000.
- [21] W. T. Norris, "Calculation of hysteresis losses in hard superconductors carrying ac: isolated conductors and edges of thin sheets," *Journal of Physics D: Applied Physics*, vol. 3, p. 489, 1970.
- [22] M. Cizek, A. M. Campbell, S. P. Ashworth, and B. A. Glowacki, "Energy dissipation in high temperature ceramic superconductors," *Applied Superconductivity*, vol. 3, pp. 509-520, 1995.
- [23] C. Kittel, "Introduction To Solid State Physics," ed: John Wiley & Sons, 2005, pp. 273-278.
- [24] C. P. Bean, "Magnetization of High-Field Superconductors," *Reviews of Modern Physics*, vol. 36, pp. 31-39, 1964.
- [25] N. Magnusson, "Semi-empirical model of the losses in HTS tapes carrying AC currents in AC magnetic fields applied parallel to the tape face," *Physica C: Superconductivity and its Applications*, vol. 349, pp. 225-234, 2001.
- [26] S. P. Ashworth and D. W. Reagor, "A novel cooling scheme for superconducting power cables," *Cryogenics*, vol. 51, pp. 161-167, 2011.
- [27] D. C. Hanselman, *Brushless permanent-magnet motor design*: McGraw-Hill, 1994.
- [28] J. Pyrhönen, T. Jokinen, and V. Hrabovcová, *Design of rotating electrical machines*: Wiley, 2008, pp. 281.
- [29] D. Bang, H. Polinder, G. Shrestha, and J. A. Ferreira, "Review of Generator Systems for Direct-Drive Wind Turbines," presented at the Electrical Power Processing / DUWIND, Delft University of Technology, Mekelweg 4, 2628 CD Delft, The Netherlands, 2008.
- [30] H. J. Gutt and A. Grüner, "Definition of power density as a general utilization factor of electrical machines," *European Transactions on Electrical Power*, vol. 8, pp. 305-308, 1998.
- [31] M. Lindner, P. Brauer, and R. Werner, "Increasing the Torque Density of Permanent-Magnet Synchronous Machines using Innovative Materials and Winding Technologies," in *9th International Multi-Conference on Systems, Signals and Devices*, Chemnitz, Germany, 2012.
- [32] T. Haring, K. Forman, T. Huhtanen, and M. Zawadzki, "Direct drive-opening a new era in many applications," in *Pulp and Paper Industry Technical Conference, 2003. Conference Record of the 2003 Annual*, 2003, pp. 171-179.

-
- [33] F. Libert and J. Soulard, "Design Study of a Direct-Driven Surface Mounted Permanent Magnet Motor for Low Speed Application," *Proceedings of Symposium on Advanced Electromechanical Motion Systems Electromotion*, vol. 1, pp. 252-257, 2003.
- [34] J. E. Rucker, "Design and analysis of a permanent magnet generator for naval applications," Dept. of Electrical Engineering and Computer Science, Massachusetts Institute of Technology, Massachusetts Institute of Technology, 2005.
- [35] B. Kristoffersen, "Electrical machine," United States Patent, 2003.
- [36] F. Libert and J. Soulard, "Investigation on Pole-Slot Combinations for Permanent Magnet Machines with Concentrated Windings," *Proceedings of the International Conference on Electrical Machines, ICEM 2004*, pp. 530-535, 2004.
- [37] M. G. Say, *The performance and design of alternating current machines; transformers, three-phase induction motors and synchronous machines*: Pitman paperbacks, 1968.
- [38] A. Matveev, R. B. Ummaneni, E. M. Husum, B. Noddeland, N. Rotevatn, and A. Røkke, "SmartTool," 2011.
- [39] (2011.10.22). *COMSOL Multiphysics*. Available: <http://www.comsol.com/products/multiphysics/>
- [40] H. E. Leiseth and R. Nilssen, "10 MW Reference Wind Turbine," 2010.
- [41] N. Bracikowski, D. Ilea, F. Gillon, M. Hecquet, and P. Brochet, "Design of permanent magnet synchronous machine in order to reduce noise under multi-physic constraints," in *Electric Machines & Drives Conference (IEMDC), 2011 IEEE International*, 2011, pp. 29-34.
- [42] D. J. Griffiths, *Introduction to electrodynamics*: Prentice Hall, 1999.
- [43] (2012). *Shape, dimensions and materials*. Available: <http://www.columbussuperconductors.com/shape.asp>
- [44] Z. Zhaoqiang, A. Matveev, S. Ovrebo, R. Nilssen, and A. Nysveen, "State of the art in generator technology for offshore wind energy conversion systems," in *Electric Machines & Drives Conference (IEMDC), 2011 IEEE International*, 2011, pp. 1131-1136.
- [45] H. Polinder and M. J. Hoeijmakers, "Eddy-current losses in the segmented surface-mounted magnets of a PM machine," *Electric Power Applications, IEE Proceedings* -, vol. 146, pp. 261-266, 1999.
- [46] K. Yamazaki and Y. Fukushima, "Effect of Eddy-Current Loss Reduction by Magnet Segmentation in Synchronous Motors With Concentrated Windings," *IEEE Transactions on Industry Applications*, vol. 47, pp. 779-788, 2011.
- [47] J. Klötzl, M. Pyc, and D. Gerling, "Permanent magnet loss reduction in PM-machines using analytical and FEM calculation," in *2010 International Symposium on Power Electronics Electrical Drives Automation and Motion (SPEEDAM)*, 2010, pp. 98-100.
- [48] M. Mirzaei, A. Binder, and C. Deak, "3D analysis of circumferential and axial segmentation effect on magnet eddy current losses in permanent magnet
-

- synchronous machines with concentrated windings," in *Electrical Machines (ICEM), 2010 XIX International Conference on*, 2010, pp. 1-6.
- [49] *Wind Turbines Connected to Grids with Voltages above 100 kV, Technical Regulations for the properties and the regulation of Wind Turbines*, Danish Energy Authority, 2004.
- [50] Z. Q. Zhu and D. Howe, "Influence of design parameters on cogging torque in permanent magnet machines," in *Electric Machines and Drives Conference Record, 1997. IEEE International*, 1997, pp. MA1/3.1-MA1/3.3.
- [51] L. Dosiek and P. Pillay, "Cogging Torque Reduction in Permanent Magnet Machines," in *Industry Applications Conference, 2006. 41st IAS Annual Meeting. Conference Record of the 2006 IEEE*, 2006, pp. 44-49.
- [52] K. Kajikawa, T. Kawano, R. Osaka, T. Nakamura, M. Sugano, M. Takahashi, and T. Wakuda, "AC losses in monofilamentary MgB₂ round wire carrying alternating transport currents," *Superconductor Science and Technology*, vol. 23, p. 045026, 2010.
- [53] J. Nagamatsu, N. Nakagawa, T. Muranaka, Y. Zenitani, and J. Akimitsu, "Superconductivity at 39 K in magnesium diboride," *Nature*, vol. 410, pp. 63-64, 2001.
- [54] T. P. Sheahen, "Introduction to high-temperature superconductivity," ed: Plenum Press, 1994, pp. 63-64.
- [55] X. D. Su, G. Witz, K. Kwasnitza, and R. Flükiger, "Fabrication of square and round Ag/Bi(2223) wires and their ac loss behaviour," *Superconductor Science and Technology*, vol. 15, p. 1184, 2002.
- [56] C. Seyong, T. Kiyoshi, K. Jung Ho, and D. Shi Xue, "AC Loss in MgB₂ Superconducting Wires at Various Operating Temperatures," *Applied Superconductivity, IEEE Transactions on*, vol. 21, pp. 3342-3346, 2011.

Appendices

This page is intentionally left blank.

Table of contents

Appendix A	Possible pole slot combinations	73
Appendix B	Specification of MgB ₂ superconductor	74
Appendix C	Derivation of power loss in slot	75
Appendix D	FEA results of reference machine.....	76
Appendix E	FEA results of Machine – 1 (176 pole 192 slots).....	88
Appendix F	FEA results of Machine – 2 (154 pole 168 slots).....	101
Appendix G	FEA results of Machine – 3 (132 pole 144 slots)	113
Appendix H	FEA results of Machine – 1 (176 pole 192 slots with 50 mm magnet).....	125
Appendix I	FEA results of reference machine with segmentation of magnet	137

List of figures

Figure D.1: Combined input and output panel of reference machine.....	76
Figure D.2: Input parameters of reference machine.	77
Figure D.3: Magnetic flux density at no-load.	77
Figure D.4: EMF plot under no-load condition.....	78
Figure D.5: EMF waveform and harmonics of phase 1 EMF.	79
Figure D.6: EMF and harmonics of line voltage 1.	79
Figure D.7: EMF waveform and harmonics of phase 2 EMF.	79
Figure D.8: EMF and harmonics of line voltage 2.	79
Figure D.9: EMF waveform and harmonics of phase 3 EMF.	79
Figure D.10: EMF and harmonics of line voltage 3.	79
Figure D.11: Zoomed in part of core with maximum flux density under full load condition. .	80
Figure D.12: Plot of full load torque.....	80
Figure D.13 Plot of amplitude and harmonics of full load torque.	81
Figure D.14: Full load PM losses.....	81
Figure D.15: Plot of full load rotor core flux density.....	82
Figure D.16: Summary of FEA simulation results.	82
Figure D.17: COMSOL plot of magnetic flux density under full load.	84
Figure D.18: variation of flux density in stator core at a point close to slot.....	84
Figure D.19: Plot of magnetic flux density in a range of 0 to 1.7 T.	85
Figure D.20: Plot of relation permeability in a range of 1 to 500 at full load condition.....	86
Figure D.21: Plot of relation permeability in a range of 1 to 200 at full load condition.....	87
Figure E.1: Combined input output panel of optimized parameters of SC Machine – 1.....	88
Figure E.2: Input parameters of SC Machine - 1.	89
Figure E.3: EMF simulation plot under no-load condition.	89
Figure E.4: EMF plot under no-load condition.	90
Figure E.5: EMF waveform and harmonics plot of phase 1.	91

Figure E.6: EMF waveform of line voltage 1.	91
Figure E.7: EMF waveform and harmonics plot of phase 2.	91
Figure E.8: EMF waveform of line voltage 2.	91
Figure E.9: EMF waveform and harmonics plot of phase 3.	91
Figure E.10: EMF waveform of line voltage 3.	91
Figure E.11: Full load simulation plot.	92
Figure E.12: Plot of full load torque.	92
Figure E.13: Plot of amplitude of full load torque and harmonics.	93
Figure E.14: Plot of full load PM losses.	93
Figure E.15: Plot of full load rotor flux density.	94
Figure E.16: Summary of FEA simulation results.	94
Figure E.17: COMSOL plot of magnetic flux density at full load.	96
Figure E.18: Variation of flux density in stator core at a point close to slot.	96
Figure E.19: Plot of magnetic flux density in a range from 0 to 1.7 T.	97
Figure E.20: Plot of relative permeability in a range from 1 to 500 at full load condition.	98
Figure E.21: Plot of relative permeability in a range from 1 to 200 at full load condition.	99
Figure E.22: Variation of flux density at the centre of the slot.	100
Figure F.1: Combined input and output panel of optimized parameters.	101
Figure F.2: Input parameters for SC machine - 2.	102
Figure F.3: EMF simulation plot at no-load condition.	102
Figure F.4: EMF waveform at no-load condition.	103
Figure F.5: Plot of EMF and harmonics of Phase - 1.	104
Figure F.6: EMF waveform of line voltage 1.	104
Figure F.7: Plot of EMF and harmonics of Phase - 2.	104
Figure F.8: EMF waveform of line voltage 2.	104
Figure F.9: Plot of EMF and harmonics of Phase - 3.	104
Figure F.10: EMF waveform of line voltage 3.	104
Figure F.11: Magnetic flux density in stator and rotor yoke at full load.	105
Figure F.12: Full load torque.	105
Figure F.13: Plot of full load torque amplitude and harmonics.	106
Figure F.14: Full load PM losses.	106
Figure F.15: Rotor core flux density at full load.	107
Figure F.16: Summary of FEA simulation results.	107
Figure F.17: COMSOL plot of magnetic flux density at full load.	109
Figure F.18: Magnetic flux density in stator and rotor yoke at full load.	109
Figure F.19: Plot of magnetic flux density at full load in range from 0 to 1.7 T.	110
Figure F.20: Relative permeability in a range from 1 to 500 at full load.	111
Figure F.21: Relative permeability in a range from 1 to 200 at full load.	112
Figure G.1: Combined input and output panel of optimized parameters.	113
Figure G.2: Input parameters for Machine - 3.	114
Figure G.3: EMF simulation plot.	114

Figure G.4: EMF plot at no-load condition.	115
Figure G.5: Plot of EMF and harmonics of Phase - 1.	116
Figure G.6: EMF waveform of line voltage 1.	116
Figure G.7: Plot of EMF and harmonics of Phase - 2.	116
Figure G.8: EMF waveform of line voltage 2.	116
Figure G.9: Plot of EMF and harmonics of Phase - 3.	116
Figure G.10: EMF waveform of line voltage 3.	116
Figure G.11: Magnetic flux density at full load.	117
Figure G.12: Torque at full load.	117
Figure G.13: Plot of full load torque and harmonics amplitude.	118
Figure G.14: Full load PM losses.	118
Figure G.15: Plot of flux density in rotor core.	119
Figure G.16: Summary of FEA simulation results.	119
Figure G.17: COMSOL plot of magnetic flux density at full load.	121
Figure G.18: Variation of flux density in stator core at a point close to slot.	121
Figure G.19: Plot of magnetic flux density in a range from 0 to 1.7 T at full load.	122
Figure G.20: Relative permeability in range of 1 to 500 at full load.	123
Figure G.21: Relative permeability in range of 1 to 200 at full load.	124
Figure H.1: Combined input output panel of SC machine - 1 with 50 mm magnet.	125
Figure H.2: Input parameters of machine -1 with 50 mm magnet.	126
Figure H.3: EMF simulation plot at no-load.	126
Figure H.4: EMF waveform of 3-phases at no-load.	127
Figure H.5: EMF and harmonics of phase voltage of phase 1.	128
Figure H.6: EMF waveform of line voltage 1.	128
Figure H.7: EMF and harmonic of phase voltage of phase 2.	128
Figure H.8: EMF waveform of line voltage 2.	128
Figure H.9: EMF and harmonic of phase voltage of phase 3.	128
Figure H.10: EMF waveform of line voltage 3.	128
Figure H.11: Magnetic flux density at full load.	129
Figure H.12: Torque at full load condition.	129
Figure H.13: Torque and harmonic content at full load.	130
Figure H.14: PM losses at full load.	130
Figure H.15: Rotor core flux density at full load.	131
Figure H.16: Summary of FEA results.	131
Figure H.17: Surface plot of magnetic flux density at full load.	133
Figure H.18: Variation of flux density in stator yoke (just above the slot).	133
Figure H.19: Surface plot of magnetic flux density in range of 0 to 1.7 T at full load.	134
Figure H.20: Relative permeability in range of 1 to 500 at full load.	135
Figure H.21: Relative permeability in range of 1 to 200 at full load.	136
Figure H.22: Variation of flux density at the center of a slot.	136
Figure I.1: Combined input/output panel of reference machine with segmentation.	137

Figure I.2: FEA results of reference machine with segmentation..... 138

Appendix A Possible pole slot combinations

S.N.	n*m	Number of slots $s = (12*n*m)$	n	m	$s-p=2*m$	Number of Poles (p)	LCM of pole and slot
1	18	216	1	18	36	180	1080
	18	216	2	9	18	198	2376
	18	216	3	6	12	204	3672
	18	216	6	3	6	210	7560
	18	216	9	2	4	212	11448
2	16	192	1	16	32	160	960
	16	192	2	8	16	176	2112
	16	192	4	4	8	184	4416
	16	192	8	2	4	188	9024
3	14	168	1	14	28	140	840
	14	168	2	7	14	154	1848
	14	168	7	2	4	164	6888
4	12	144	1	12	24	120	720
	12	144	2	6	12	132	1584
	12	144	3	4	8	136	2448
	12	144	4	3	6	138	3312
	12	144	6	2	4	140	5040
5	10	120	1	10	20	100	600
	10	120	2	5	10	110	1320
	10	120	5	2	4	116	3480

(Ref: SmartMotor patent US6664692 B1)

Appendix B Specification of MgB₂ superconductor

STAC010

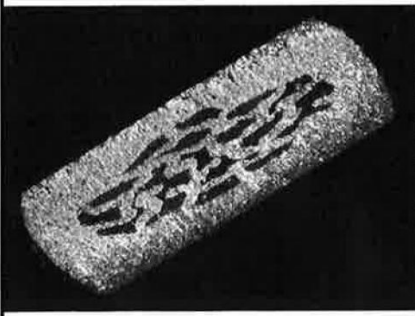
 <p>COLUMBUS</p>	RAPPORTO DI CONTROLLO <i>Inspection Report</i>				N° MC	
	<input type="checkbox"/> IN APPROVVIGIONAMENTO <i>on purchasing</i>		<input checked="" type="checkbox"/> IN FABBRICAZIONE <i>on manufacturing</i>		Pag. 1 of 1	
COMMESSA/Job CS0501	LOTTO/Lot	COMPONENTE/Item code MULTI1	DISEGNO/Drawing 651RC10501	POS/Item	REV./Rev 0	BOLLALAVORAZ./Work note
IMPIANTO plant	CLIENTE /customer		PCF N° PCF8010501/C????	REV./Rev. 3	POS/Item	
SPECIFICA/Specification			REV./Rev.	STAMPIGLIATURE/Stamps		
DESCRIZIONE PRODOTTO/Item Description Cavo multifilamentare stabilizzato MgB₂			MFT233_0.75			

Temperature T (K) and magnetic field B(T):

T/B	0	0,1	0,2	0,3	0,4	0,5	0,6	0,7	0,8	0,9	1	1,1	1,2	1,3	1,4	1,5	1,6	1,7	1,8
16 Ic							496		433		381		340		299		260		234
Jc							336		293,4		258,1		230,4		202,6		176,2		158,5
Jcs							2120		1850		1628		1453		1278		1111		1000
18 Ic																			
Jc																			
Jcs																			
20 Ic					415		344		288		235		205		171		144		122
Jc					281,2		233,1		195,1		159,2		138,9		115,9		97,56		82,66
Jcs					1774		1470		1231		1004		876,1		730,8		615,4		521,4
22 Ic																			
Jc																			
Jcs																			
24 Ic		304			223		166		128		97		75		56		43		30
Jc		206			151,1		112,5		86,72		65,72		50,81		37,94		29,13		20,33
Jcs		1299			953		709,4		547		414,5		320,5		239,3		183,8		128,2
26 Ic																			
Jc																			
Jcs																			
28 Ic																			
Jc																			
Jcs																			
30 Ic	71	50	28	17	11	7													
Jc	48,1	33,88	18,97	11,52	7,453	4,743													
Jcs	303,4	213,7	119,7	72,65	47,01	29,91													
32 Ic																			
Jc																			
Jcs																			

Critical Temperature T(K) Vs Magnetic Field B(T):

B	0	0,1	0,2	0,3	0,4	0,5	0,6	0,7	0,8	0,9	1	1,1	1,2	1,3	1,4	1,5	1,6	1,7	1,8	
T	33,5																			

	Thickness (mm):	0,76	Width (mm):	2
	Tot.Cr.Sect.(mm ²):	1,476	Sup.Cr.Sect.(mm ²):	0,234
	Filling Factor (%):	15,8	Total Cable Length (m):	
	Net weigh (kg):			
	Annotations:			

COGNOME <i>Name</i>					
FIRMA <i>Signature</i>					
DATA <i>Date</i>	14.10.2011				
ENTE <i>Department</i>	Quality dept.				

(Courtesy: Columbus Superconductor, Italy via SINTEF Energy AS, Trondheim, Norway)

Appendix C Derivation of power loss in slot

Let, the area of the slot = A_{slot} and length of the slot = L

Since the whole area is not filled with copper winding, assume the filling factor of copper = F

The effective area of slot containing copper = $A_{slot,eff} = A_{slot} \times F$

Power loss (P) = I^2R

Here, Copper density = J_{ac} and conductivity of copper = σ

Current in the slot (I) = $J_{ac} \cdot A_{slot,eff}$

And, the resistance of the winding in one slot (R) = $L / (\sigma \cdot A_{slot,eff})$

Now,

$$\begin{aligned} \text{Power loss in one slot (P)} &= (J_{ac} \cdot A_{slot,eff})^2 \cdot \frac{L}{\sigma \cdot A_{slot,eff}} \\ &= J_{ac}^2 \cdot \frac{A_{slot,eff}}{\sigma} \cdot L \end{aligned}$$

$$\text{Power loss in slot per unit length (P}_{loss}) = J_{ac}^2 \cdot \frac{A_{slot,eff}}{\sigma}$$

Appendix D FEA results of reference machine

1. Input/output panel

The screenshot displays the SmartTool V3.3 software interface, divided into three main sections: Input panel, Control, and Output panel.

Input panel: This section is used to define machine parameters. It includes radio buttons for 'inner [Rotor] outer' (selected) and 'motor | generator'. Under 'Machine key numbers', parameters include Rated mechanical power (10000 kW), Rated rotational speed (12.95 rpm), and Desired rated voltage (3310 V). 'Machine geometry' includes Machine inner diameter (11600 mm), Magnet length (20 mm), Magnet pitch/pole pitch (0.9), Slot width/slot pitch (0.5), Slot depth/slot width (0.5), Number of poles (198), and Number of slots (216). 'Energy density' includes Current loading (rms) (47247.1 A/m). 'Winding data' includes Copper fill factor under wedge (0.5) and Number of parallel branches (6). 'Slot wedge' includes Thickness slot wedge (0 mm). At the bottom, there are buttons for 'Set existing machine para...', 'Regular input' (selected), 'Geometry input', 'Save des ign', and 'Load des ign'.

Control: This panel contains several functional buttons: 'Calculate', 'Optimize', 'Optimization limits', 'Slot/Pole advice', 'Winding vis ualization', 'Advanced', 'Cost data', 'FEA', 'Save to Excel', and 'Struct to Works pace'.

Output panel: This panel displays the results of the simulation. It is divided into several sub-sections:

- Geometry (main) and winding:** Lists parameters such as Stack length (1218.4 mm), Length with end windings (1479.3 mm), Outer active diameter (12141.2 mm), Inner active diameter (11600 mm), Diameter at air gap (11857.1 mm), Slot pitch (172.6 mm), Pole pitch (188 mm), Slot depth (43.1 mm), Slot width (86.3 mm), Stator back iron thickness (92.6 mm), Rotor back iron thickness (103.6 mm), Weight of active materials (90459.86 kg), Rotor moment of inertia (1460904 kg*m^2), Number of turns (25), and Copper operating temperature (80 deg C).
- Characteristics:** Shows Torque (7373974 Nm), Efficiency (96.1%), and cos_phi (0.8366).
- Electromagnetic values:** Lists Frequency (21.37 Hz), RMS line voltage (3365.9 V), RMS phase induced voltage (1692.9 V), RMS phase current (1957.17 A), Flux density in tooth (1.18 T), Average flux density in air gap (0.59 T), Active power (9545.6 kW), Phase inductance (4051.7 μH), Synchronous pu reactance (0.5478), RMS Copper current density (4.381 A/mm^2), and RMS current loading (47247.1 A/m).
- Losses:** Lists Losses in winding (334380 W), No Load Losses in magnets (36149.45 W), No Load Losses in teeth (12143.47 W), No Load Losses in stator yoke (11527.05 W), No Load Losses in rotor yoke (206.04 W), and Stator loss per area (7873 W/m^2).
- Coefficients:** Lists Distribution factor (0.958), AC/DC Loss factor (1.2), and Magnetic air gap shear force (43047 N/m^2).
- Cost:** Lists Material cost of windings (6092 NOK), Material cost of magnets (6020 NOK), Material cost of stator laminate (41836 NOK), Material cost of rotor back iron (36512 NOK), and Total active cost (90460 NOK).

Figure D.1: Combined input and output panel of reference machine.

$$C = \frac{S}{D^2 \cdot L \cdot n} = \frac{10000 / 0.8366}{11.86^2 \cdot 1.22 \cdot 12.95} = 5.37$$

Note: The parameters in red color indicate that losses due to harmonics are not included.

2. Machine Parameters:

Set Existing Machine Parameters

Electrical parameters: motor | generator

Number of slots, Ns:

Number of poles, Np:

Electrical frequency, f: [Hz]

Rotational speed, n: [rpm]

RMS phase current, I_{ph_rms}: A

Current loading, ac: A/m

Winding details:

Number of parallel branches, n_{pb}:

Slot fill factor, excl. slot wedge, k_{cu_nowedge}:

Number of turns, n_s:

Temperatures:

Machine operating temperature, temp_{win}: [°C]

Dimensions: inner | Rotor | outer

Outer stator radius, r_{so}: [mm]

Inner stator radius, r_{si}: [mm]

Tooth width, straight, w_{ts}: [mm]

Slot shape Rectangular Parallelogram

Slot width, w_s: [mm]

Slot depth, d_s: [mm]

Slot wedge thickness, th_{sw}: [mm]

Semi magnetic slot wedge? mag_{sw}:

Air gap length, g: [mm]

Permanent magnet thickness, th_{pm}: [mm]

Permanent magnet width, w_{pm}: [mm]

Rotor yoke thickness, th_{br}: [mm]

Active length, L: [mm]

Figure D.2: Input parameters of reference machine.

Simulation results:

3. EMF Simulation Plot

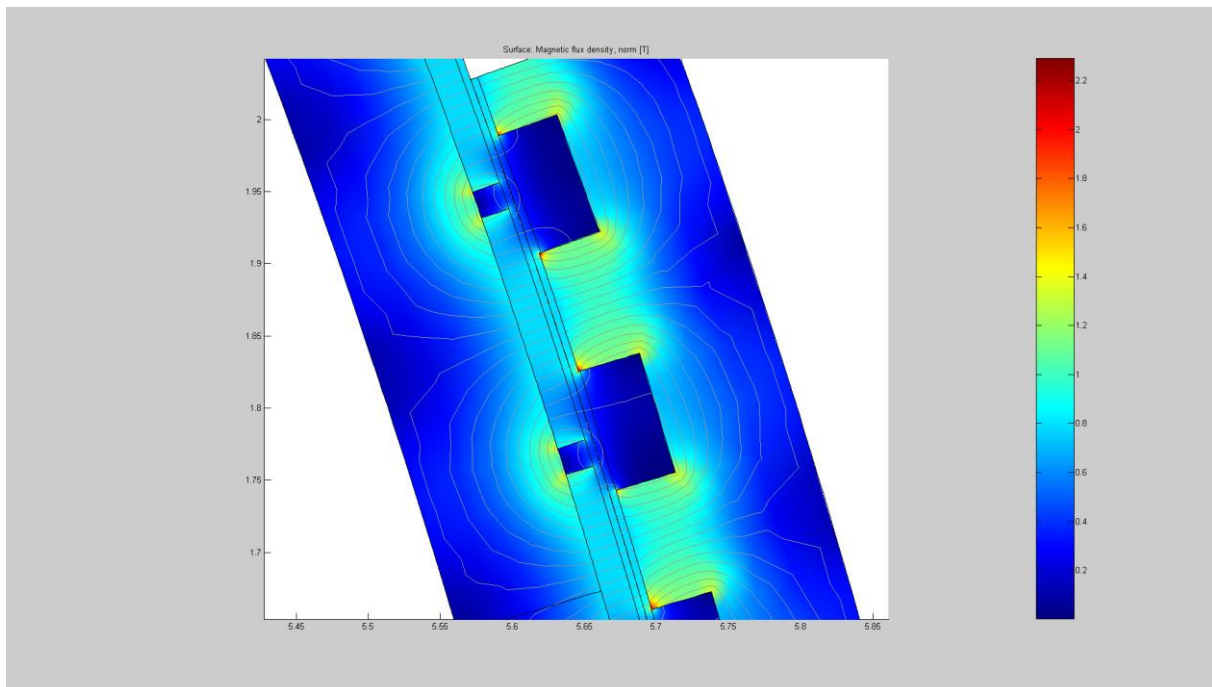


Figure D.3: Magnetic flux density at no-load.

4. One period EMF Excitation

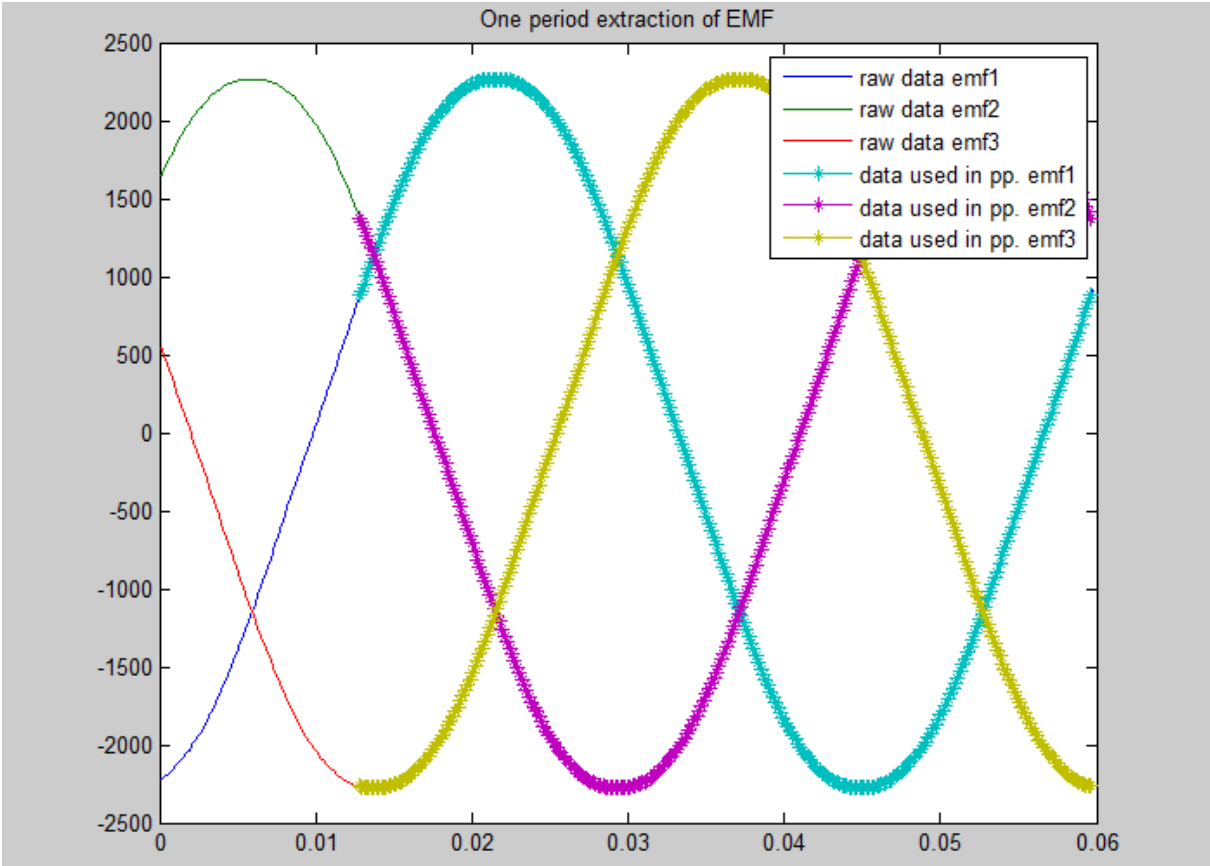


Figure D.4: EMF plot under no-load condition.

5. FEA results of EMF simulation

Parameters	Reference machine	Reference machine
	Phase EMF	Line EMF
Mean first harmonic peak, V	2302.9	3988.8
Mean peak voltage, V	2276.2	4026.7
Phase voltage, 1. harmonics (rms), V	1628	2820
Phase voltage maximum (rms), V	1610	2847
THD (%)	1.14%	1.13%

6. Phase and line EMF waveforms

Phase EMFs

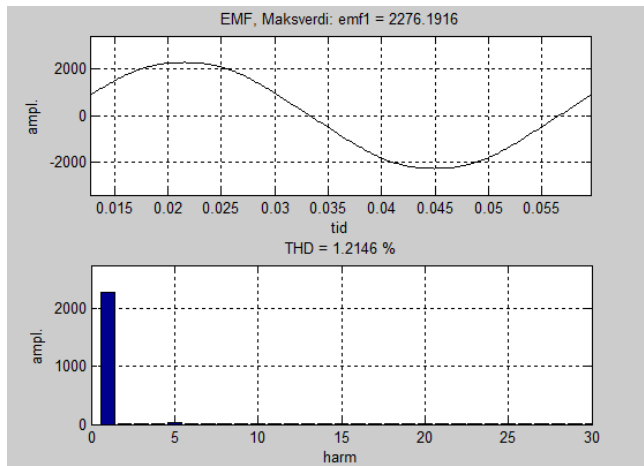


Figure D.5: EMF waveform and harmonics of phase 1 EMF.

Line EMFs

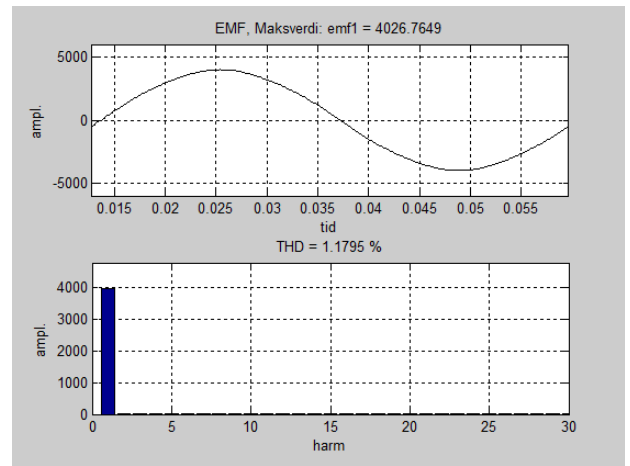


Figure D.6: EMF and harmonics of line voltage 1.

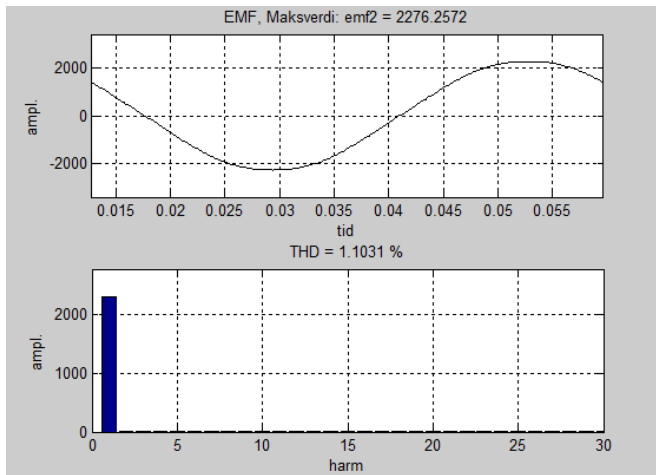


Figure D.7: EMF waveform and harmonics of phase 2 EMF.

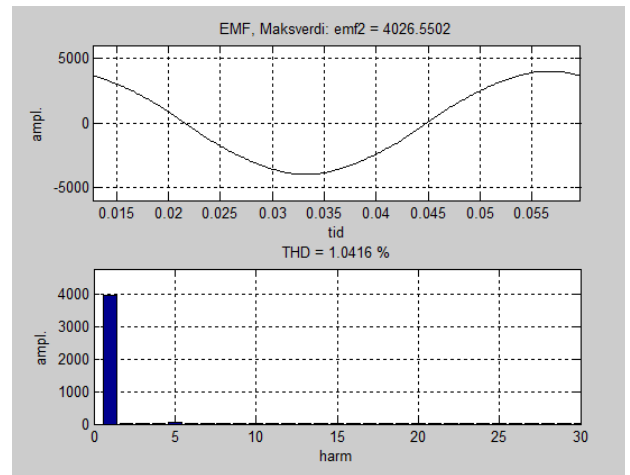


Figure D.8: EMF and harmonics of line voltage 2.

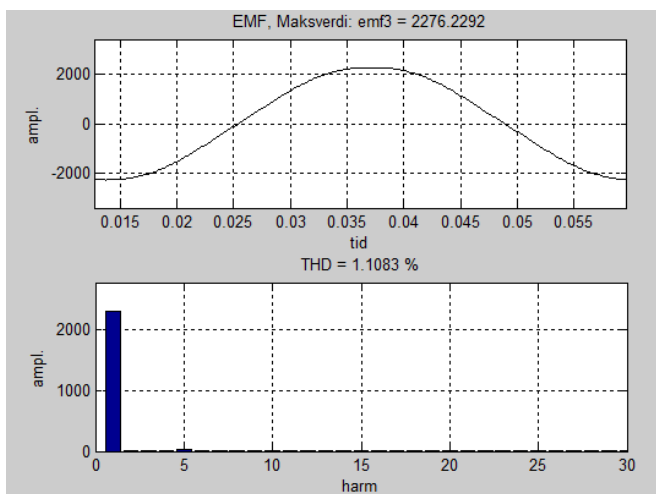


Figure D.9: EMF waveform and harmonics of phase 3 EMF.

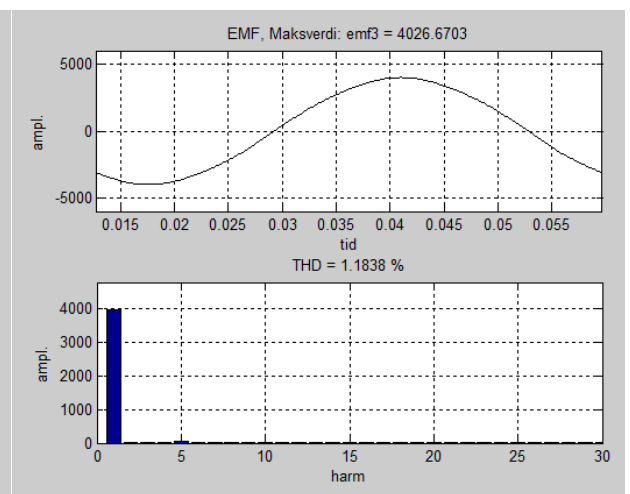


Figure D.10: EMF and harmonics of line voltage 3.

7. Full Load Simulation plot

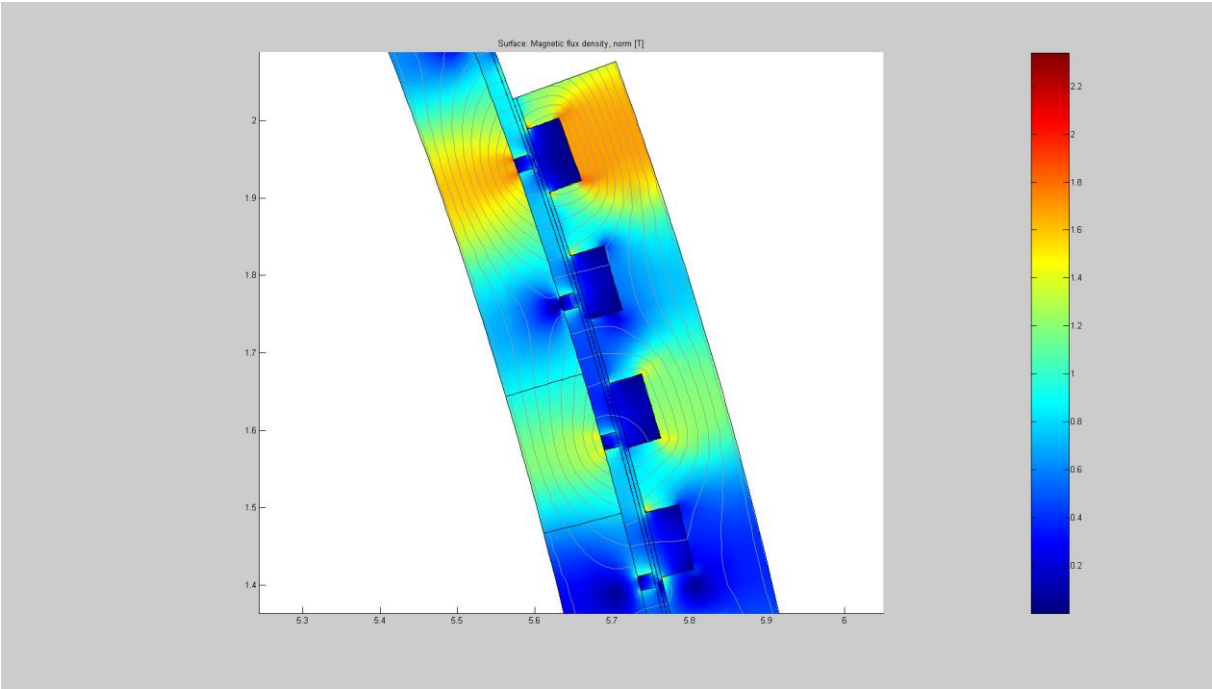


Figure D.11: Zoomed in part of core with maximum flux density under full load condition.

8. Full load torque

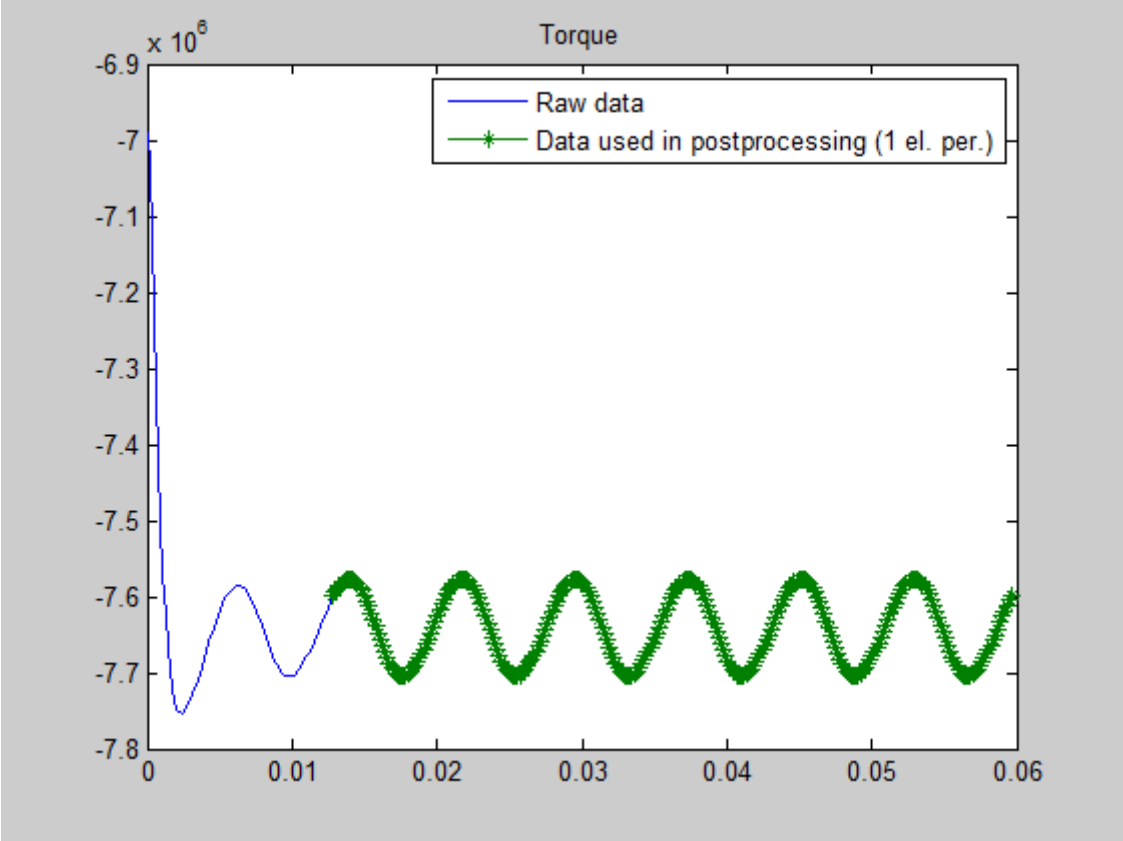


Figure D.12: Plot of full load torque.

9. Full load torque Harmonics

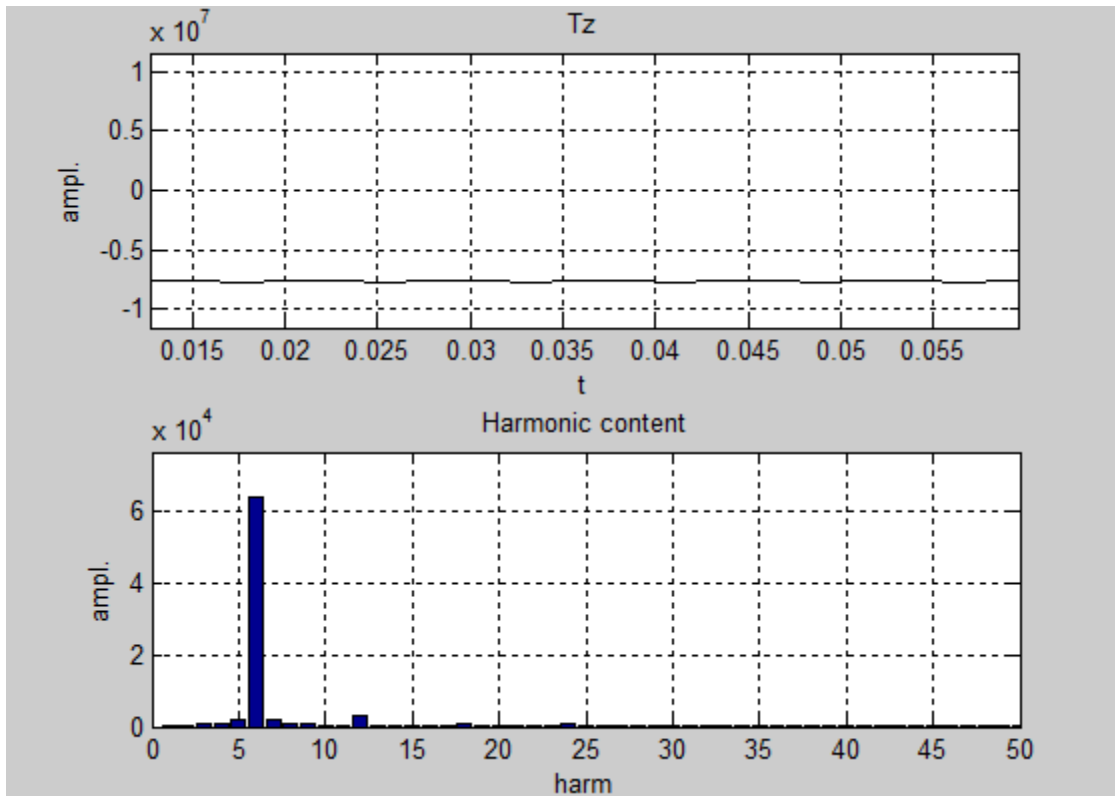


Figure D.13 Plot of amplitude and harmonics of full load torque.

10. Full load PM losses

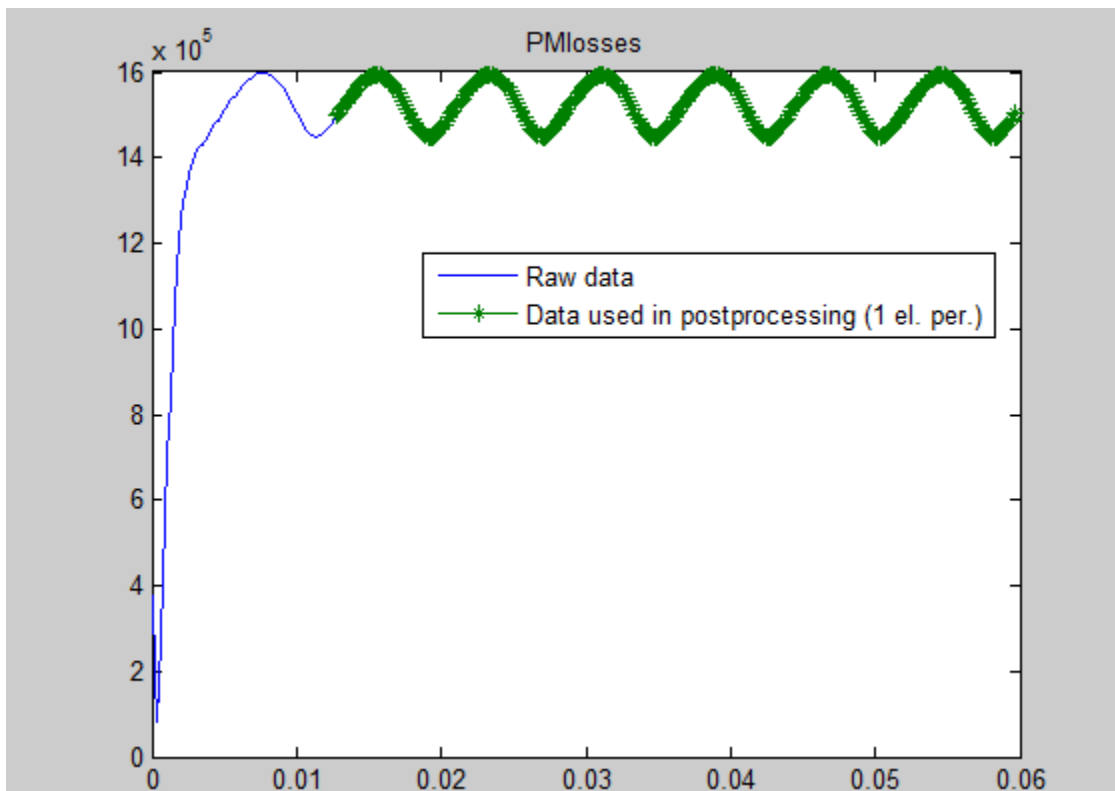


Figure D.14: Full load PM losses.

11. Full load rotor core flux density plot 1

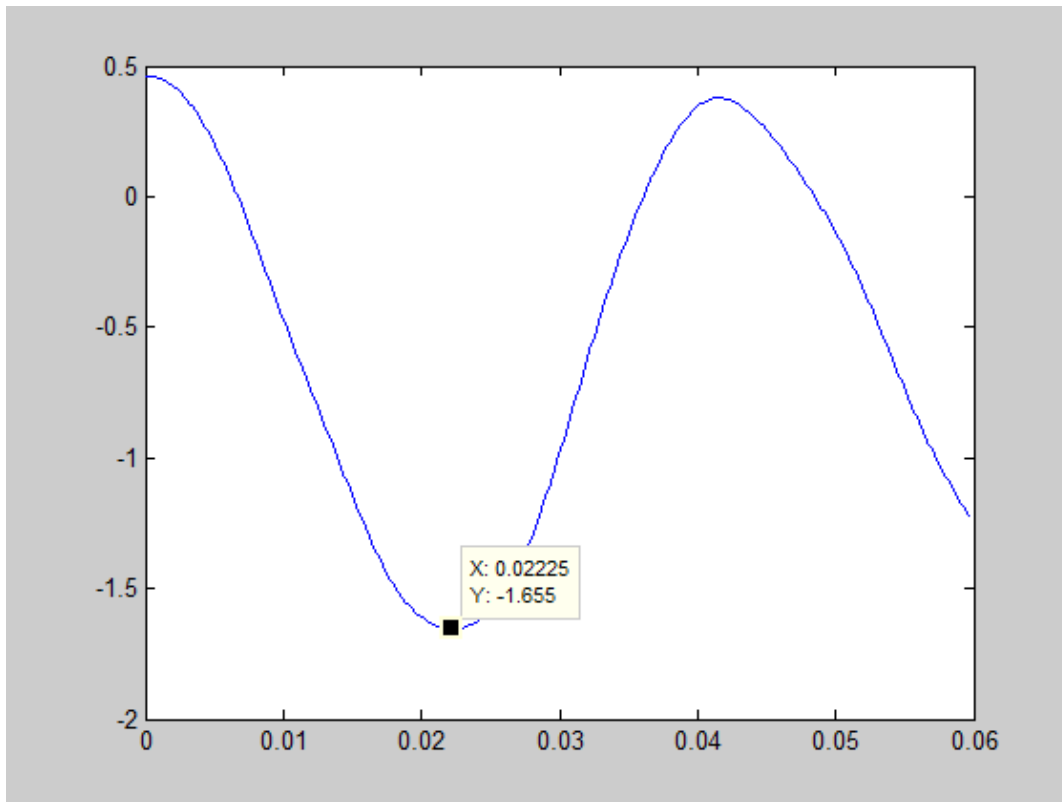


Figure D.15: Plot of full load rotor core flux density.

12. Smarttool FEA simulation results

Phase inductance	3987 μ H
Induced voltage	
Phase voltage, 1. harmonic (rms)	1628 V
Phase voltage, maximum (rms)	1610 V
Total harmonic distortion (THD)	1.142 %
Torque	
Cogging torque amplitude at noload	393.2422
Mean torque at full load	-7640158.5
Torque ripple amplitude at full load (pu)	-0.84046 %
Losses	
Iron loss in stator at noload	23592.9432
Iron loss in rotor at noload	1561.7988
Induced loss in magnets at noload	677415.676
Iron loss in stator at full load	60757.1016
Iron loss in rotor at full load	36787.0476
Induced loss in magnets at full load	1526113.25

OK Write to command window

Figure D.16: Summary of FEA simulation results.

13. Simulation results

Cogging torque results:

Cogging torque amplitude at no-load :393.2 N·m

No-load Loss results:

Average PM loss : 677416 W

Max stator core loss : 23592.9 W

Max rotor core loss : 1561.8 W

Where $B_{max} = 0.609154$ T and $B_{off} = 0.575204$ T

Full load simulation results:

Total torque results:

Mean torque (offset) : -7640.1 kN·m

Peak torque : -7576.8 kN·m

Torque ripple amplitude at full load (pu) : -0.84 %

Full load Loss results:

Average PM loss : 1526113 W

Max stator core loss : 60757.1 W

Max rotor core loss : 36787 W

Where $B_{max} = 1.6545$ T and $B_{off} = 0.596516$ T

14. Surface plot of magnetic flux density at full load

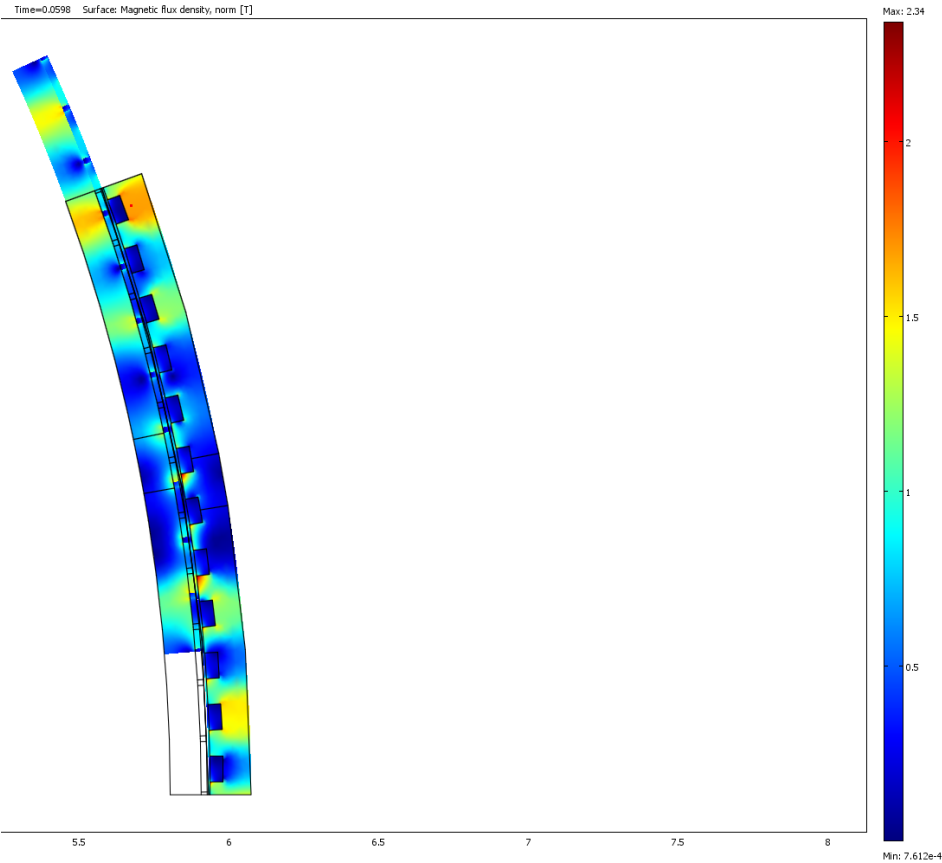


Figure D.17: COMSOL plot of magnetic flux density under full load.

15. Flux variation in Stator yoke

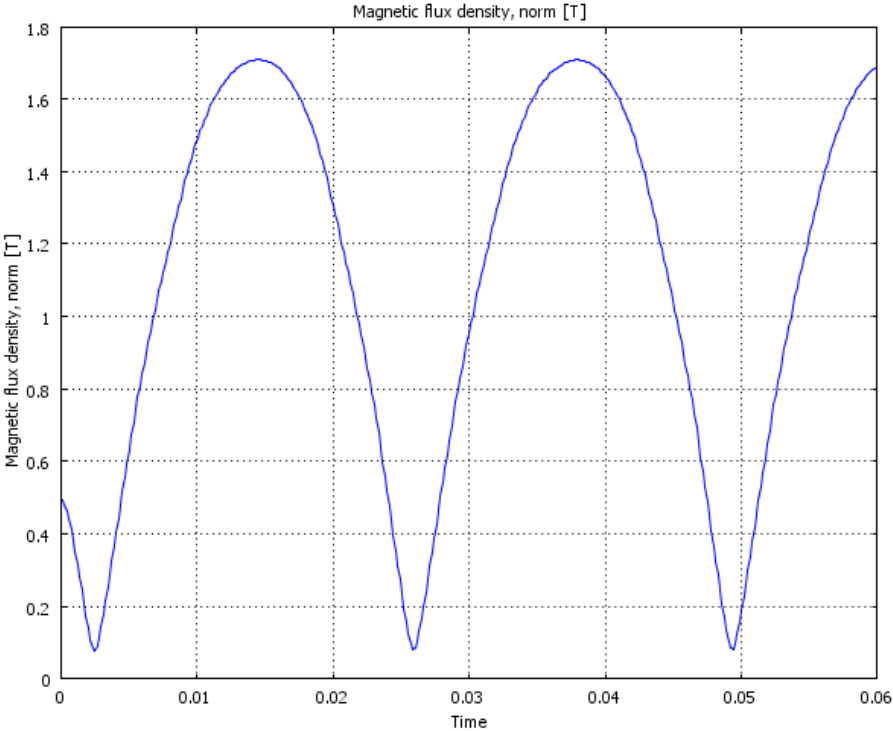


Figure D.18: variation of flux density in stator core at a point close to slot.

16. Magnetic flux density in range B=0 to 1.7

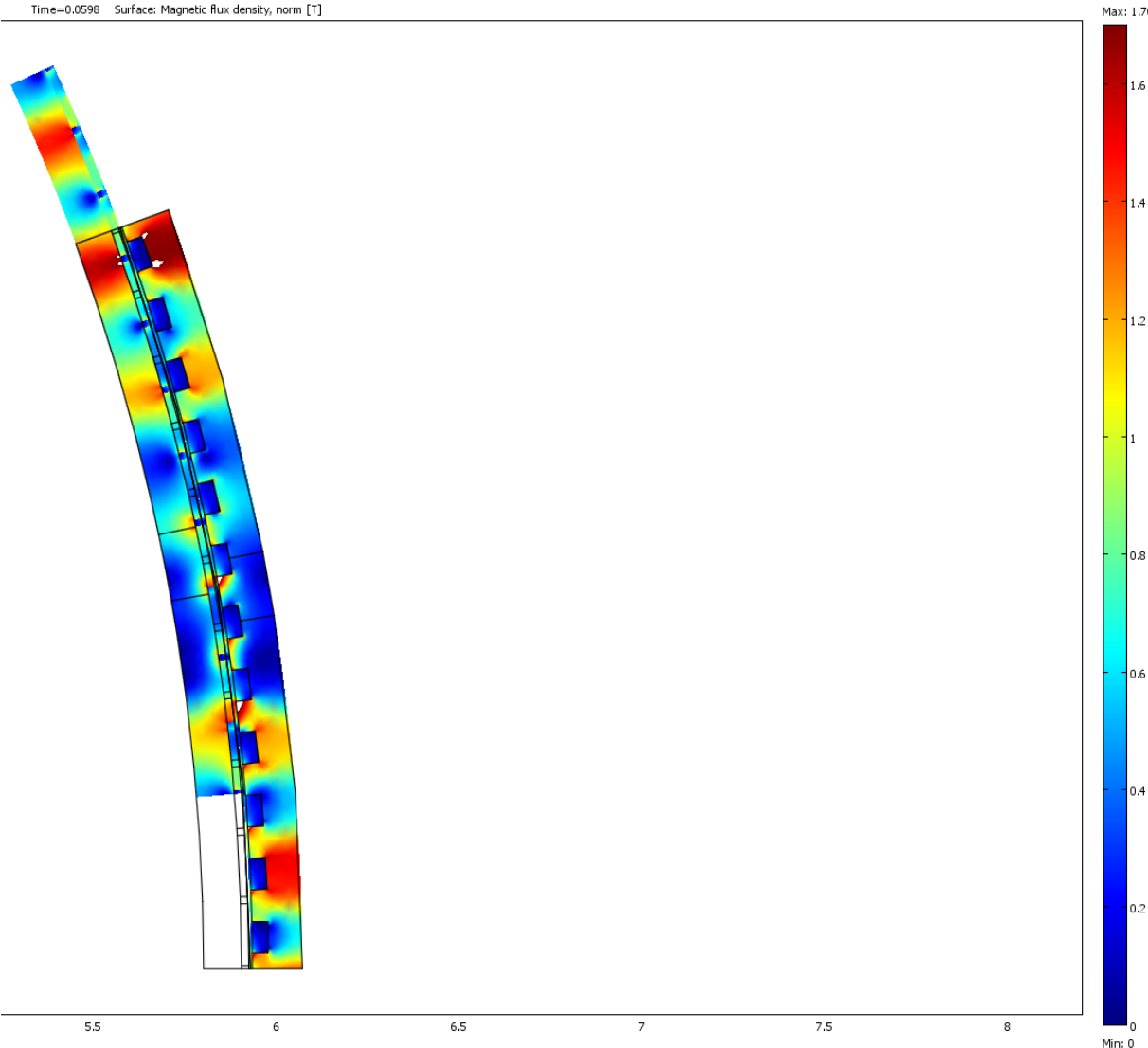


Figure D.19: Plot of magnetic flux density in a range of 0 to 1.7 T.

17. Relative permeability plot at full load condition

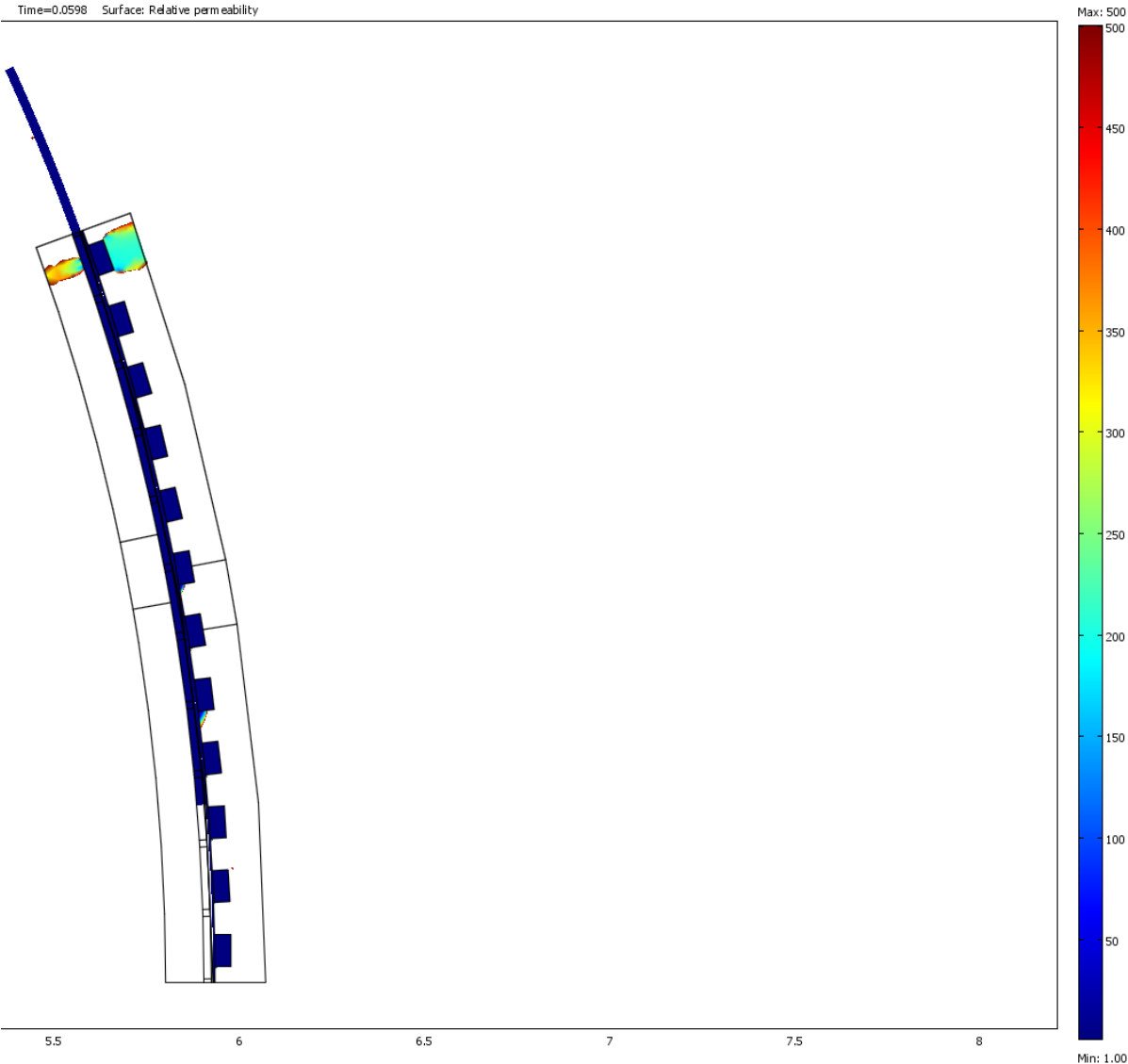


Figure D.20: Plot of relation permeability in a range of 1 to 500 at full load condition.

18. Relative permeability plot at full load condition (Range: 1 to 200)

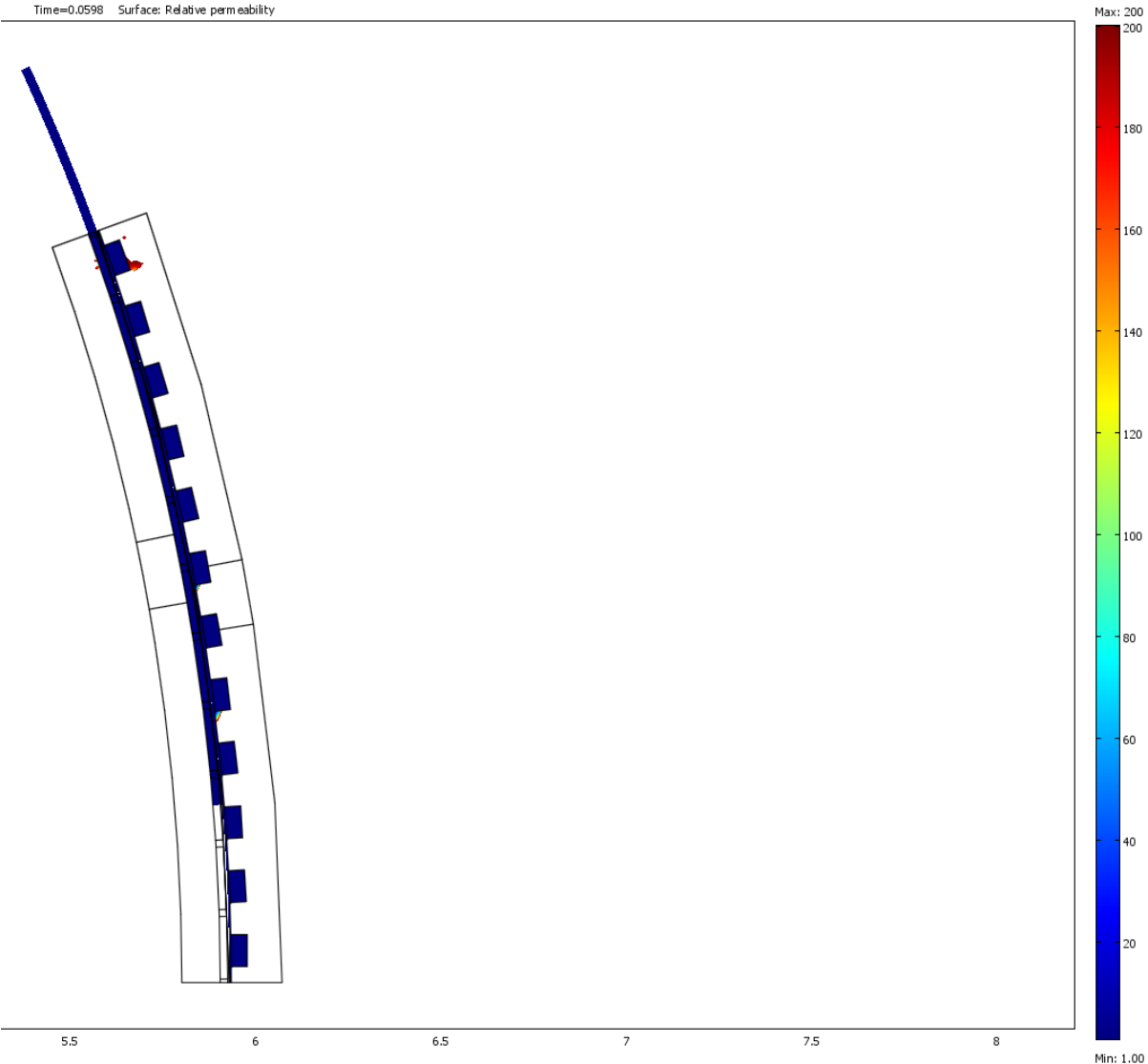


Figure D.21: Plot of relation permeability in a range of 1 to 200 at full load condition.

Appendix E FEA results of Machine – 1 (176 pole 192 slots)

1. Input/output panel

SmartTool V3.3

Input panel

inner | Rotor | outer motor | generator

Machine key numbers

Rated mechanical power: 10000 kW

Rated rotational speed: 12.95 rpm

Desired rated voltage: 3300 V

Air gap length: 10 mm

Copper operating temperature: 80 deg C

Machine geometry

Machine outer diameter: mm
 Machine inner diameter: 8000.02 mm

Magnet length: 30 mm

Magnet pitch/pole pitch: 0.9

Slot width/slot pitch: 0.222

Slot depth/slot width: 1.267

Number of poles: 176

Number of slots: 192

Vary pole/slot configuration (optimization only):

Energy density

Copper current density (rms): 145 A/mm²
 Current loading (rms):
 Stator loss per area:

Flux density in stator yoke: 0.4 T

Flux density in rotor yoke: 0.5 T

Winding data

Copper fill factor under wedge: 0.08

Number of parallel branches: 6

Slot wedge

Thickness slot wedge: 3 mm

Semimagnetic wedge?

Regular input:
 Geometry input:

Control

Output panel

Geometry (main) and winding

Stack length:	1007.5	mm
Length with end windings:	1174.9	mm
Outer active diameter:	8648.2	mm
Inner active diameter:	8000	mm
Diameter at air gap:	8301.9	mm
Slot pitch:	136	mm
Pole pitch:	148	mm
Slot depth:	38.2	mm
Slot width:	30.2	mm
Stator back iron thickness:	129.4	mm
Rotor back iron thickness:	115.9	mm
Weigth of active materials:	62590.38	kg
Rotor moment of inertia:	474943.	kg*m ²
Number of turns:	34	
Copper operating temperature:	80	deg C

Characteristics

Torque:	7373974	Nm
Efficiency:	99.9	%
cos_phi:	0.8047	

Electromagnetic values

Frequency:	18.99	Hz
RMS line voltage:	3284.7	V
RMS phase induced voltage:	1528.1	V
RMS phase current:	2178.34	A
Flux density in tooth:	0.99	T
Average flux density in air gap:	0.77	T
Active power:	9972.3	kW
Phase inductance:	4331.5	µH
Synchronous pu reactance:	0.5937	
RMS Copper current density:	145	A/mm ²
RMS current loading:	90761.5	A/m

Losses

Losses in winding:	11.37	W
No Load Losses in magnets:	3549.75	W
No Load Losses in teeth:	5776.37	W
No Load Losses in stator yoke:	4492	W
No Load Losses in rotor yoke:	14.45	W
Stator loss per area:	390	W/m ²

Coefficients

Distribution factor:	0.958	
AC/DC Loss factor:	1.2	
Magnetic air gap shear force:	106190	N/m ²

Cost

Material cost of windings:	189	NOK
Material cost of magnets:	5206	NOK
Material cost of stator laminate:	33753	NOK
Material cost of rotor back iron:	23442	NOK
Total active cost:	62590	NOK

Figure E.1: Combined input output panel of optimized parameters of SC Machine – 1.

$$C = \frac{S}{D^2 L n} = \frac{10000 / 0.805}{8.3^2 \cdot 1.007 \cdot 12.95} = 13.83$$

Note: The parameters in red color indicate that losses due to harmonics are not included.

2. Machine Parameters:

Set Existing Machine Parameters

Electrical parameters: motor | generator

Number of slots, Ns:

Number of poles, Np:

Electrical frequency, f: [Hz]

Rotational speed, n: [rpm]

RMS phase current, I_{ph_rms}: A

Current loading, ac: A/m

Winding details:

Number of parallel branches, n_{pb}:

Slot fill factor, excl. slot wedge, k_{cu_nowedge}:

Number of turns, n_s:

Temperatures:

Machine operating temperature, temp_{win}: [°C]

Dimensions: inner (Rotor) | outer

Outer stator radius, r_{so}: [mm]

Inner stator radius, r_{si}: [mm]

Tooth width, straight, w_{ts}: [mm]

Slot shape Rectangular Parallelogram

Slot width, w_s: [mm]

Slot depth, d_s: [mm]

Slot wedge thickness, th_{sw}: [mm]

Semi magnetic slot wedge? mag_{sw}:

Air gap length, g: [mm]

Permanent magnet thickness, th_{pm}: [mm]

Permanent magnet width, w_{pm}: [mm]

Rotor yoke thickness, th_{br}: [mm]

Active length, L: [mm]

Figure E.2: Input parameters of SC Machine - 1.

3. EMF Simulation Plot

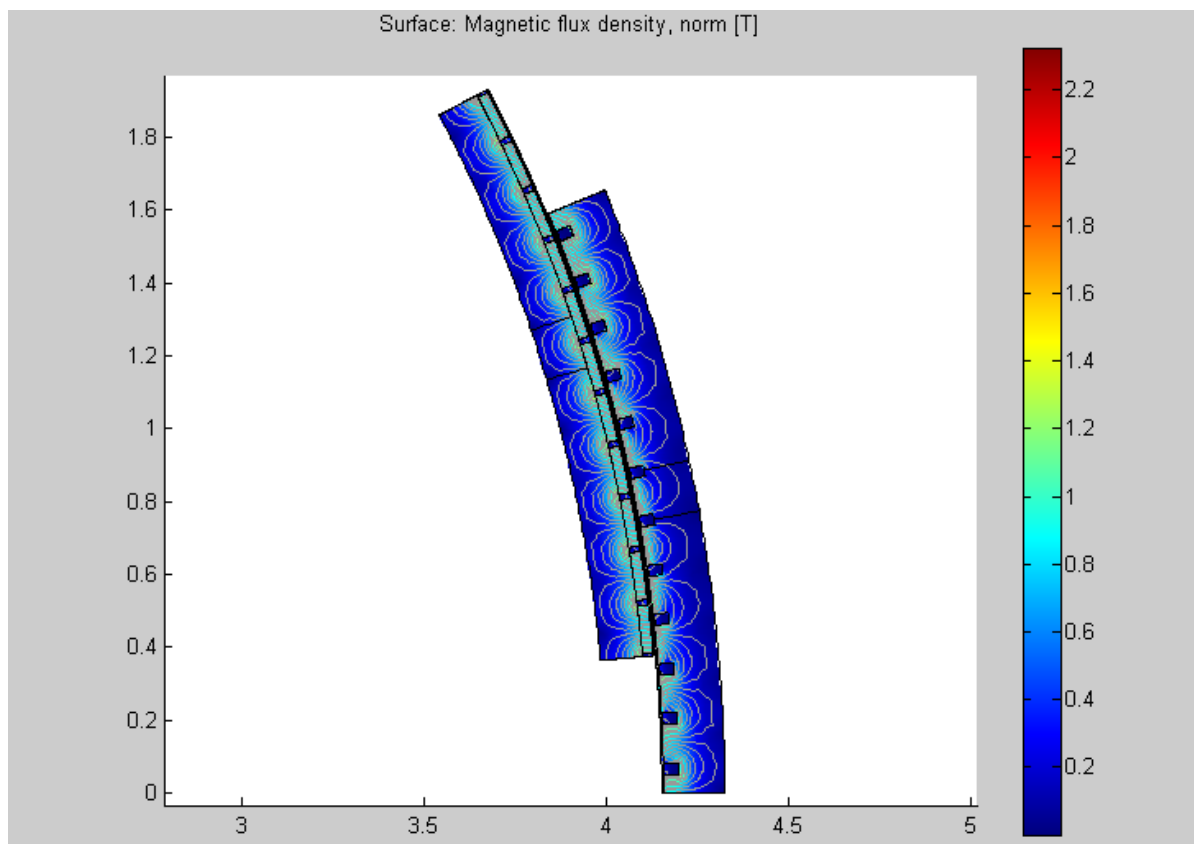


Figure E.3: EMF simulation plot under no-load condition.

4. One period EMF Excitation

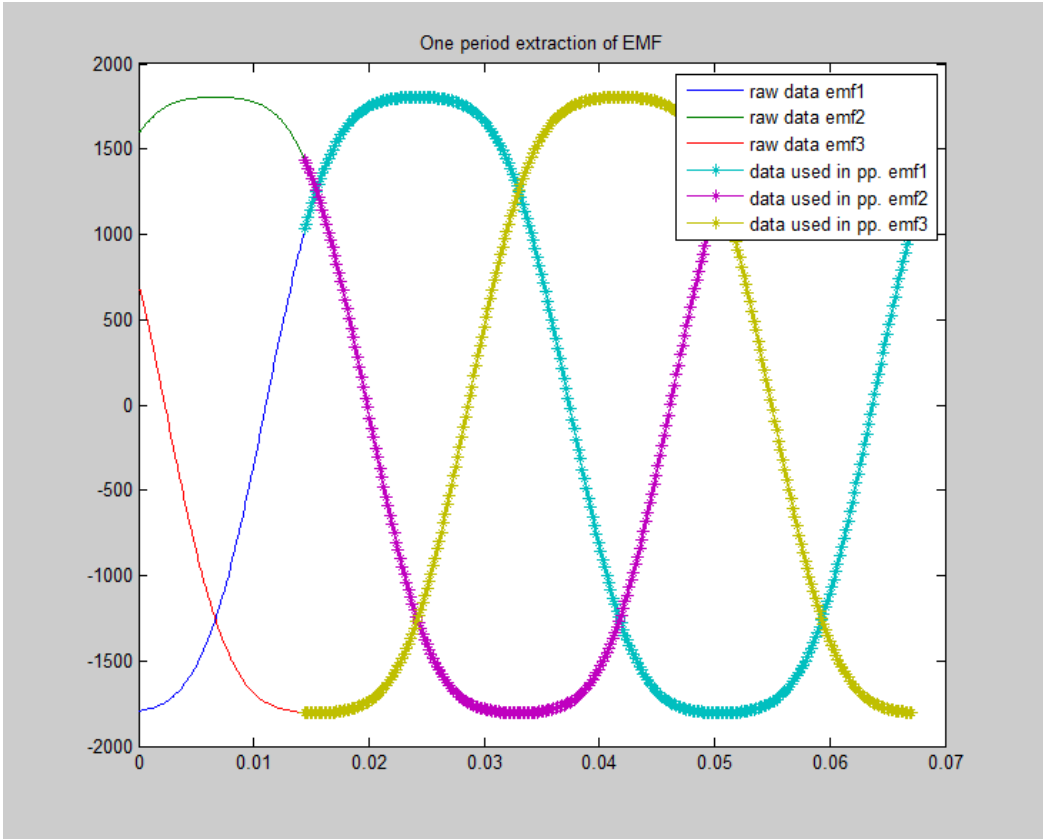


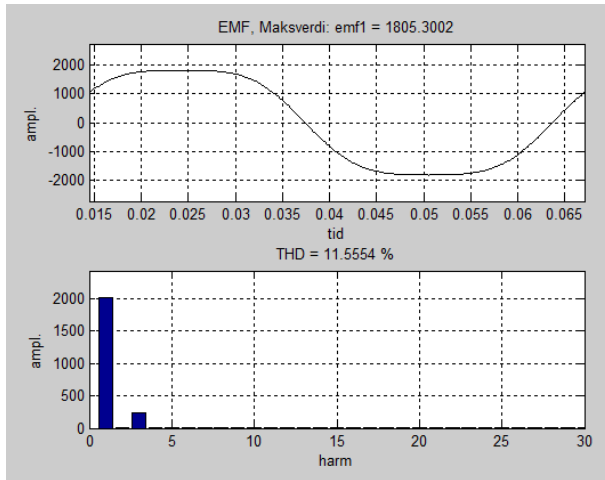
Figure E.4: EMF plot under no-load condition.

5. FEA results of EMF simulation

Parameters	Machine – 1	Machine – 1
	Phase EMF	Line EMF
Mean first harmonic peak, V	2026.8	3510.5
Mean peak voltage, V	1805.3	3487.7
Phase voltage, 1. harmonics (rms), V	1433	2482
Phase voltage maximum (rms), V	1277	2466
THD (%)	11.7 %	0.95 %

6. Phase and line EMF waveforms

Phase EMF



Line EMF

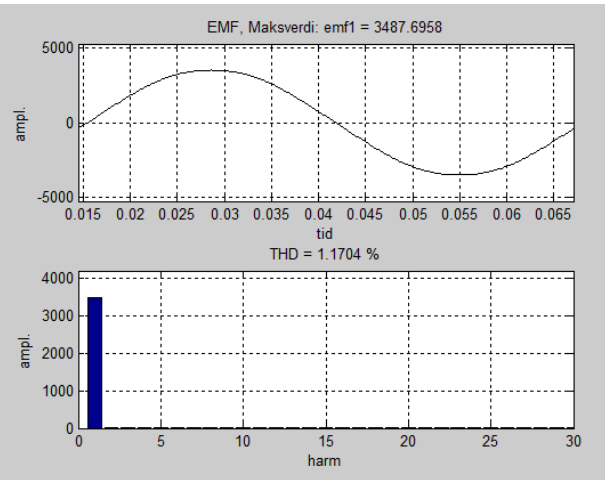


Figure E.5: EMF waveform and harmonics plot of phase 1.

Figure E.6: EMF waveform of line voltage 1.

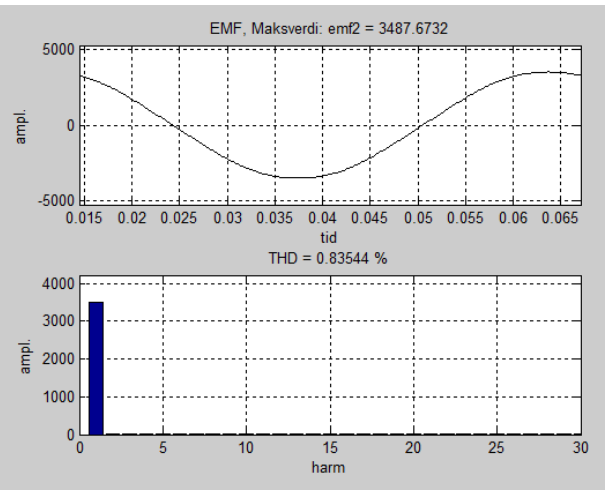
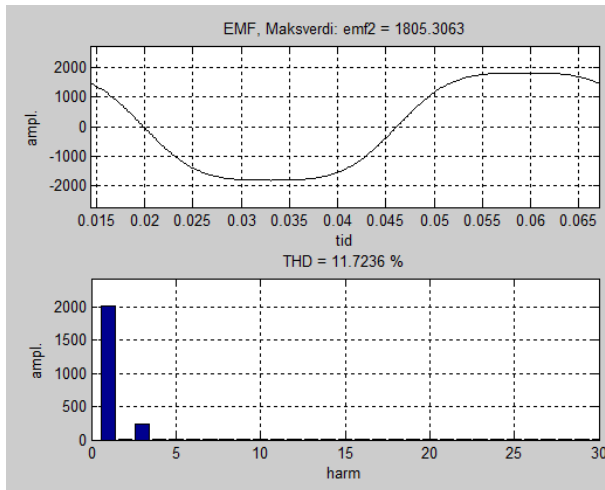


Figure E.7: EMF waveform and harmonics plot of phase 2.

Figure E.8: EMF waveform of line voltage 2.

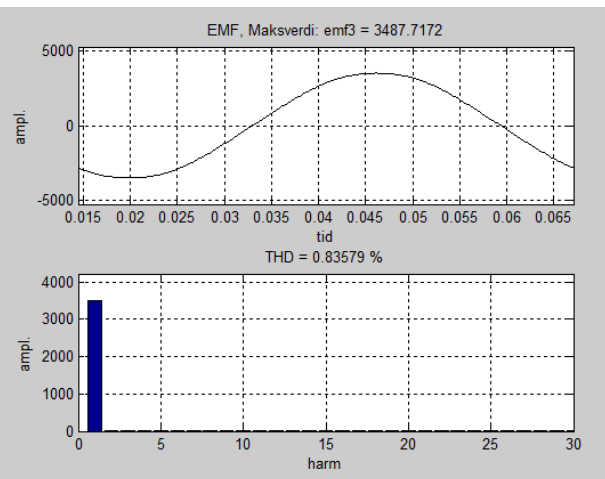
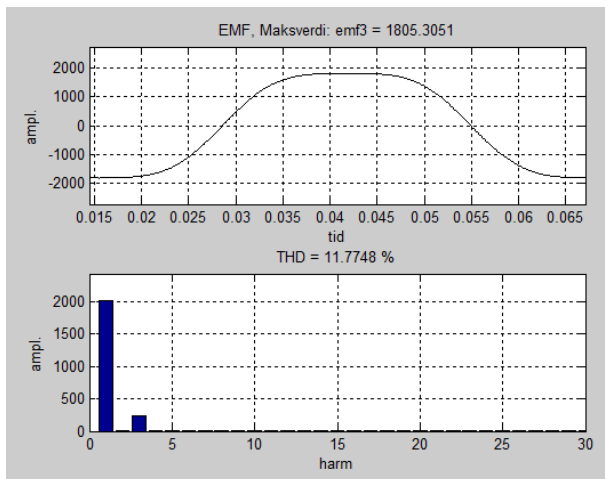


Figure E.9: EMF waveform and harmonics plot of phase 3.

Figure E.10: EMF waveform of line voltage 3.

7. Full Load Simulation plot

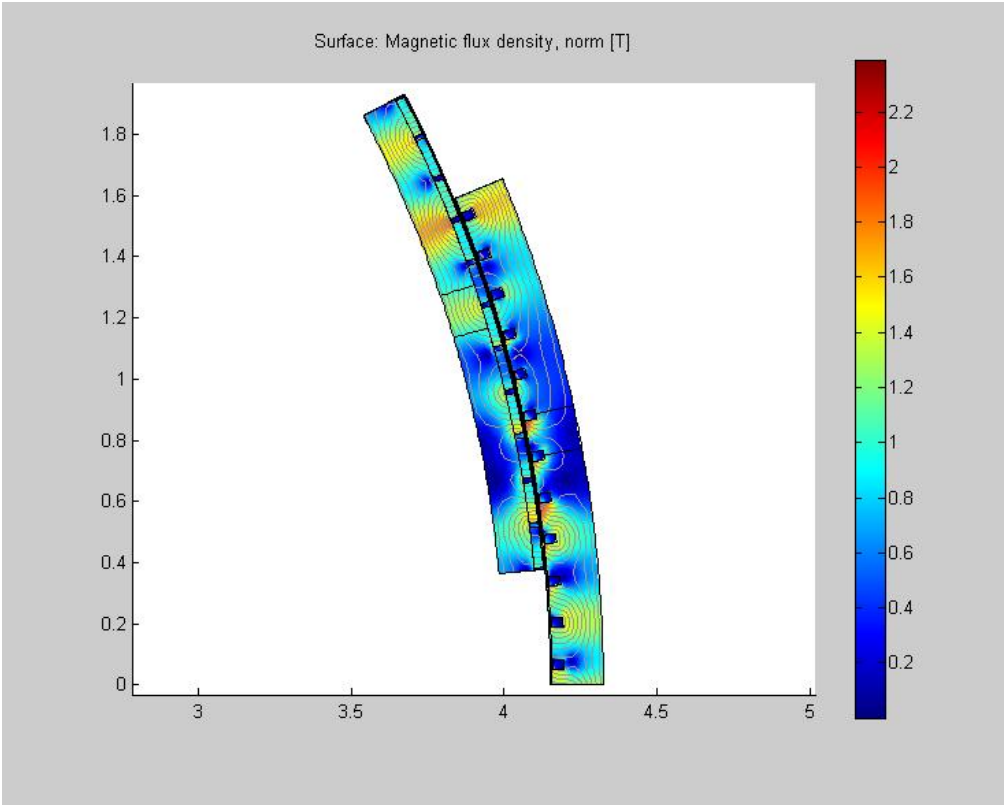


Figure E.11: Full load simulation plot.

8. Full load torque one period data 1

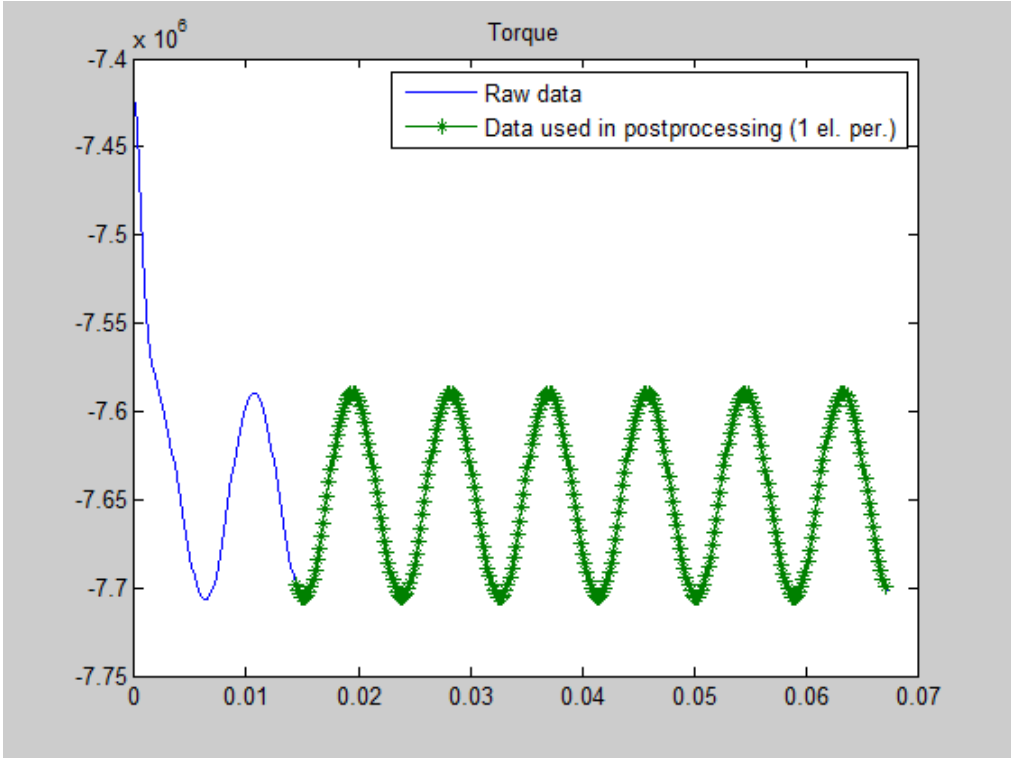


Figure E.12: Plot of full load torque.

9. Full load torque Harmonics

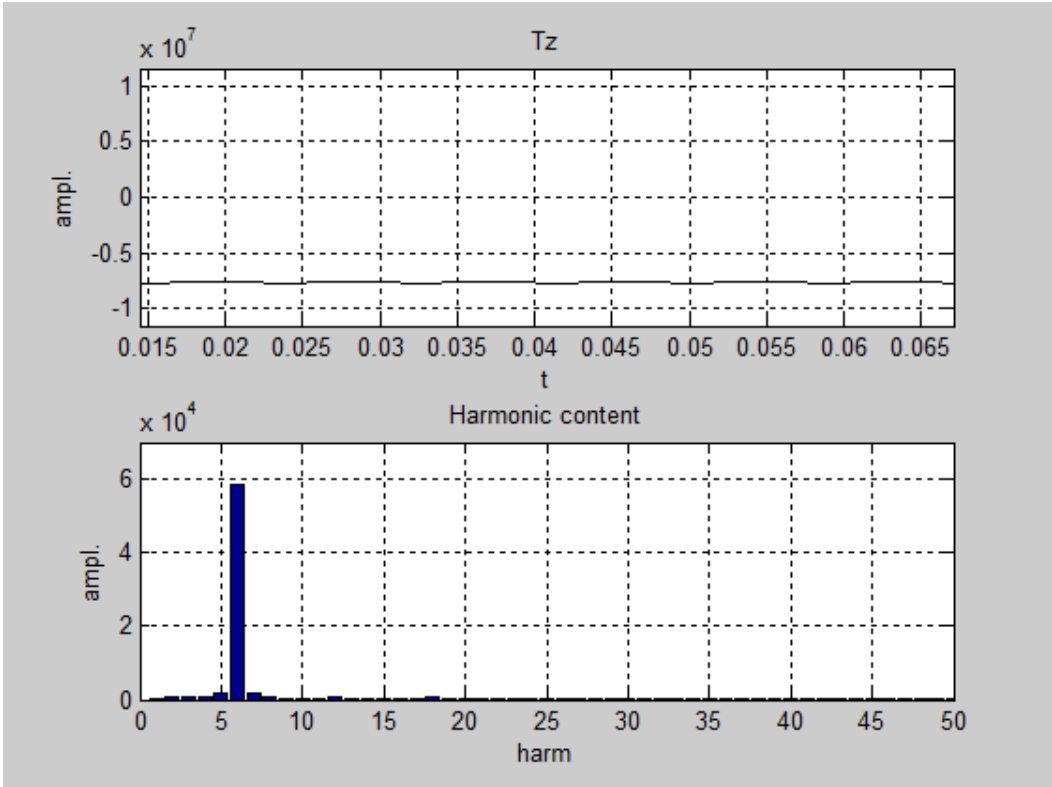


Figure E.13: Plot of amplitude of full load torque and harmonics.

10. Full load PM losses

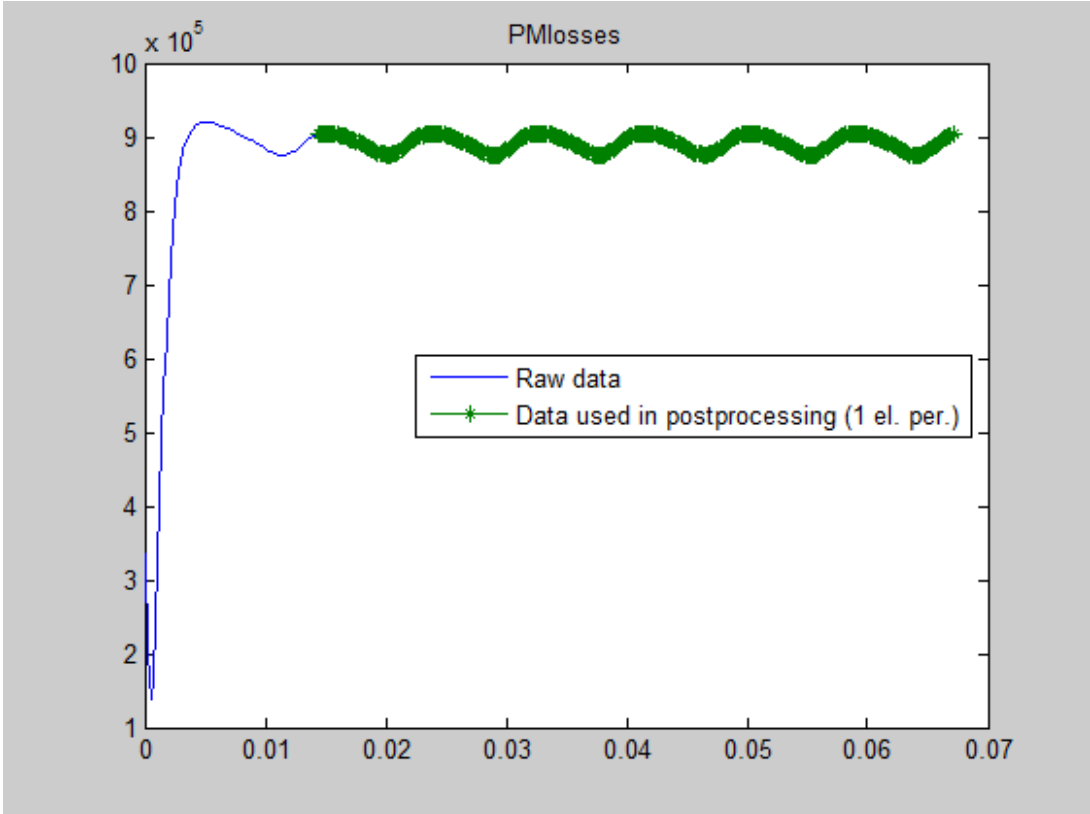


Figure E.14: Plot of full load PM losses.

11. Full load rotor core flux density

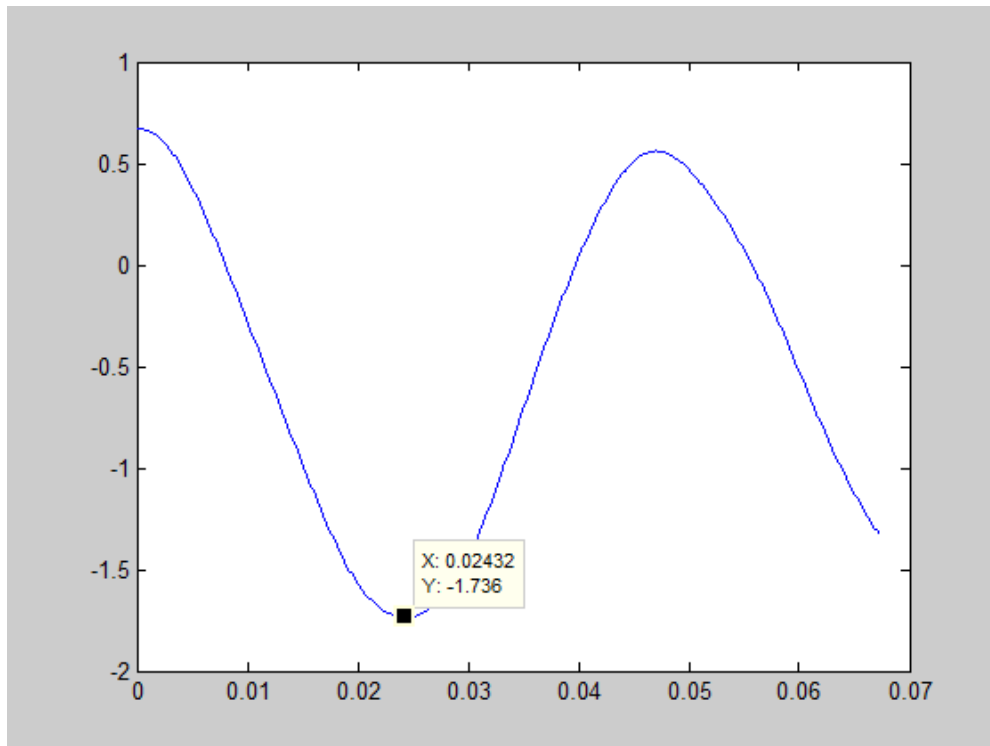


Figure E.15: Plot of full load rotor flux density.

12. Smarttool FEA simulation results

Phase inductance	5124 μ H
Induced voltage	
Phase voltage, 1. harmonic (rms)	1433 V
Phase voltage, maximum (rms)	1277 V
Total harmonic distortion (THD)	11.6846 %
Torque	
Cogging torque amplitude at noload	302.8753
Mean torque at full load	-7647105.6
Torque ripple amplitude at full load (pu)	-0.76093 %
Losses	
Iron loss in stator at noload	14640.6378
Iron loss in rotor at noload	223.4747 W
Induced loss in magnets at noload	17923.8996
Iron loss in stator at full load	36721.8251
Iron loss in rotor at full load	27327.1075
Induced loss in magnets at full load	891624.021
<input type="button" value="OK"/> <input type="button" value="Write to command window"/>	

Figure E.16: Summary of FEA simulation results.

13. FEA simulation results

No-load Loss results:

Average PM loss = 17923.9 W

Max stator core loss = 14640.6 W

Max rotor core loss = 223.475 W

Where $B_{max} = 0.534045$ T and $B_{off} = 0.52795$ T

Full load simulation results:

Loss results:

Average PM loss = 891624 W

Max stator core loss = 36721.8 W

Max rotor core loss = 27327.1 W

Where $B_{max} = 1.73587$ T and $B_{off} = 0.533757$ T

SmartTool FEA simulation results:

Phase inductance = 5124 μ H

Induced voltage

Line voltage, 1. harmonic (rms) = 1433 V

Line voltage, maximum (rms) = 1277 V

Total harmonic distortion (THD) = 11.6846 %

Torque

Cogging torque amplitude at noload = 302.8753 Nm

Mean torque at full load = -7647105.6256 Nm

Torque ripple amplitude at full load (pu) = -0.76093 %

14. Surface plot of magnetic flux density at full load

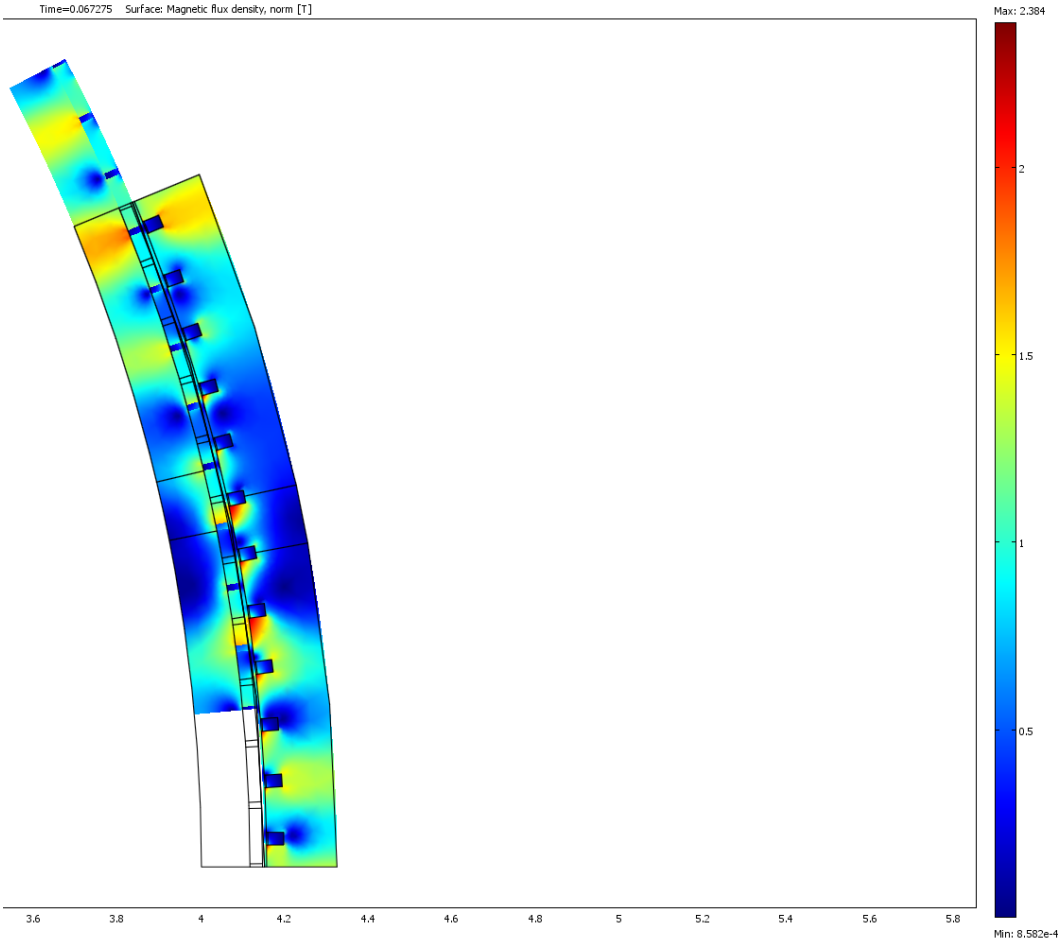


Figure E.17: COMSOL plot of magnetic flux density at full load.

15. Variation of flux density in Stator yoke

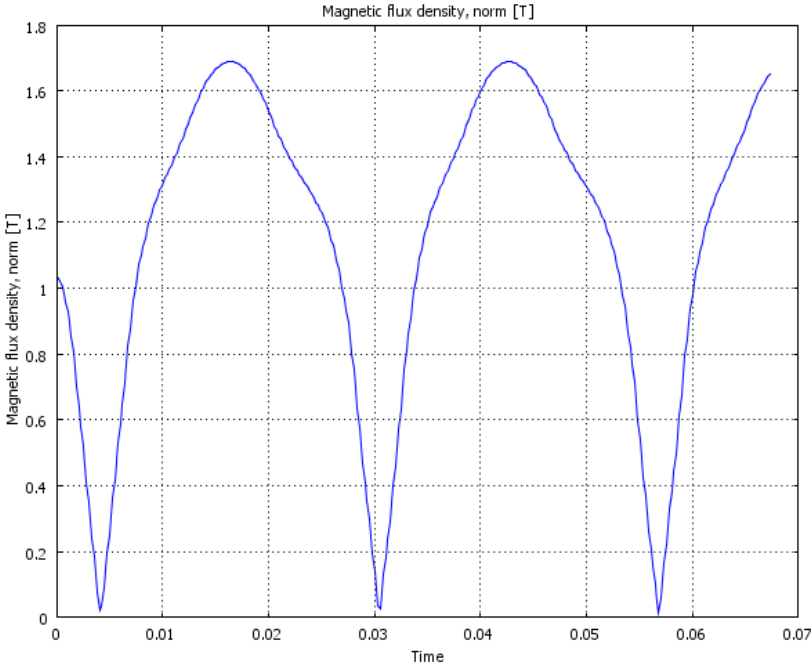


Figure E.18: Variation of flux density in stator core at a point close to slot.

16. Surface plot of magnetic flux density in range of B = 0 to 1.7

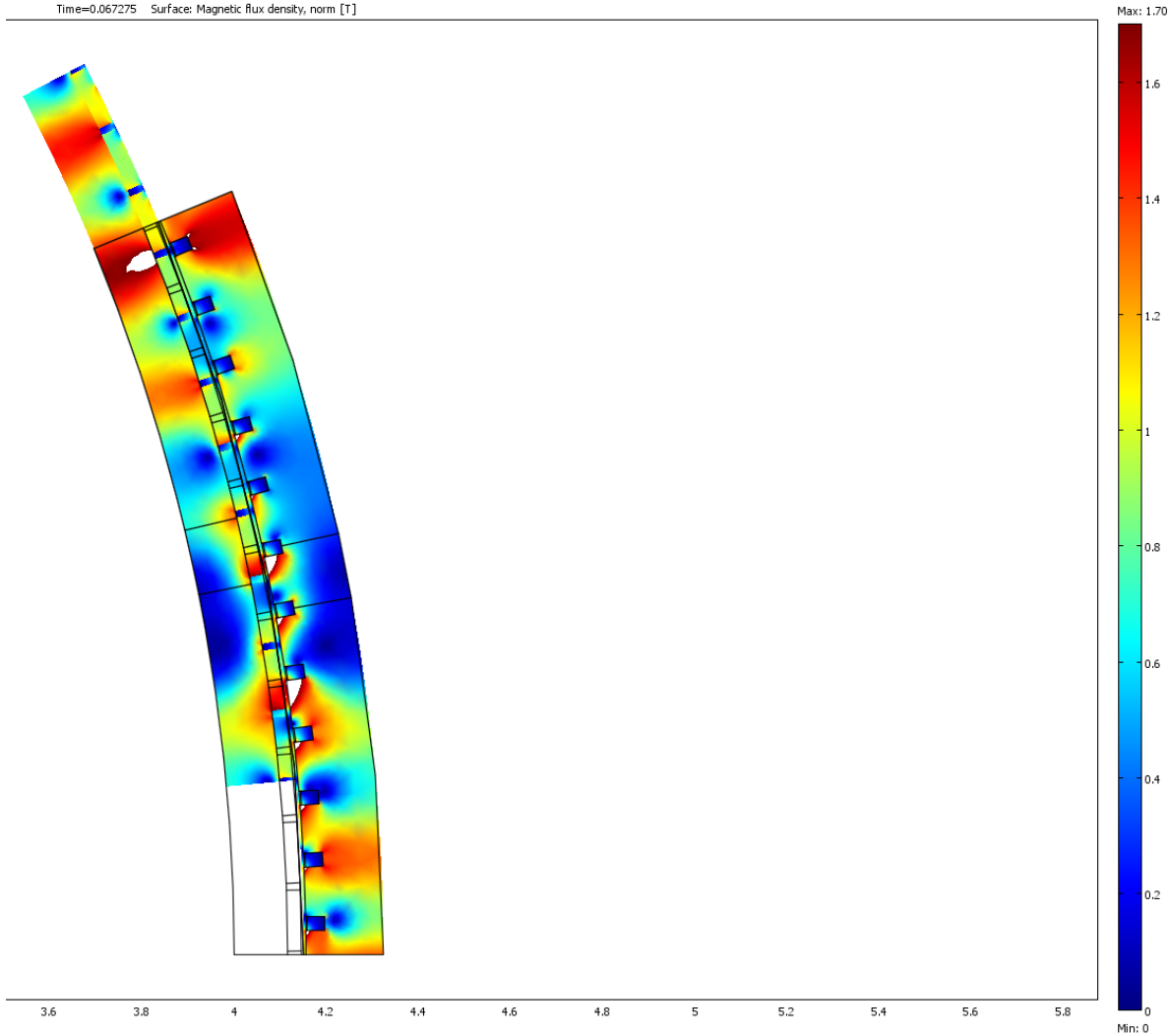


Figure E.19: Plot of magnetic flux density in a range from 0 to 1.7 T.

17. Relative permeability plot at full load condition (Range: 1 to 500)

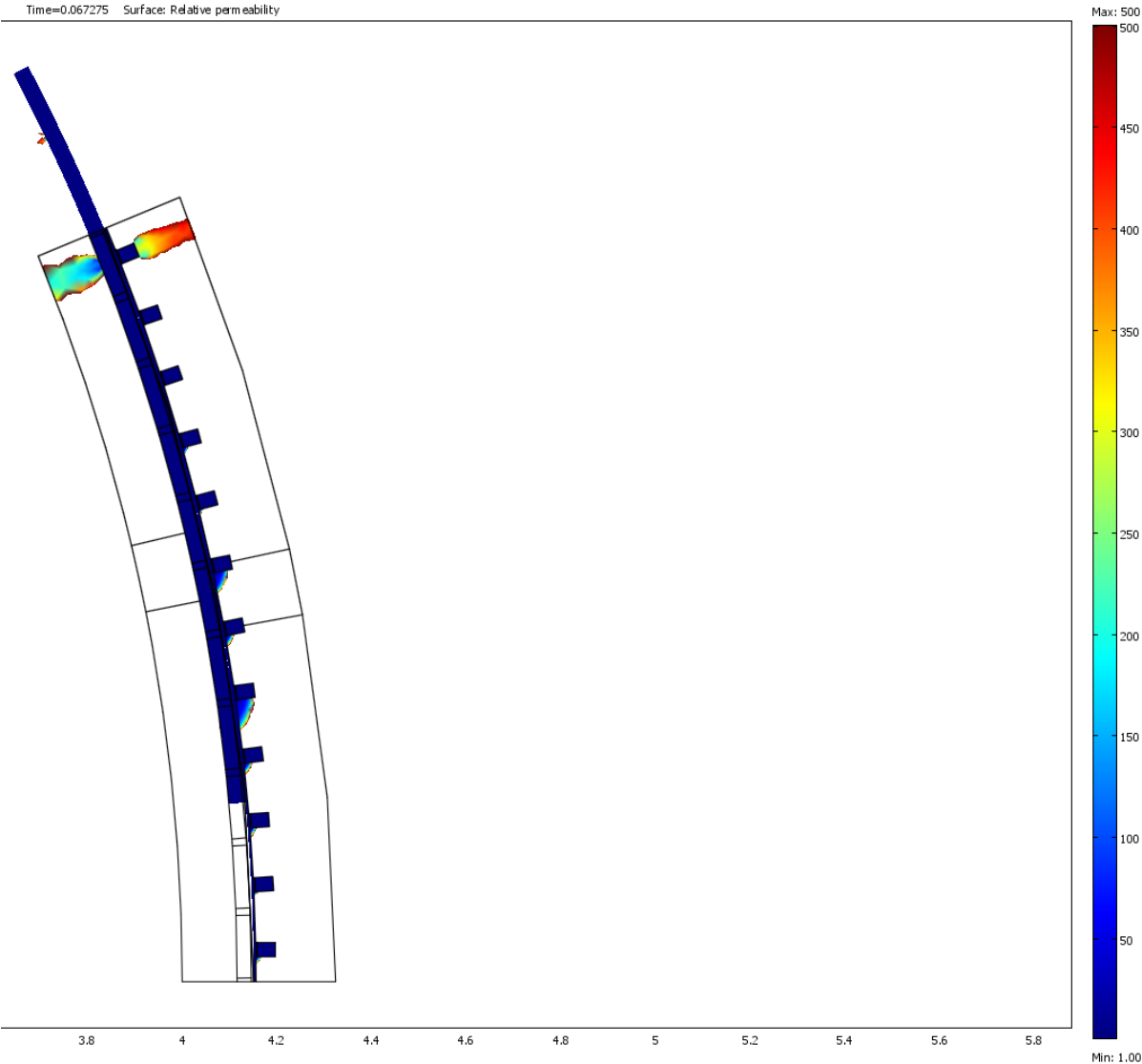


Figure E.20: Plot of relative permeability in a range from 1 to 500 at full load condition.

18. Relative permeability plot at full load condition (Range: 1 to 200)

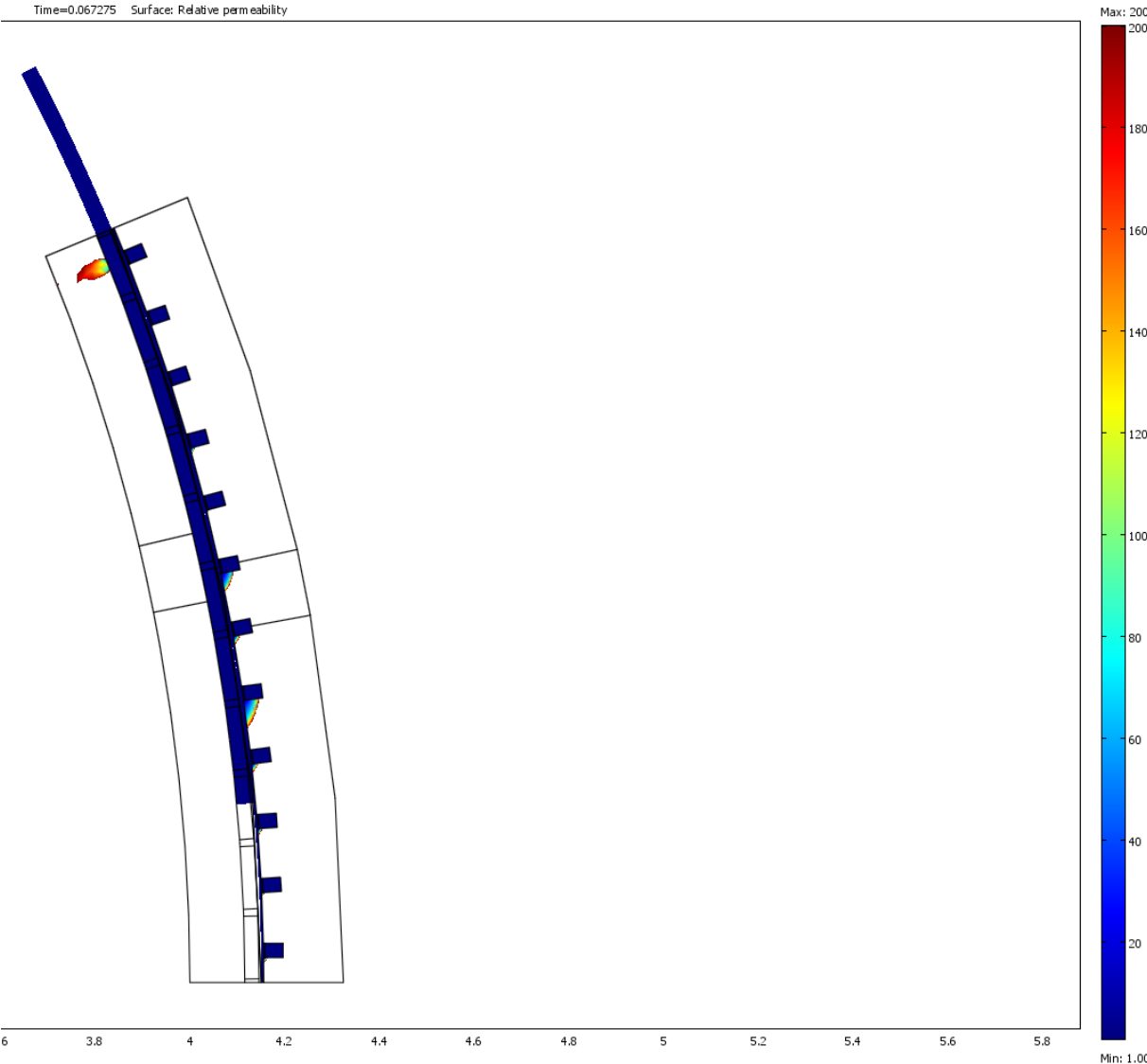


Figure E.21: Plot of relative permeability in a range from 1 to 200 at full load condition.

19. Flux density at the center of the slot

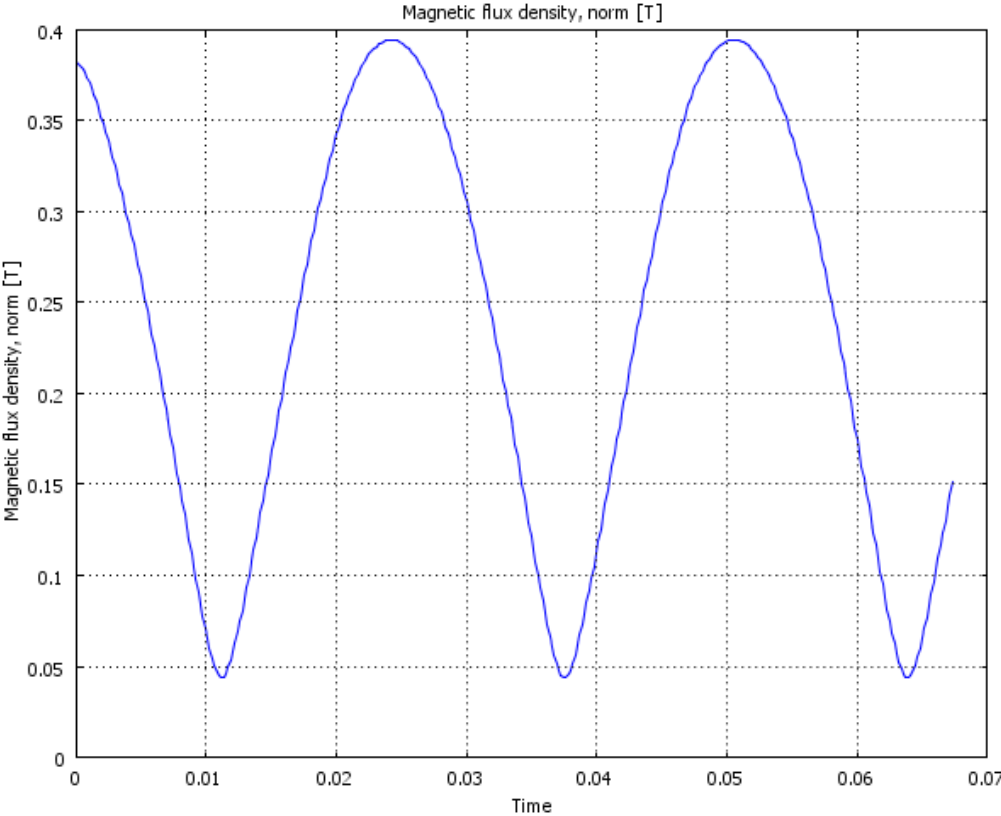


Figure E.22: Variation of flux density at the centre of the slot.

Appendix F FEA results of Machine – 2 (154 pole 168 slots)

1. Input/output panel

The screenshot displays the SmartTool V3.3 software interface, divided into three main sections: Input panel, Control, and Output panel.

Input panel: This section contains various input fields and checkboxes for machine configuration. It includes options for 'inner (Rotor) outer' and 'motor | generator'. Key parameters include:

- Machine key numbers: Rated mechanical power (10000 kW), Rated rotational speed (12.95 rpm), Desired rated voltage (3300 V).
- Machine geometry: Machine inner diameter (8000.02 mm), Magnet length (30 mm), Magnet pitch/pole pitch (0.9), Slot width/slot pitch (0.193), Slot depth/slot width (1.267), Number of poles (154), Number of slots (168).
- Energy density: Copper current density (rms) (160 A/mm²), Flux density in stator yoke (0.4 T), Flux density in rotor yoke (0.45 T).
- Winding data: Copper fill factor under wedge (0.08), Number of parallel branches (6).
- Slot wedge: Thickness slot wedge (3 mm).

Control panel: This panel contains several buttons for simulation and optimization: Calculate, Optimize, Optimization limits, Slot/Pole advice, Winding visualization, Advanced, Cost data, FEA, Save to Excel, and Struct to Works pace.

Output panel: This panel displays the results of the simulation and optimization. It is divided into several sub-sections:

- Geometry (main) and winding:** Stack length (1009.4 mm), Length with end windings (1197.8 mm), Outer active diameter (8759.3 mm), Inner active diameter (8000 mm), Diameter at air gap (8366.6 mm), Slot pitch (156.6 mm), Pole pitch (170.5 mm), Slot depth (38.3 mm), Slot width (30.2 mm), Stator back iron thickness (152.5 mm), Rotor back iron thickness (148.3 mm), Weight of active materials (74947.77 kg), Rotor moment of inertia (591790. kgm²), Number of turns (37), Copper operating temperature (80 deg C).
- Characteristics:** Torque (7373974 Nm), Efficiency (99.9 %), cos_phi (0.7927).
- Electromagnetic values:** Frequency (16.62 Hz), RMS line voltage (3280.8 V), RMS phase induced voltage (1503.4 V), RMS phase current (2214.56 A), Flux density in tooth (0.97 T), Average flux density in air gap (0.78 T), Active power (9975.8 kW), Phase inductance (4993 μH), Synchronous pu reactance (0.6096), RMS Copper current density (160 A/mm²), RMS current loading (87182.5 A/m).
- Losses:** Losses in winding (12.47 W), No Load Losses in magnets (2410.65 W), No Load Losses in teeth (5058.45 W), No Load Losses in stator yoke (4626.82 W), No Load Losses in rotor yoke (8.8 W), Stator loss per area (365 W/m²).
- Coefficients:** Distribution factor (0.958), AC/DC Loss factor (1.2), Magnetic air gap shear force (104361 N/m²).
- Cost:** Material cost of windings (170 NOK), Material cost of magnets (5256 NOK), Material cost of stator laminate (39367 NOK), Material cost of rotor back iron (30154 NOK), Total active cost (74948 NOK).

Figure F.1: Combined input and output panel of optimized parameters.

$$C = \frac{S}{D^2 Ln} = \frac{10000/0.80}{8.4^2 \cdot 1.00 \cdot 12.95} = 13.7$$

Note: The parameters in red color indicate that losses due to harmonics are not included.

2. Machine Parameters:

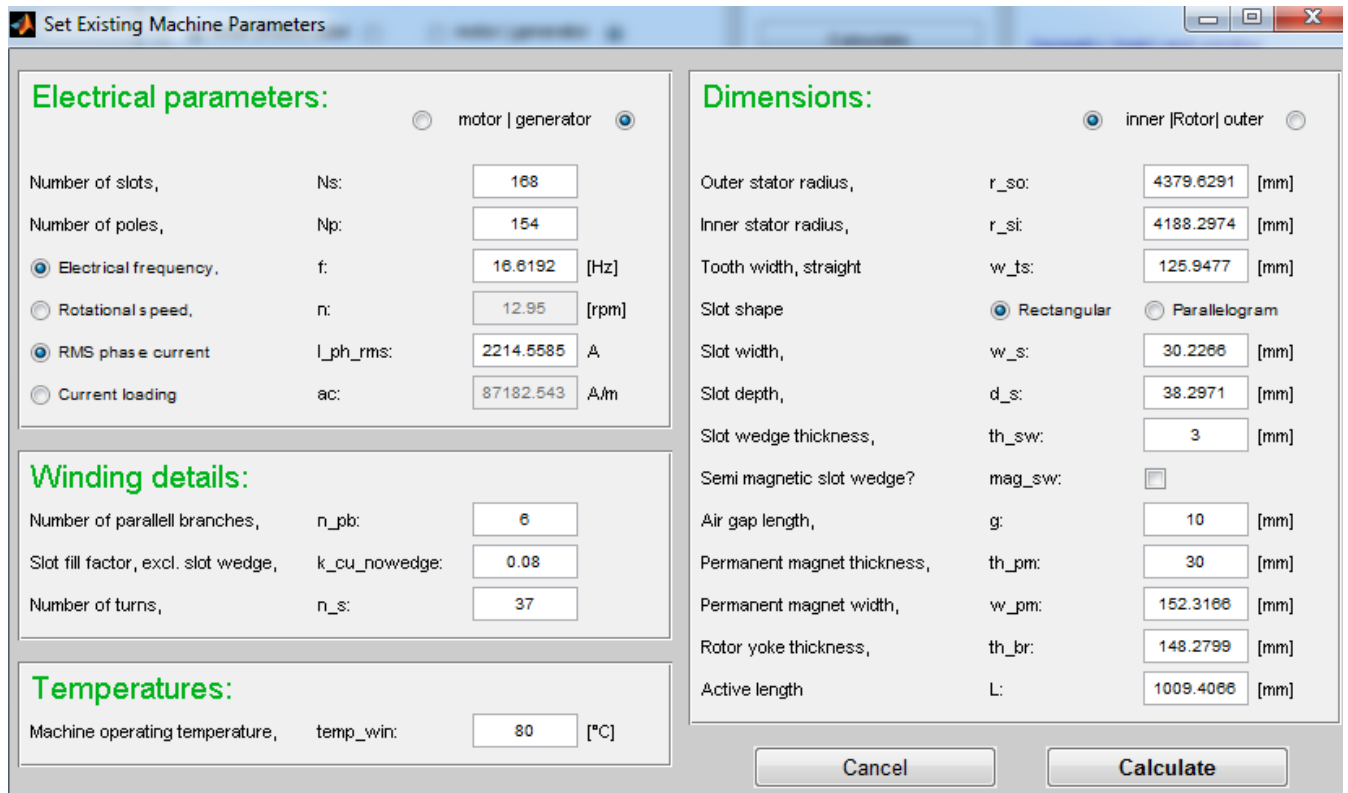


Figure F.2: Input parameters for SC machine - 2.

3. EMF Simulation Plot

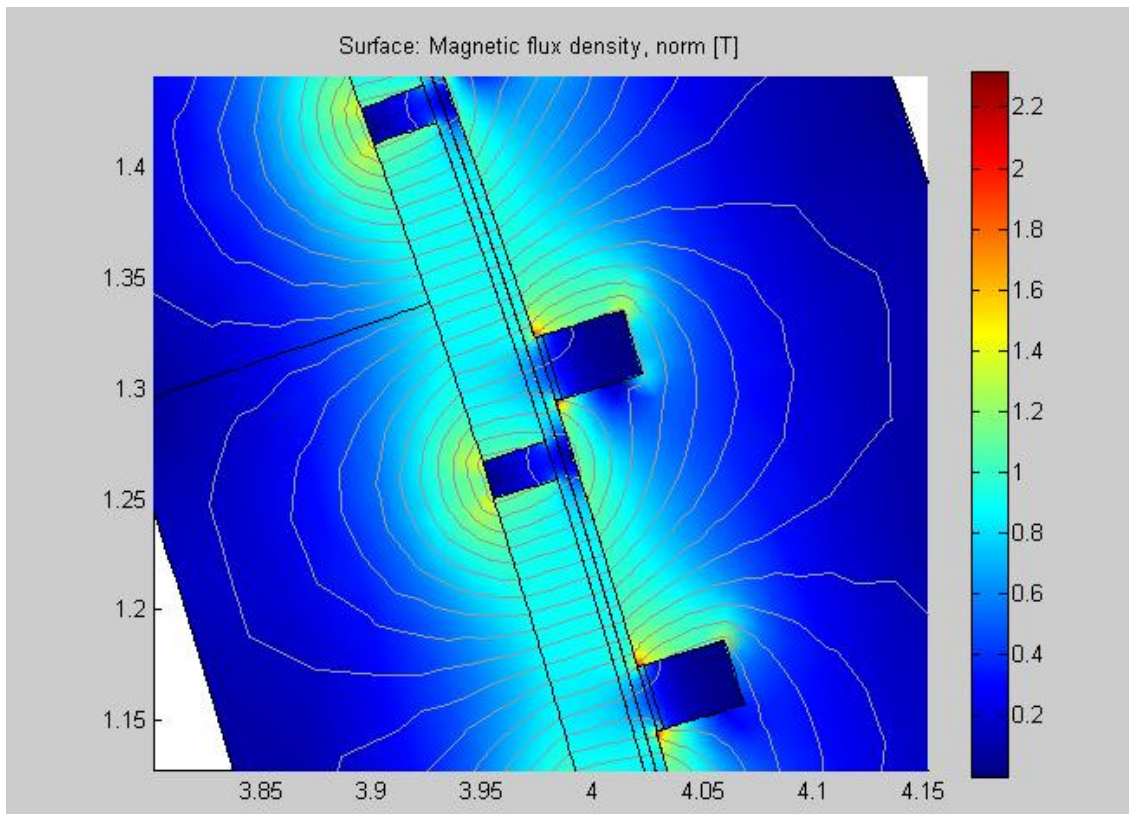


Figure F.3: EMF simulation plot at no-load condition.

4. One period EMF Excitation

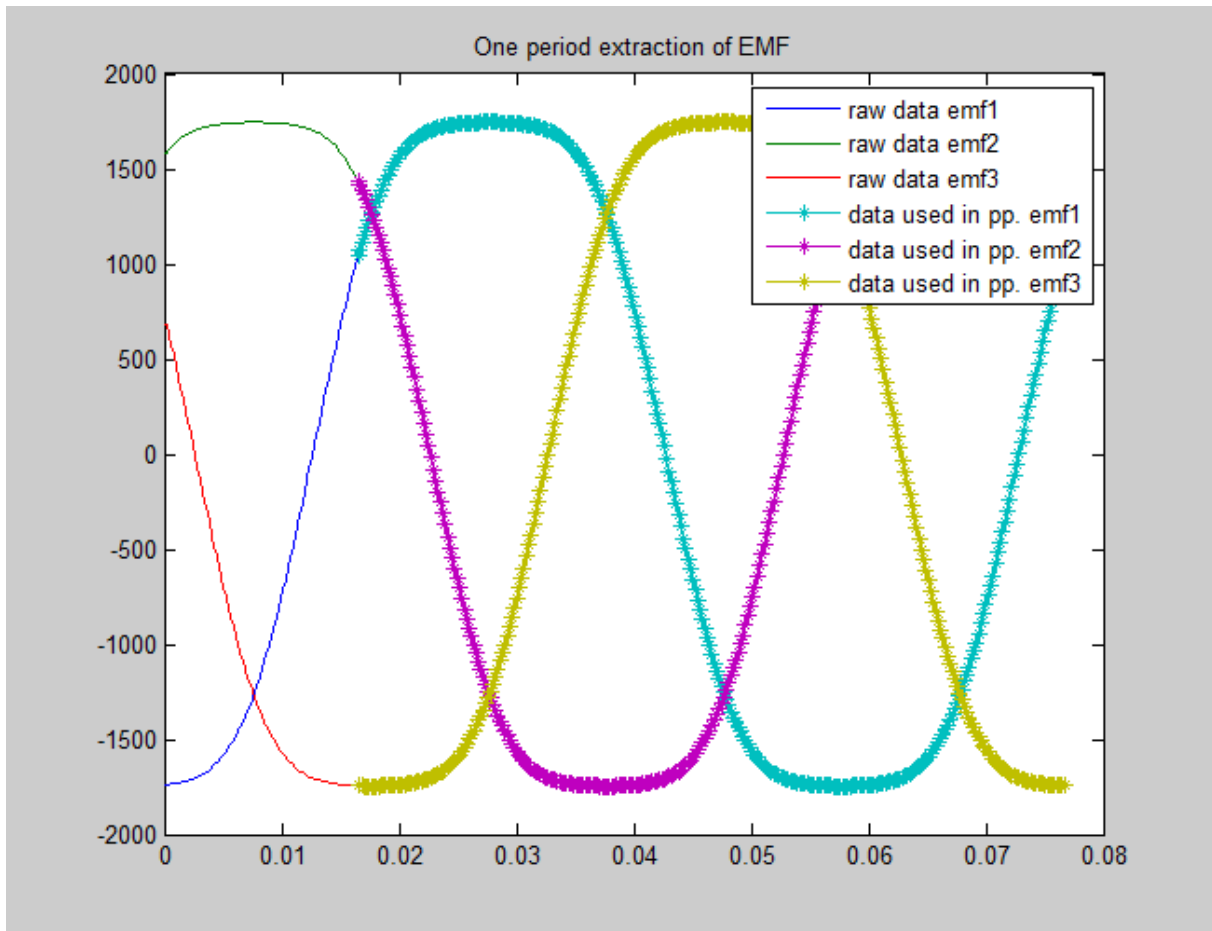


Figure F.4: EMF waveform at no-load condition.

5. EMF Simulation results

Parameters	Machine – 2	Machine – 2
	Phase EMF	Line EMF
Mean first harmonic peak, V	1986.2	3440.2
Mean peak voltage, V	1745.8	3406.7
Phase voltage, 1. harmonics (rms), V	1404	2432
Phase voltage maximum (rms), V	1234	2409
THD (%)	13.2 %	1.15 %

6. Phase and line EMFs

Phase EMFs

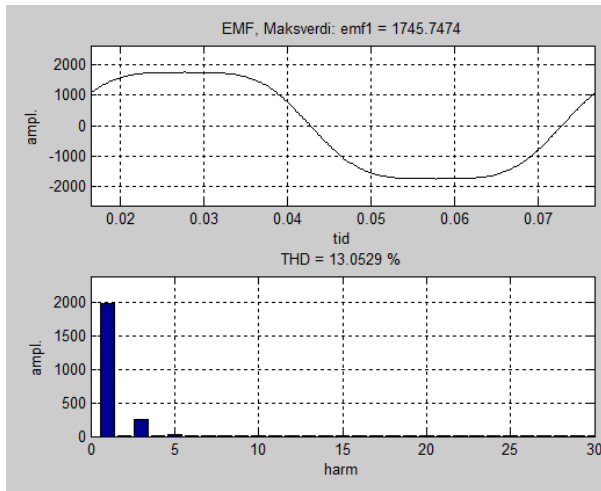


Figure F.5: Plot of EMF and harmonics of Phase - 1.

Line EMFs

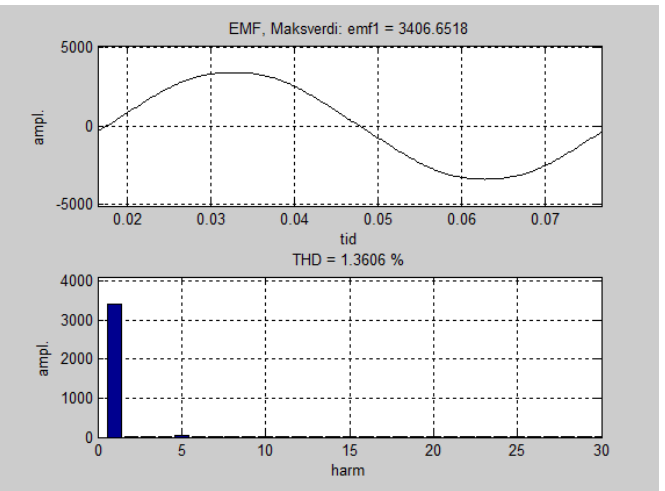


Figure F.6: EMF waveform of line voltage 1.

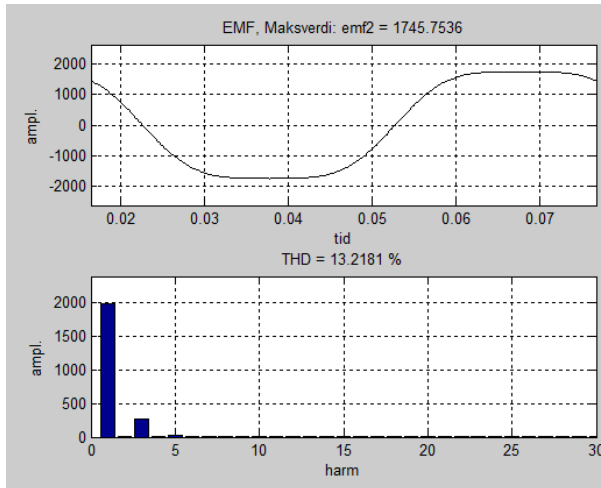


Figure F.7: Plot of EMF and harmonics of Phase - 2.

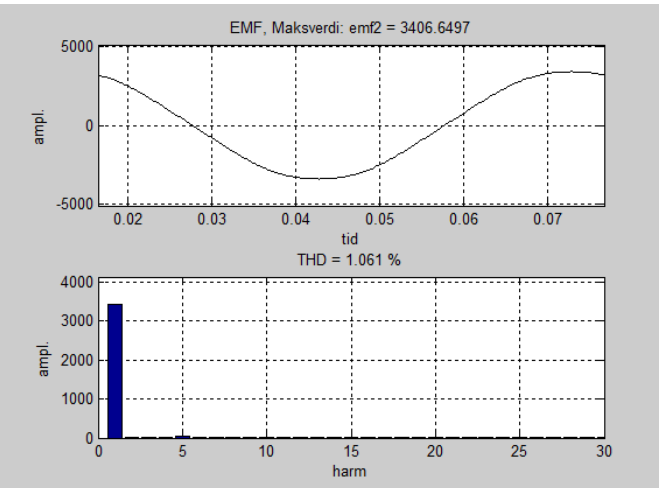


Figure F.8: EMF waveform of line voltage 2.

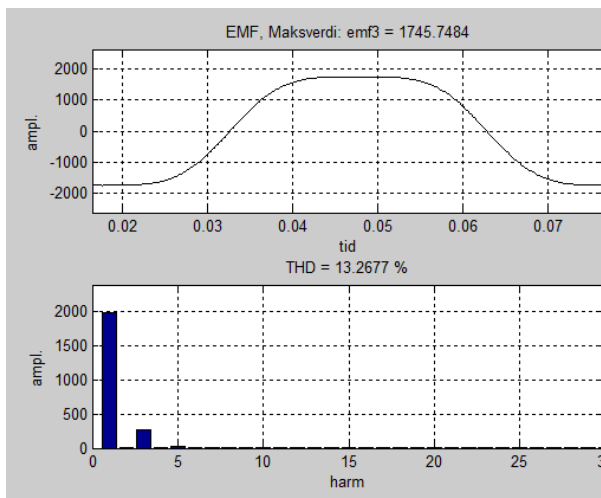


Figure F.9: Plot of EMF and harmonics of Phase - 3.

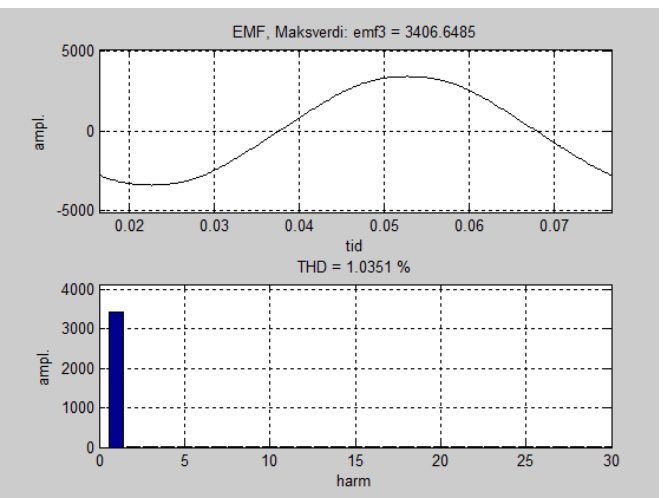


Figure F.10: EMF waveform of line voltage 3.

7. Full Load Simulation plot

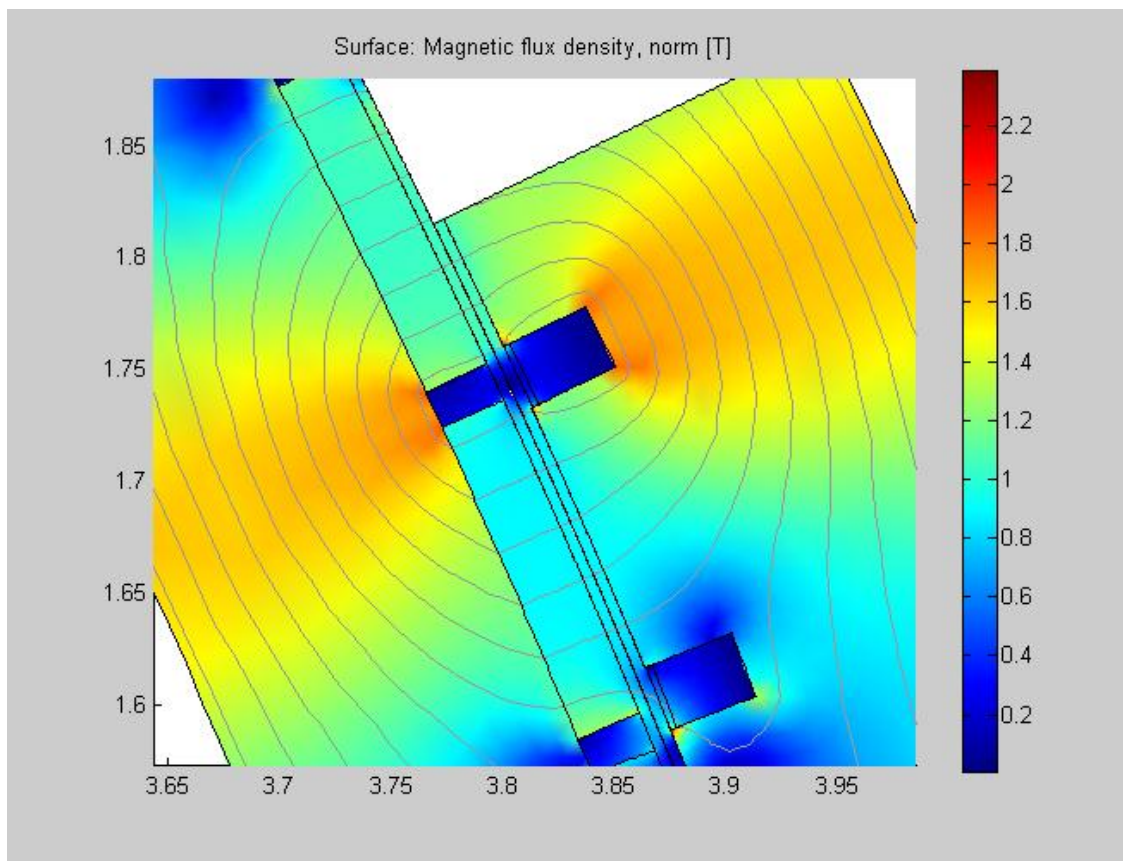


Figure F.11: Magnetic flux density in stator and rotor yoke at full load.

8. Full load torque

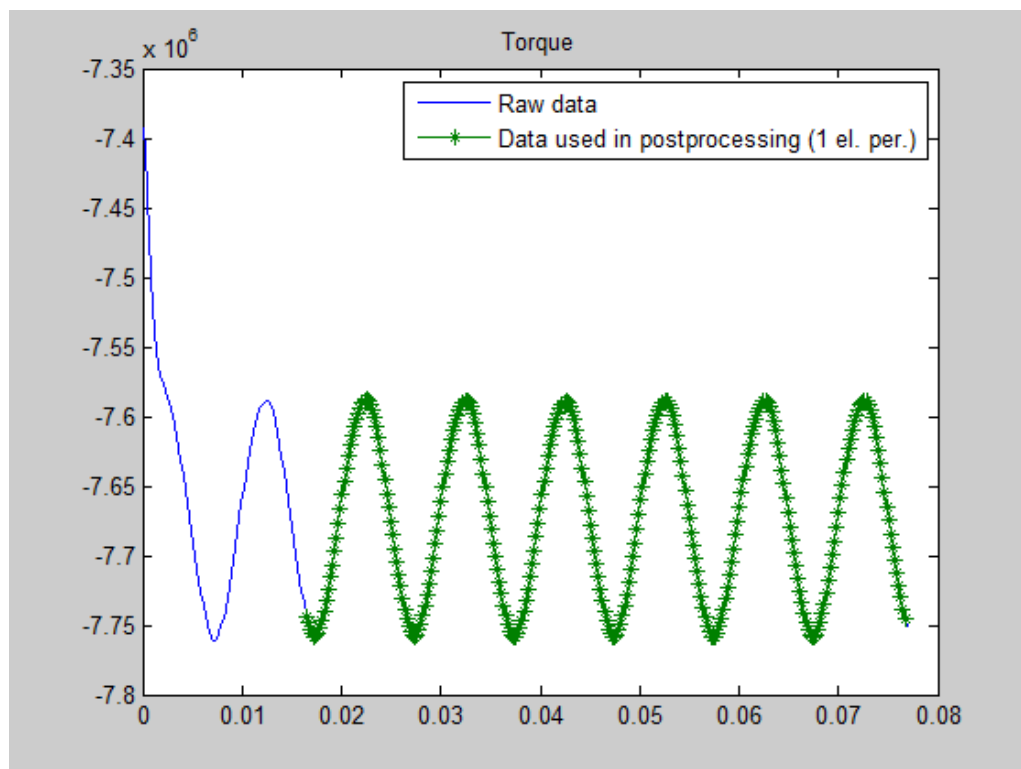


Figure F.12: Full load torque.

9. Full load torque Harmonics

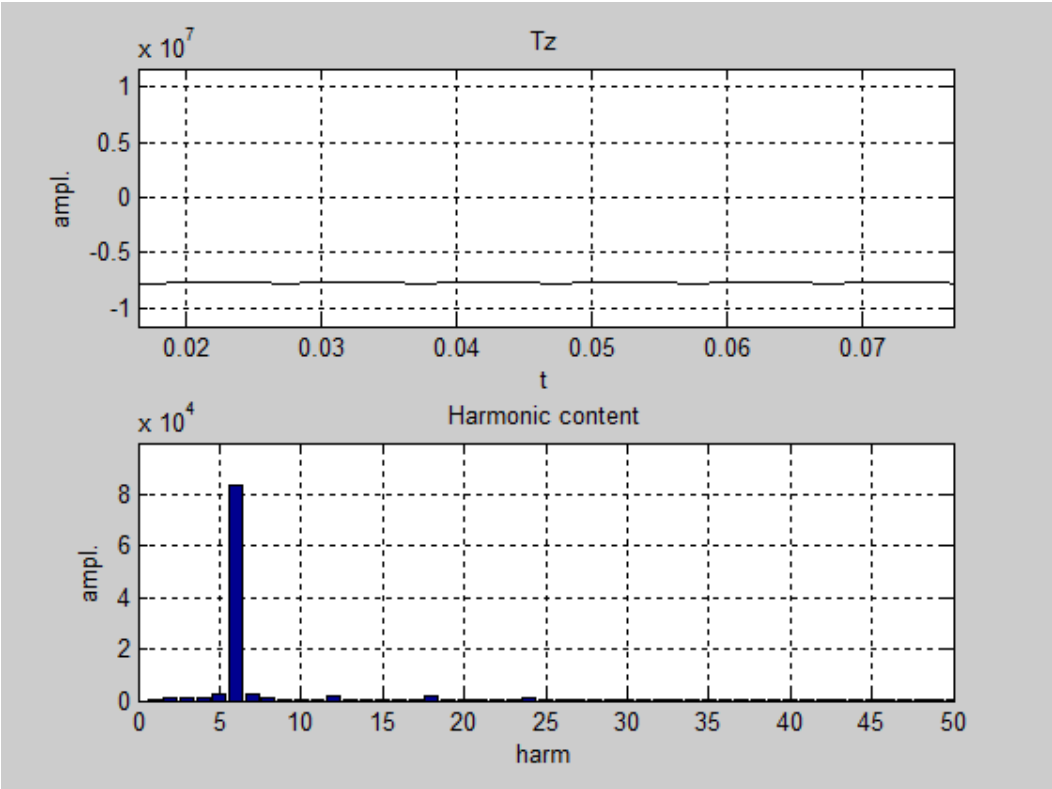


Figure F.13: Plot of full load torque amplitude and harmonics.

10. Full load PM losses

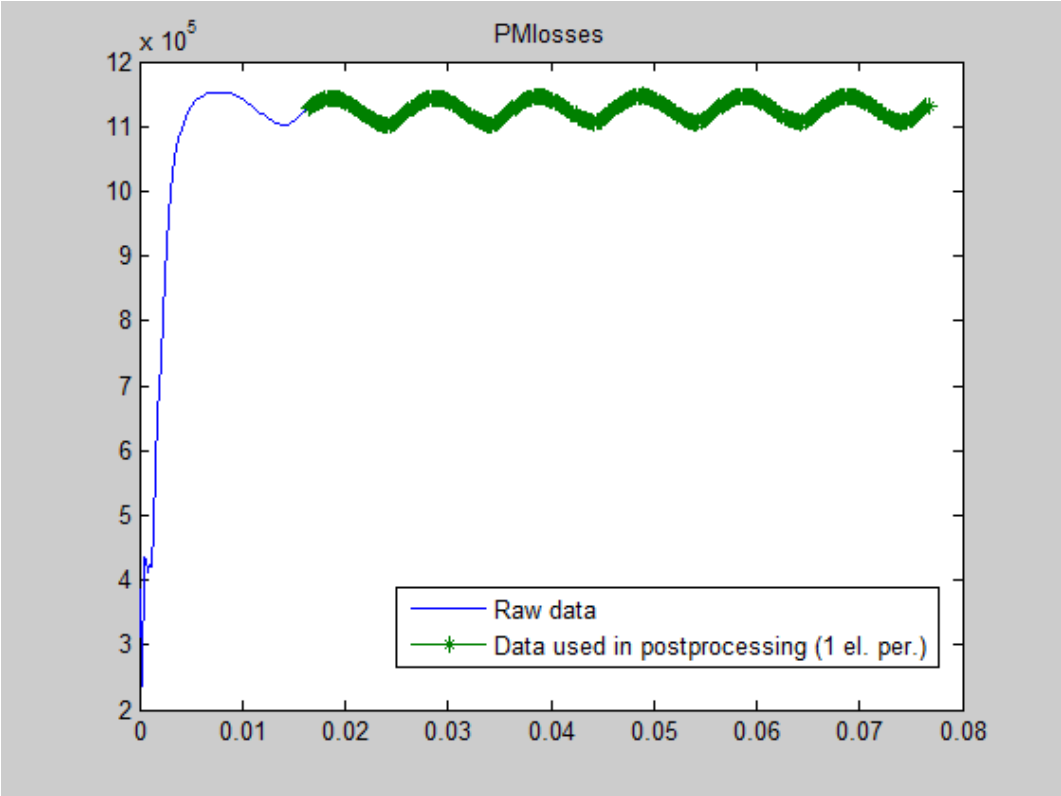


Figure F.14: Full load PM losses.

11. Full load rotor core flux density

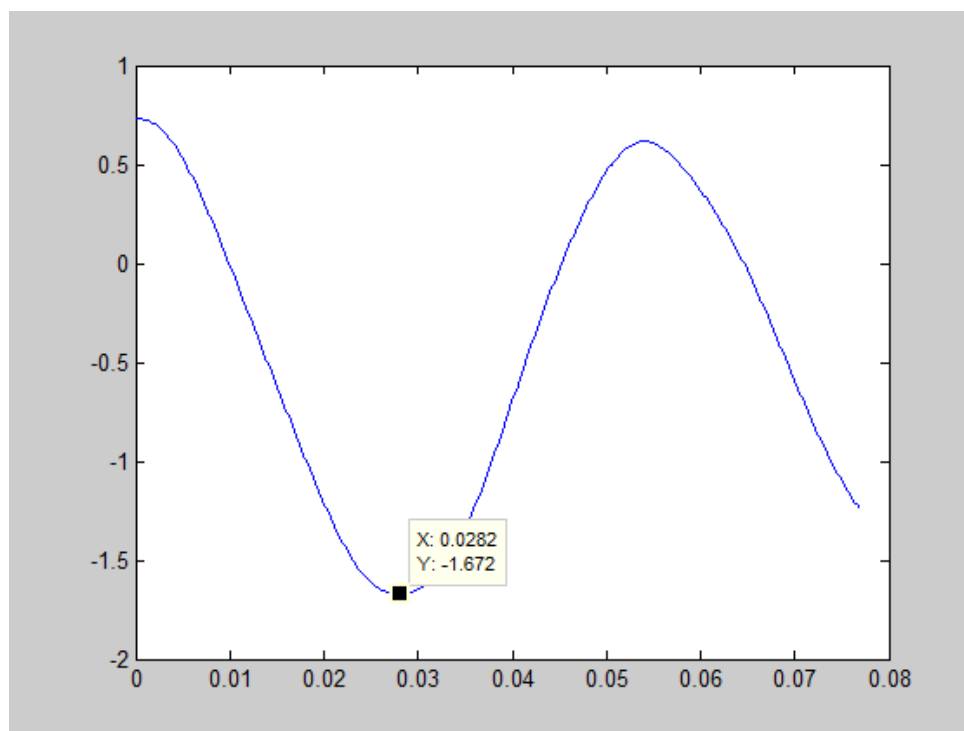


Figure F.15: Rotor core flux density at full load.

12. Smarttool FEA simulation results

Phase inductance	5797 μ H
Induced voltage	
Phase voltage, 1. harmonic (rms)	1404 V
Phase voltage, maximum (rms)	1234 V
Total harmonic distortion (THD)	13.1795 %
Torque	
Cogging torque amplitude at noload	1587.0363
Mean torque at full load	-7671708.6
Torque ripple amplitude at full load (pu)	-1.1147 %
Losses	
Iron loss in stator at noload	14681.8852
Iron loss in rotor at noload	237.3728 W
Induced loss in magnets at noload	16743.9667
Iron loss in stator at full load	40621.2773
Iron loss in rotor at full load	30872.5648
Induced loss in magnets at full load	1126867.85

OK Write to command window

Figure F.16: Summary of FEA simulation results.

No load simulation:

Loss results:

Average PM loss = 16744 W

Max stator core loss = 14681.9 W

Max rotor core loss = 237.373 W

Where $B_{max} = 0.476345$ T and $B_{off} = 0.471694$ T**Full load simulation:**

Loss results:

Average PM loss = 1.12687e+006 W

Max stator core loss = 40621.3 W

Max rotor core loss = 30872.6 W

Where $B_{max} = 1.67174$ T and $B_{off} = 0.471099$ T**SmartTool FEA simulation results:**Phase inductance = 5797 μ H

Induced voltage

Line voltage, 1. harmonic (rms) = 1404 V

Line voltage, maximum (rms) = 1234 V

Total harmonic distortion (THD) = 13.1795 %

Torque

Cogging torque amplitude at noload = 1587.0363 Nm

Mean torque at full load = -7671708.6463 Nm

Torque ripple amplitude at full load (pu) = -1.1147 %

13. Surface plot of magnetic flux density at full load

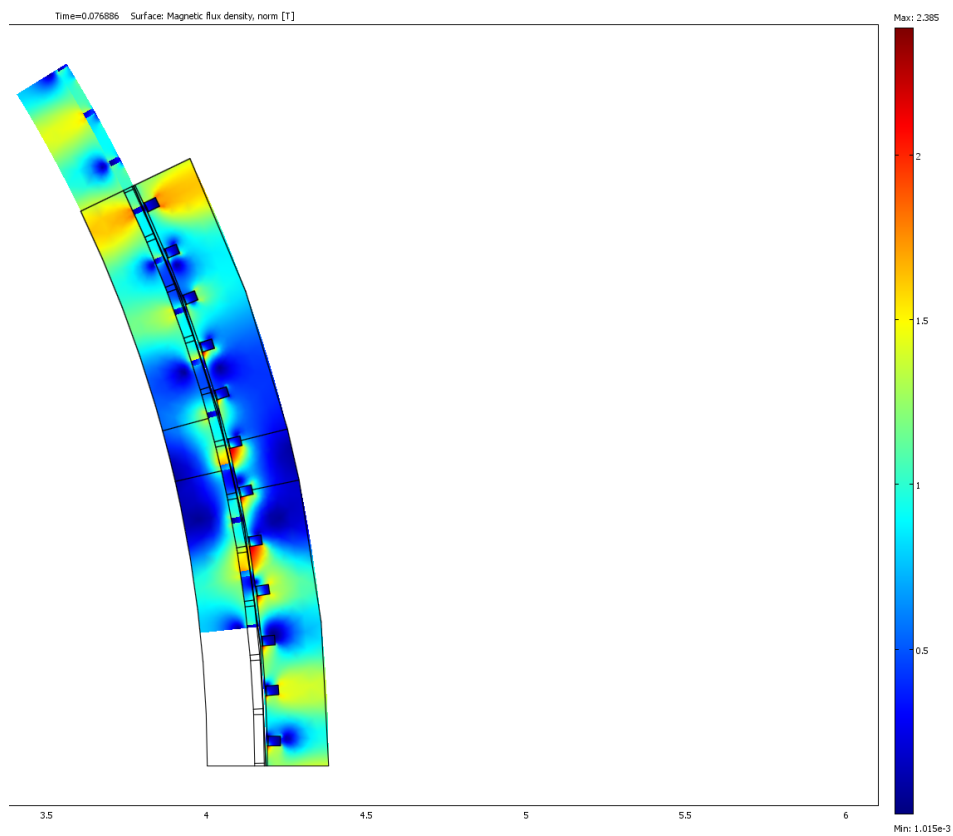


Figure F.17: COMSOL plot of magnetic flux density at full load.

14. Surface plot of magnetic flux density at full load in range of B=0 to 2 T

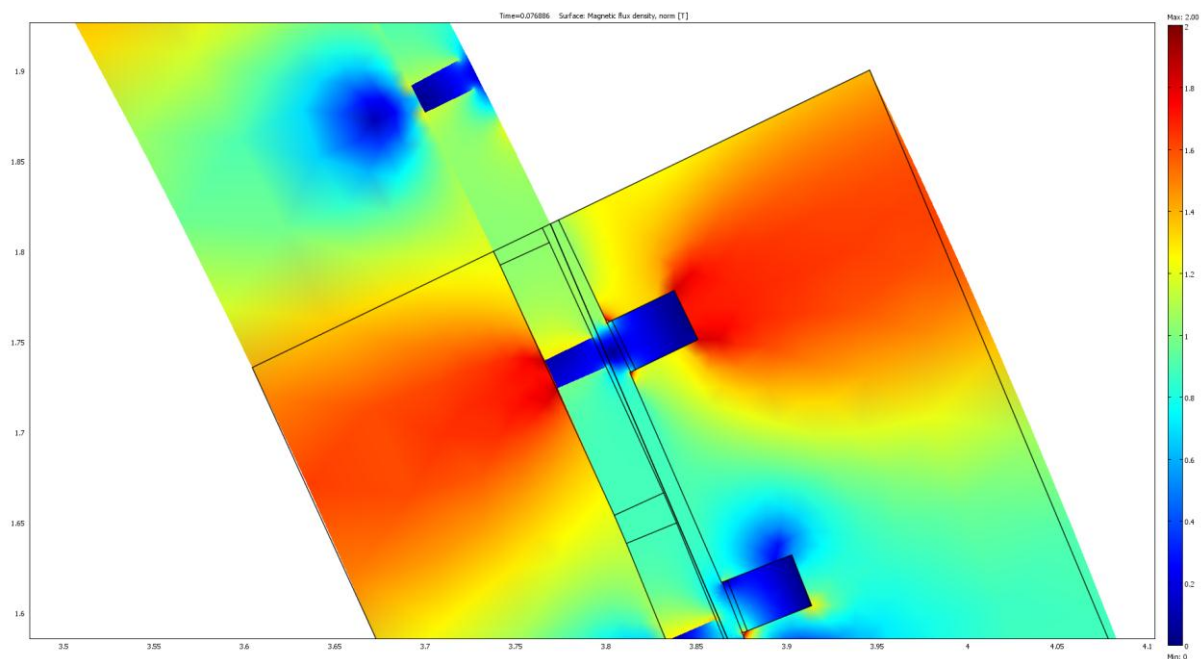


Figure F.18: Magnetic flux density in stator and rotor yoke at full load.

15. Surface plot of magnetic flux density at full load in range of B = 0 to 1.7

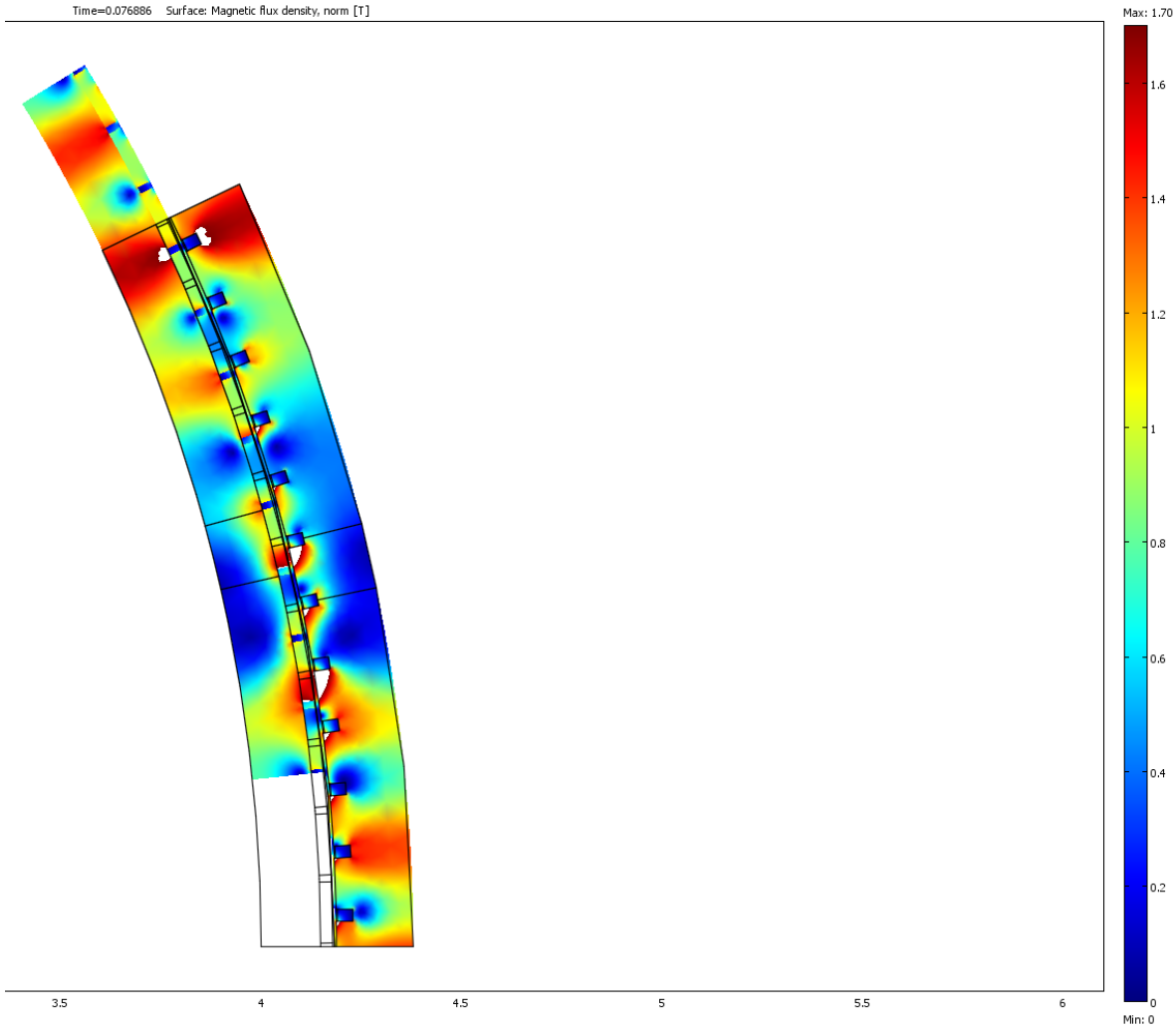


Figure F.19: Plot of magnetic flux density at full load in range from 0 to 1.7 T.

16. Relative permeability plot at full load condition (Range: 1 to 500)

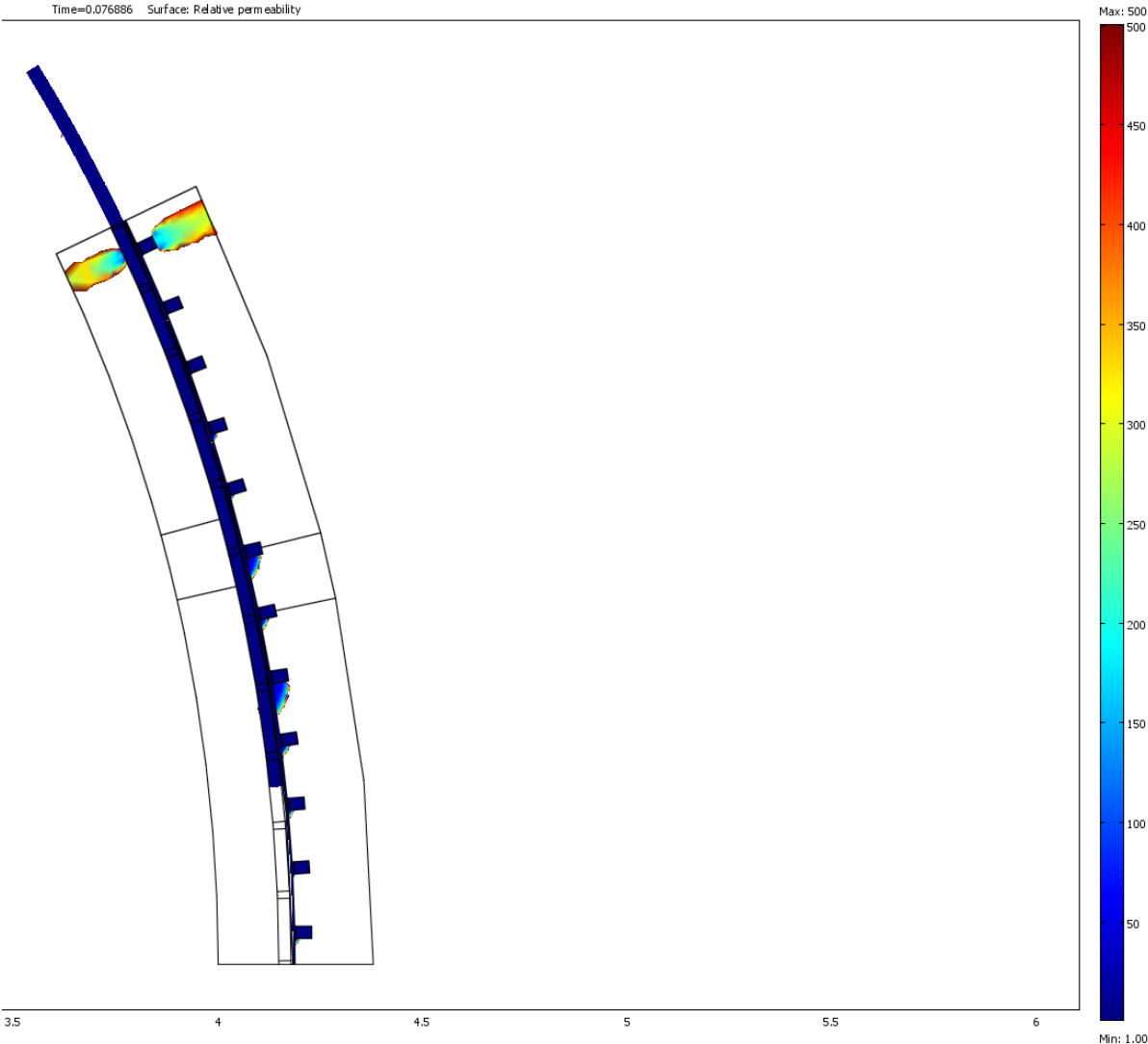


Figure F.20: Relative permeability in a range from 1 to 500 at full load.

17. Relative permeability plot at full load condition (Range: 1 to 200)

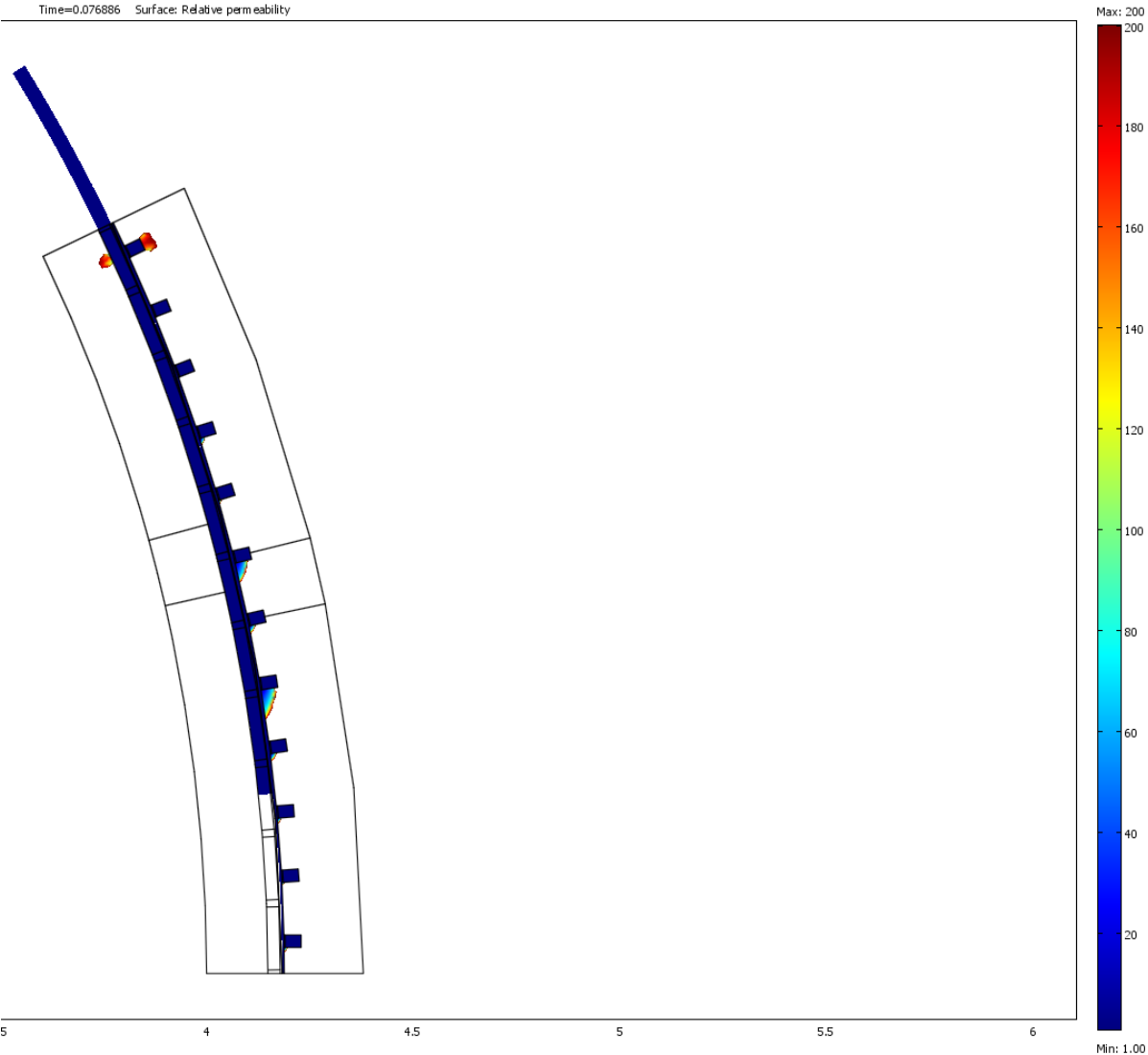


Figure F.21: Relative permeability in a range from 1 to 200 at full load.

Appendix G FEA results of Machine – 3 (132 pole 144 slots)

1. Input/output panel

The screenshot displays the SmartTool V3.3 software interface, divided into three main sections: Input panel, Control, and Output panel.

Input panel: This section contains various input parameters for the machine design. It includes radio buttons for 'inner [Rotor] outer' (selected) and 'motor | generator'. Under 'Machine key numbers', parameters like Rated mechanical power (10000 kW), Rated rotational speed (12.95 rpm), and Desired rated voltage (3298 V) are shown. 'Machine geometry' includes Machine outer diameter (7800 mm) and Machine inner diameter (30 mm). 'Energy density' shows Copper current density (rms) at 190 A/mm². 'Winding data' includes Copper fill factor under wedge (0.08) and Number of parallel branches (6). 'Slot wedge' shows Thickness slot wedge (3 mm). A 'Set existing machine para...' button is also present.

Control: This central panel contains several functional buttons: Calculate, Optimize, Optimization limits, Slot/Pole advice, Winding visualization, Advanced, Cost data, FEA, Save to Excel, and Struct to Works pace.

Output panel: This section displays the results of the optimization. It is divided into several categories:

- Geometry (main) and winding:** Stack length (1006.8 mm), Length with end windings (1221.9 mm), Outer active diameter (8750.6 mm), Inner active diameter (7800 mm), Diameter at air gap (8254.3 mm), Slot pitch (180.3 mm), Pole pitch (196.2 mm), Slot depth (37.9 mm), Slot width (29.9 mm), Stator back iron thickness (204.6 mm), Rotor back iron thickness (192.1 mm), Weight of active materials (93741.76 kg), Rotor moment of inertia (698002. kg*m²), Number of turns (42), and Copper operating temperature (20 deg C).
- Characteristics:** Torque (7373974 Nm), Efficiency (99.9%), and cos_phi (0.7623).
- Electromagnetic values:** Frequency (14.25 Hz), RMS line voltage (3332.7 V), RMS phase induced voltage (1468.2 V), RMS phase current (2268.33 A), Flux density in tooth (0.93 T), Average flux density in air gap (0.78 T), Active power (9981.6 kW), Phase inductance (6133.9 µH), Synchronous pu reactance (0.6472), RMS Copper current density (190 A/mm²), and RMS current loading (88066.7 A/m).
- Losses:** Losses in winding (12.25 W), No Load Losses in magnets (1134.95 W), No Load Losses in teeth (4027.26 W), No Load Losses in stator yoke (4029.64 W), No Load Losses in rotor yoke (3.79 W), and Stator loss per area (308 W/m²).
- Coefficients:** Distribution factor (0.958), ACDC Loss factor (1.2), and Magnetic air gap shear force (107499 N/m²).
- Cost:** Material cost of windings (147 NOK), Material cost of magnets (5172 NOK), Material cost of stator laminate (50198 NOK), Material cost of rotor back iron (38226 NOK), and Total active cost (93742 NOK).

Figure G.1: Combined input and output panel of optimized parameters.

$$C = \frac{S}{D^2 L n} = \frac{10000 / 0.762}{8.255^2 \cdot 1.07 \cdot 12.95} = 13.9$$

Note: The parameters in red color indicate that losses due to harmonics are not included.

2. Machine Parameters:

Set Existing Machine Parameters

Electrical parameters: motor | generator

Number of slots, Ns: 144

Number of poles, Np: 132

Electrical frequency, f: 14.245 [Hz]

Rotational speed, n: 12.95 [rpm]

RMS phase current, I_{ph_rms}: 2268.3347 A

Current loading, ac: 88066.729 A/m

Winding details:

Number of parallel branches, n_{pb}: 6

Slot fill factor, excl. slot wedge, k_{cu_nowedge}: 0.08

Number of turns, n_s: 42

Temperatures:

Machine operating temperature, temp_{win}: 20 [°C]

Dimensions: inner [Rotor] outer

Outer stator radius, r_{so}: 4375.3031 [mm]

Inner stator radius, r_{si}: 4132.1486 [mm]

Tooth width, straight, w_{ts}: 153.2537 [mm]

Slot shape: Rectangular Parallelogram

Slot width, w_s: 29.9222 [mm]

Slot depth, d_s: 37.9114 [mm]

Slot wedge thickness, th_{sw}: 3 [mm]

Semi magnetic slot wedge?, mag_{sw}:

Air gap length, g: 10 [mm]

Permanent magnet thickness, th_{pm}: 30 [mm]

Permanent magnet width, w_{pm}: 175.2938 [mm]

Rotor yoke thickness, th_{br}: 192.1453 [mm]

Active length, L: 1006.7828 [mm]

Buttons: Cancel, Calculate

Figure G.2: Input parameters for Machine - 3.

3. EMF Simulation Plot

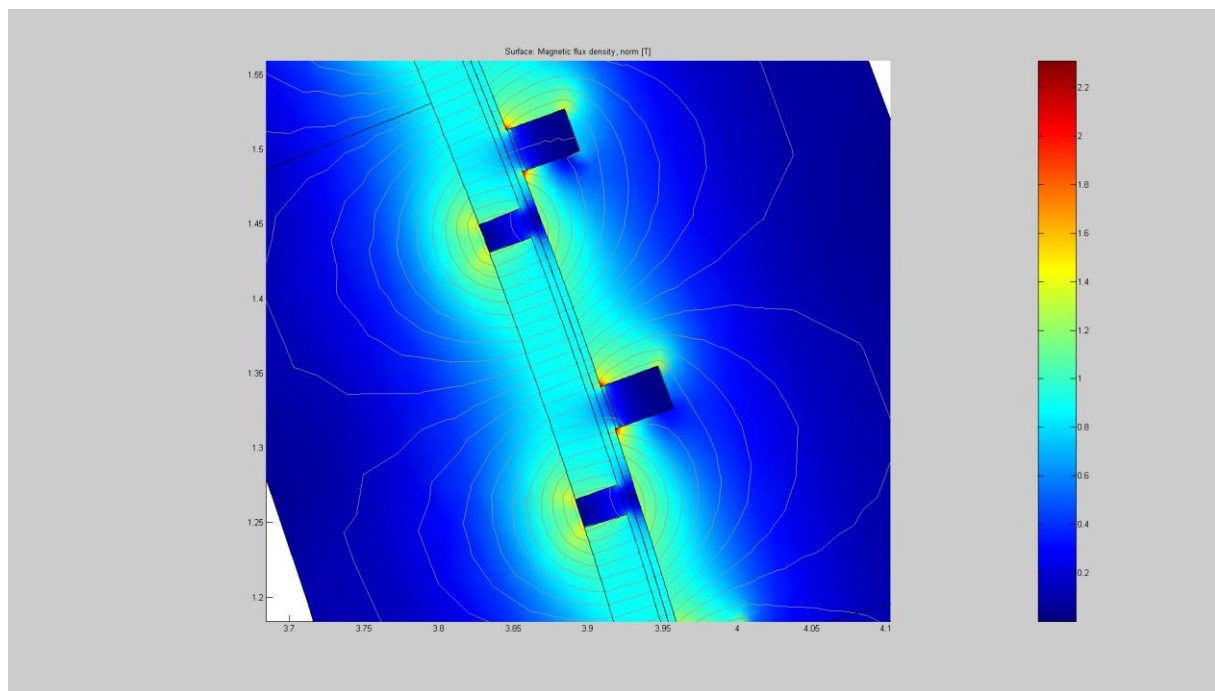


Figure G.3: EMF simulation plot.

4. One period EMF Excitation

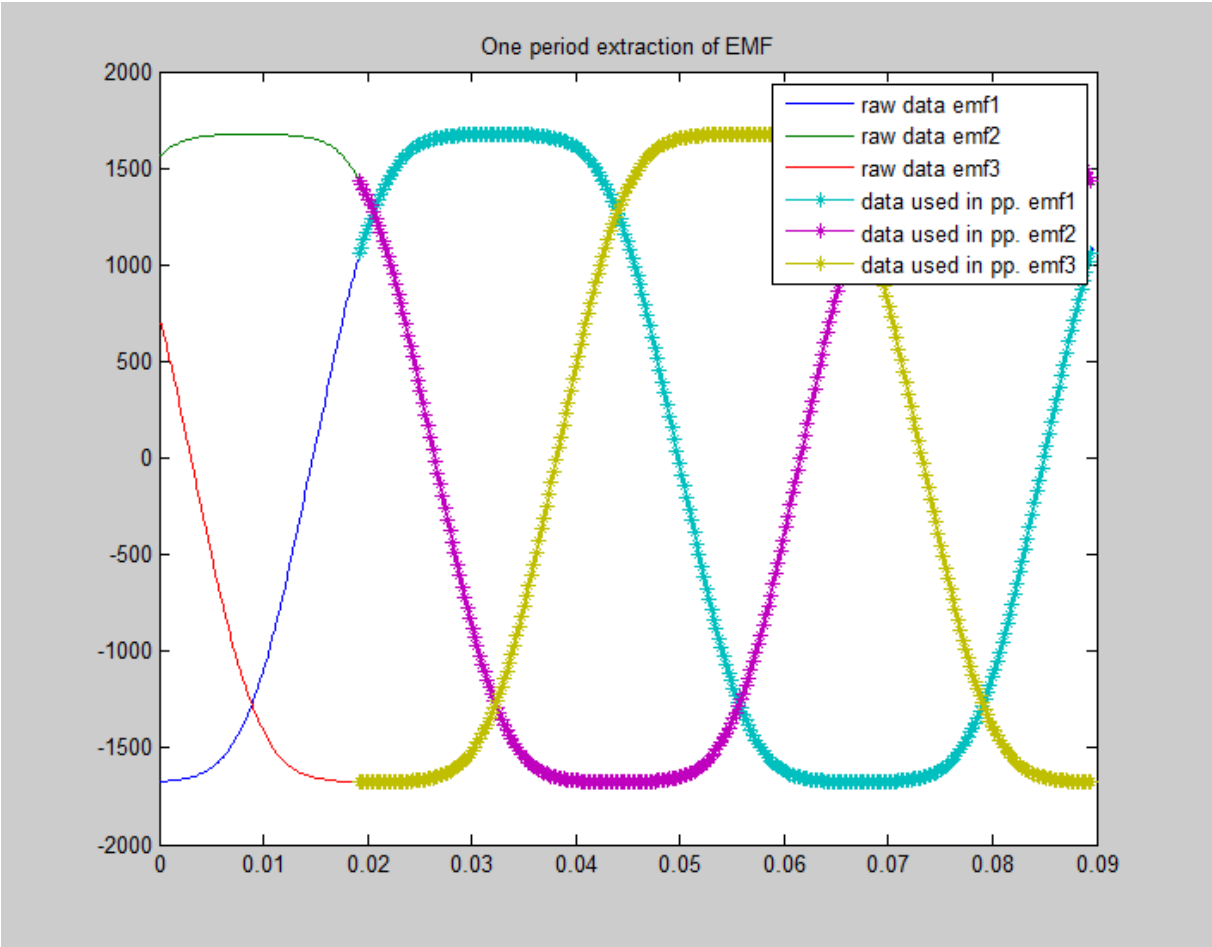


Figure G.4: EMF plot at no-load condition.

5. EMF simulation results

Parameters	Machine – 3	Machine – 3
	Phase EMF	Line EMF
Mean first harmonic peak, V	1937.2	3355.4
Mean peak voltage, V	1677.1	3303.4
Phase voltage, 1. harmonics (rms), V	1370	2372
Phase voltage maximum (rms), V	1186	2336
THD (%)	15.0 %	1.52 %

6. Phase and Line EMFs

Phase EMF

Line EMF

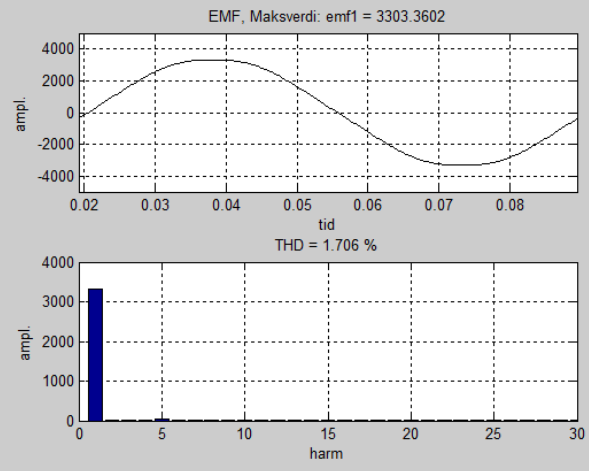
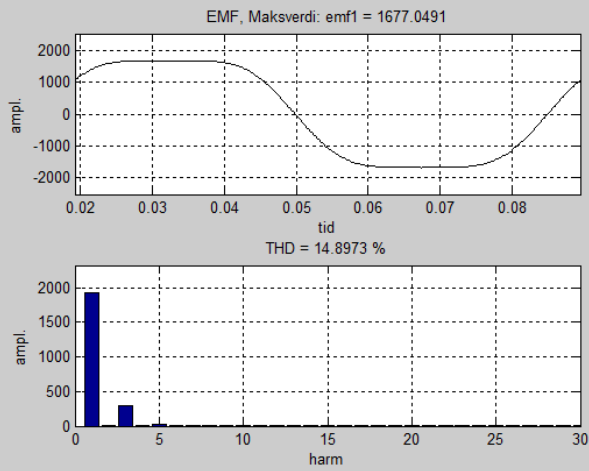


Figure G.5: Plot of EMF and harmonics of Phase - 1.

Figure G.6: EMF waveform of line voltage 1.

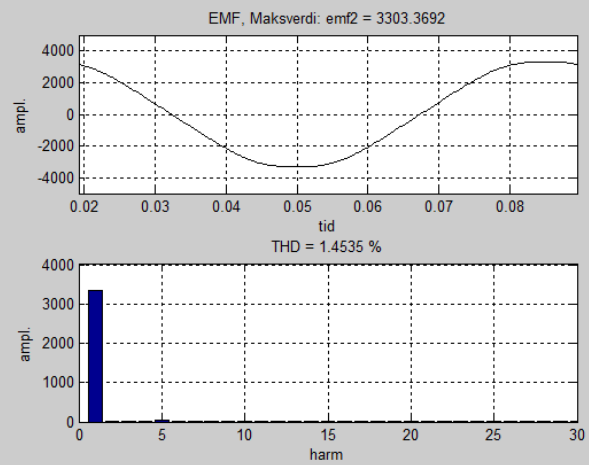
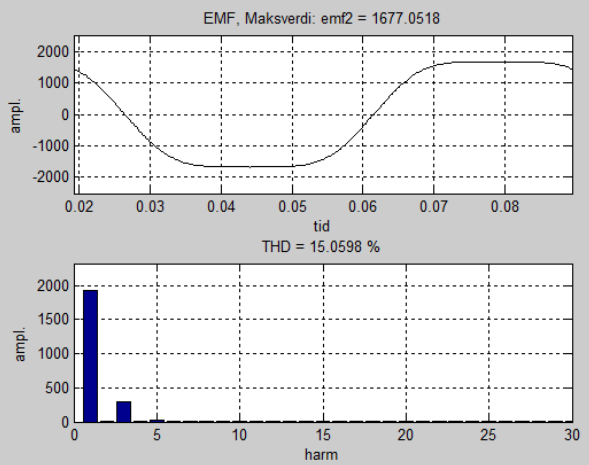


Figure G.7: Plot of EMF and harmonics of Phase - 2.

Figure G.8: EMF waveform of line voltage 2.

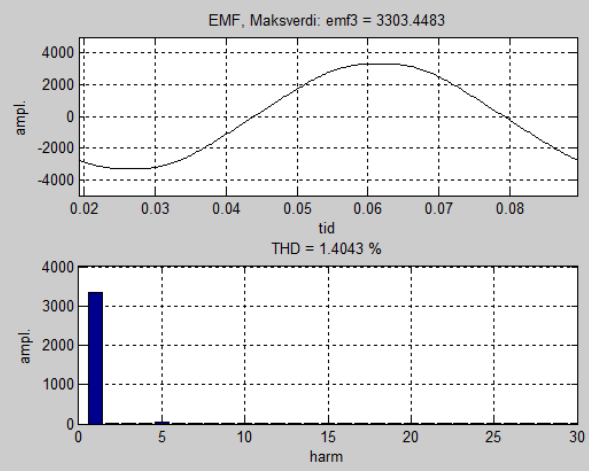
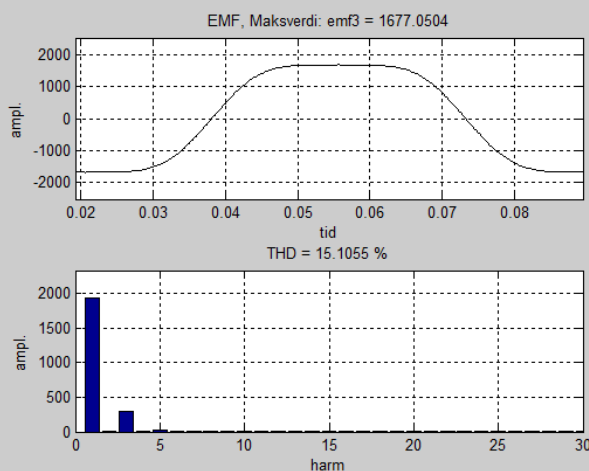


Figure G.9: Plot of EMF and harmonics of Phase - 3.

Figure G.10: EMF waveform of line voltage 3.

7. Full Load Simulation

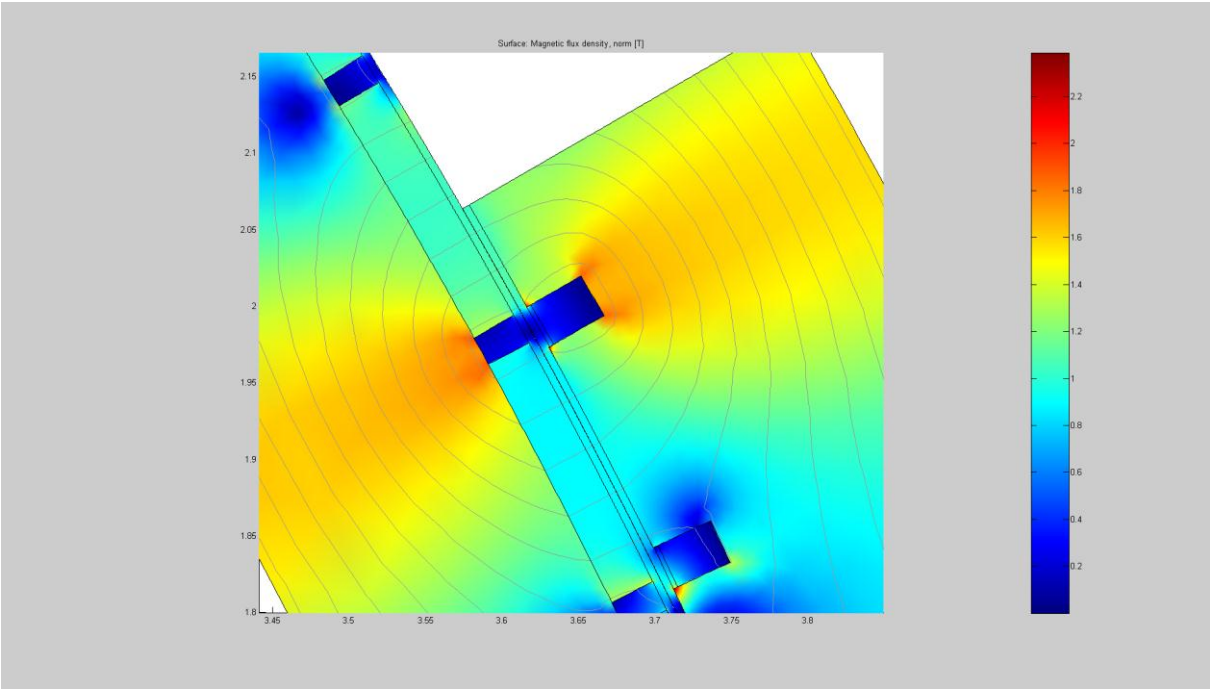


Figure G.11: Magnetic flux density at full load.

8. Full load torque

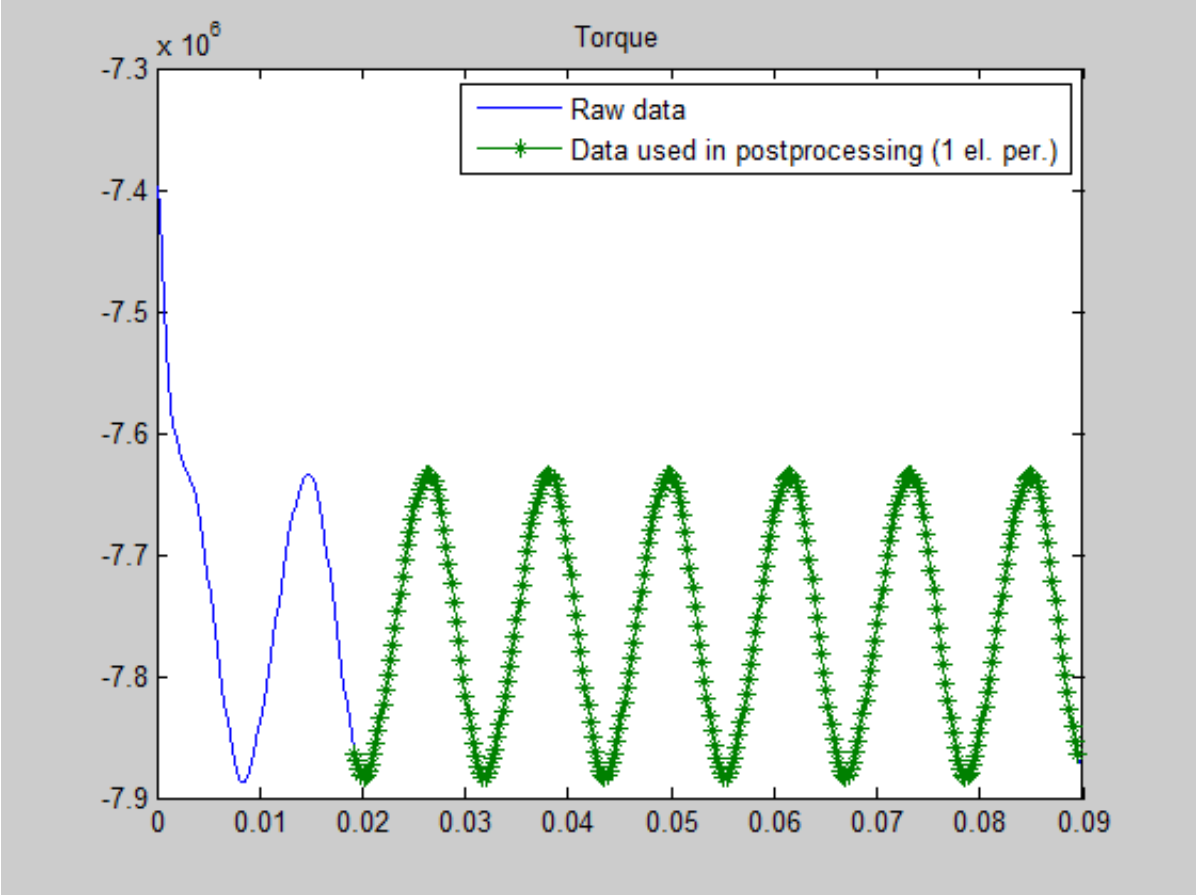


Figure G.12: Torque at full load.

9. Full load torque Harmonics

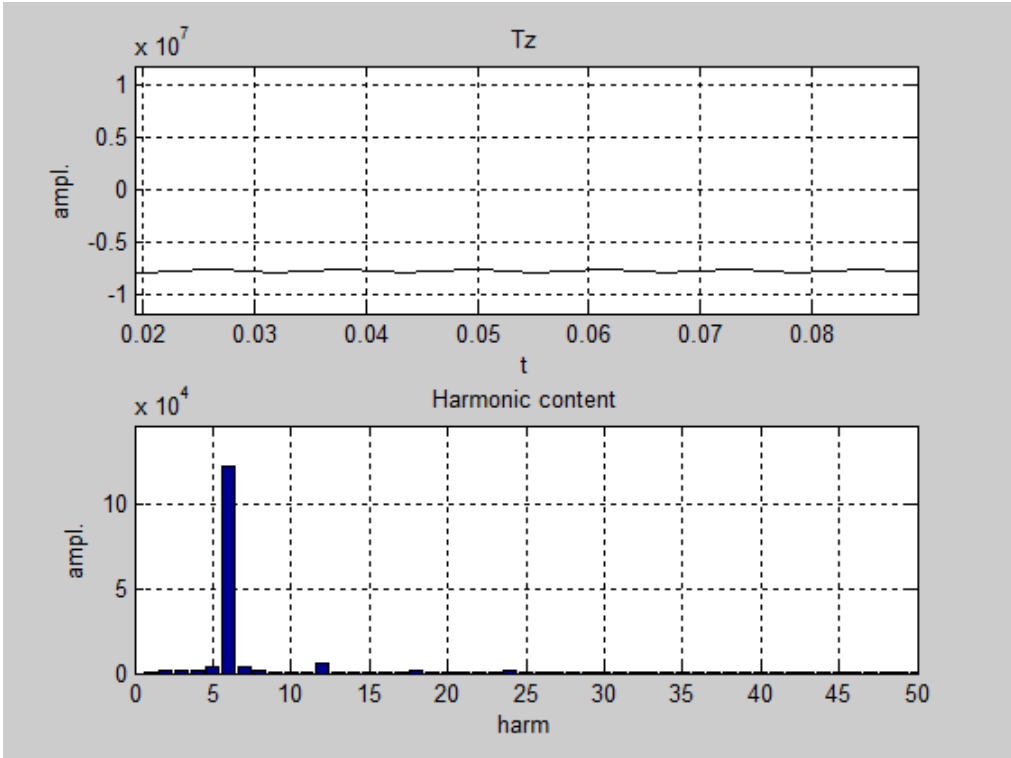


Figure G.13: Plot of full load torque and harmonics amplitude.

10. Full load PM losses

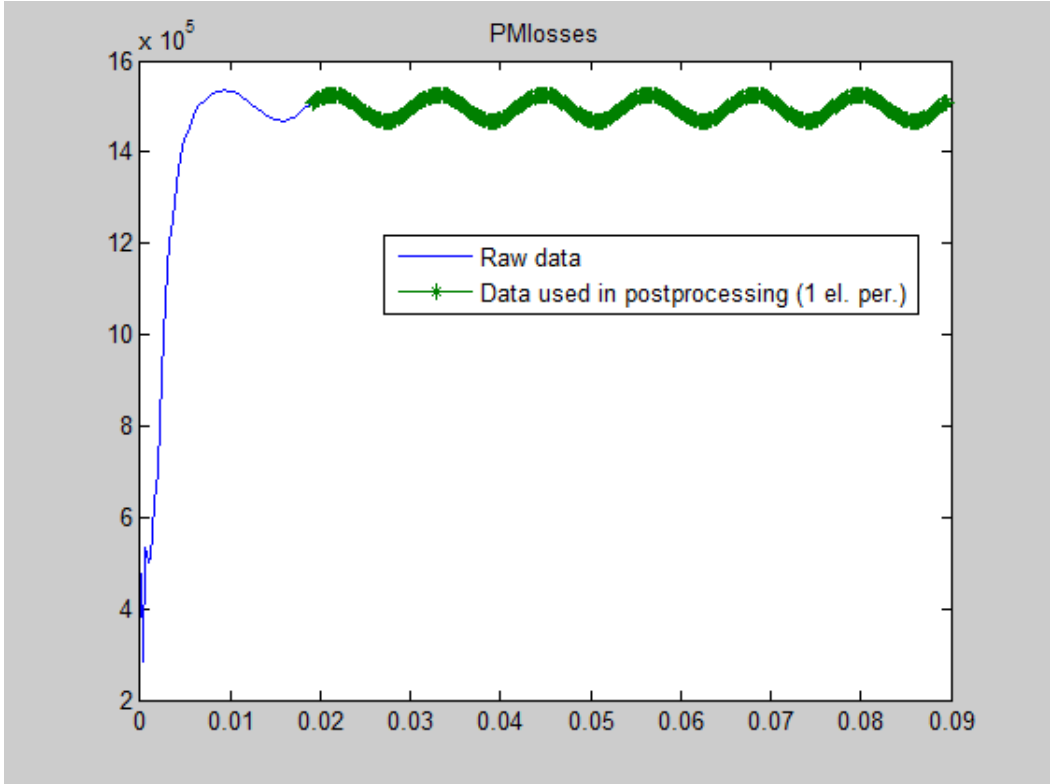


Figure G.14: Full load PM losses.

11. Full load rotor core flux density

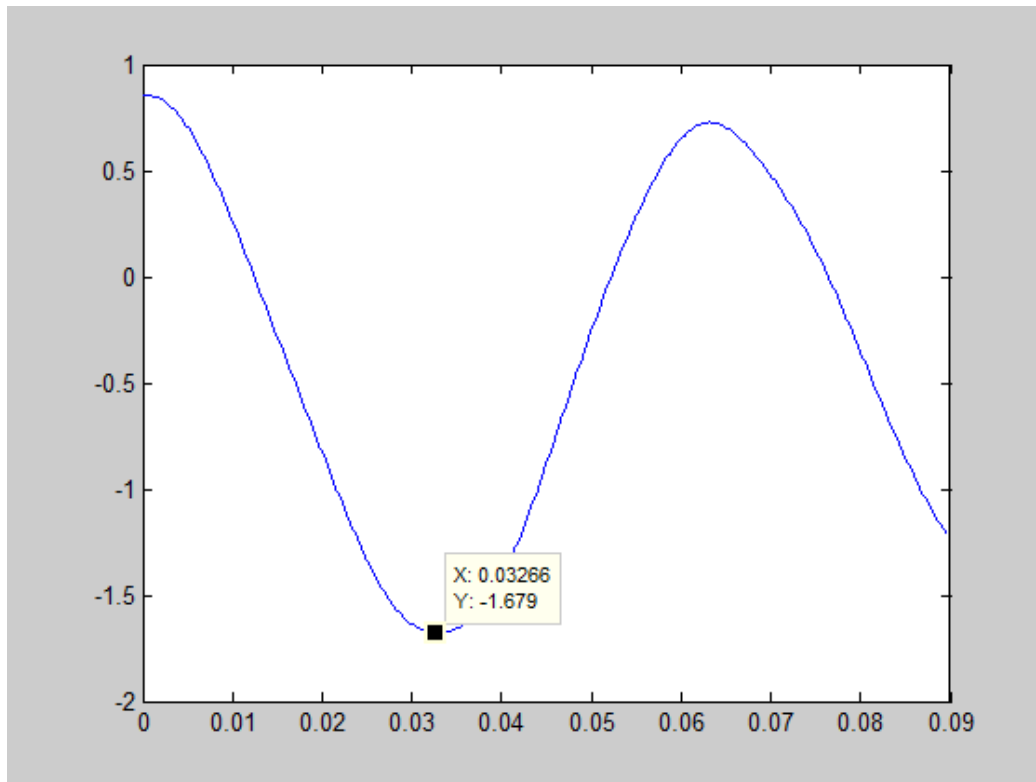


Figure G.15: Plot of flux density in rotor core.

12. Smarttool FEA simulation results

Phase inductance	6963 μ H
Induced voltage	
Phase voltage, 1. harmonic (rms)	1370 V
Phase voltage, maximum (rms)	1186 V
Total harmonic distortion (THD)	15.0209 %
Torque	
Cogging torque amplitude at noload	4744.6994
Mean torque at full load	-7756743.3
Torque ripple amplitude at full load (pu)	-1.6035 %
Losses	
Iron loss in stator at noload	14649.7336
Iron loss in rotor at noload	330.6925 W
Induced loss in magnets at noload	14092.7725
Iron loss in stator at full load	43461.9903
Iron loss in rotor at full load	36649.7419
Induced loss in magnets at full load	1497058.90

OK Write to command window

Figure G.16: Summary of FEA simulation results.

No load simulation:

Loss results:

Average PM loss = 14092.8 W

Max stator core loss = 14649.7 W

Max rotor core loss = 330.692 W

Where $B_{max} = 0.42093$ T and $B_{off} = 0.416171$ T

Full load simulation:

Loss results:

Average PM loss = 1.49706e+006 W

Max stator core loss = 43462 W

Max rotor core loss = 36649.7 W

Where $B_{max} = 1.67971$ T and $B_{off} = 0.41261$ T

SmartTool FEA simulation results:

Phase inductance = 6963 μ H

Induced voltage

Line voltage, 1. harmonic (rms) = 1370 V

Line voltage, maximum (rms) = 1186 V

Total harmonic distortion (THD) = 15.0209 %

Torque

Cogging torque amplitude at no-load = 4744.6994 Nm

Mean torque at full load = -7756743.3977 Nm

Torque ripple amplitude at full load (pu) = -1.6035 %

13. Surface plot of magnetic flux density at full load

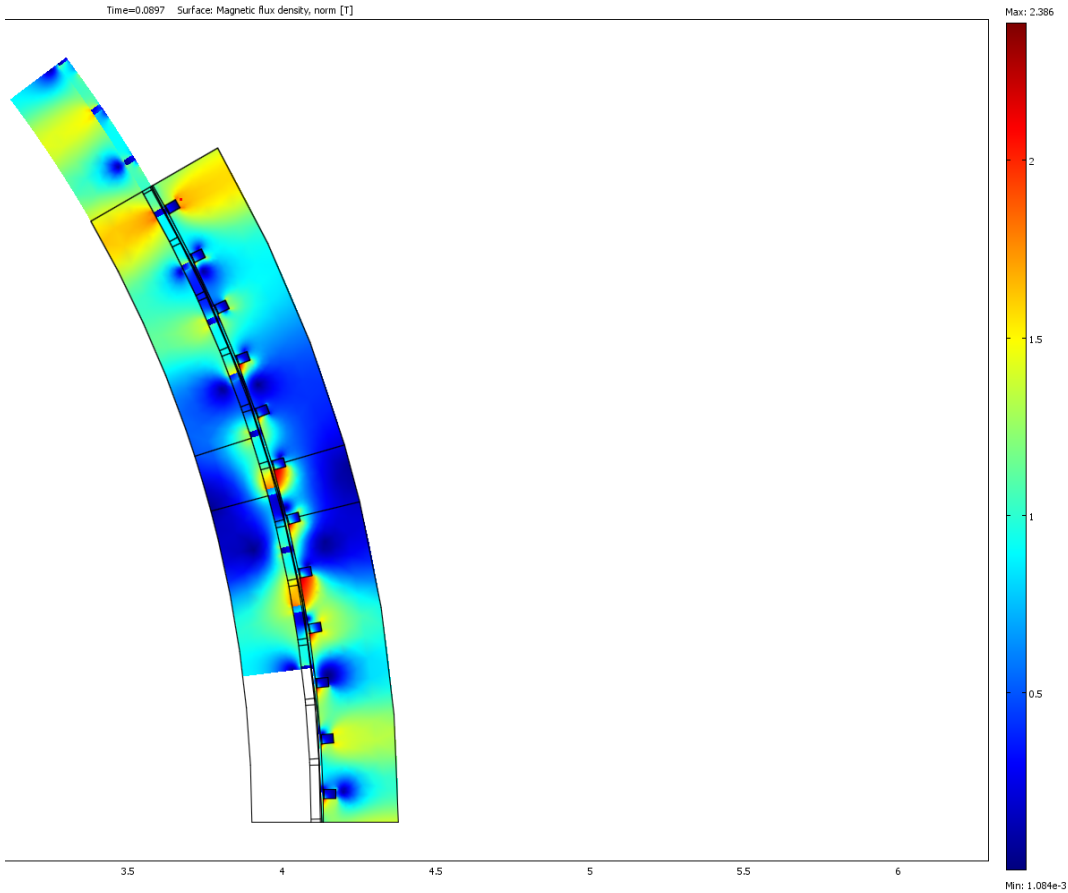


Figure G.17: COMSOL plot of magnetic flux density at full load.

14. Flux variation in stator yoke

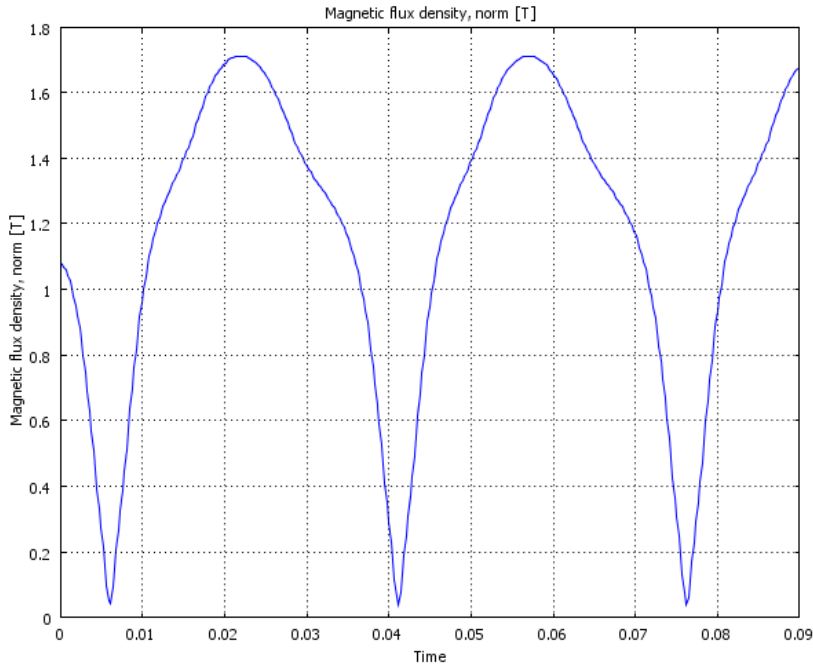


Figure G.18: Variation of flux density in stator core at a point close to slot.

15. Magnetic flux density in range of B = 0 to 1.7

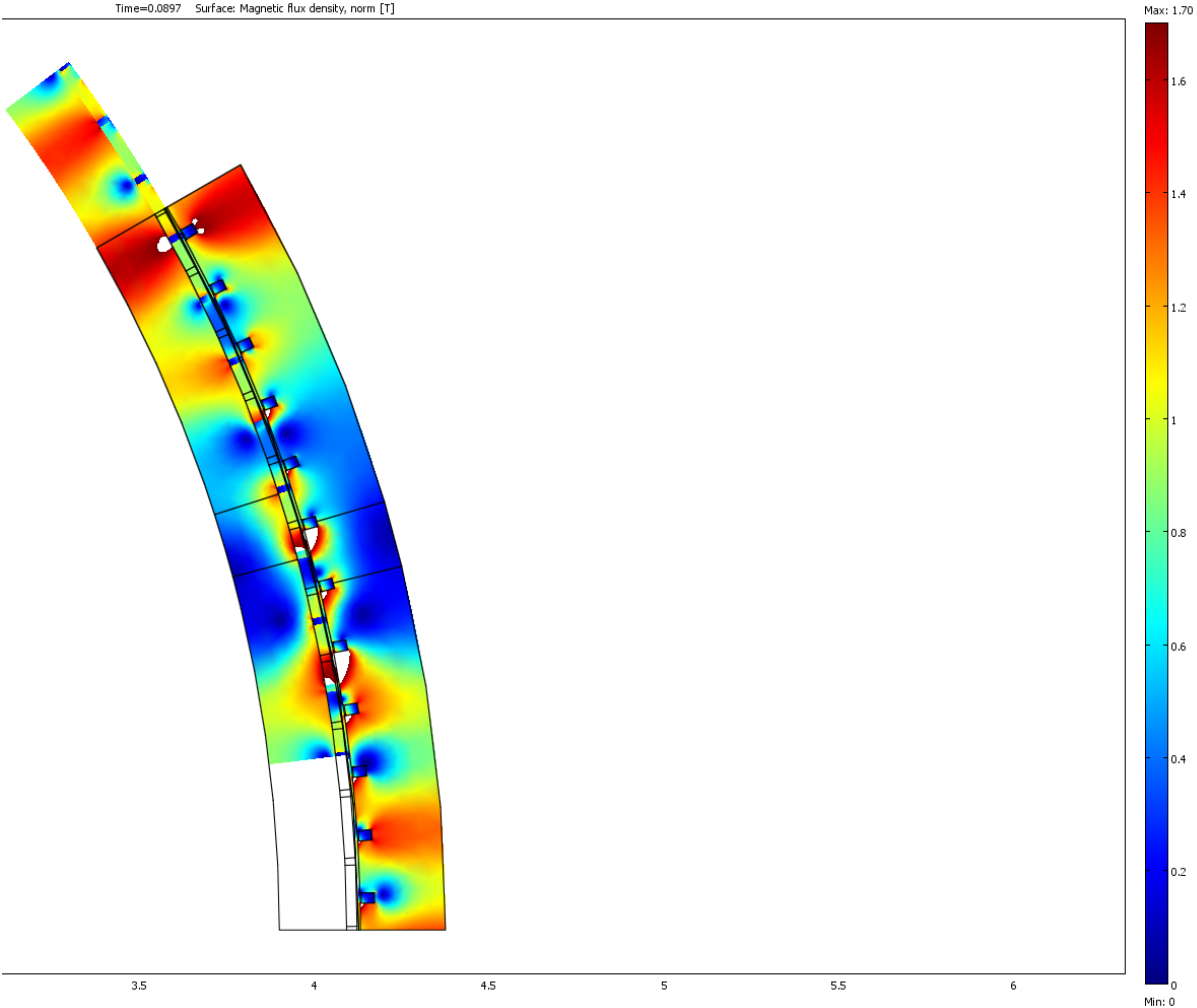


Figure G.19: Plot of magnetic flux density in a range from 0 to 1.7 T at full load.

16. Relative permeability plot at full load condition (Range: 1 to 500)

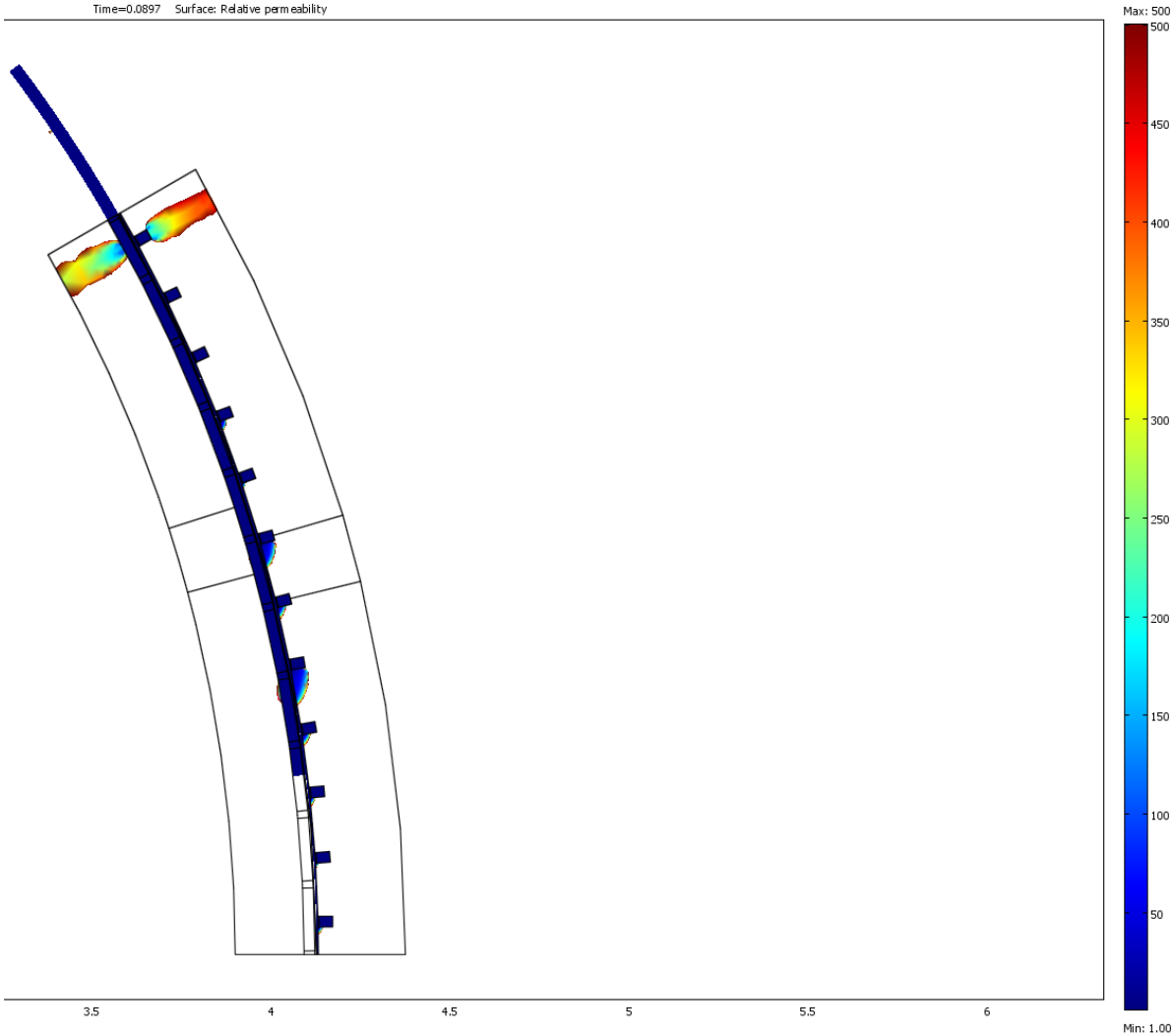


Figure G.20: Relative permeability in range of 1 to 500 at full load.

17. Relative permeability plot at full load condition (Range: 1 to 200)

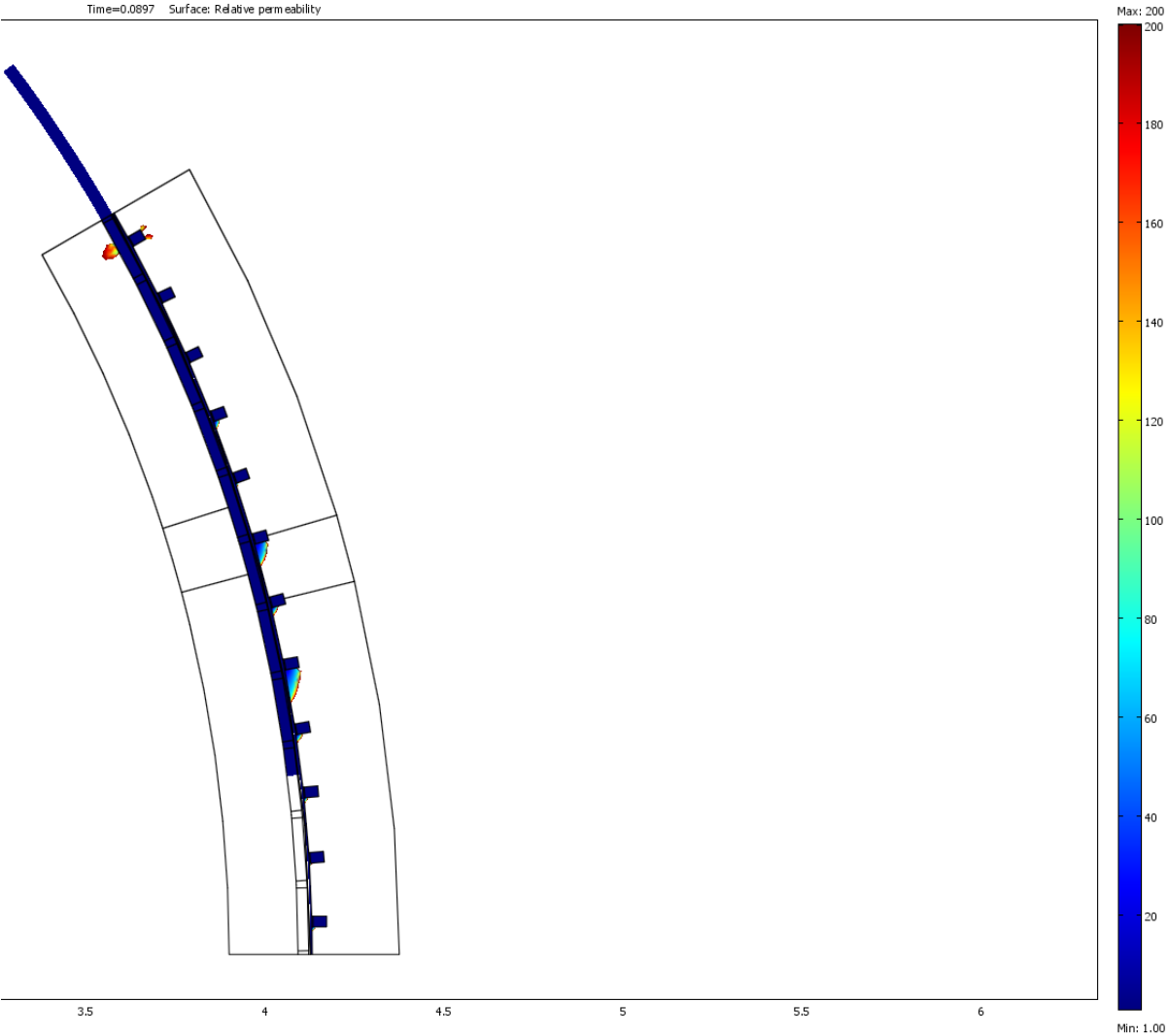


Figure G.21: Relative permeability in range of 1 to 200 at full load.

Appendix H FEA results of Machine – 1 (176 pole 192 slots with 50 mm magnet)

1. Input/output panel

The screenshot displays the SmartTool V3.3 software interface, divided into three main sections: Input panel, Control, and Output panel.

Input panel: Contains various input fields and controls. At the top, there are radio buttons for 'inner [Rotor] outer' (selected) and 'motor | generator'. Below are sections for 'Machine key numbers' (Rated mechanical power: 10000 kW, Rated rotational speed: 12.95 rpm, Desired rated voltage: 3300 V), 'Machine geometry' (Machine inner diameter: 8000 mm, Magnet length: 50 mm, Magnet pitch/pole pitch: 0.9, Slot width/slot pitch: 0.222, Slot depth/slot width: 1.267, Number of poles: 176, Number of slots: 192), 'Energy density' (Copper current density (rms): 130 A/mm²), 'Winding data' (Copper fill factor under wedge: 0.08, Number of parallel branches: 6), and 'Slot wedge' (Thickness slot wedge: 3 mm). There are also buttons for 'Set existing machine para.', 'Save design', and 'Load design'.

Control panel: Contains several buttons: 'Calculate', 'Optimize', 'Optimization limits', 'Slot/Pole advice', 'Winding visualization', 'Advanced', 'Cost data', 'FEA', 'Save to Excel', and 'Struct to Works pace'.

Output panel: Displays calculated results. It is divided into several sub-sections:

- Geometry (main) and winding:** Stack length: 1010.7 mm, Length with end windings: 1178 mm, Outer active diameter: 8567.4 mm, Inner active diameter: 8000 mm, Diameter at air gap: 8294.1 mm, Slot pitch: 135.9 mm, Pole pitch: 147.9 mm, Slot depth: 38.2 mm, Slot width: 30.2 mm, Stator back iron thickness: 92.9 mm, Rotor back iron thickness: 92 mm, Weight of active materials: 53443.92 kg, Rotor moment of inertia: 451412. kg*m², Number of turns: 35, Copper operating temperature: 20 deg C.
- Characteristics:** Torque: 7373974 Nm, Efficiency: 99.8 %, cos_phi: 0.9091.
- Electromagnetic values:** Frequency: 18.99 Hz, RMS line voltage: 3341.4 V, RMS phase induced voltage: 1757.1 V, RMS phase current: 1893.47 A, Flux density in tooth: 1.1 T, Average flux density in air gap: 0.85 T, Active power: 9962 kW, Phase inductance: 3557.3 uH, Synchronous pu reactance: 0.4167, RMS Copper current density: 130 A/mm², RMS current loading: 81289.4 A/m.
- Losses:** Losses in winding: 7.4 W, No Load Losses in magnets: 4420.46 W, No Load Losses in teeth: 7115.71 W, No Load Losses in stator yoke: 7440.22 W, No Load Losses in rotor yoke: 13.54 W, Stator loss per area: 551 W/m².
- Coefficients:** Distribution factor: 0.958, AC/DC Loss factor: 1.2, Magnetic air gap shear force: 106053 N/m².
- Cost:** Material cost of windings: 189 NOK, Material cost of magnets: 8653 NOK, Material cost of stator laminate: 25989 NOK, Material cost of rotor back iron: 18612 NOK, Total active cost: 53444 NOK.

Figure H.1: Combined input output panel of SC machine - 1 with 50 mm magnet.

$$C = \frac{S}{D^2 Ln} = \frac{10000/0.909}{8.3^2 \cdot 1.01 \cdot 12.95} = 12.2$$

Note: The parameters in red color indicate that losses due to harmonics are not included.

2. Machine Parameters:

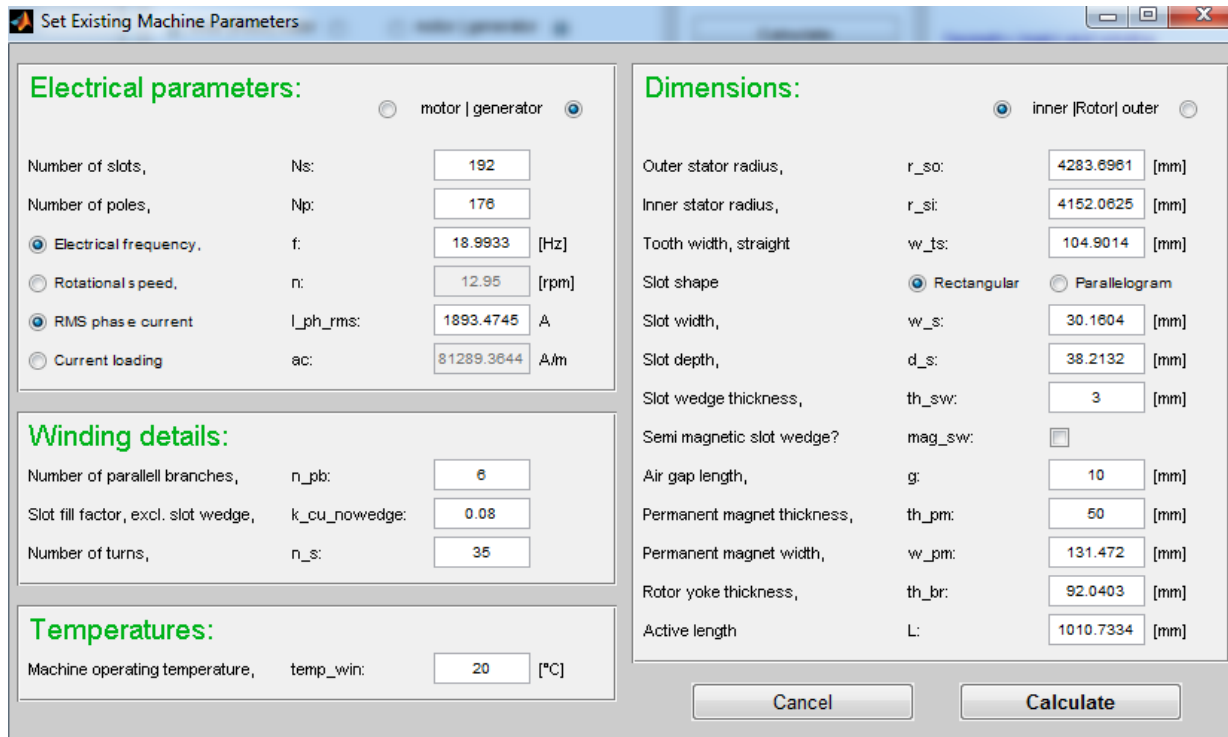


Figure H.2: Input parameters of machine -1 with 50 mm magnet.

3. EMF Simulation Plot

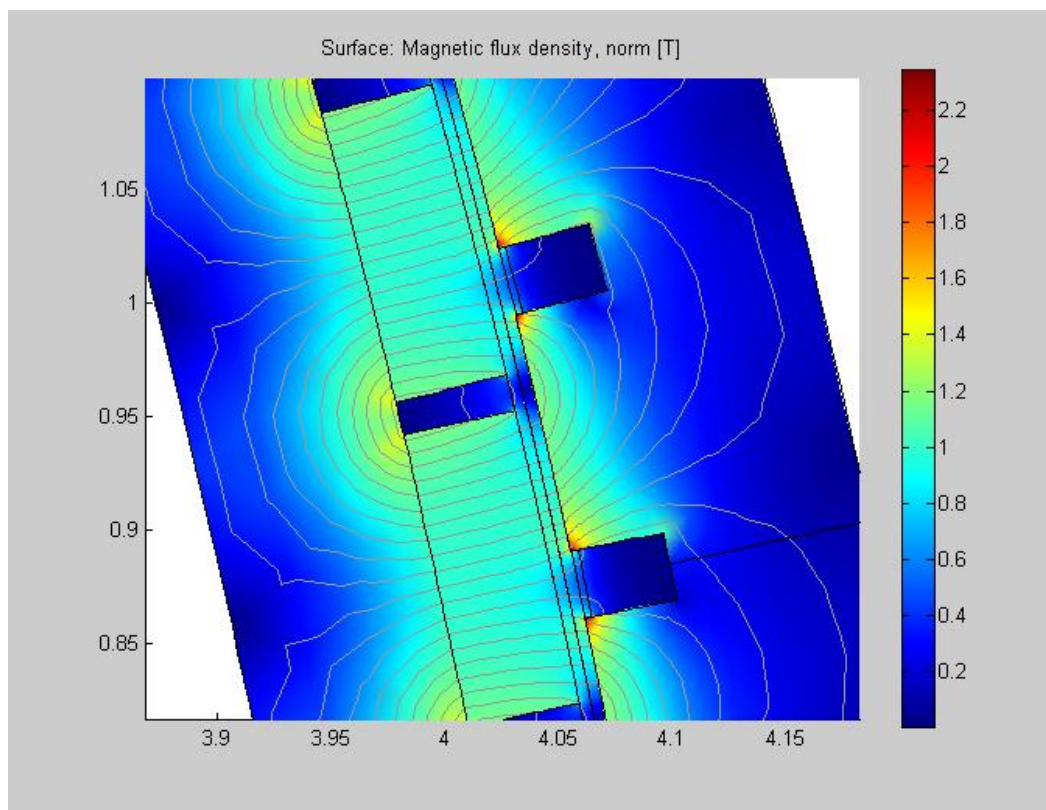


Figure H.3: EMF simulation plot at no-load.

4. One period EMF Excitation

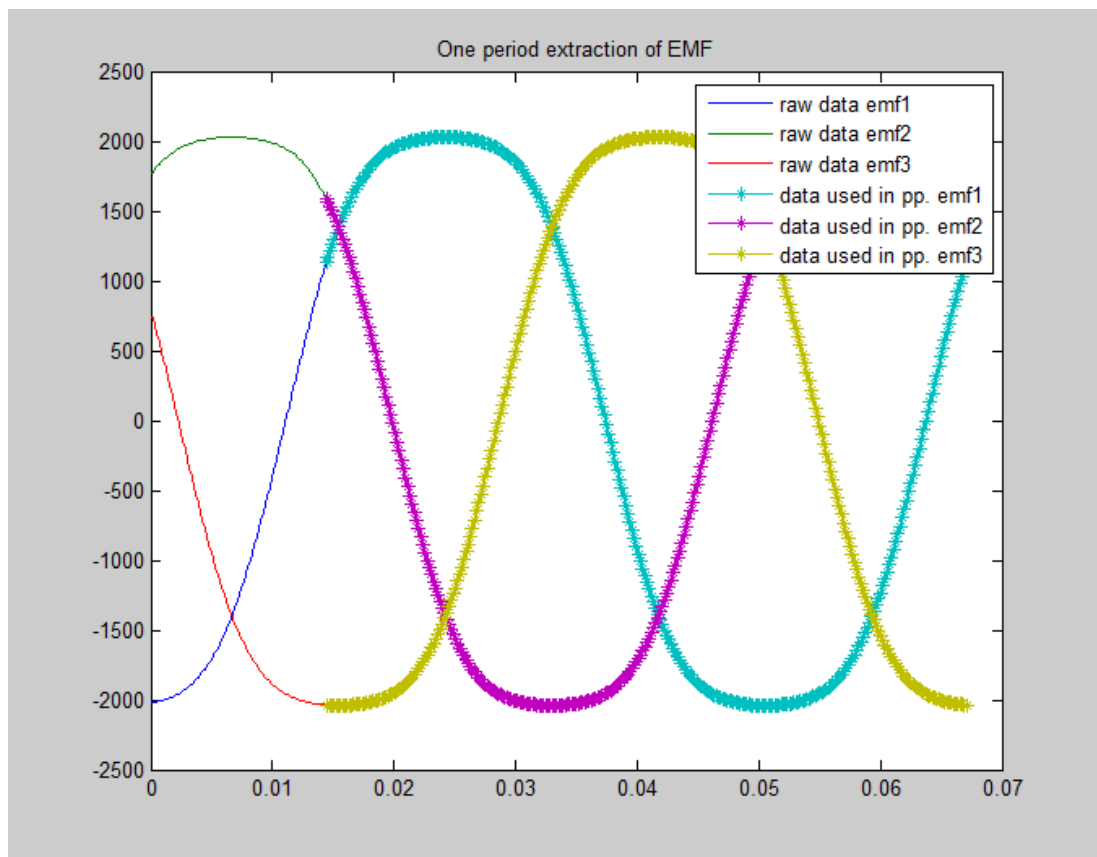


Figure H.4: EMF waveform of 3-phases at no-load.

5. EMF Simulation results:

Parameters	Machine – 1	Machine – 1
	(50 mm magnet)	(50 mm magnet)
	Phase EMF	Line EMF
Mean first harmonic peak, V	2273.5	3937.8
Mean peak voltage, V	2038.9	3911.8
Phase voltage, 1. harmonics (rms), V	1608	2784
Phase voltage maximum (rms), V	1442	2766
THD (%)	11.1 %	1.13%

6. Phase and Line EMFs

Phase EMF

Line EMF

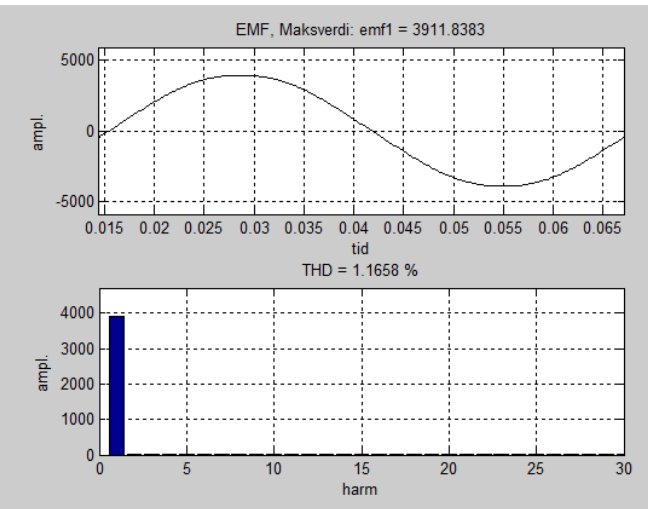
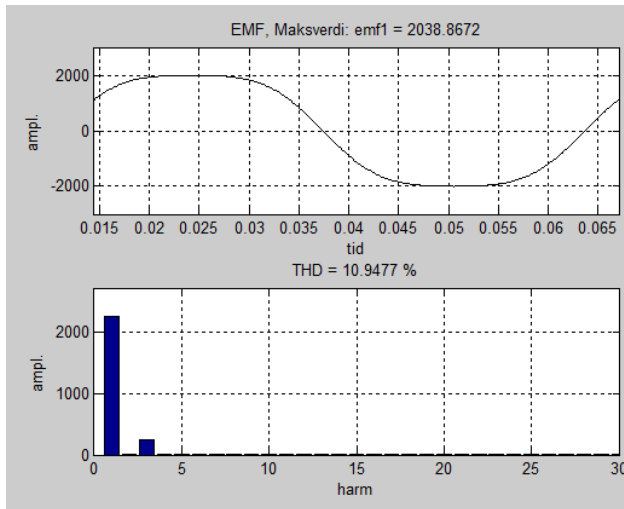


Figure H.5: EMF and harmonics of phase voltage of phase 1.

Figure H.6: EMF waveform of line voltage 1.

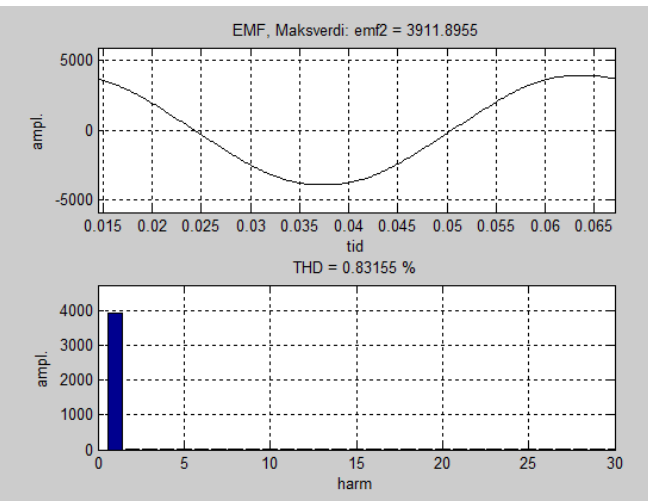
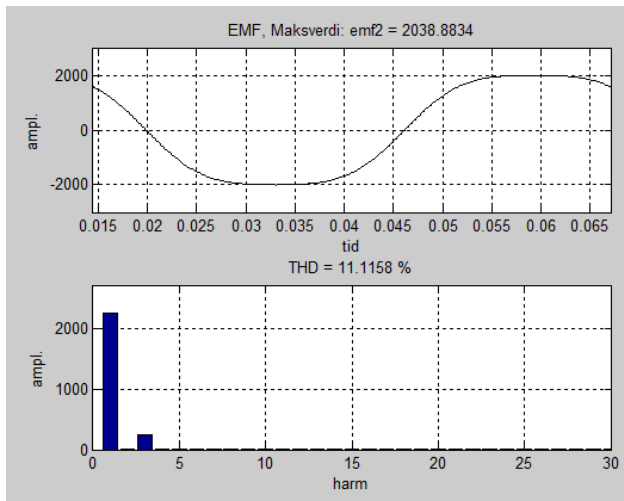


Figure H.7: EMF and harmonic of phase voltage of phase 2.

Figure H.8: EMF waveform of line voltage 2.

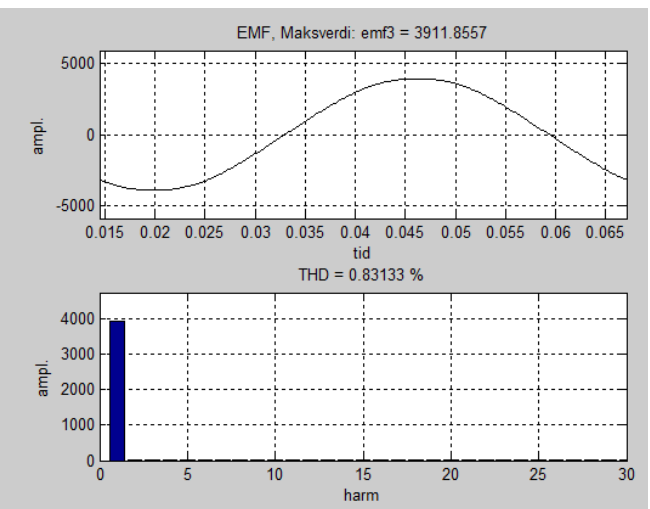
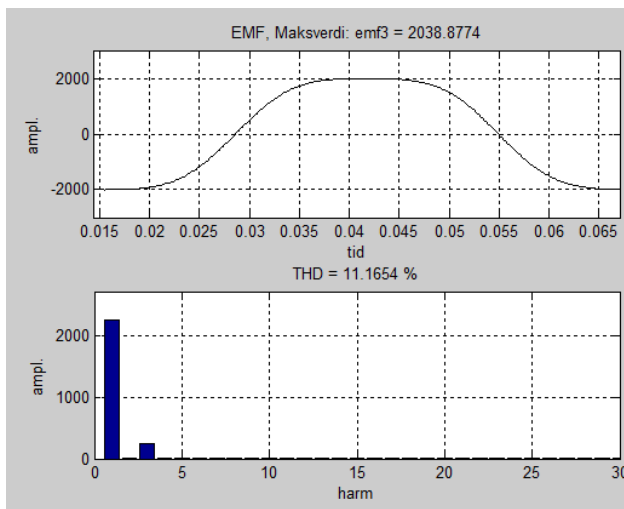


Figure H.9: EMF and harmonic of phase voltage of phase 3.

Figure H.10: EMF waveform of line voltage 3.

7. Full Load Simulation plot

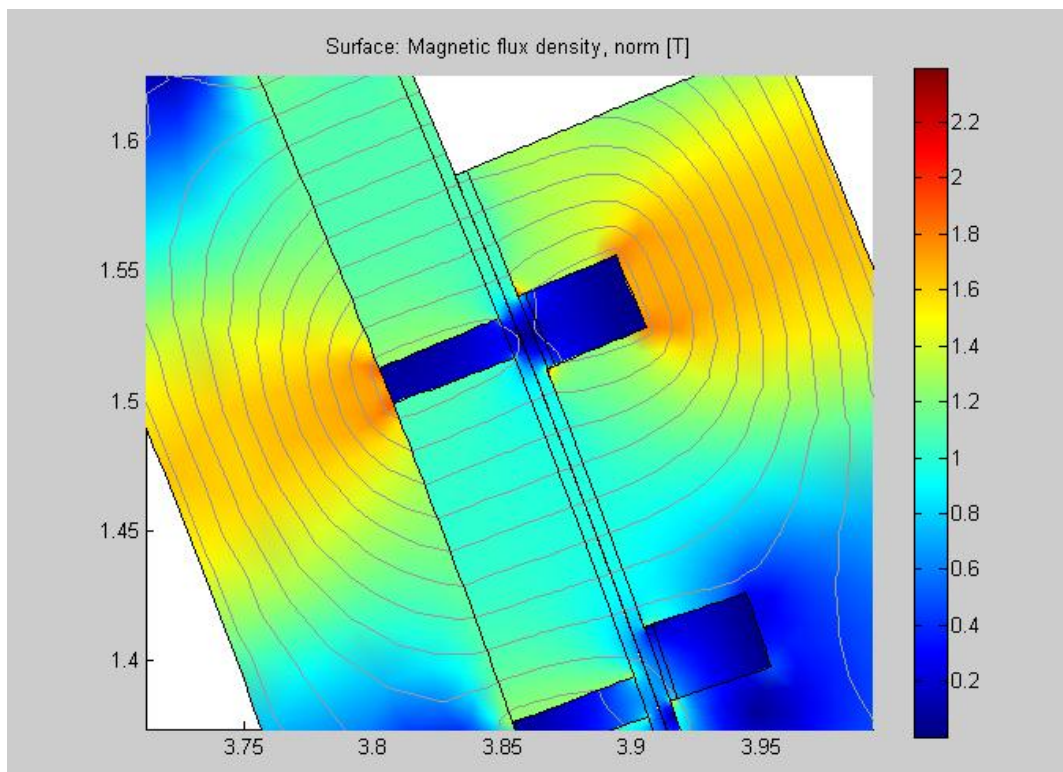


Figure H.11: Magnetic flux density at full load.

8. Full load torque

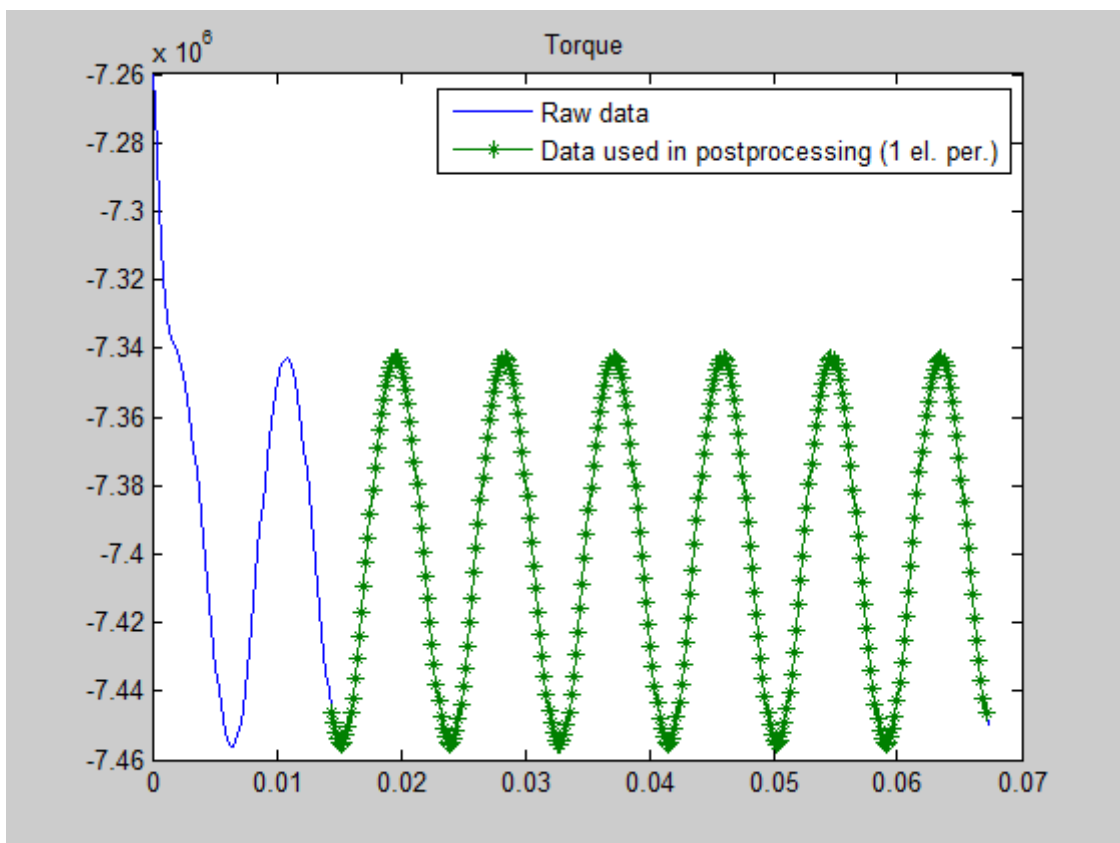


Figure H.12: Torque at full load condition.

9. Full load torque Harmonics

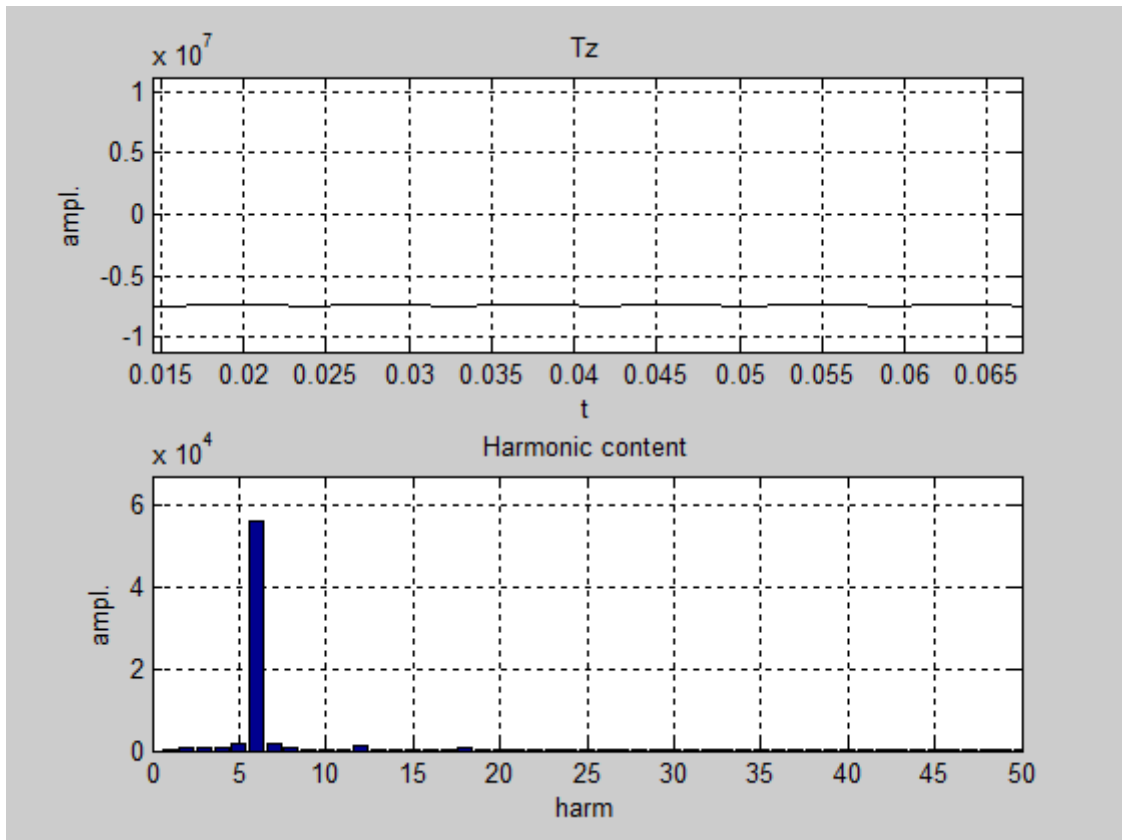


Figure H.13: Torque and harmonic content at full load.

10. Full load PM losses

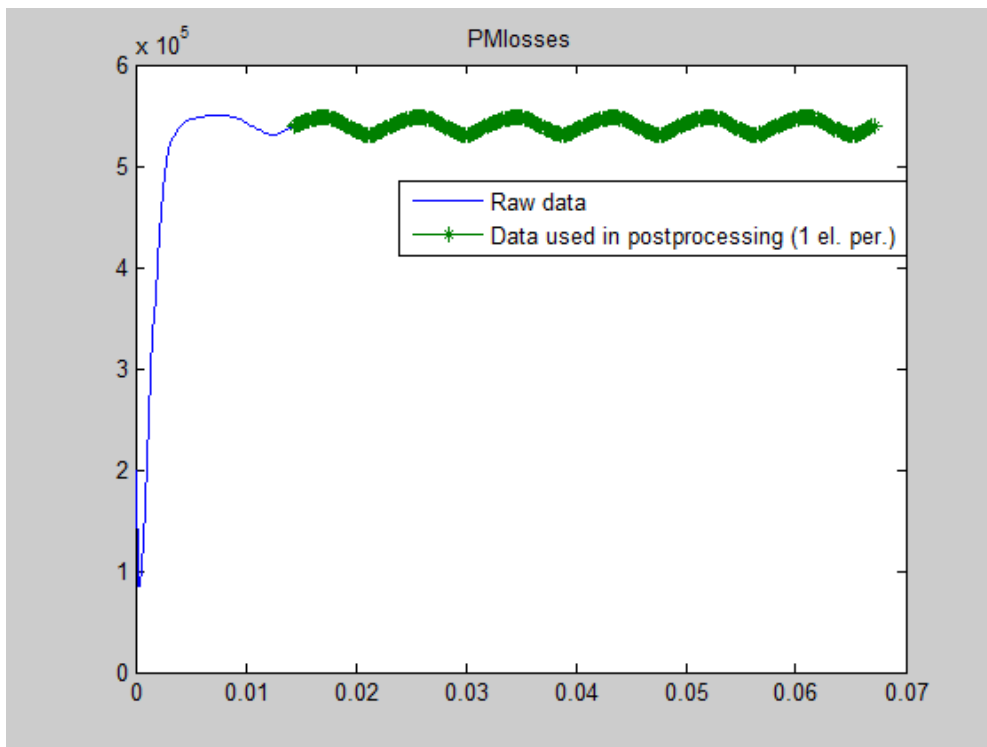


Figure H.14: PM losses at full load.

11. Full load rotor core flux density

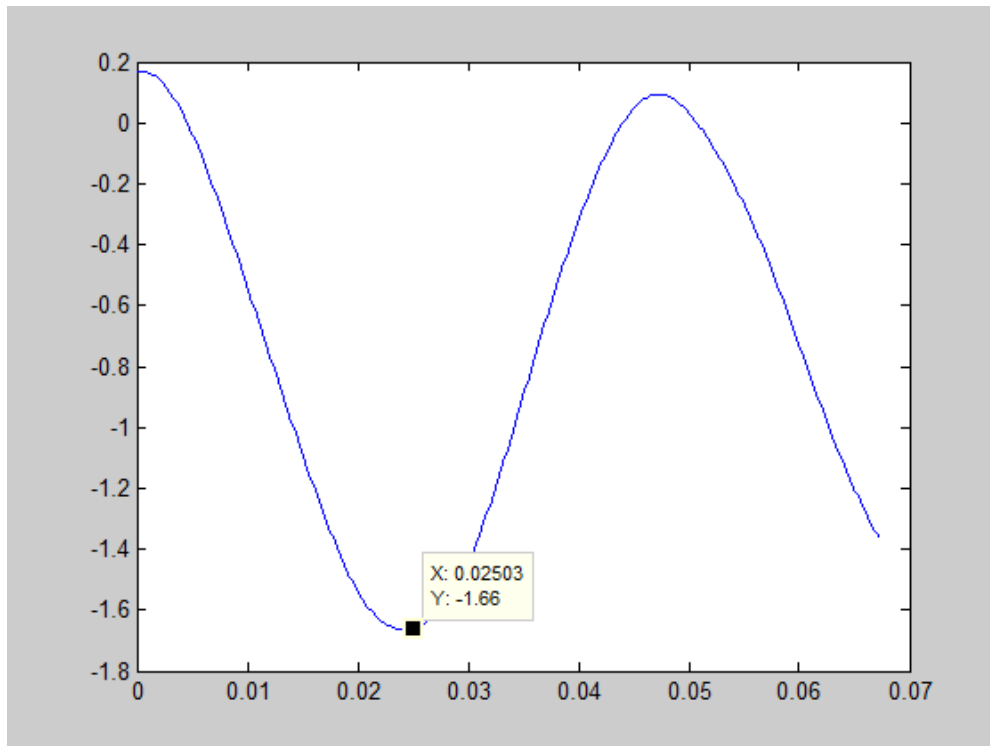


Figure H.15: Rotor core flux density at full load.

12. Smarttool FEA simulation results

Phase inductance	4635 μ H
Induced voltage	
Phase voltage, 1. harmonic (rms)	1608 V
Phase voltage, maximum (rms)	1442 V
Total harmonic distortion (THD)	11.0763 %
Torque	
Cogging torque amplitude at noload	107.3969
Mean torque at full load	-7398141.6
Torque ripple amplitude at full load (pu)	-0.76148 %
Losses	
Iron loss in stator at noload	15396.3902
Iron loss in rotor at noload	156.627 W
Induced loss in magnets at noload	18282.3427
Iron loss in stator at full load	27528.9453
Iron loss in rotor at full load	13112.1575
Induced loss in magnets at full load	540242.558
<input type="button" value="OK"/> <input type="button" value="Write to command window"/>	

Figure H.16: Summary of FEA results.

No load simulation:

Loss results:

Average PM loss = 18282.3 W

Max stator core loss = 15396.4 W

Max rotor core loss = 156.627 W

Where $B_{max} = 0.74988$ T and $B_{off} = 0.744438$ T**Full load simulation:**

Loss results:

Average PM loss = 540243 W

Max stator core loss = 27528.9 W

Max rotor core loss = 13112.2 W

Where $B_{max} = 1.66388$ T and $B_{off} = 0.747241$ T**SmartTool FEA simulation results:**Phase inductance = 4635 μ H

Induced voltage

Line voltage, 1. harmonic (rms) = 1608 V

Line voltage, maximum (rms) = 1442 V

Total harmonic distortion (THD) = 11.0763 %

Torque

Cogging torque amplitude at no-load = 107.3969 Nm

Mean torque at full load = -7398141.6876 Nm

Torque ripple amplitude at full load (pu) = -0.76148 %

13. Surface plot of magnetic flux density at full load

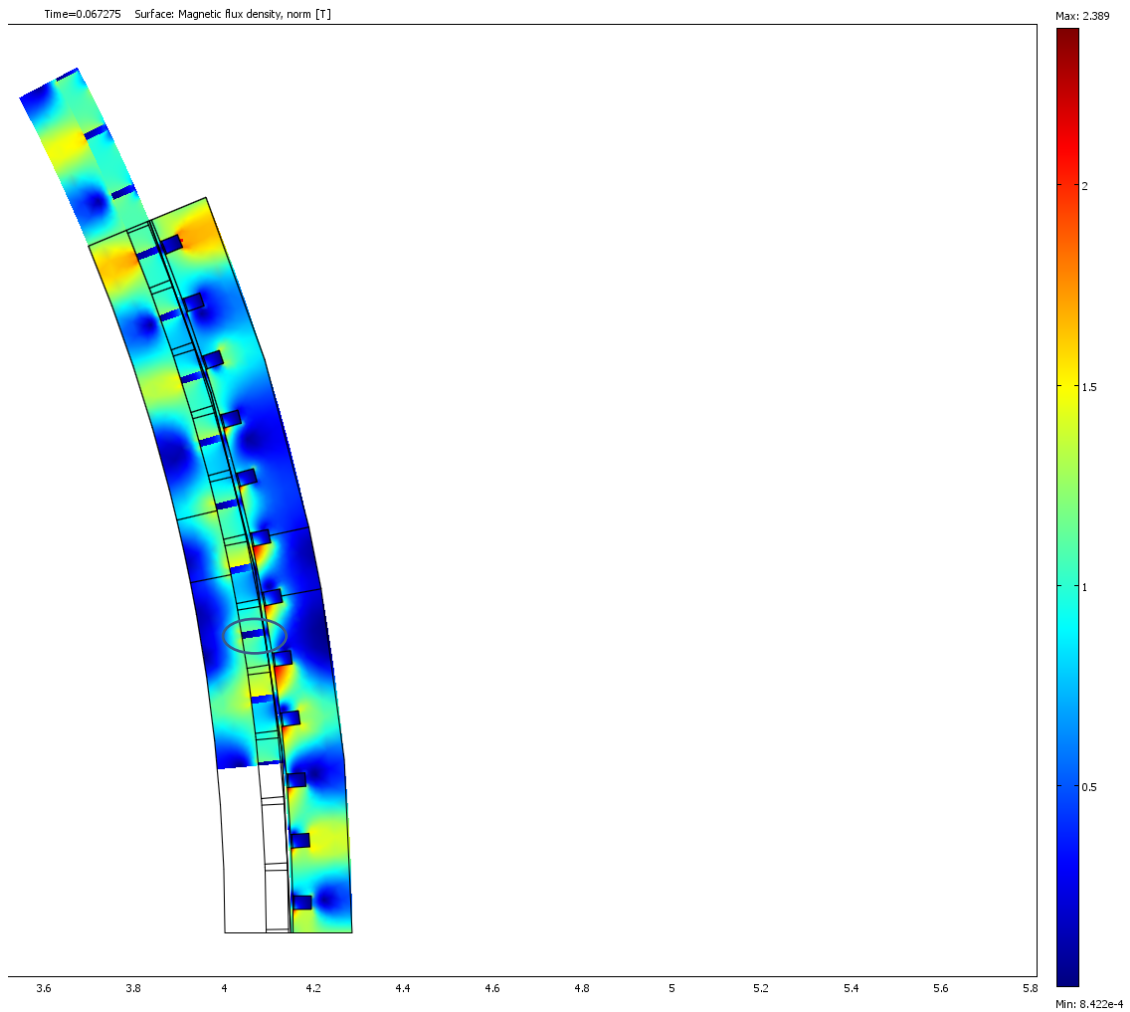


Figure H.17: Surface plot of magnetic flux density at full load.

14. Variation of flux density in stator yoke (just above the slot)

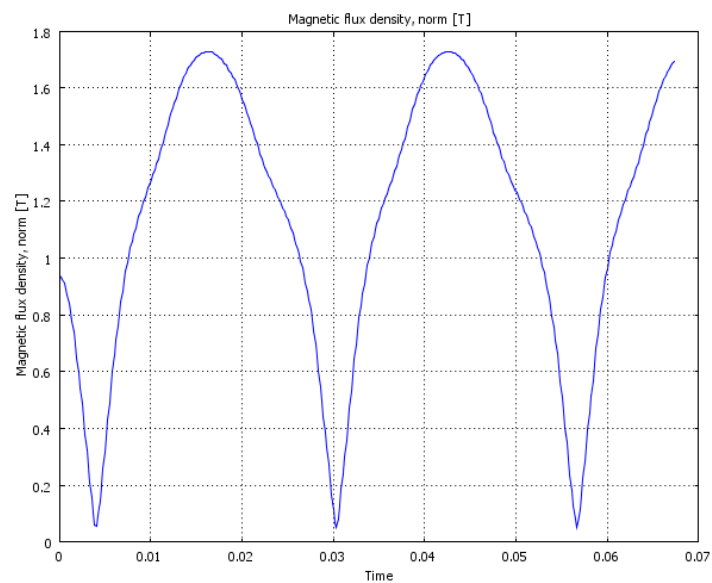


Figure H.18: Variation of flux density in stator yoke (just above the slot).

15. Magnetic flux density in range of B = 0 to 1.7 T

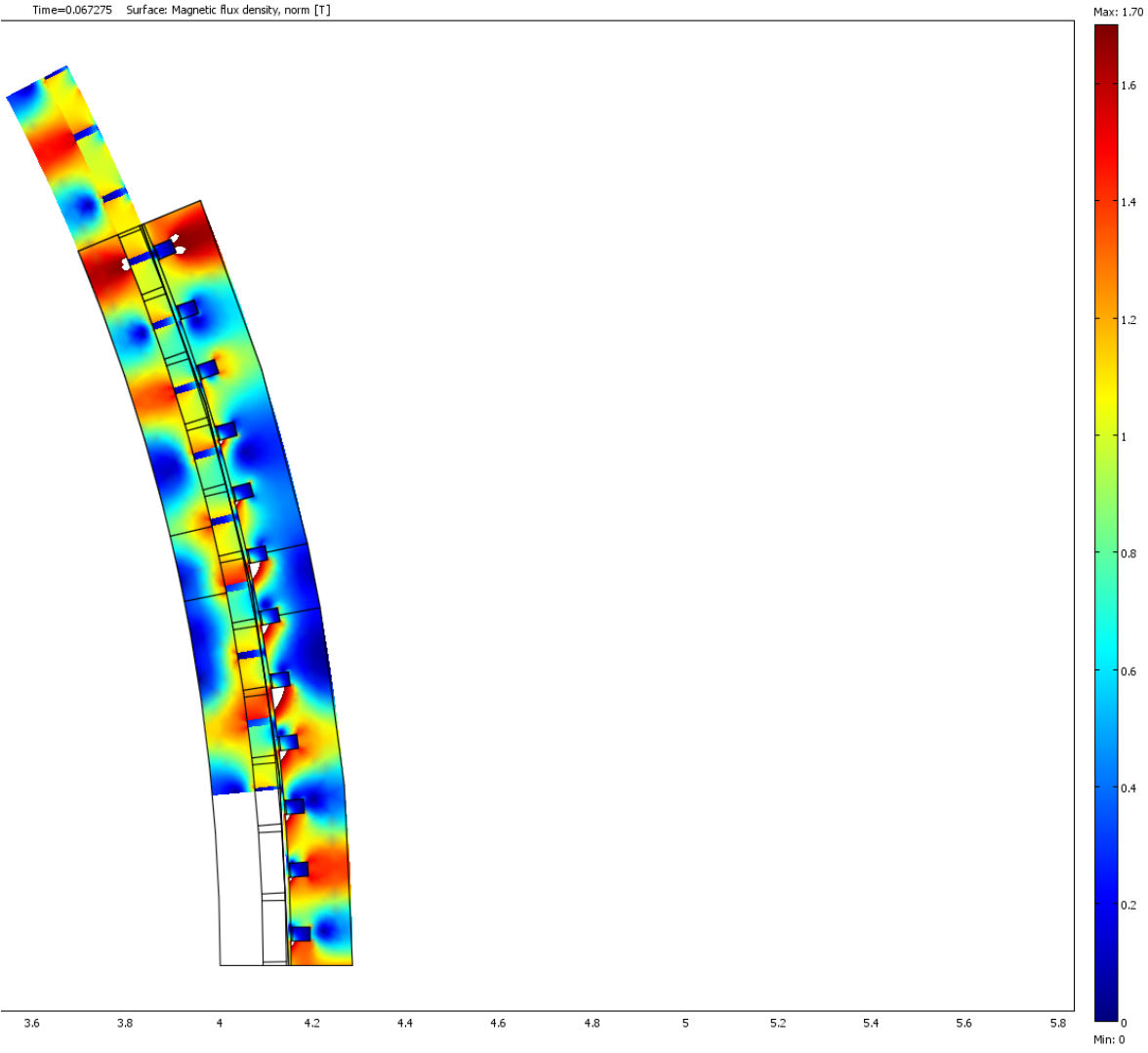


Figure H.19: Surface plot of magnetic flux density in range of 0 to 1.7 T at full load.

16. Relative permeability plot at full load condition (Range: 1 to 500)

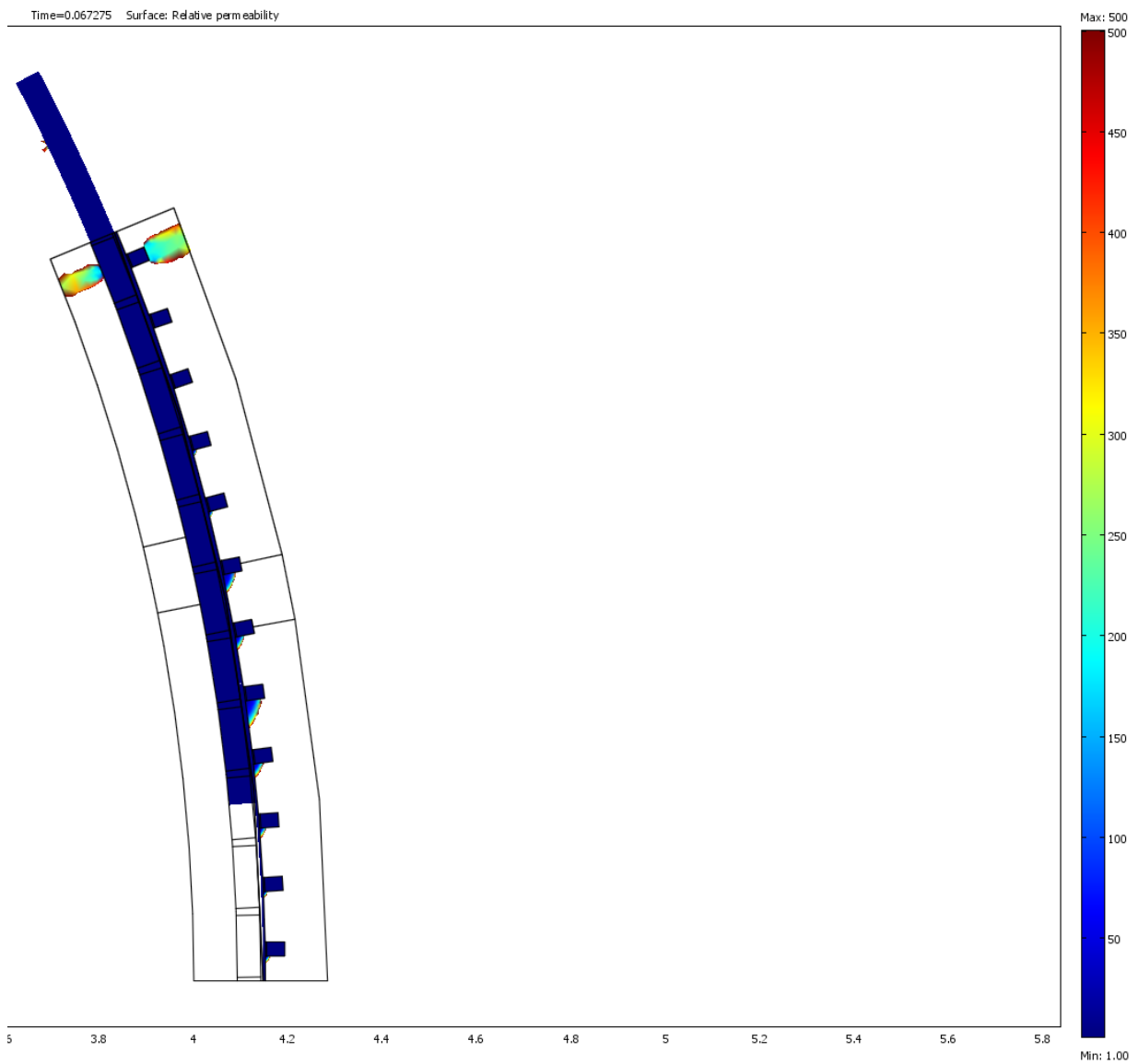


Figure H.20: Relative permeability in range of 1 to 500 at full load.

17. Relative permeability plot at full load condition (Range: 1 to 200)

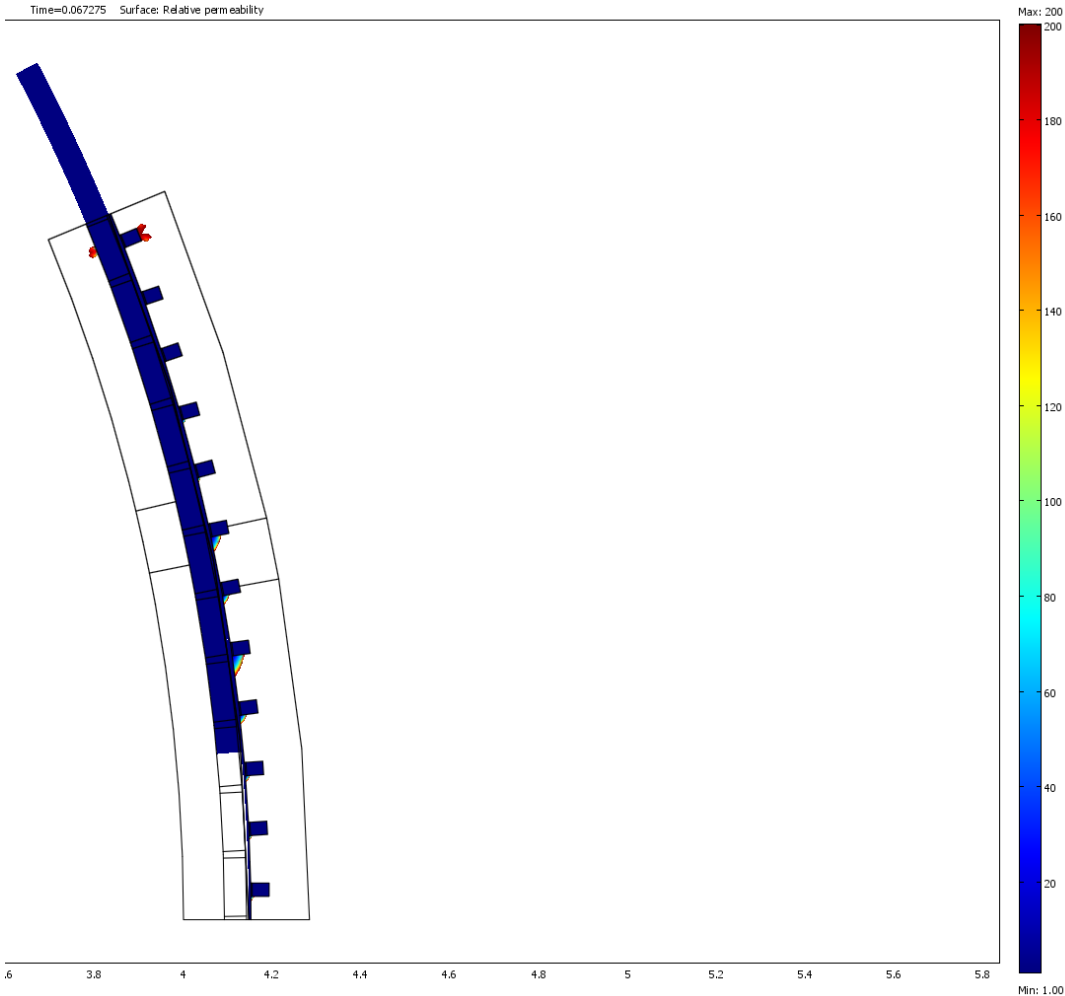


Figure H.21: Relative permeability in range of 1 to 200 at full load.

18. Flux density variation at the center of a slot

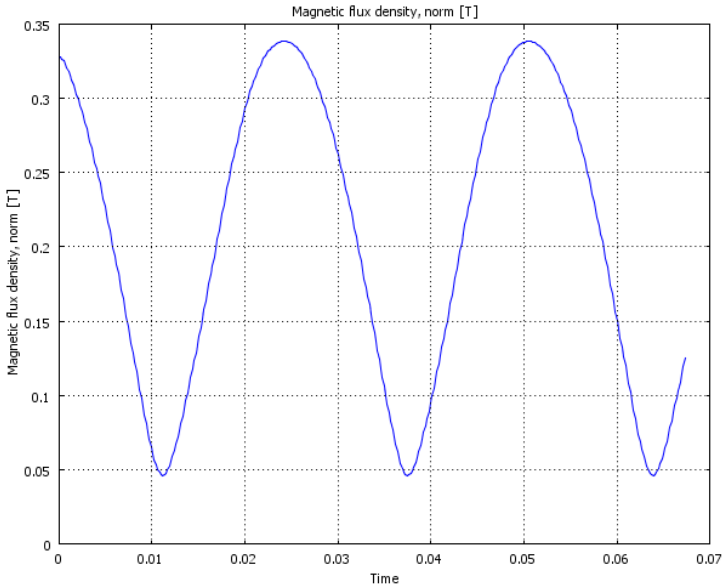


Figure H.22: Variation of flux density at the center of a slot.

Appendix I FEA results of reference machine with segmentation of magnet

The pole magnet of the reference machine is segmented into 17 parts in circumferential direction.

1. Input/output panel

The screenshot displays the SmartTool V3.3 software interface, divided into three main sections: Input panel, Control, and Output panel.

Input panel: This section contains various input parameters for the machine. It includes radio buttons for 'inner | Rotor | outer' (selected) and 'motor | generator' (selected). Under 'Machine key numbers', parameters include Rated mechanical power (10000 kW), Rated rotational speed (12.95 rpm), and Desired rated voltage (3300 V). 'Machine geometry' includes Machine outer diameter (11600 mm), Magnet length (20 mm), Magnet pitch/pole pitch (0.9), Slot width/slot pitch (0.5), Slot depth/slot width (0.5), Number of poles (198), and Number of slots (216). 'Energy density' includes Copper current density (rms) (47247.1 A/m), Stator loss per area, Flux density in stator yoke (0.55 T), and Flux density in rotor yoke (0.55 T). 'Winding data' includes Copper fill factor under wedge (0.5) and Number of parallel branches (6). 'Slot wedge' includes Thickness slot wedge (0 mm) and Semimagnetic wedge? (unchecked). A 'Set existing machine para...' button is present. At the bottom, there are radio buttons for 'Regular input' (selected) and 'Geometry input', along with 'Save design' and 'Load design' buttons.

Control: This section contains several buttons for simulation and optimization: 'Calculate', 'Optimize', 'Optimization limits', 'Slot/Pole advice', 'Winding visualization', 'Advanced', 'Cost data' (highlighted with a dashed border), 'FEA', 'Save to Excel', and 'Struct to Workspace'.

Output panel: This section displays the results of the simulation, categorized into several groups:

- Geometry (main) and winding:** Stack length (1222.8 mm), Length with end windings (1483.7 mm), Outer active diameter (12141.2 mm), Inner active diameter (11600 mm), Diameter at air gap (11857.1 mm), Slot pitch (172.6 mm), Pole pitch (188 mm), Slot depth (43.1 mm), Slot width (86.3 mm), Stator back iron thickness (92.6 mm), Rotor back iron thickness (103.6 mm), Weight of active materials (90780.72 kg), Rotor moment of inertia (1466186 kg*m²), Number of turns (24), and Copper operating temperature (80 deg C).
- Characteristics:** Torque (7373974 Nm), Efficiency (96.4 %), and cos_phi (0.8375).
- Electromagnetic values:** Frequency (21.37 Hz), RMS line voltage (3251.6 V), RMS phase induced voltage (1631.1 V), RMS phase current (2038.72 A), Flux density in tooth (1.18 T), Average flux density in air gap (0.59 T), Active power (9616.6 kW), Phase inductance (3747.3 μH), Synchronous pu reactance (0.5464), RMS Copper current density (4.381 A/mm²), and RMS current loading (47247.1 A/m).
- Losses:** Losses in winding (335249. W), No Load Losses in magnets (125.54 W), No Load Losses in teeth (12187.38 W), No Load Losses in stator yoke (11568.72 W), No Load Losses in rotor yoke (206.79 W), and Stator loss per area (7866 W/m²).
- Coefficients:** Distribution factor (0.958), AC/DC Loss factor (1.2), and Magnetic air gap shear force (42892 N/m²).
- Cost:** Material cost of windings (6108 NOK), Material cost of magnets (6042 NOK), Material cost of stator laminate (41987 NOK), Material cost of rotor back iron (36644 NOK), and Total active cost (90781 NOK).

Figure I.1: Combined input/output panel of reference machine with segmentation.

Note: The parameters in red color indicate that losses due to harmonics are not included.

2. FEA results of reference machine with segmentation of magnet

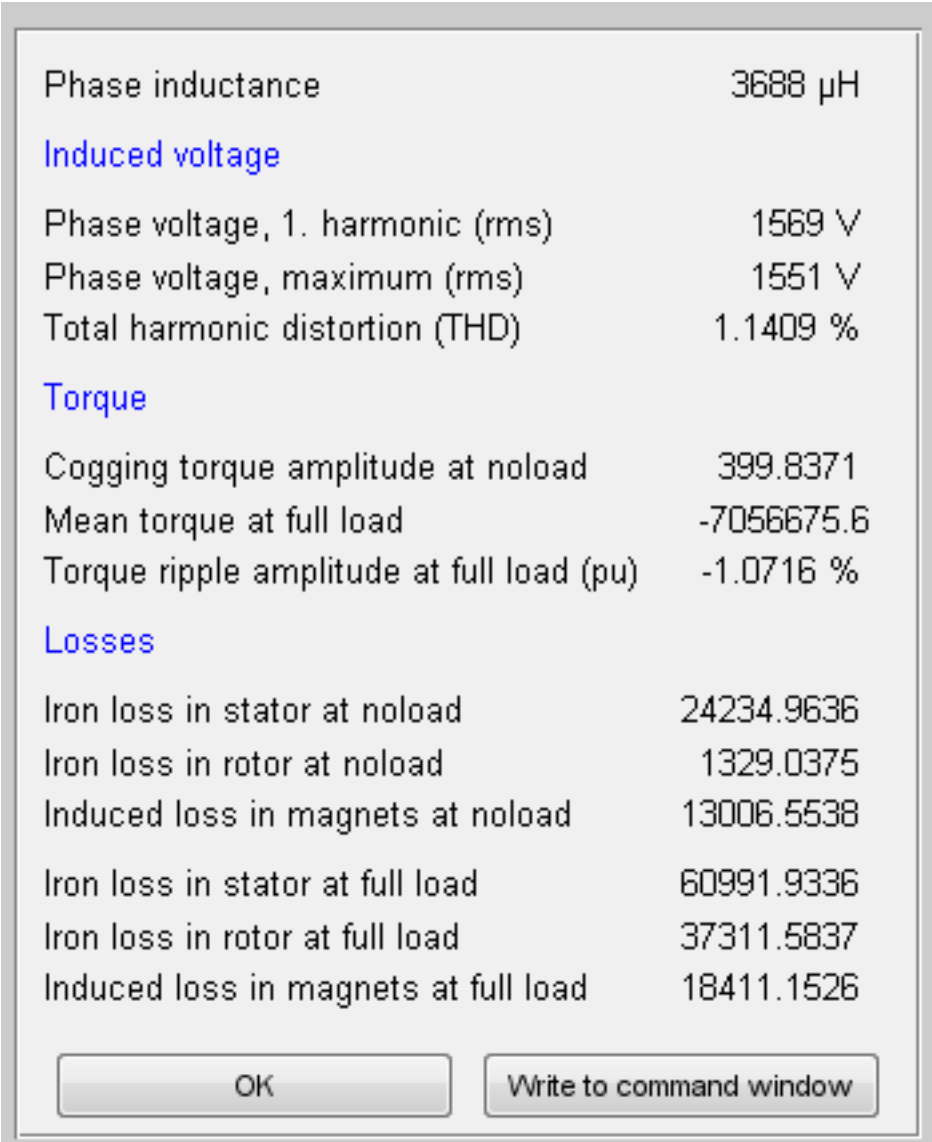


Figure I.2: FEA results of reference machine with segmentation.